UDK 66:54(05) CODEN HMIDA 8 ISSN 0367–598 X

6

Hemijska industrija

Vol. 68

Časopis Saveza hemijskih inženjera

Chemical Industry

Posebna sekcija:
Polimeri

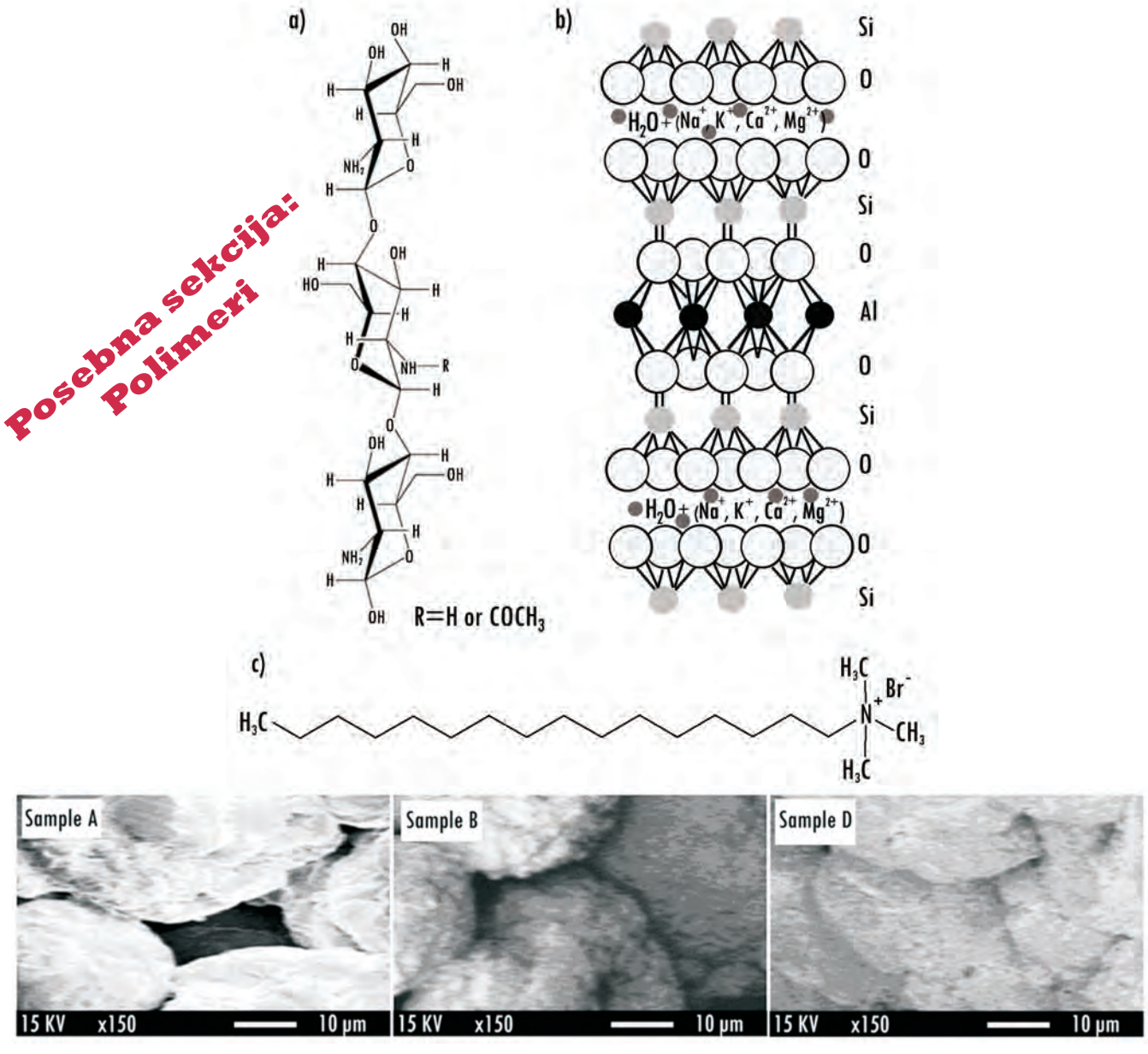

BEOGRAD, NOVEMBAR-DECEMBAR 2014.

HMIDA 8, 68 (6) 653-825 (2014)

GENERALNI POKROVITELJ

Hemofarm

HEMOFARM KONCERN

VRŠAC, Beogradski put bb, tel. 013/821-345, 821-027, 821-129
BEOGRAD, Prote Mateje 70, tel. 011/344-26-63, faks: 344-17-87
E-pošta: info@hemofarm.com

IZDAVANJE ČASOPISA POMOGLA JE:

INŽENJERSKA KOMORA SRBIJE
Bulevar vojvode Mišića 37
11000 Beograd

SUIZDAVAČI

Tehnološko-metalurški fakultet
Univerziteta u Beogradu, Beograd

Prirodno-matematički fakultet Univerziteta
u Novom Sadu, Novi Sad

Hemijski fakutet
Univerziteta u Beogradu
Beograd

ITNMS
Institut za tehnologiju nuklearnih i drugih
mineralnih sirovina, Beograd

HIP PETROHEMIJA
HIP Petrohemija a.d. Pančevo

Tehnološki fakultet Univerziteta
u Novom Sadu, Novi Sad

NU Institut za hemiju,
tehnologiju i metalurgiju
Univerziteta u Beogradu,
Beograd

nevena
„Nevena Color“ d.o.o.
Leskovac

Tehnološki fakultet Univerziteta
u Nišu, Leskovac

dcp-hemigal
DCP Hemigal, Leskovac

Chemical Industry
Химическая промышленность

Hemijska industrija

Časopis Saveza hemijskih inženjera Srbije
Journal of the Association of Chemical Engineers of Serbia
Журнал Союза химических инженеров Сербии

VOL. 68 **Beograd, novembar–decembar 2014** **Broj 6**

Izdavač
Savez hemijskih inženjera Srbije
Beograd, Kneza Miloša 9/I

Glavni urednik
Branko Bugarski

Zamenica glavnog i odgovornog urednika
Nevenka Bošković-Vragolović

Urednici
Katarina Jeremić, Ivana Banković-Ilić, Maja Obradović, Dušan Mijin

Članovi uredništva
Milorad Cakić, Željko Čupić, Željko Grbavčić, Katarina Jeremić, Miodrag Lazić, Slobodan Petrović, Milovan Purenović, Aleksandar Spasić, Dragoslav Stoiljković, Radmila Šećerov-Sokolović, Slobodan Šerbanović, Nikola Nikačević, Svetomir Milojević

Članovi uredništva iz inostranstva
Dragomir Bukur (SAD), Jiri Hanika (Češka Republika), Valerij Meshalkin (Rusija), Ljubiša Radović (SAD), Constantinos Vayenas (Grčka)

Likovno-grafičko rešenje naslovne strane
Milan Jovanović

Redakcija
11000 Beograd, Kneza Miloša 9/I
Tel/fax: 011/3240-018
E-pošta: shi@yubc.net
www.ache.org.rs

Izlazi dvomesečno, rukopisi se ne vraćaju

Za izdavača
Tatijana Dudukoviċ

Sekretar redakcije
Slavica Desnica

Izdavanje časopisa pomaže
Republika Srbija, Ministarstvo prosvete, nauke i tehnološkog razvoja

Uplata pretplate i oglasnog prostora vrši se na tekući račun Saveza hemijskih inženjera Srbije, Beograd, broj 205-2172-71, Komercijalna banka a.d., Beograd

Kompjuterska priprema
Vladimir Panić

Štampa
Razvojno-istraživački centar grafičkog inženjerstva, Tehnološko-metalurški fakultet, Univerzitet u Beogradu, Karnegijeva 4, 11000 Beograd

Indeksiranje
Radovi koji se publikuju u časopisu *Hemijska Industrija* ideksiraju se preko *Thompson Reuters Scietific®* servisa *Science Citation Index - Expanded™* i *Journal Citation Report (JCR)*, kao i domaćeg *SCIndeks* servisa Centra za evaluaciju u obrazovanju i nauci

SADRŽAJ

SADRŽAJ Nastavak

CONTENTS

Polymers

CONTENTS Continued

The preparation and thermal properties of chitosan/bentonite composite beads

Vesna Teofilović[1], Jelena Pavličević[1], Oskar Bera[1], Mirjana Jovičić[1], Jaroslava Budinski-Simendić[1], Katalin Mészáros Szécsényi[2], Ayse Aroguz[3]

[1]*University of Novi Sad, Faculty of Technology, Novi Sad, Serbia*
[2]*University of Novi Sad, Faculty of Sciences, Novi Sad, Serbia*
[3]*Istanbul University, Engineering Faculty, Istanbul, Turkey*

Abstract

The biopolymer composites are often used as remarkable adsorbents in treatment of wastewater due to their biodegradable and nontoxic nature. The chitosan/bentonite composite beads, in this study, were obtained by addition of clay into the polymer using solution process. The bentonite was modified with surfactant cetyltrimethyl ammonium bromide (CTAB) before the composite preparation. The morphology of beads was examined by scanning electron microscopy (SEM). Thermal properties of the composite beads were studied by simultaneous thermogravimetry coupled with differential scanning calorimetry (SDT) and differential scanning calorimetry (DSC). TG results showed that the complex decomposition mechanism of the composites depends on the preparation procedure. It was observed that the concentration of NaOH used for composites precipitation affects the final structure of beads. The influence of preparation procedure on the glass transition temperature *T*g of chitosan/bentonite samples was not found (*T*g values for all samples were about 144 °C).

Keywords: chitosan/bentonite composite beads, thermal decomposition, DSC.

Available online at the Journal website: http://www.ache.org.rs/HI/

Polymers

SCIENTIFIC PAPER

UDC 678.577.11:543.456:54

Hem. Ind. **68** (6) 653–659 (2014)

doi: 10.2298/HEMIND130905088T

The water pollution is a result of nearly all aspects of human activities: domestic, industrial and agricultural [1]. One of the biggest producers of wastewater is the dyeing industry. The wastewater is characterized by high organic pollutant content, deep color and significant impact on water quality. Color is wastewater contaminant that can be easily noticed, because even a very small amount of dyes in water is highly visible [2]. Disposing of the colored wastewater has caused a great interest for the human health and sea life [3,4]. Dyes are very inert, therefore it is hard to remove them from wastewaters. Second obstacle for the removal of dyes is the low saturation of wastewater with dye particles. Due to high costs of removal of very small amounts of pollutants from wastewater, the application of conventional processes of dye removal at a large scale is very expensive [3]. Currently, many adsorption methods using chitosan composites are being developed to adsorb dyes as a substitute for conventional wastewater treatment methods [5].

Chitosan is a partially deacetylated polysaccharide, produced from chitin, the world second most important natural polymer [6–8]. The most important resources for production of chitin are two sea arthropods: shrimps and crabs. Chitosan has different characteristics than any other biopolymer, particularly because of the presence of primary amino groups. It is classified as a natural polymer consisting of randomly distributed α-(1,4)-glucosamine and *N*-acetyl-D-glucosamine units (Fig. 1a). Due to the variety of its functional properties it can be used for synthesis of composite materials with other polymers [9]. Amino and hydroxyl groups in the structure of chitosan can serve as the active sites for removal of heavy metals and dyes [10]. If amino groups of chitosan are cationized, they strongly adsorb anionic dyes by electrostatic attraction in the acidic media [11]. However, depending on the pH values, chitosan can either form gel or can be dissolved, because it is very sensitive to pH [12]. Cross-linking reagents such as glyoxal, formaldehyde, glutaraldehyde, epichlorohydrin, ethylene glycon diglycidyl ether and isocyanates have been used to improve chitosan's performance as an adsorbent [13].

One of the many forms of chitosan for the dye removal by adsorption is its gel-bead form. It is used for adsorption in batch or fixed-bed column systems, deposited on an adequate substrate [14–16]. Chitosan is non-toxic, non-corrosive and safe to handle [17,18], which make it feasible in wastewater treatment. The main reasons for the success of chitosan is that it can bind dyes in low concentrations compared to metal salts and is also efficient in cold water. It does not leave residual metals that can cause secondary contam-

Correspondence: V. Teofilović, Research assistant, University of Novi Sad, Faculty of Technology, Boulevard cara Lazara 1, Novi Sad, Serbia.
E-mail: vesnavele@gmail.com
Paper received: 3 September, 2013
Paper accepted: 6 December, 2013

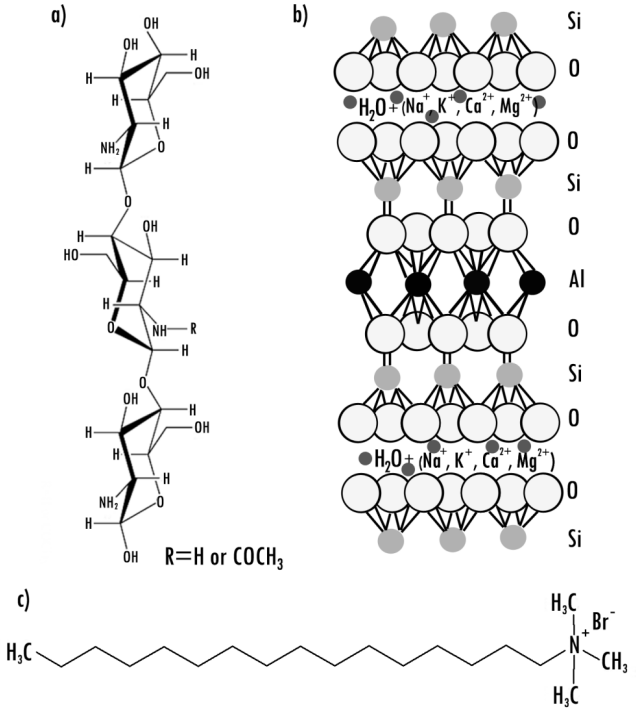

Figure 1. a) Chemical structure of chitosan, b) schematic illustration of layered structure of bentonite and c) chemical structure of CTAB.

ination problems. The low concentrations of chitosan reduce the volume of produced sludge compared for example to alum. Chitosan considerably increases the density of the sludge and facilitates its drying compared to the sludge produced with metal salts. In addition, chitosan is biodegradable, so the sludge can be efficiently degraded by micro-organisms.

Bentonite is a 2:1 type aluminosilicate, its unit layer consists of one Al^{3+} octahedral sheet between two Si^{4+} sheets [19]. Because of its large surface area and surface energy, the bentonite exhibits strong adsorption capability. However, negatively charged surface and large amount of exchangeable positive ions make natural bentonite highly hydrophilic and its surface is covered with a layer of water, blocking thus in part its adsorption capability for organic pollutants. By exchanging the occupation of sites on the bentonite surface by organic cations (such as cationic surfactants, quaternary ammonium surfactants), the surface properties can be changed from hydrophilic to hydrophobic. Therefore, bentonite should be modified before use as adsorbent for removal of pollutants from wastewater [1,20–22].

This paper is focused on the synthesis of chitosan/ /bentonite composite beads for colored wastewater treatment. The influence of the preparation procedure of composite beads on the morphology and thermal behavior of biopolymer composites was studied.

EXPERIMENTAL

Materials

Chitosan (Fig. 1a) of degree of deacetylation >85% was purchased from Aldrich. Bentonite (Fig. 1b) used in this study was obtained from the MTA, Ankara, Turkey. The clay cation exchange capacity (*CEC*) was 95 meq per 100 g of the clay. This value was estimated directly by exchanging sodium with an ethylenediamine complex of Cu(II) [23]. Cetyltrimethyl ammonium bromide (CTAB) (Fig. 1c), NaOH and acetic acid were of analytical grade and obtained from HIMEDIA.

Sample preparation

Bentonite was firstly dried at 110 °C for 2 h and sieved through 200 μm sieve. The dry bentonite was modified in the following way: 1 g of bentonite was suspended in 100 ml of distilled water at room temperature. CTAB, as a quaternary ammonium surfactant interacts with bentonite by exchanging its sodium ions with quaternary ion. Therefore, CTAB was dissolved in hot water (1 wt. %), slowly poured into the bentonite suspension and stirred for 24 h at ambient temperature. The modified bentonite (mass of 0.5 g) was filtered off, washed three times with deionized water and dried under vacuum. The final product was crushed into powder and sieved again. In order to obtain 2 wt.% of chitosan solution, chitosan was suspended in water at 120 °C for 25 min and then dissolved by addition of acetic acid in a sterile medium. The homogeneous

solution was obtained after stirring for 48 h. Four different chitosan/bentonite composite beads (table 1) were prepared using the following procedure: modified clay was swelled by 50 ml of deionized water, added to 50 ml chitosan solution and stirred at 60 °C overnight. Chitosan shows the polycationic nature in acidic media, and hence, it is suitable for intercalation in bentonite by means of cationic exchange processes, due to the Coulombic interactions between NH_3^+ groups of chitosan and the negative sites in the bentonite structure [24]. The chitosan droplets formed a bead shape in the solution of NaOH used for precipitation and remained there for 12 h. The filtered chitosan/clay beads were washed by deionized water and stored in the same water. The mean diameter of the beads was 2.5–3.0 mm.

Scanning electron microscopy (SEM)

The structure of obtained chitosan/bentonite composites was studied using scanning electron microscope JEOL JSM-6460 at magnifications from 10^3 to 2×10^6 at 15 kV.

Thermogravimetry coupled with differential scanning calorimetry (TG–DSC analysis)

The thermal decomposition of chitosan/bentonite beads was followed by means of simultaneous TG/DSC using TA Instruments SDT Q600 setup. The measurements were performed employing open alumina crucible and a corresponding empty referent crucible. All experiments were done in the temperature range from ambient temperature to 350 °C in flowing air atmosphere (100 cm^3/min) with a heating rate of 20 °C/min. After precipitation, all beads were cut to obtain sample mass about 2.5 mg.

Differential scanning calorimetry (DSC)

The enthalpy changes and glass transition temperatures were measured by differential scanning calorimeter DSC Q20, TA Instruments. The instrument was calibrated using an indium standard. After precipitation, all beads were cut to obtain sample mass about 2.5 mg. All measurements were performed under the nitrogen atmosphere, at the purge gas flow rate of 50 cm^3/min. The experiments were done from 30 to 225 °C, with a heating rate of 10 °C/min.

RESULTS AND DISCUSSION

Figure 2 shows the morphology of three different chitosan/bentonite composite beads. From SEM images it can be seen that beads formed at high NaOH concentration have more irregular spherical shape (sample D), so we may conclude that surface changes of chitosan/bentonite composite beads depend on preparation method and conditions.

Figure 3a presents TG curves of prepared chitosan/bentonite beads. TG/DTG/DSC curves of sample A are presented in Fig. 3b. As the samples were kept under water, the first mass losses up to around 220 °C most probably belong to evaporation of water molecules [25] bonded at different binding sites. The mass loss to 215 °C in all four samples is 13.0±0.5% meaning that the water adsorptivity of the samples is about the same, regardless to the preparation mode. In samples prepared at lower NaOH concentration the mechanism of water evaporation strongly depends on the bentonite content (Fig. 4a), while in samples prepared at higher NaOH concentration is practically independent of composition (Fig. 4b). The water evaporation and the decomposition of the matrix are not separable, but

Table 1. The code and description of obtained chitosan/bentonite beads (sample name, the volume of chitosan/bentonite solution, the weight content of chitosan/bentonite composites powder, the volume of NaOH solution and the molarity of NaOH solution)

Sample code	Chitosan/clay solution, ml	Chitosan/clay powder, wt.%	NaOH, ml	NaOH, mol/dm^3
A	5	4	10	1
B	3	6	10	1
C	2	5	10	5
D	3	6	10	5

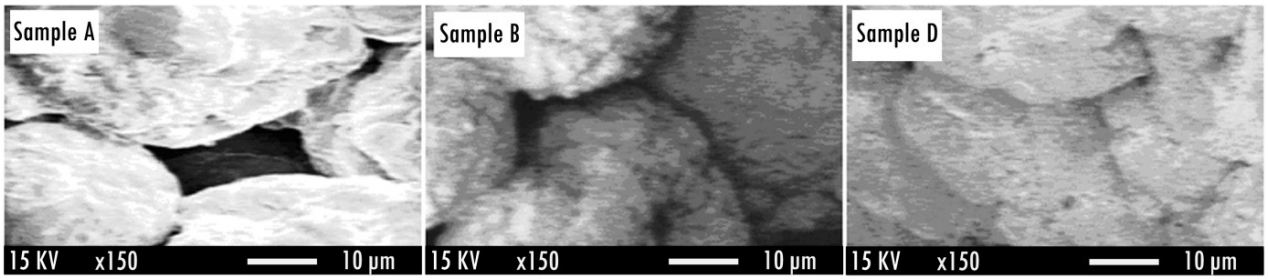

Figure 2. SEM Micrographs of samples A, B and D.

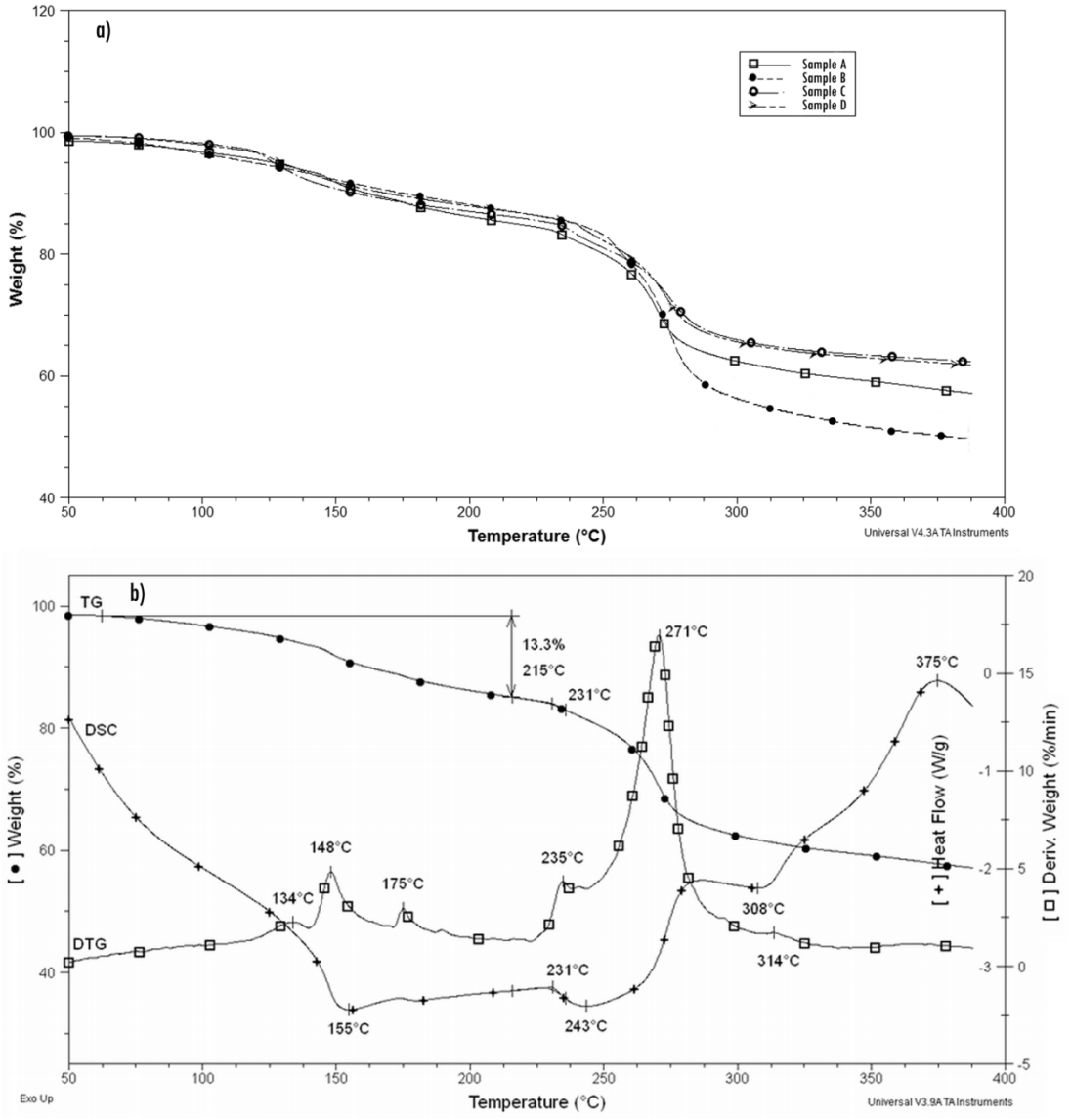

Figure 3. a) TG Curves of prepared chitosan/bentonite beads and b) TG/DTG/DSC curves for sample A.

the decomposition of the matrix probably starts around 230 °C (Fig. 3a).

The processes are endothermic up to ~250 °C (Fig. 3b). Above 250 °C, the decomposition in air is highly exothermic for samples prepared at lower NaOH concentration. The exothermic effects accompanying the decomposition are significantly lower for composites prepared at higher NaOH concentration, in agreement with their more compact structure which prevents the good contact of the beads with air.

As the processes in the whole temperature range are accompanied with mass loss, there is no possibility to determine physical changes in the matrix. However, curves recorded using DSC equipment may be used for a qualitative estimation of the water binding energies (Fig. 5). The glass transition temperature for all chitosan/bentonite samples was estimated at 144 °C, and it was found to be independent from the preparation procedure. A significantly higher enthalpy change (393.6 J/g) for water evaporation was found for the sample (A), with highest chitosan/clay powder content prepared at lower NaOH concentration. Taking into account the shapes of DTG and DSC curves, as well as the enthalpy values of water removal, it can be concluded that the method of preparation of chitosan/ /bentonite beads significantly affects their morphology, as well as the interaction of the boundary layer of the solid phase with water. Furthermore, the experimental work is necessary to prove if this observation could be used as a basis for dye removal by chitosan/bentonite composites.

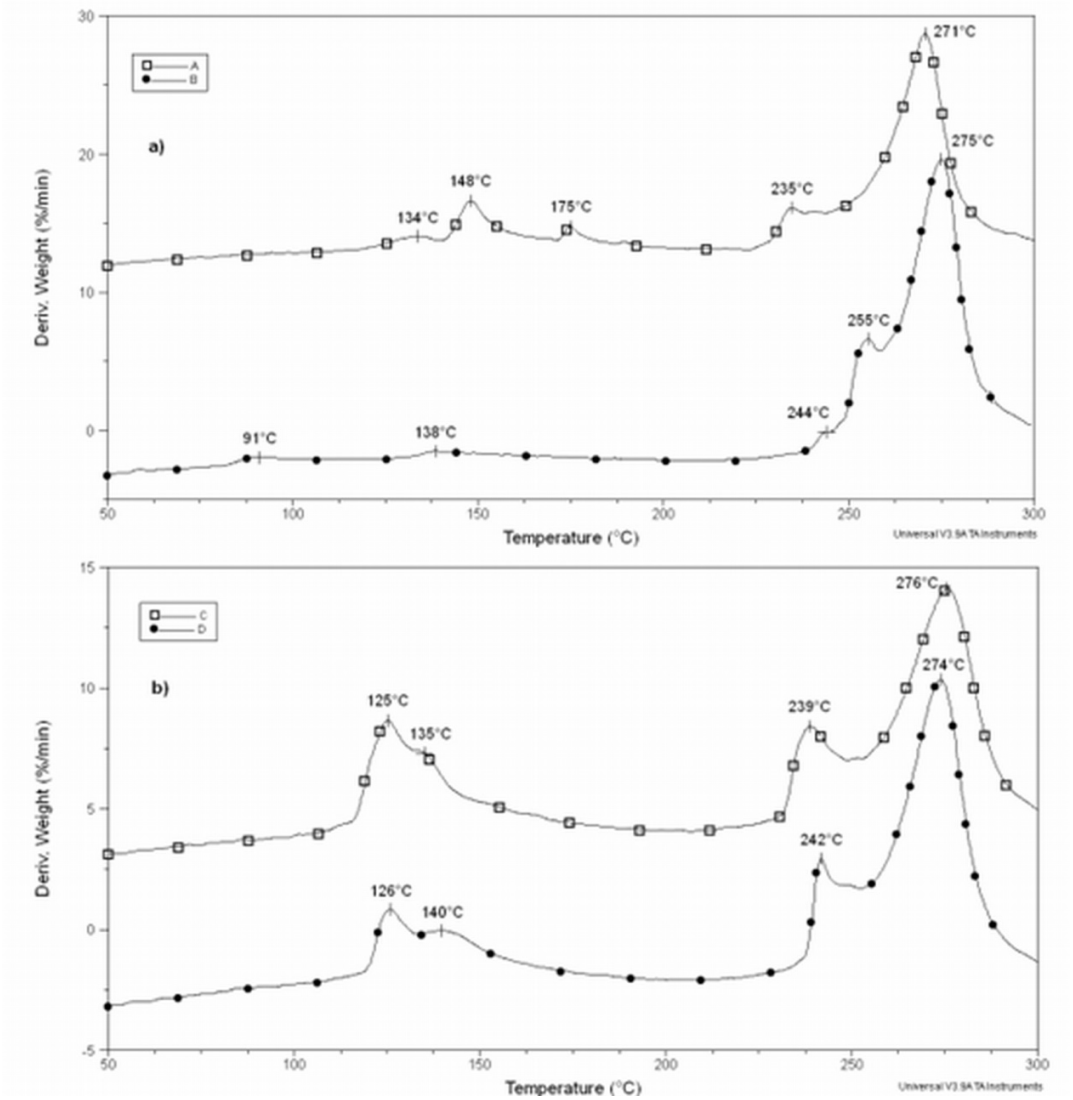

Figure 4. a) DTG Curves of samples prepared at lower (a) and at higher (b)NaOH concentration.

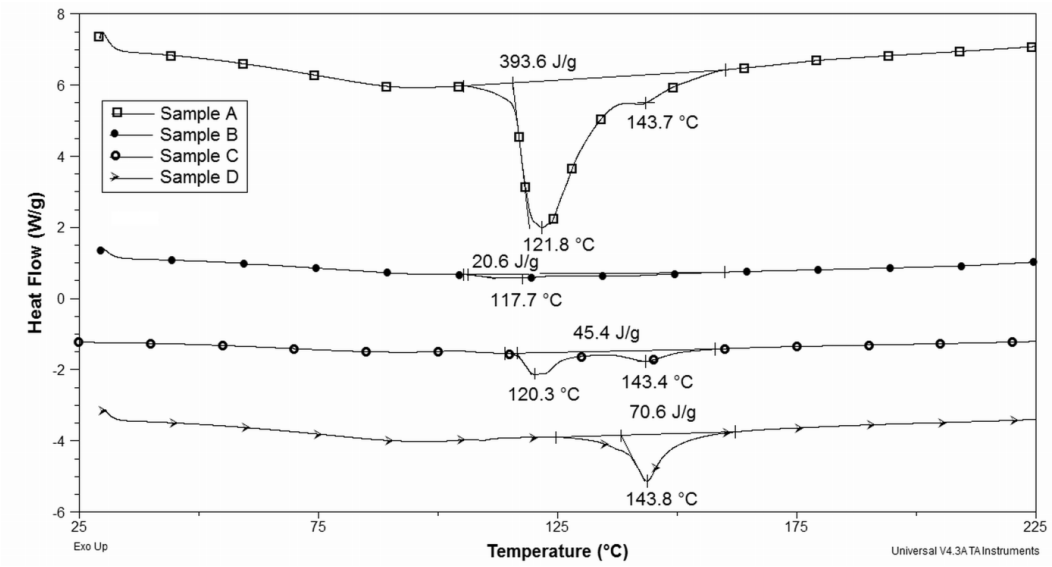

Figure 5. DSC Thermograms of chitosan/bentonite beads.

CONCLUSIONS

This paper was aimed to optimize the preparation procedure of biopolymer/clay composite beads based on chitosan and bentonite intended for wastewater purification. It was found that the preparation procedure affects the morphology and the thermal behaviour of the composites: beads formed at higher basicity of the solution have more irregular spherical shape. The results of thermal measurements refer to the dependence of water adsorption capability on the morphology of the composites. The highest water binding energy belongs to the composite prepared with higher chitosan/bentonite ratio precipitated in solution with lower basicity. The glass transition temperature for all chitosan/bentonite beads was determined at 144 °C.

Acknowledgement

This work is financially supported by Ministry of Education, Science and Technological Development of the Republic of Serbia (III45022 and ON172014) and Provincial Secretariat of Vojvodina for Science and Technological Development (114-451-2396/2011-01).

REFERENCES

[1] F. Renault, B. Sancey, P.M. Badot, G. Crini, Chitosan for coagulation/flocculation processes – An eco-friendly approach, Eur. Polym. J. **45** (2009) 1337–1348.

[2] J. Guo, S. Chen, L. Liu, B. Li, P. Yang, L. Zhang, Y. Feng, Adsorption of dye from wastewater using chitosan–CTAB modified bentonites, J. Colloid Interf. Sci. **382** (2012) 61–66.

[3] G. Crini, P.M. Badot, Traitement et épuration des eaux industrielles polluées, PUFC Press, Besançon, 2007.

[4] W.S. Wan Ngaha, L.C. Teonga, M.A.K.M. Hanafiaha, Adsorption of dyes and heavy metal ions by chitosan composites: A review, Carbohyd. Polym. **83** (2011) 1446–1456.

[5] Y. El Mouzdahira, A. Elmchaouria, R. Mahbouba, A. Gilb, S.A. Korili, Equilibrium modeling for the adsorption of methylene blue from aqueous solutions on activated clay minerals, Desalination **250** (2010) 335–338.

[6] G.A.F. Roberts, Chitin chemistry, London, MacMillan, 1992.

[7] K. Kurita, Chitin and chitosan: functional biopolymers from marine crustaceans, Mar. Biotechnol. **8** (2006) 203–206.

[8] M. Rinaudo, Chitin and chitosan: properties and applications, Prog. Polym. Sci. **31** (2006) 603–632.

[9] Japanese Chitin and Chitosan Society, Chitin and chitosan handbook, Gihodo, Tokyo, 1995, pp. 460–483.

[10] F.-C. Wua, R.-L. Tseng, R.-S. Juang, Kinetic modeling of liquid-phase adsorption of reactive dyes and metal ions on chitosan, Water Res. **35** (2001) 613–618.

[11] M.N.V. Ravi Kumar, A review of chitin and chitosan applications, React. Funct. Polym. **46** (2000) 1–27.

[12] M.-S. Chiou, P.-Y. Ho, H.-Y. Li , Adsorption of anionic dyes in acid solutions using chemically cross-linked chitosan beads, Dyes. Pigments **60** (2004) 69–84.

[13] G. Crini, P.M. Badot, Application of chitosan, a natural aminopolysaccharide, for dye removal from aqueous solutions by adsorption processes using batch studies: a review of recent literature. Prog. Polym. Sci. **33** (2008) 399–447.

[14] M.G. Peter, Applications and environmental aspects of chitin and chitosan, J. Macromol. Sci., A **32** (1995) 629––640.

[15] G. Skjak-Braek, T. Anthonsen T, P. Standford, Chitin and chitosan, Elsevier Applied Science, New York, 1989.

[16] J. Roussy, M. Van Vooren, B.A. Dempsey, E. Guibal, Influence of chitosan characteristics on the coagulation and the flocculation of bentonite suspensions, Water Res. **39** (2005) 3247–3258.

[17] J. Bratby, Coagulation and flocculation in water and wastewater treatment, 2nd ed., IWA Publishing, 2007.

[18] B. Bolto, J. Gregory, Organic polyelectrolytes in water treatment. Water Res. **41** (2007) 2301–2324.

[19] J.M. Wei, R.L. Zhu, J.X. Zhu, F. Ge, P. Yuan, H.P. He, Simultaneous sorption of crystal violet and 2-naphthol to bentonite with different CECs, J. Hazard. Mater. **166** (2009) 195–199.

[20] Q. Li, Q.Y. Yue, H.J. Sun, Y. Su, B.Y. Gao, A comparative study on the properties, mechanisms and process designs for the adsorption of non-ionic or anionic dyes onto cationic-polymer/bentonite, J. Environ. Manage. **91** (2010) 1601-1611.

[21] Z.X. Chen, X.Y. Jin, Z. Chen, M. Megharaj, R. Naidu, Removal of methyl orange from aqueous solution using bentonite-supported nanoscale zero-valent iron, J. Colloid Interface Sci. **363** (2011) 601–607.

[22] A.A. Tayel, S.H. Moussa, W.F. El-Tras, N.M. Elguindy, K. Opwis, Antimicrobial textile treated with chitosan from Aspergillus niger mycelial waste, Int. J. Biol. Macromol. **49** (2011) 241–245.

[23] F. Bergaya, M. Vayer, CEC of clays: Measurement by adsorption of a copper ethylenediamine complex, Appl. Clay Sci. **12** (1997) 275–280.

[24] M. Darder, M. Colilla, E. Ruiz-Hitzky, Biopolymer-clay nanocomposites based on chitosan intercalated in montmorillonite. Chem. Mater. **15** (2003) 3774–3780.

[25] T. Mlčoch, J. Kučerík, Hydration and drying of various polysaccharides studied using DSC, J. Therm. Anal. Calorim. **113** (2013) 1177–1185.

IZVOD

DOBIJANJE I TOPLOTNA SVOJSTVA HITOZAN/BENTONIT KOMPOZITNIH GRANULA

Vesna Teofilović[1], Jelena Pavličević[1], Oskar Bera[1], Mirjana Jovičić[1], Jaroslava Budinski-Simendić[1], Katalin Mészáros Szécsényi[2], Ayse Aroguz[3]

[1]*Univerzitet u Novom Sadu, Tehnološki fakultet, Novi Sad, Srbija*
[2]*Univerzitet u Novom Sadu, Prirodno–matematički fakultet, Novi Sad, Srbija*
[3]*Istanbul University, Engineering Faculty, Istanbul, Turkey*

(Naučni rad)

Zbog biorazgradivosti i netoksičnosti, biopolimerni kompoziti se često koriste kao izuzetni adsorbenti u tretmanu obojenih otpadnih voda. U ovom radu, hitozan/bentonit kompozitne granule dobijene su dodatkom gline u rastvor polimera. Pre pripreme kompozita, bentonit je modifikovan cetiltrimetil-amonijum-bromidom (CTAB). Morfologija granula je ispitana pomoću skenirajuće elektronske mikroskopije (SEM). Toplotna svojstva hitozan/bentonit granula su ispitana istovremenom termogravimetrijom i diferencijalno skenirajućom kalorimetrijom (SDT) i diferencijalnom skenirajućom kalorimetrijom (DSC). Pokazano je da molarnost baze (NaOH) koja se koristi za taloženje granula utiče na konačnu strukturu kompozita. Rezultati dobijeni sa TG/DTG i odgovarajućih DSC krivi su pokazali da složeni mehanizam dekompozicije kompozita hitozan/glina zavisi od postupka pripreme uzoraka i da se sastoji od četiri koraka. Uticaj koncentracije baze na razgradnju određen je poređenjem DTG krivi uzoraka sa istim sadržajem praha hitozan/glina, ali različitim sadržajem NaOH. Utvrđeno je da temperatura prelaska u staklasto stanje ne zavisi od postupka pripreme, a za sve uzorke hitozan/bentonit granula je detektovana na oko 144 °C.

Ključne reči: Hitozan/bentonit Kompozitne granule • Termička dekompozicija • DSC

Drying of polymer powder in fluidized bed. Modelling of multizone dryer

Nickolay M. Ostrovskii

Hipol a.d., Odžaci, Serbia

Abstract

The process of drying of porous polymer powder (polypropylene) intended to remove the solvent (heptane) is analyzed. The dryer consists of two stages (apparatus) with multizone fluidized bed. The mathematical model of the process in multizone fluidized bed is proposed. The rate-limiting step, depending on diameter of polymer particles, is determined. It was found that in relatively large particles (>200 μm) the rate of drying is limited by intraparticle diffusion. A way to decrease the energy consumption in drying has been also discussed and verified in experiments.

Keywords: polymer powder drying, fluidized bed, rate limiting step, multizone dryer, mathematical model.

Available online at the Journal website: http://www.ache.org.rs/HI/

Polymers

SCIENTIFIC PAPER

UDC 676.742.3:66.047:51

Hem. Ind. **68** (6) 661–671 (2014)

doi: 10.2298/HEMIND131016007O

Many polymerization processes are carried out in suspension, which consists of liquid monomer itself (or its solution in some solvent) and of growing polymer particles. At the reactor exit, porous polymer particles should separate from the suspension. If the liquid is not ease vaporable, then first centrifugation and next drying stages are used for separation. An example of such a process is the propylene polymerization over solid Ziegler–Natta catalysts in heptane or hexane solution. After centrifugation, the polymer powder (50––500 μm) contains 15–20% of heptane in its pores.

For such a powder (as well as for corns, inorganic and pharmaceutical materials) the fluidized-bed drying is widely used. It provides a good mixing of powder, easy heat application, a relatively homogeneous temperature and a continuous process operation (Fig. 1).

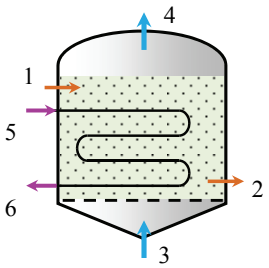

Figure 1. Schematic diagram of fluidized-bed dryer. 1, 2 – particles flow; 3, 4 – gas flow; 5, 6 – heat-transfer flow.

Most of the gas passes through the fluidized bed in the form of bubbles, which almost do not contain solids. Bubbles merge and disintegrate in the bed, and collapse at the exit of bed. Thus, the fluid provides almost ideal mixing of solids, and prevents from local overcooling and particles agglomeration.

On the other hand, bubbles diameter (3–10 cm) considerably exceeds the typical particles diameter (0.02–1 mm). This reduces the interface area (gas––particles) that becomes equal to the external surface of bubbles, and consequently, slows down the rate of mass transfer (rate of drying).

Therefore, the bubble fragmentation in fluidized bed is desirable. It is possible in so-called “organized fluidized bed” with small-volume packing, grates, or even with immersed heaters (like in Fig. 1).

The size of polymer particles varies from 20 to 550 μm. The particles size distribution, coupled with the mixing of solid phase, generates the distribution of particles residence time in a fluidized bed. That is why at the exit of bed, there is always a mixture containing particles from “almost dry” to “almost wet”. The distribution of particles moisture determines the average polymer moisture that should satisfy the requirements of polymer quality (0.1%).

The mathematical model of drying process should include all peculiarities (mentioned above) if the purpose of modelling is a detail analysis and optimization. Heat balance equations should enclose a fluid convection, an interphase heat transfer, and a mixing of solid phase. Mass balance equations (for both fluid and solid moisture) also should represent phase flow velocities, an interphase mass transfer, and a moisture transfer inside particles.

Such a model is constructed in present paper and is applied to the drying of polypropylene powder in multistage dryer with fluidized bed. For the solid phase moisture and temperature the model of “exchange interaction“ between zones is used. The rate limiting step is examined, depending on particles size and moisture. The energy efficiency is also analysed in order to decrease the heat consumption.

Correspondence: Hipol a.d., Gračački put b.b., 25250 Odžaci, Serbia Serbia.

E-mail: nikolaj.ostrovski@hipol.rs

Paper received: 16 October, 2013

Paper accepted: 7 February, 2014

Total heat balance of the process

Let us consider the structure of energy consumption in a drying process. The heat is consumed for the heating of polymer powder, heptane and nitrogen to the drying temperature, as well as for heptane evaporation:

$$\left(G_{LPS}+G_{MPS}\right)Q_W = G_S\left(Cp_S+\frac{G_H}{G_S}Cp_H\right)\left(T_S-T_S^o\right)+ \\ +F_G\,Cp_G\,\rho_G\left(T_G-T_G^o\right)+G_H\,Q_H \tag{1}$$

Specific consumption of water steam depends on input moisture of polymer powder (heptane concentration), $W_o = G_H/(G_S + G_H)$:

$$\frac{G_{LPS}+G_{MPS}}{G_S}=\frac{1}{Q_W}\left(Cp_S+\frac{W_o}{1-W_o}Cp_H\right)\left(T_S-T_S^o\right)+ \\ +\frac{F_G\,\rho_G}{G_S}\frac{Cp_G}{Q_W}\left(T_G-T_G^o\right)+\frac{W_o}{1-W_o}\frac{Q_H}{Q_W} \tag{2}$$

The Eq. (2) is illustrated in Fig. 2. It is seen that the total consumption of steam is much higher than required for heptane evaporation. It means that probably some potential opportunities exist for the saving of heat energy. For example, almost half water steam is supplied for a heating of nitrogen. Its mass flow ($F_G\rho_G$) depends on dryer capacity and optimal fluidization velocity, and therefore cannot be decreased. Meanwhile, the contribution of nitrogen in total heat balance of the process is quite low (less than 12%), because of low heat capacity (Cp_G) and low difference of temperatures ($T_G - T_S$).

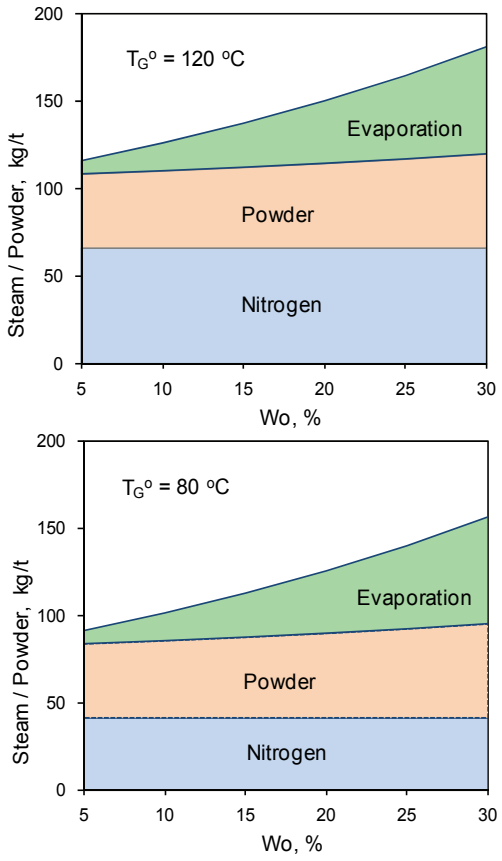

Figure 2. Specific consumption of water steam for the polymer drying as a function of input moisture of powder. (Hipol a.d., 2007).

Thus, the temperature of input nitrogen (T_G^o) can be optimized in order to decrease the energy consumption (Fig. 2). Besides, when the temperature T_G^o is decreased from 120 to 80 °C, the middle-pressure steam (MPS, 11 bar) can be replaced by low-pressure steam (LPS, 2 bar).

Nevertheless, a decreasing of T_G^o can cause some undesirable changes in drying dynamics, which is impossible to estimate on the base of only total heat balance. For this purpose, a detail modelling of dryer is necessary based on drying kinetics (Eqs. (11)–(17)), equations of mass and heat balance (Eqs. (18)–(26)), and fluidized bed hydrodynamics (Eqs. (27)–(30)).

Process in particle

For the description of heptane concentration inside particle (moisture of particle, w_r) the diffusion equation can be used [1–3]:

$$\frac{\partial w_r}{\partial t}=D_P\left(\frac{\partial^2 w_r}{\partial r^2}+\frac{s}{r}\frac{\partial w_r}{\partial r}\right) \tag{3}$$

It not represents the actual mechanism of moisture transfer in porous particles, which is the combination of diffusion, capillary and surface phenomena [3]. Nevertheless, it gives the possibility to estimate the rate of particles drying or corresponding time.

At the particle center the symmetry condition is valid:

$$r = 0:\ \mathrm{d}w_r/\mathrm{d}r = 0 \tag{4}$$

At the external particle surface, the diffusion flux from the particle is equal to the rate of mass transfer through the external laminar layer of fluid:

$$r = R_P:\ D_P\frac{S_P}{V_P}\frac{d\,w_r}{d\,r}=\frac{k_m}{\rho_P}\frac{S_P}{V_P}\left(C-C_E\right) \tag{5}$$

Defining the dimensionless radius, $\phi = r/R_P$, we obtain:

$$\phi = 1:\ \frac{\mathrm{d}w_r}{\mathrm{d}\phi}=\frac{\mathrm{Bi}}{\rho_P}\left(C-C_E\right),\ \mathrm{Bi}=\frac{k_m R_P}{D_P} \tag{6}$$

The mass transfer Biot number (Bi) indicates the ratio of external mass transfer and internal diffusion. Let's try to estimate the value of Bi. An effective dif-

fusivity in porous particle depends on its moisture $\psi(w)$, porosity (ε_P), and porous tortuosity (h):

$$D_P(w) = \psi(w) D_m \varepsilon_P / h \quad (7)$$

Molecular diffusivity in gas phase (heptane in nitrogen) consist of D_{mG}, from 7×10^{-2} to 9×10^{-2} cm^2/s, and in liquid phase D_{mL}, from 3×10^{-5} to 8×10^{-5} cm^2/s [4]. The particle porosity varies in the range 0.15–0.25 and the tortuosity, h, in range 4–6 [5].

The most complicated is ψ parameter, which represents an influence of surface tension and osmotic and capillary effects [3]. It decreases with w and vary in the interval 0.02–0.1.

The mass transfer coefficient, k_m, is usually changed within 10–100 cm/s [6]. Then, Biot number values reach 10^2–10^3 (in the case of gas phase diffusion) and 10^5–10^6 (liquid phase diffusion).

Because of Bi >> 1, the rate of external mass transfer is always higher than the rate of internal diffusion, which is therefore the rate limiting step of the process.

In the case of small particles (<1 mm), it is not necessary to calculate the moisture distribution inside particles, and it is sufficient to estimate the integral (average) moisture:

$$W = \int_0^{R_P} 3\frac{r^2}{R_P^3} w_r(r)\,dr \quad (8)$$

Because of Bi >>1, at the particle surface ($r = R_P$) we have $w_r(R_P) = W_E$. Thus, after integrating Eqs. (3) and (8) we obtain the well-known approximate solution:

$$w = \frac{W - W_E}{W_o - W_E} \approx \frac{6}{\pi^2} \exp\left(-\pi^2 \frac{D_P}{R_P^2} t\right) \quad (9)$$

The example of drying dynamics of polymer particles, according to Eq. (9), is presented in Fig. 3a. Drying time is proportional to particle diameter as square. For example, in the case of d_P = 50 μm, the moisture reducing from 16 to 1.6 %, requires the only 0.2 min. Meanwhile, for particles having diameter d_P = 350 μm, this time is increased up to 12 min.

In a fluidized bed (even with uniform particles), the non-uniform distribution of residence time $f(t)$ exists (Fig. 4), which is tended to a normal distribution with increasing of n [2]:

$$f(t) = \frac{1}{\tau_Z (n-1)!} \left(\frac{t}{\tau_Z}\right)^{n-1} \exp\left(-\frac{t}{\tau_Z}\right)$$

That is why the average moisture, $\langle w \rangle$, differs from the moisture estimated by Eq. (9). For the bed having only one stage, the Eq. (10) can be used for $\langle w \rangle$ calculation (Fig. 3b):

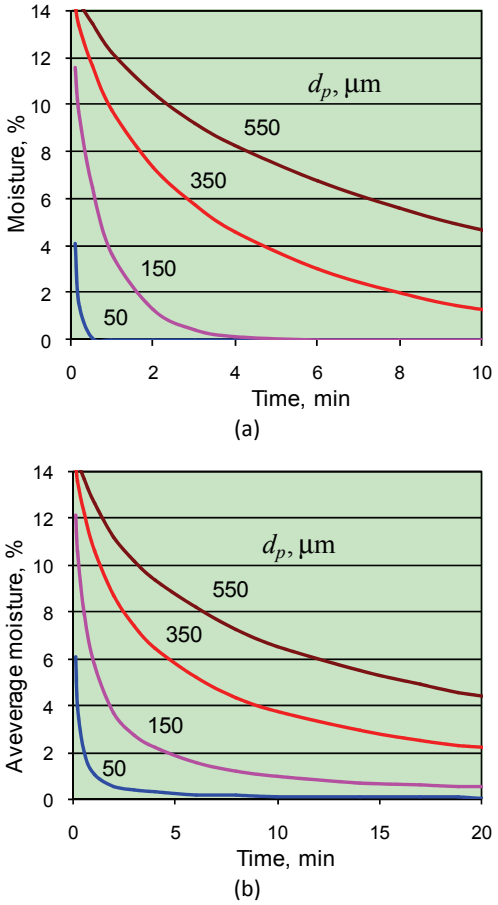

Figure 3.a) Particle drying dynamics in accordance with Eq. (9) and b) particle drying dynamics in fluidized bed in accordance with Eq. (10); W_O = 16%, W_E = 0.1%; $D_P = 1\cdot10^{-7}$ cm^2/s.

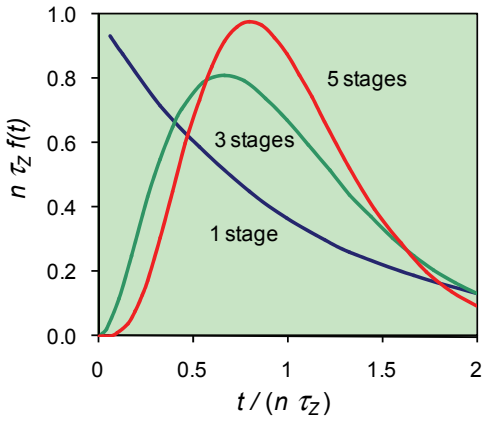

Figure 4. Distribution function of particles residence time in multi-stage (n) fluidized bed.

$$\langle w \rangle = \frac{1}{\tau_Z} \int_0^{\infty} \exp(-t/\tau_Z)\, w(t)\, dt \approx \approx \frac{6}{\pi^2} \left(1 + \pi^2 \frac{D_P}{R_P^2} \tau_Z\right)^{-1} \quad (10)$$

From the comparison of Fig. 3a and b, it is seen that the drying time in fluidized bed (under particles mixing) is two times longer than without mixing. Such an influence of residence time distribution should be taken into account during analysis of fluidized bed dryer.

Mass transfer in fluidized bed

Another peculiarity of fluidized bed is the influence of external mass transfer. The rate of gas-solid mass transfer in fluidized bed is lower than in the case of single freely settling particle. The reason is a bubbling regime of gas flow (about 90 %) passing through the suspension phase (Fig. 5). In this case the bubbles external surface determines the rate of mass transfer.

In any *j*-th zone of the bed (having volume V_j) the rate of mass transfer is given by

$$R_m = \beta_T V_j \frac{\rho_F}{\varepsilon_F}\left(W_j - W_E\right),\ W_E = H\,C_E \qquad (11)$$

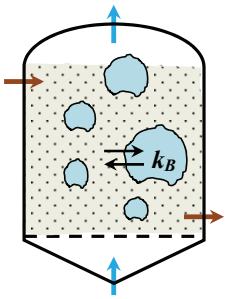

Figure 5. Interphase mass transfer in fluidized bed.

The value of total coefficient, β_T, depends on local coefficients:

1) β_P – inside particle to its surface, S_P:

$$\beta_P = k_P(S_P/V_P)(1-\varepsilon_F) = k_P(6/d_P)(1-\varepsilon_F) \qquad (12)$$

2) β_B – into bubble through its surface, S_B:

$$\beta_B = k_B(S_B/V_B)\varepsilon_F = k_B(6/d_B)\varepsilon_F \qquad (13)$$

Here $(S_B/V_B)\varepsilon_F = a_B$ and $(S_P/V_P)(1-\varepsilon_F) = a_P$ are specific areas of bubbles and particles in the unit of bed volume (cm^2_i/cm^3_{bed}). So, the coefficients β_P, β_B, and also β_T, have the same unit ($cm^3_{gas}/(cm^3_{bed}$ s)). Because of successive steps (12) and (13), their rates are equal each other in quasi-steady state and equals to R_m. Then, the total coefficient, β_T, is defined by formula:

$$\frac{1}{\beta_T} = \frac{1}{\beta_P} + \frac{1}{\beta_B} \qquad (14)$$

The local transfer coefficient in bubble (k_B, $cm^3_{gas}/(cm^2_{bubble}$ s)) depends on hydrodynamic regime in fluidized bed, namely on bubble diameter (d_B) and on its velocity (u_B), which is indirectly dependent on particles diameter (d_P) [2]:

$$k_B = \left(\frac{d_B^{5/4}}{a + b d_B^{1/4}} + \frac{d_B^{3/2}}{c u_B^{1/2}}\right)^{-1} \qquad (15)$$

a, *b* and *c* are empirical parameters.

The local transfer coefficient in particle (k_P, $cm^3_{gas}/(cm^2_{particle}$ s)) approximates the diffusion flux inside particle, similarly to first member of Eq. (5):

$$k_P a_P \left(W - W_E\right) \approx \varepsilon_P \frac{D_P}{R_P}\frac{\rho_L}{\rho_G} a_P \frac{\mathrm{d}W}{\mathrm{d}\phi} \qquad (16)$$

Then k_P can be defined by formula:

$$k_P = \frac{2 D_P \varepsilon_P}{d_P\,\Delta\phi}\frac{\rho_L}{\rho_G},\ \Delta\phi = 1 - \delta_o\left(W/W_o\right)^{1/3} \qquad (17)$$

The parameter $\Delta\phi$ is a formal dimensionless depth of a dry zone in particle, through which the moisture is diffused. It is increased from $1-\delta_o$ at the beginning, when $W = W_O$, to ~1 at the end of the process, when $W \approx W_E$. Thus, the coefficient k_P (or D_P) is decreased in drying process, which is typical for capillary-porous materials [3].

Anticipated values of parameters β_B and β_P are presented in Fig. 6. They were calculated using formulas (12)–(17) under conditions of drying of polypropylene powder.

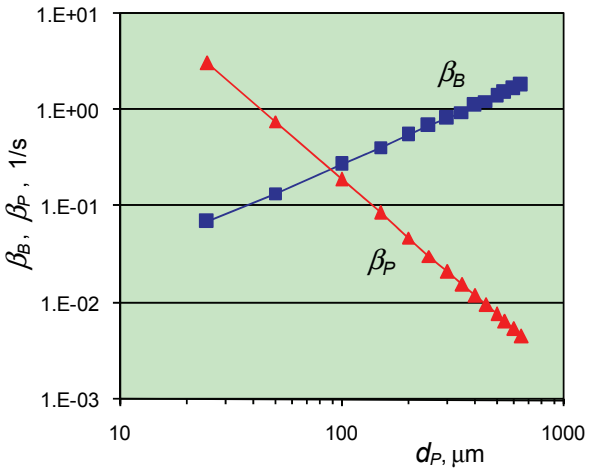

Figure 6. Dependencies of mass-transfer coefficients on particle diameter.

In contrast to mass transfer under the blowing of a single particle, there is a little difference between the intensity of external (through bubble surface) and internal (through particle surface) mass transfer here (Fig. 6).

In the case of relatively large particles (>200 μm), $\beta_P < \beta_B$, therefore the rate of process is limiting by moisture diffusion in particles, and $\beta_T \approx \beta_P$. In the case of fine particles (<50 μm), $\beta_B < \beta_P$, therefore the rate of process is limiting by mass transfer in bubbles, and

$\beta_T \approx \beta_B$. In transition region (50–200 μm), the formula (14) should be used.

In polymerization process, the polydisperse particles are usually formed, and their size distribution depends on the catalyst type (Fig. 7). That is why particles separation along the height of fluidized bed always takes place. Consequently, the distribution of particles residence time in a dryer becomes rather complicated. These are the main reasons of application of multi-stage fluidized bed dryer in industry.

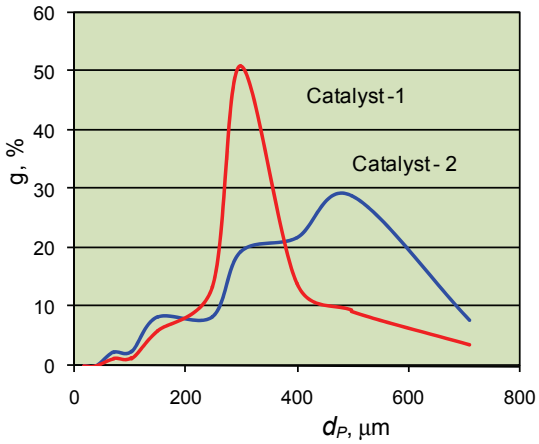

Figure 7. The distribution of polypropylene particles size depending on polymerization catalyst; initial moisture W_O (% of heptane): catalyst 1: 16–18%; catalyst 2: 17–25%.

Zones of fluidization in dryer

The simplified scheme of drying of polypropylene powder (PP) is presented in Fig. 8. Each stage of dryer is divided in two parts by vertical curtain wall. The powder is transferred from the left part to the right part under this wall. The heat is supplied in dryers by two ways: 1 – by heating of fluidized bed using water low-pressure steam (LPS, 2 bar), supplying in heat radiators; 2 – by heating of fluid (N_2) in heat exchangers using water middle-pressure steam (MPS, 11 bar).

Because of these peculiarities of dryer design (Nara Machinery, Japan), the hydrodynamic regime in process vessels is quite complicated (Fig. 9). Each fluidization vessel can be divided in three groups of zones distinguished by hydrodynamic conditions. Upper zones (1, 6 and 7, 12) are located over radiators. Middle zones (2, 5 and 8, 11) occupy the majority of a bed volume, where radiators are allocated. Lower zones (3, 4 and 9, 10) represent the space between radiators and gas distributors (perforated metal grates).

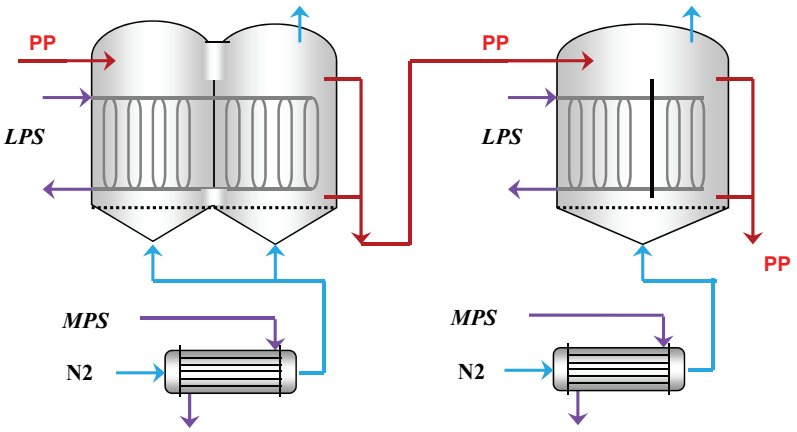

Figure 8. The principle circuit of PP drying.

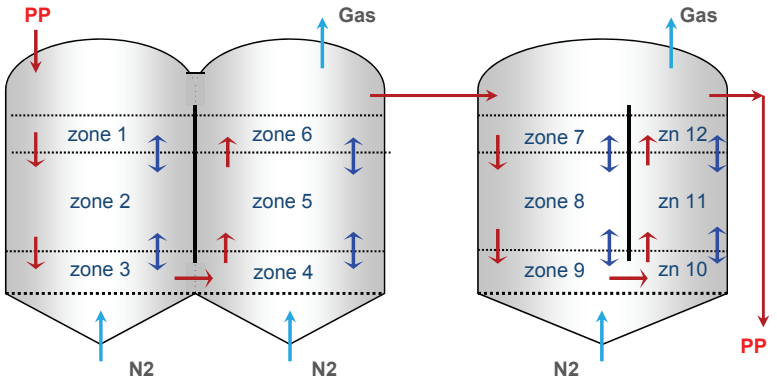

Figure 9. Solids flow scheme in dryers; ↓ – flow; ↕ – mixing.

Mathematical model of the process

Each mentioned zone we can consider to be completely mixed stage, which is typical for a fluidized bed [2,6]. For the drying process modelling, four equations are necessary in each zone. They are: moisture concentrations in gas and solid phases, as well as gas and solid temperatures. Thus, for dryer with 12 zones, this implies a model with 48 equations. Besides, heat balance equations in radiators and in heat exchangers should be formulated.

Gas phase (bubbles)

The moisture concentration in gas (C) and the gas temperature (T_G) are changed due to the gas streaming and interphase transfer:

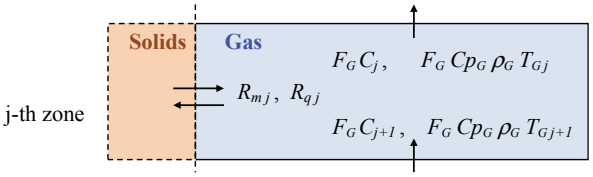

Rates of mass and heat transfer:

$$R_{mj} = \beta_T V_j \frac{\rho_F}{\varepsilon_F}\left(W_j - W_E\right),\ R_{qj} = \alpha_T V_j \left(T_{Gj} - T_{Sj}\right) \tag{18}$$

Balance equations:

$$F_G\left(C_j - C_{j+1}\right) = R_{mj}\ ,\ F_G Cp_G \rho_G \left(T_{Gj} - T_{Gj+1}\right) = R_{qj} \tag{19}$$

Dense phase (particles)

The process in a dense phase is much more complicated. Except the main flow of solids (input-output, G_S), the interstage particles transfer takes place. This transfer is the result of fluidization and is interpreted often as particles diffusion (axial dispersion). Such a flux provides an interchange of moisture and heat between zones. Thus, corresponding rate coefficients of these mass (D_S) and heat (λ_S) transfer can be defined by formula:

$$D_{Sj} = D_F \frac{F_j}{L_j}\rho_F\ \left(1-\varepsilon_F\right),\ \lambda_{Sj} = \lambda_F \frac{F_j}{L_j} \tag{20}$$

In a heat balance, a significant role plays the heating of solids by immersed radiator (R_R) and the cooling by heptane evaporation (Q_H). The rate of heating is proportional to the difference of temperature in zones 2, 5, 8 and 11, and in radiators:

$$R_{Rj} = \alpha_R V_j \left(T_{Rj} - T_{Sj}\right) \tag{21}$$

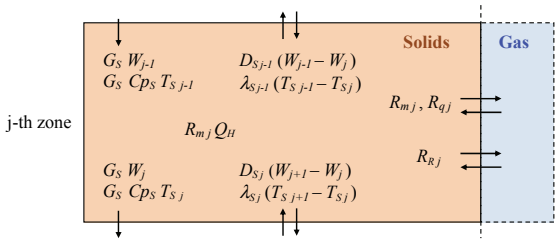

Mass and heat balance equations in a j-th zone:

$$G_S\left(W_j - W_{j-1}\right) = D_{Sj}\left(W_{j+1} - W_j\right) + \\ + D_{Sj-1}\left(W_{j-1} - W_j\right) - R_{mj} \tag{22}$$

$$Cp_S G_S\left(T_{Sj} - T_{Sj-1}\right) = \lambda_{Sj}\left(T_{Sj+1} - T_{Sj}\right) + \\ + \lambda_{Sj-1}\left(T_{Sj-1} - T_{Sj}\right) + R_{qj} + R_{Rj} + R_{mj} Q_H \tag{23}$$

Heating

Heat balance equation in a radiator:

$$G_{LPSj} Cp_{LPS}\left(T_{LPS} - T_{Rj}\right) + G_{LPSj} Q_W = R_{Rj} \tag{24}$$

Balance equation in a heat exchanger (for the heating of N_2):

$$F_G Cp_G \rho_G\left(T_G - T_G^o\right) = \\ = G_{MPS} Cp_{MPS}\left(T_{MPS} - T_G\right) + G_{MPS} Q_W \tag{25}$$

Overall heat balance in a fluidized bed:

$$Cp_S\left(G_S T_S - G_S^o T_S^o\right) + \left(G_S^o - G_S\right) Q_H = \\ = F_G Cp_G \rho_G\left(T_G^o - T_G\right) + G_{LPS} Q_W \tag{26}$$

Fluidization parameters

Most hydrodynamic characteristics of fluidized bed depend on Archimedes and Reynolds numbers:

$$\mathrm{Ar} = \frac{g d_P^3 \rho_P \rho_G}{\mu_G^2}\ ,\ \mathrm{Re}_P = \frac{u_G d_P \rho_G}{\mu_G} \tag{27}$$

Particular Reynolds numbers: current (Re_P), start of fluidization (Re_{PF}), and start of particle transport (Re_{PT}) are functions of Archimedes number. They give the possibility to calculate corresponding gas velocities [7]:

$$\mathrm{Re}_P = \frac{\mathrm{Ar}}{18 + 5.22\ \mathrm{Ar}^{0.5}},\ \mathrm{Re}_{PF} = \frac{\mathrm{Ar}}{1400 + 5.22\ \mathrm{Ar}^{0.5}}, \\ \mathrm{Re}_{PT} = \frac{\mathrm{Ar}}{18 + 0.61\ \mathrm{Ar}^{0.5}} \tag{28}$$

For the calculation of heat transfer coefficients (h_q, h_R) the Nusselt number is used [7]:

$$\mathrm{Nu}_q = \frac{h_q d_P}{\lambda_G} = 0.4\left(\frac{\mathrm{Re}}{\varepsilon_F}\right)^{2/3} \mathrm{Pr}^{1/3},$$

$$\mathrm{Nu}_R = \frac{h_R d_P}{\lambda_G} = 0.75\left(1 - \frac{d_c}{L_c}\right)^{0.14} \mathrm{Ar}^{0.22} \qquad (29)$$

In a fluidized bed hydrodynamics a bed porosity (ε_F), particles „diffusivity“ (D_F), and an effective heat conductivity of the bed (λ_F) are also very important [2]:

$$\varepsilon_F = \left(\frac{18\mathrm{Re} + 0.36\mathrm{Re}^2}{\mathrm{Ar}}\right)^{0.21}, \quad D_F = \frac{\alpha^2 d_B}{3\delta}\frac{\varepsilon_F}{u_F}\left(u_G - u_F\right)^2,$$

$$\lambda_F = D_F C p_S \rho_F \qquad (30)$$

Here α and δ are empirical functions of bubbles diameter.

The model should also include well-known equations for heat transfer coefficient in heat exchangers; for physical properties of nitrogen, heptane, water steam and polymer powder; for pressure drop in fluidized bed, etc. [4,6].

Modelling of drying process

First, the modelling of standard drying regime has been done (Fig. 10). It provides a drying of PP powder (3.8–4.1 t/h) from initial moisture of 15–18% to final moisture less than 0.1%. The temperature in 1st and 5th zone, and powder moisture at the exit of dryers are in a good agreement with experimental data (Fig. 10). From this simulation of drying process the following parameters were estimated: D_P , from 2.5×10^{-7} to 3.0×10^{-7} cm^2/s; D_F, 80–120 cm^2/s; d_B, 5–7 cm. The rest of parameters were calculated using the above formulas.

The bubbles diameter (d_B) is determined by distance between tubes of immersed steam radiator [8,9]. The axial dispersion of particles (D_F), calculated by (30), is also corresponded to latter estimations [10]. Finely, the effective intra-particle diffusivity (D_P) lies in the interval of values predicted by formula (7) at D_{mL} = 6.6×10^{-5} cm^2/s, ε_P = 0.2, h = 5, and ψ = 0.1.

Using these parameters, two regimes of drying process were simulated: 1st – at the N_2 inlet temperature T_G^o = 120 °C, and 2nd – at T_G^o = 80 °C. The results are presented in Fig. 11.

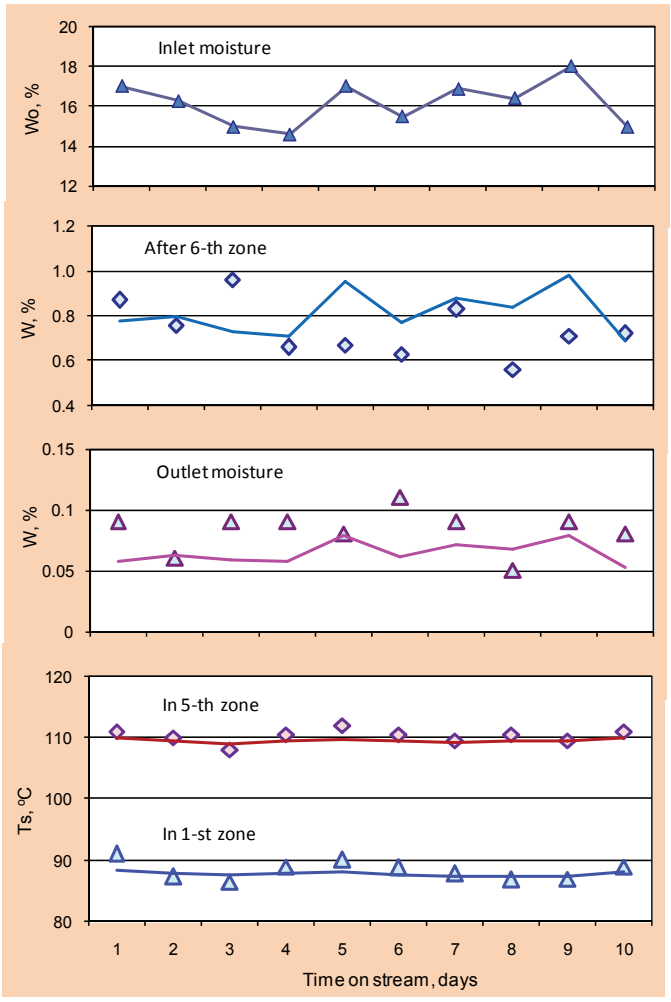

Figure 10. Results of standard regime modelling. G_S = 3.8-4.1 t/h, T_G^o = 120 °C. Points – experimental data; Lines – calculated values.

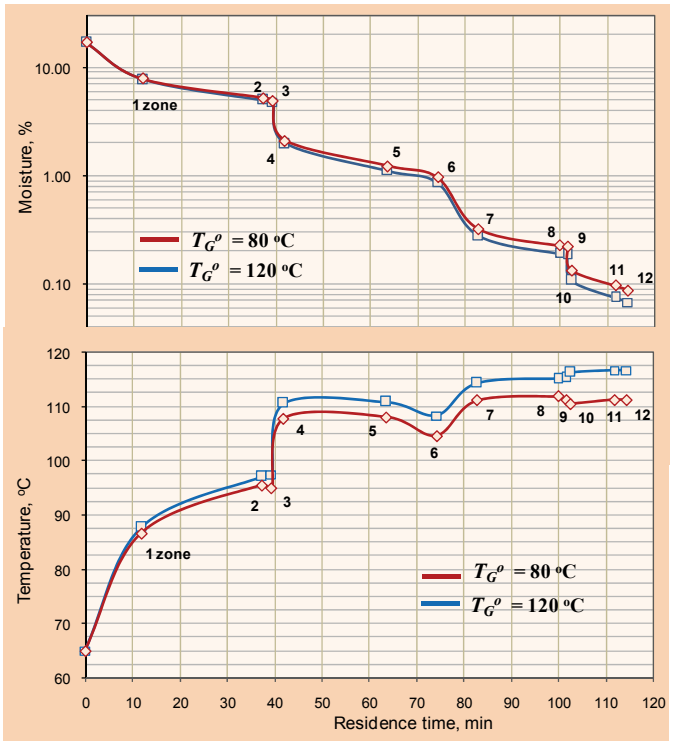

Figure 11. Results of dryer modeling: the influence of T_G^o. G_S = 3.94 t/h. Numbers indicate a zone number.

It is seen from Fig. 11 that supposed decrease in energy consumption, which has been made in Section „Total heat balance of the process“ and Fig. 2, is quite possible. The decreasing of T_G^o only slightly increases the outlet powder moisture, which remains lower than 0.1%.

Nitrogen mass flows, as well as flow rates of low-pressure steam (LPS) and middle-pressure steam (MPS) for these two regimes, are presented in Figs. 12 and 13. It is seen, that the decreasing of MPS by 130 kg/h increases the consumption of LPS by 110 kg/h without remarkable changing in zone temperature, and without loss of drying quality. It happens because the gas moisture (heptane content in N_2) affects the rate of drying much stronger than the gas temperature.

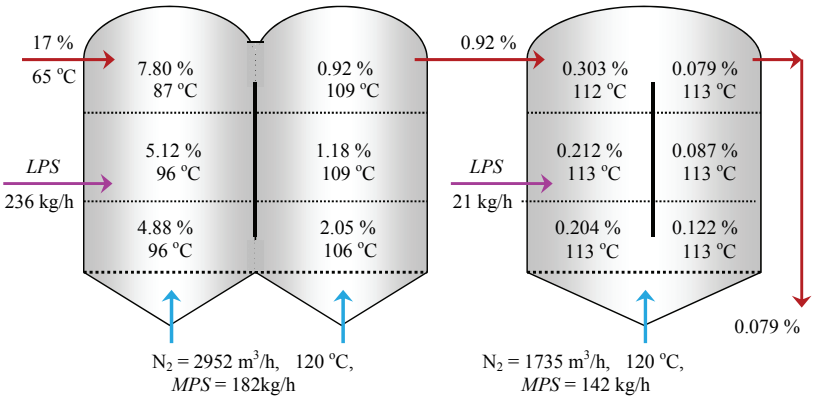

Figure 12. Results of standard regime modelling. G_S = 3.94 t/h of dry powder. T_G^o = 120 °C. Numbers – powder moisture and temperature in zones.

For the experimental verification of these regimes (and for the model validation), the trial run of dryer was carried out, and the results are presented in Fig. 14. The nitrogen inlet temperature T_G^o has been varied from 120 to 95 °C, and the inlet moisture of polymer – from 15 to 25%. It is clearly seen from Fig. 14 that the average outlet moisture is in acceptable correlation with the average inlet moisture at all nitrogen temperatures. The best illustration for the possibility of T_G^o decreasing is an operation at 95 and 120 °C at approximately the same inlet moisture of 22% (see interval from 95th to 170th days). Both cases (95 and 120 °C)

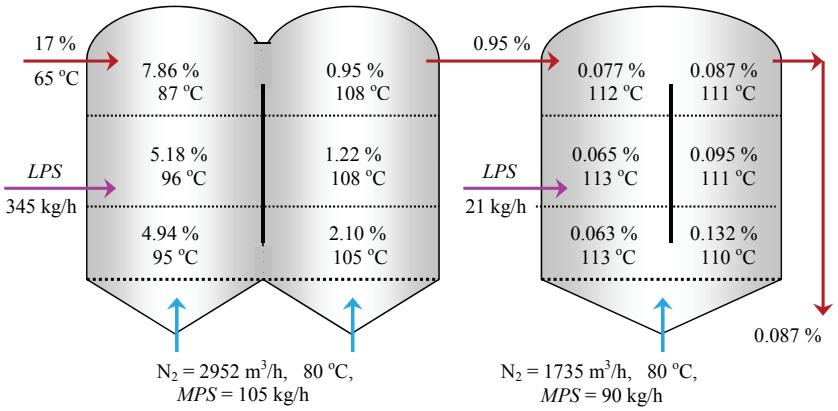

Figure 13. Results of modified regime modelling. G_S = 3.94 t/h of dry powder. T_G^o = 80 °C. Numbers – powder moisture and temperature in zones.

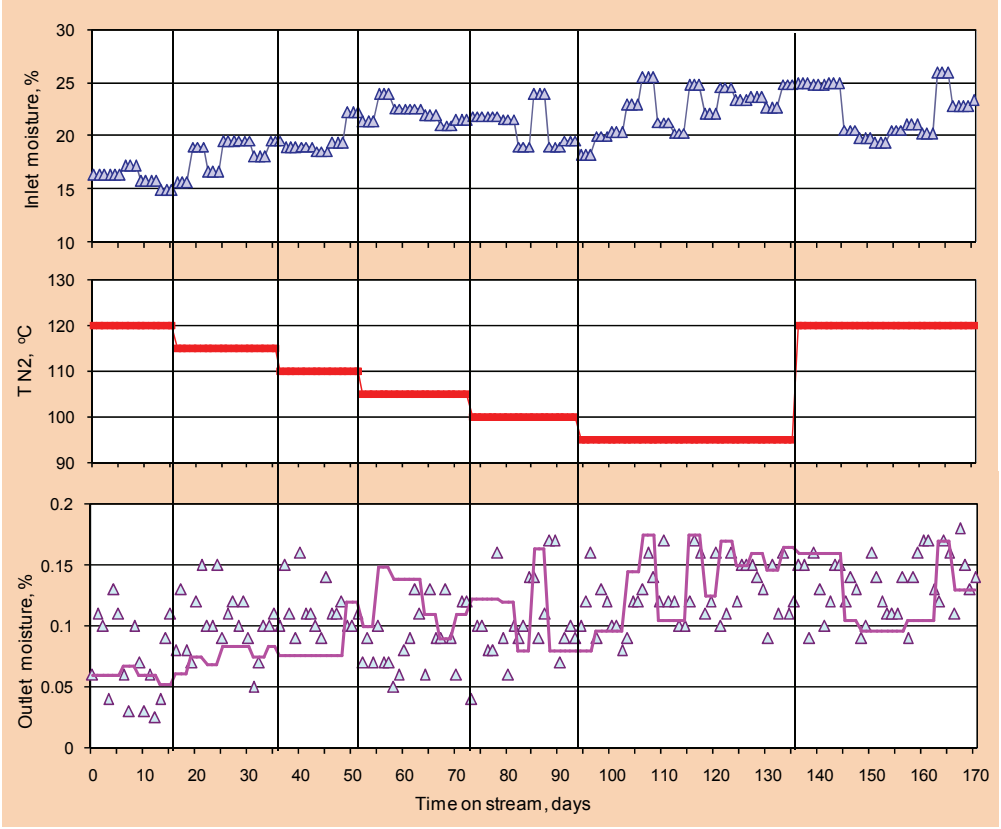

Figure 14. Trial run of dryer. G_S = 3.9–4.0 t/h of dry powder. T_G^o = 95-120 °C. Points – experimental values. Lines – calculated outlet moisture.

provide almost the same average outlet moisture of 0.12–0.13%.

These experiments open up the possibility to replace the middle-pressure steam (MPS) by low-pressure steam (LPS) for the heating of nitrogen.

CONCLUSIONS

The simulation based on the Multizone Model showed good agreement with experimental data. It was demonstrated that proposed model could also predict hydrodynamic and thermal behavior of multizone fluidized bed dryer with immersed heating tubes.

The model consists of plausible values of mass and heat transfer parameters.

The application of presented model is proved to be fruitful in optimization of dryer operation and of energy consumption.

Nomenclature

a_B, a_P specific area of bubble and particle [cm^2/cm^3 or m^2/m^3]

a_R specific area of radiator [m^2/m^3]
C, C_E current and equilibrium moisture content in gas [g/cm^3 or kg/m^3]
Cp_G, Cp_L, Cp_S heat capacity of gas, liquid and solid [J/(g K) or kJ/(kg K)]
Cp_{LPS}, Cp_{MPS} heat capacity of water steam [kJ/kg K]
d_B, d_P bubbles and particles diameter [cm]
d_c diameter of radiator pipe [cm]
D_m molecular diffusivity [cm^2/s]
D_P effective diffusivity in particles [cm^2/s]
D_F particles diffusivity (axial dispersion) in fluidized bed [cm^2/s, or m^2/h]
D_S inter-zone particles transfer [kg/h]
F_G gas flow rate [cm^3/s, or m^3/h]
F_j cross-section area in j-th zone [m^2]
h tortuosity of porous structure
h_q interphase heat-transfer coefficient [$kJ/(m^2\ h\ K)$]
h_R „radiator-to-bed“ heat-transfer coefficient [$kJ/(m^2\ h\ K)$]
H Henry coefficient [cm^3/g]
G_S flow rate of dry particles [kg/h]
G_{LPS}, G_{MPS} flow rate of water steam [kg/h]
k_m external mass-transfer coefficient [$cm^3/(cm^2\ s)$]
k_B, k_P local mass-transfer coefficient in bubble and particle [$cm^3/(cm^2\ s)$]
L_j height of j-th zone in bed [m]
L_c distance between pipes in radiator [cm]
R_P particles radius [cm]
R_m rate of mass transfer [g/s, or kg/h]
R_R rate of „radiator-to-bed“ heat-transfer [kJ/h]
R_q rate of interphase heat transfer [kJ/h]
r coordinate inside particle [cm]
Q_H, Q_W heat of vaporization of heptane and water [kJ/kg]
s particle shape parameter (0 – plate, 1 – cylinder, 2 – sphere)
S_B, S_P external surface of bubble and particle [cm^2 or m^2]
T_G, T_S, T_R temperature of gas bed and radiator [°C]
T_{LPS}, T_{MPS} temperature of water steam [°C]
u_G gas velocity [cm/s, or m/s]
u_F minimum fluidization velocity [cm/s, or m/s]
V_j volume of j-th zone [cm^3, or m^3]
V_B, V_P volume of bubble and particle [cm^3]
W, W_E current and equilibrium moisture of particles [g/g or kg/kg]
w dimensionless moisture Eq. (7))

Greek symbols

$\alpha_R = h_R a_R$ total „radiator-to-bed“ heat-transfer coefficient [$kJ/(m^3\ h\ K)$]
$\alpha_T = h_q\ a_B$ total interphase heat-transfer coefficient [$kJ/(m^2\ h\ K)$]
β_T total interphase mass-transfer coefficient [1/s or 1/h]
β_B, β_P total mass-transfer coefficient in bubbles and particles [1/h]
ε_P porosity of particles
ε_S, ε_F void fraction of a fixed and fluidized bed
ψ empirical parameter (Eq. (5))
$\phi = r/R_P$ dimensionless radius of particles
ρ_P polymer particles density [g/cm^3 or kg/m^3]
ρ_S, ρ_F density of fixed and fluidized bed [g/cm^3 or kg/m^3]
ρ_G, ρ_L density of gas and liquid [g/cm^3 or kg/m^3]
μ_G, μ_L viscosity of gas and liquid [g/(cm s)]
λ_G, λ_L heat conductivity of gas and liquid [J/(cm s K)]
λ_F heat conductivity of fluidized bed [kJ/(m h K)]
λ_S inter-zone heat transfer [kJ/(h K)]
τ_Z residence time of particles in bed [min or h]

Aknowledgments

The author would like to acknowledge G. Mijatović and B. Dimić for survey work on the trial run of dryer.

REFERENCES

[1] A.V. Lykov, Theory of energy and mass transfer, Prentice-Hall, Englewood Cliffs, NJ, 1961.
[2] D. Kunii, O. Levenspiel, Fluidization Engineering, 2nd ed. Butterworth-Heinemann, Boston, MA, 1991.
[3] A.V. Lykov, Heat and mass transfer (Handbook), Energia, Moscow, 1972 (in Russian).
[4] R.C. Reid, J.M. Prausnitz, T.K. Sherwood, The properties of gases and liquids, McGraw-Hill, New York, 1977.
[5] J.A. Debling, W.H. Ray, Heat and mass transfer effects in multistage polymerization processes, Ind. Eng. Chem. Research **34** (1995) 3466–3480.
[6] Perry’s Chemical Engineers’ Handbook, McGraw-Hill, New York, 1984.
[7] Fluidization, J.F. Davidson, D. Harrison, Eds., Academic Press, London, 1971.
[8] M. Schreiber, T.W. Asegehegn, H.J. Krautz, Numerical and Experimental Investigation of Bubbling Gas- Solid Fluidized Beds with Dense Immersed Tube Bundles, Ind. Eng. Chem. Research **50** (2011) 7653–7666.
[9] M. Rudisuli, T.J. Schildhauer, S.M.A. Biollaz, J.R. van Ommen, Radial Bubble Distribution in a Fluidized Bed with Vertical Tubes, Ind. Eng. Chem. Research **51** (2012) 13815–13824.
[10] S. Sanaei, N. Mostoufi, R. Radmanesh, R. Sotudeh-Gharebagh, C. Guy, J. Chaouki, Hydrodynamic Characteristics of Gas- Solid Fluidization at High Temperature, Canadian J. Chem. Eng. **88** (2010) 1–11.

IZVOD

SUŠENJE POLIMERNOG PRAHA U FLUIDIZOVANOM SLOJU. MODELIRANJE VIŠESLOJNE SUŠNICE

Nikolaj M. Ostrovski

Hipol a.d., Odžaci, Serbia

(Naučni rad)

Analiziran je proces sušenja poroznih čestica polimera (polipropilena) sa ciljem uklanjanja rastvarača (heptana). Sušnica uključuje dva stadijuma (aparata) sa fluidizovanim slojem u kojima postoje nekoliko zona sušenja. Predložen je matematički model procesa u fluidizovanom sloju sa različitim zonama. Određen je limitirajući stupanj sušenja u zavisnosti od prečnika polimernih čestica. Pronađeno je da u relativno krupnim česticama (>200 μm) brzina sušenja se limitira difuzijom unutar čestica. U malim česticama (<50 μm) proces limitira prenos mase kroz spoljašnu površinu mehuriča gasnog fluida (azota). Model je pokazao zadovoljavajuću saglasnost sa eksperimentalnim podacima i korišćen je za optimizaciju rada sušnice. Data je analiza načina smanjenja potrošnje energije koje su ispitane u eksperimentima na industrijskom postrojenju.

Ključne reči: Sušenje polimernog praha • Fluidizovani sloj • Limitirajući stupanj • Zone sušenja • Matematički model

Electrochemical synthesis of electroconducting polymers

Milica M. Gvozdenović[1], Branimir Z. Jugović[2], Jasmina S. Stevanović[3], Branimir N. Grgur[1]

[1]*Faculty of Technology and Metallurgy, University of Belgrade, Belgrade, Serbia*
[2]*Insitute of Technical Science, Serbian Academy of Science and Arts, Belgrade, Serbia*
[3]*Institute of Chemistry Technology and Metallurgy, University of Belgrade, Belgrade, Serbia*

Abstract

Electroconducting polymers from the group of synthetic metals are extensively investigated due to numerous properties perspective in practical application. These materials may be synthesized by both chemical and electrochemical procedures. Chemical synthesis is suitable when bulk quantities of the polymer are necessary and up to date it presents dominant commercial method of producing electroconducting polymers. Nevertheless, the electrochemical synthesis has its advantages; it avoids usage of oxidants since conducting polymeric material is obtained at anode upon application of positive potential, leading to increased purity. On the other hand, since the polymer is deposited onto electrode, further electrochemical characterization is facilitated. Owing to actuality of the research in the field, this text aims to describe important aspects of electrochemical synthesis of electroconducting polymers, with special emphasis to polyaniline and polypyrrole.

Keywords: electrochemical synthesis, anode, polyaniline, polypyrrole.

Available online at the Journal website: http://www.ache.org.rs/HI/

Polymers

REVIEW PAPER

UDC 621.772/.774:544.6:678:620.193

Hem. Ind. **68** (6) 673–684 (2014)

doi: 10.2298/HEMIND131122008G

From an unexpected discovery of polyacetylene conductivity in the late seventies, later awarded by the Nobel Prize in Chemistry in 2000, the field of electroconducting polymers is still expanding. Although the term "electroconducting polymers" nowadays covers a large group of polymeric materials, with both ionic and electronic conductivity, commonly this term refers to polymeric materials with electronic conductivity originated from the specificity of the molecular structure [1,2], often called "synthetic metals" and the following text will be dedicated exclusively to this group of electroconducting polymers. By studying the mechanism of electrical conductivity it was soon realized that the basic request for macroscopic electrical conductivity was existence of conjugated double bounds, while necessary condition was doping [3]. Although the term doping was taken from traditional semiconductors terminology and it refers to a completely different process, *i.e.*, oxidation (rarely reduction) during which the stoichiometric amount ions (dopants) are introduced into polymer backbone [4]. Moreover, doping often refers to a process in which polyaniline polymer chain is protonated and recent studies indicate that protonation of polypyrrole is also possible [5]. The presence of a large quantity of ions in the polymer alters its structure bringing completely new and unique properties such as: controllable electrical conductivity, reversible doping/dedoping (oxidation/reduction) process, optical activity, corrosion stability etc. [6]. Mentioned properties are considered in the field of: rechargeable power sources [7–9], electrochemical capacitors [10–12], electrochromic devices [13–15], sensors [16–18], magnetic shielding materials [19–21], corrosion protection [22–26], etc.

Although, at the very beginning, the electroconducting polymers were synthesized chemically [3], with deeper insight into the polymerization mechanism, it became clear that electroconducting polymers can also be obtained by electrochemical methods. Both chemical and electrochemical synthesis refers to oxidative polymerization however, other alternative approaches such as: photochemically initiated or enzyme catalyzed polymerization were also reported [4,27].

Although suitable for smaller quantity of the desired electroconducting polymer, the electrochemical synthesis has some advantages. The electrochemical synthesis involves the direct oxidation of the monomer at the anode, so there is no need of an oxidizing agent. On the other hand, in most cases, the polymer is deposited on electrode facilitating further analysis. Having in mind the popularity of polyaniline and polypyrrole in both theoretical and practical aspects, the following text, apart from the general discussion, will be dedicated to the principles of electrochemical synthesis of polyaniline and polypyrrole.

The complexity of electrochemical synthesis

As stated before, the electrochemical synthesis refers to the oxidation of the monomer and growth of the polymer chain onto anode. Since the oxidation is carried out by applying a positive potential or current, the electrochemical polymerization avoids application

Correspondence: M.M. Gvozdenović, Faculty of Technology and Metallurgy, University of Belgrade, Karnegijeva 4, 11120 Belgrade, Serbia.
E-mail: popovic@tmf.bg.ac.rs
Paper received: 22 November, 2013
Paper accepted: 7 February, 2014

of the oxidant, thus achieving greater purity of the desired polymer. On the other hand, growth of the polymers occurs simultaneously with insertion of dopant anions in accordance to generalized stoichiometric equation:

$$n\mathrm{M} + ny\mathrm{A}^- \xrightarrow{\text{oxidation}} [\mathrm{M}^{y+}(\mathrm{A}^-)^{y-}]_n + n(2+y)e^-$$

where, M refers to monomer and A refers to dopant anion whose role is to compensate the positive charge at anode, while *y* is doping degree defined as ratio between the number of charges in the polymer and the number of monomer units [28]. Although the experimental demands for electrochemical formation of electroconducting polymers are simple, the mechanism itself is quite complicated.

Relying on the knowledge of the mechanism of chemical synthesis, it is generally accepted that the first step of the mechanism of electrochemical polymerization is formation of the primary cation-radicals by monomer oxidation at the anode [4,29–32]. These species have essential role in the outcome of the electrochemical polymerization. If being too reactive, they can react with other compounds in the electrolyte, or react with monomers at the "wrong" positions. If, on the other hand being too stable, they may diffuse from the anode before it comes to the further reaction so there will be no formation of electroconductive polymer film [30]. After the primary cation-radicals were formed, the further formation of dimers occurs trough deprotonation and rearomatization [4,32]. The growth of the polymer is achieved by further oxidation and reactions of cation-radicals or cation-radicals and monomers [4]. In order to obtain electroconductive polymer film on the electrode, it is necessary that radical coupling and the continual growth of the polymer occur in the vicinity of the electrode, otherwise, it is possible that cation-radicals and dimers diffuse from the electrode surface (intensive mixing reduces polymerization yield) [4]. The yield can also be reduced by the possible undesired side reactions of cation-radicals and nucleophilic species present in the electrolyte [34].

Once the polymer layer is formed, further polymerization will take place on the modified electrode. This explains the fact that the potential required for the oxidation of the already formed polymer is lower than the potential required for the oxidation of the monomer and the formation of radical cations [6]. Explanation of the kinetics of nucleation and growth processes during electrochemical synthesis of electroconducting polymers relies on the theory of electrochemical metal deposition [6,34]. According to the theory, two types of nucleation are possible, instantaneous and progressive with three types of the growth process: one-dimensional (1D), two-dimensional (2D) and three-dimensional (3D). Instantaneous nucleation refers to constant number of nuclei growing without further formation, while progressive nucleation refers to constant generation of the nuclei [35]. Growth in only one direction refers to 1D growth, perpendicular to the electrode surface, 2D growth is characterized by nuclei with preferences to growth parallel to the electrode surface, while 3D growth implies similar rates of growth in both perpendicular and parallel directions [6].

Factors influencing electrochemical synthesis of electroconducting polymers

Bearing in mind the similarity of the proposed mechanisms of chemical and electrochemical synthesis of electroconducting polymers, it is reasonable to expect that similar factors influencing chemical would exhibit influence on electrochemical synthesis of electroconducting polymers [36]. Beside composition of reaction solution, *i.e*., electrolyte, and temperature, the electrochemical synthesis is subjected to the influence of the electrode material and selected electrochemical technique [37–40].

Electrode material

Although, as mentioned previously, the electrochemical synthesis proceeds without use of oxidants, the nature of the electrode influences the ease of the monomer oxidation and on the other hand deposition of the polymer is dependent on the surface energy of the electrode and its hydrophobic/hydrophilic nature. The major limitations of electrochemical synthesis of electroconductive polymers on numerous metals and alloys are relatively high potentials required for monomer oxidation. At these potentials most metals are either dissolved (iron, steel, copper,…), or form low or even nonconductive passive layers (aluminum and its alloys). This problem is of particular importance when electrochemical synthesis is performed for the purpose of corrosion protection [22,23,25,41,42].

However, the electrochemical synthesis can be easily, by proper design of experimental set-up, performed on so called inert electrodes, such as: Pt, Au, graphite, glassy carbon, ITO glass, etc. [7,43–45].

Electrochemical techniques

Some of the properties of electroconducting polymers obtained electrochemically are dependent on the choice of electrochemical polymerization techniques [4]. Generally, electrochemical techniques used for synthesis of electroconducting polymers can be classified in: galvanostatic, potentiostatic, potentiodynamic.

Galvanostatic technique refers to formation of electroconducting polymer at constant rate (current density). The polymer film, obtained at the end of the polymerization is in doped, *i.e*., conductive form [6]. This technique allows control of the polymer film thickness by adjusting the duration of the polymerization pro-

cess. For its simplicity, galvanostatic technique is the suitable for practical application. Implementation of galvanostatic technique requires proper selection of the polymerization current density, since potential increases during polymerization, as a consequence of resistance increase due to the growth of the polymer film at the electrode. Increase of the potential favors side reactions thus reducing the polymerization efficiency [28].

Potentiostatic polymerization technique refers to application of a constant positive (for oxidative polymerization) potential. It is necessary to choose the potential high enough for polymerization to proceed. On the other hand, potential has to be low enough to avoid undesired secondary reactions and over oxidation of the polymer [6,28,46]. Similar to galvanostatic polymerization, the obtained polymer is in doped state. It is also possible to use a modified pulse potentiostatic technique [46]. This technique involves application of alternating anodic and cathodic pulses of constant potential. During the duration of anodic pulse, the electrochemical polymerization and deposition of the polymer are occurred, while dedoping of the polymer occurs during cathodic pulse. The parameters of the pulse potentiostatic technique, namely: lower (cathodic) and upper (anodic) limit potentials with additional cathodic and anodic pulse times, have influence on the morphology of the formed polymer [48].

Potentiodynamic technique refers to the application of cyclic voltammetry technique for electrochemical polymerization. In this case, the electrode is subjected to cyclic regular change of the potential during which electroconducting polymer changes between its nonconducting (dedoped) and conducting (doped) form [6]. It was shown that nanostructured electroconducting polymers can be obtained by potentiodynamic electrochemical synthesis [49].

Electrochemical synthesis of electroconducting polymers are usually performed in three-electrode cell arrangement, although galvanostatic synthesis can be performed in two electrode system [4]. In three electrode cell, working electrode operates as anode on which polymerization and deposition of the polymer occur. Reduction of solvent, dissolved oxygen or other compound of the electrolyte occurs at counter electrode, while reference electrode serves for the potential control. Three electrodes can all share the same compartment (one compartment cell) or they can be organized in two compartments (one for counter and working electrodes and one for reference electrode) or three compartments (each electrode has its compartment). If working and counter electrodes are in the same compartment, the reactions occurring on the counter electrode cannot be neglected. The most common reaction at counter electrode is the reduction of water (if aqueous electrolytes are used) or other additives from electrolyte, and this problem might be overcome by intentional addition of auxiliary reagent such as electroactive metal ion or ferricyanide or by use of three compartments of electrochemical cell, which are common for laboratory investigations [4]. The cell geometry also plays important role, especially for practical purposes.

Apart from standard electrochemical cells, Wallace *et al*. developed new electrochemical flow cell for potentiodynamic synthesis of colloids or water soluble electroconducting polymers. In this cell the anode was separated from two cathodes by ion exchange membrane, with anodic and cathodic electrolytes passed through these separated compartments [39,50,51]. Anode is made of porous material with developed surface area while flowing electrolyte prevents deposition of the polymer. Anolite, beside monomer, contains stabilizer polyethylene or polyvinyl alcohol, which favors formation of colloids.

Electrolyte

Composition of electrolytes used for electrochemical synthesis of electroconducting polymers involves, beside selected monomer, solvent and acid which serves as source of dopants ion and in some cases may contain some additional compounds [1,2,28,40,51,52].

Apart from being capable to dissolve monomer, the solvent has to be as pure as possible, and stable at potentials of interest for the polymerization. For example, the presence of dissolved oxygen may be problematic due to reaction with radical intermediates and it can be also reduced at counter electrode and forms hydroxide [4]. Interaction of the solvent, monomers and electrode materials cannot be neglected even before the polymerization is initiated since they will all have impact on monomer adsorption onto electrode. Once the polymerization is started, the properties of solvent will have influence on solubility of the polymer. On the other hand, as stated before, nucleophilicity of the solvent should be also considered, the nucleophilic solvent would react with radicals and thus preventing the normal course of the electrochemical polymerization [4,36].

Most of the electrochemical syntheses of electroconducting polymers are performed in aqueous electrolytes bearing in mind the price, easy handling, environmental concerns, and the fact that various dopants may be used. However, various organic solvents were also investigated, such as: acetonitile, dichlormethane, nitrobenzene, propylene carbonate and recently the application of ionic liquids was also considered [4,38,53–55].

Dopants or counter ions are incorporated into polymer structure during electrochemical polymerization fulfilling the request of electroneutrality by compen-

sating positive charge on anode. Since their amount is on stoichiometric levels, it is reasonable to expect that their presence and properties would dramatically influence the morphology, conductivity, electrochemical activity and the polymerization process as well [4,56,57]. As expected, dopants have to be both chemically and electrochemically stable. If dopant is electroactive at potentials lower than those required for polymerization of the monomer, than they can be only used for potentiostatic synthesis [4].

Temperature has also impact on electrochemical synthesis of electroconducting polymers, not only influencing the kinetics of the process, but also influencing the extent of undesired side reactions. Free radicals obtained in anodic process react with oxygen in reaction that is highly sensitive to temperature; therefore the increase in temperature has adverse impact on electrochemical syntheses through decrease of the polymerization efficiency [4].

Electrochemical synthesis of polyaniline

It is believed that polyaniline is the oldest known electroconducting polymer since it was used in textile industry as a cotton dye over a century ago [58]. The increased interest in polyaniline dates from the discovery of its conductivity in the form of emeraldine salt and existence of different oxidation forms, as given in general scheme in Fig. 1 [40,59–62].

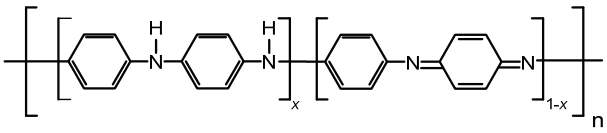

Figure 1. General scheme of polyaniline.

Fully reduced form refers to leucoemeraldine base (x = 1), half-oxidized form refers to emeraldine base (x = 0.5), while fully oxidized form is pernigraniline base (x = 0). None of these forms is conductive [42,63,64]. The only conductive form of polyaniline, the emeraldine salt, can be obtained by doping or protonation of emeraldine base [65]. The unique property of polyaniline forms is mutual conversion by both chemical and electrochemical reactions, which are followed by color and conductivity changes [64].

Electrochemical polymerization of aniline in acidic electrolytes leads to formation of green conductive emeraldine salt. Emeraldine salt can be easily oxidized to dark blue perninganiline salt or be transformed in reaction with alkali to violet pernigraniline base. Emeraldine salt can also be reduced to transparent leucoemeraldine base, or transformed in reaction with alkali to blue emeraldine base. Both the reduction and oxidation of conductive emeraldine salt are followed by decrease of conductivity [64].

The mechanism of electrochemical polymerization of aniline

As in case of chemical, the electrochemical synthesis of polyaniline is always carried out in strong acidic solutions (pH < 2), since increase in pH would lead to formation of short conjugation oligomers [4,65,66].

The generally accepted mechanism of electrochemical synthesis of polyaniline [4,30,68,69] is given in Fig. 2.

As mentioned before, first step of the polymerization process refers to formation of radical cation by oxidation of monomers at anode. Formation of primary radical cation (aniline radical cation), is believed to be the rate-determining step [68–70]. The existence of aniline radical cation was experimentally confirmed when substances capable of retarding the process were added which supported the radical mechanism. The oxidation of aniline monomer is irreversible process, occurring at potential of about 0.9 V (*vs*. standard calomel electrode), which is higher than polyaniline redox potential [30]. Formation of the radical cation is than followed by coupling of the radicals at *N*- and *p*- positions with elimination of two protons. The formed dimers and lately oligomers are than subjected to further oxidation along with aniline. Oxidation potential of dimers and oligomers are lower than oxidation potential of aniline [62]. Radical cations, formed from oligomers and aniline radical cations, are than coupled leading to chain propagation. Polyaniline is doped by anions from electrolyte. The unique feature of electrochemical formation of polyaniline is the fact that nitrogen atom is involved in formation of radical cation, unlike most of others electroconducting polymers whose radical cation is formed on carbon atom. Nitrogen is also present in conjugated system of double bonds explaining the fact that electrical conductivity of polyaniline depends both on oxidation and protonation levels [4,59,65].

It was claimed that electrochemical synthesis of polyaniline is an autocatalytic process, meaning that further formation of the polymer on already deposited polymer proceeds faster than on the bare electrode, *i.e*., the more polyaniline is formed on anode, the higher is the rate of the polymerization process [4,30,40,70–72]. The autocatalytic synthesis of aniline was experimentally confirmed during electrochemical polymerization of aniline by cyclic voltammetry technique. It was evidenced that current increased over time for potentials higher than 0.8 V (*vs*. saturated Calomel Electrode) and that anodic peak potentials decreased. The increased intensity of the anodic peak currents was connected to increased polymerization rate, while decrease of the anodic peak potentials was

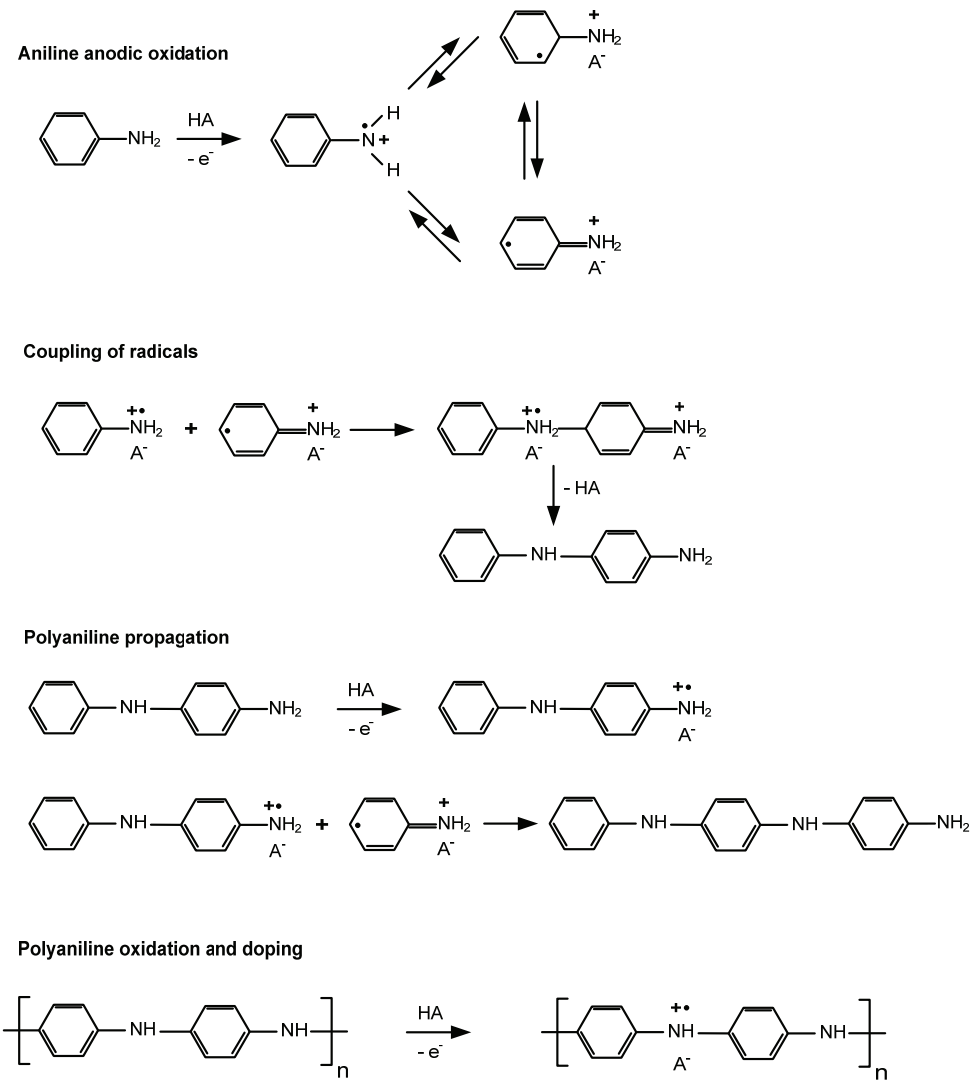

Figure 2. Mechanism of electrochemical synthesis of polyaniline.

assigned to facilitated electrochemical polymerization [70].

Factors influencing electrochemical synthesis of polyaniline

Electrochemical synthesis of polyaniline proceeds easily on inert electrodes in strong acidic aqueous electrolytes containing aniline, according to described mechanism. As expected, parameters such as: electrode (anode) materials, choice of solvent, composition of electrolyte, temperature, have influence on properties of obtained polyaniline [4,6,30,45,58].

If potentiodynamic technique is used for electrochemical synthesis of polyaniline, the several characteristic peaks appear on cyclic voltammograms, as it can be seen in Fig. 3.

First anodic peak at potential of ~0.2 V refers to doping characterizing transformation of leucoemeraldine base to emeraldine salt, further increase of potential leads to appearance of another anodic peak at 0.8 V characteristic to formation of fully oxidized pernigraniline salt [7,62,73]. Between mentioned well defined anodic peaks, small peaks at potentials ~0.4 V refer to formation of degradation and hydrolysis products [62]. If galvanostatic polymerization is used for electrochemical formation of polyaniline (insert of Fig. 3), chronopotentiograms are characterized by fast potential increase during which electrode surface is covered by polyaniline film and potential plateau at which polymerization proceeds on already formed polymer [7,45].

If polyaniline has to be obtained electrochemically as protective coating on active metals and their alloys, dissolution or passivation by nonconductive oxides would occur, since aniline polymerization potential is quite high, laying in potential region of either active metal dissolution, (iron, mild steels, copper,…) or formation of non-conductive oxides (aluminum) [22,23,25,26,42,74,75]. Two approaches were pro-

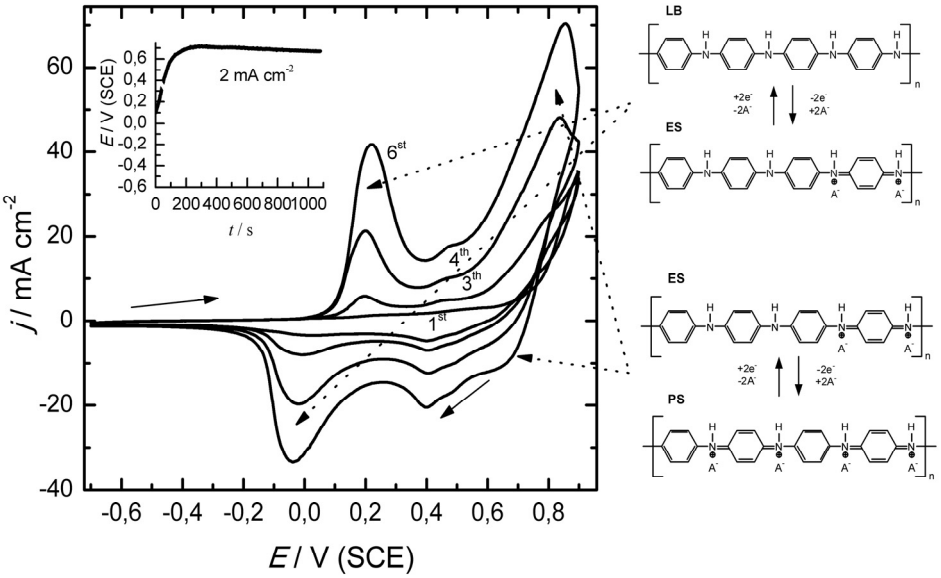

Figure 3. Electrochemical synthesis of polyaniline at graphite electrode by cyclic voltammetry (v = 20 mV s^{-1}) from 1.0 mol dm^{-3} HCl containing 0.25 mol dm^{-3} aniline. Inset: chronopotentiometric curve (j = 2.5 mA cm^{-2}) of electrochemical synthesis of polyaniline from the same electrolyte. (Reprinted from Materials Chemistry and Physics, vol. 125, Issue 3, M. M. Gvozdenović , B. Z. Jugović, T. Lj. Trišović, J.S. Stevanović and B. N. Grgur, "Electrochemical characterization of polyaniline electrode in ammonium citrate containing electrolyte", pp. 601–605, Copyright 2004, with permission from Elsevier).

posed, the application of electrode surface pre-treatments or electrolytes capable of formation of passive, but still conductive layers on which undisturbed polymerization would occur [4,22,75].

As in case with chemical synthesis the electrochemical synthesis is practically always carried out in very acidic electrolytes (pH < 2) [42,64,67]. Okamoto and Kotaka were investigated galvanostatic electrochemical synthesis of polyaniline in pH range between 0.2 and 3.7, using UV spectroscopy for determination of existence of emeraldine salt and occurrence of oligomers. They pointed out that emeraldine salt was formed at pH lower than 1.7, while increase of pH resulted in formation of films with spectra characteristic for oligomers [56].

Anions inserted during electropolymerization of aniline usually originate from acid, present their conjugated base, and exhibit influence on morphology, conductivity and redox properties of obtained polyaniline [35,57,76–78]. It was experimentally evidenced that polyaniline doped by highly hydrated ions originating from hydrochloric acid, sulfuric acid, nitric acid, *p*-toluenesulfonic acid, sulfosalicylic acid exhibited more open and swollen structures, while small ions, for example ClO_4^- or BF_4^- are responsible for more compact structures [79]. It was showed that doping of polyaniline with chiral dopants was also possible, resulted in emeraldine salt film with strong circular dichroism, meaning that chirality was introduced into polyaniline by the use of specific types of dopants [5,50]. Addition of polyelectrolytes can lead to incorporation of their polyanions as dopants into electroconducting polymer matrix [4]. Some of the researches have shown that addition of inert salts into electrolyte resulted in polyaniline with increased molecular weight [4,80]. Addition of alcohols into electrolyte also exhibited influence on morphology of obtained polyaniline leading to one dimensional growth, this effect was explained by solvation of polyaniline by alcohol molecules due to intermolecular bonding by hydrogen bonds [81].

Electrochemical synthesis of polypyrrole

Besides polyaniline, polypyrrole is certainly one of the most extensively investigated electroconducting polymer. Both electrical conductivity and chemical stability of polypyrrole originate from heteroatomic and extended π-conjugated backbone structure. This structure is not sufficient for conductivity on its own. However, conductivity achieved by doping largely exceeds those of other electroconducting polymers, which is a good prerequisite for practical application [82]. Unlike polymerization of aniline, polymerization of pyrrole can be successfully performed in neutral aqueous environment and variety of organic solvents can be also used [83].

The mechanism of electrochemical polymerization of pyrrole

According to generally accepted mechanism of electrochemical polymerization of pyrrole, the first step refers to formation of the primary radical cation, as seen in Fig. 4 [36].

Unpaired electron and positive charge are delocalized and quantum mechanical calculations reveal that

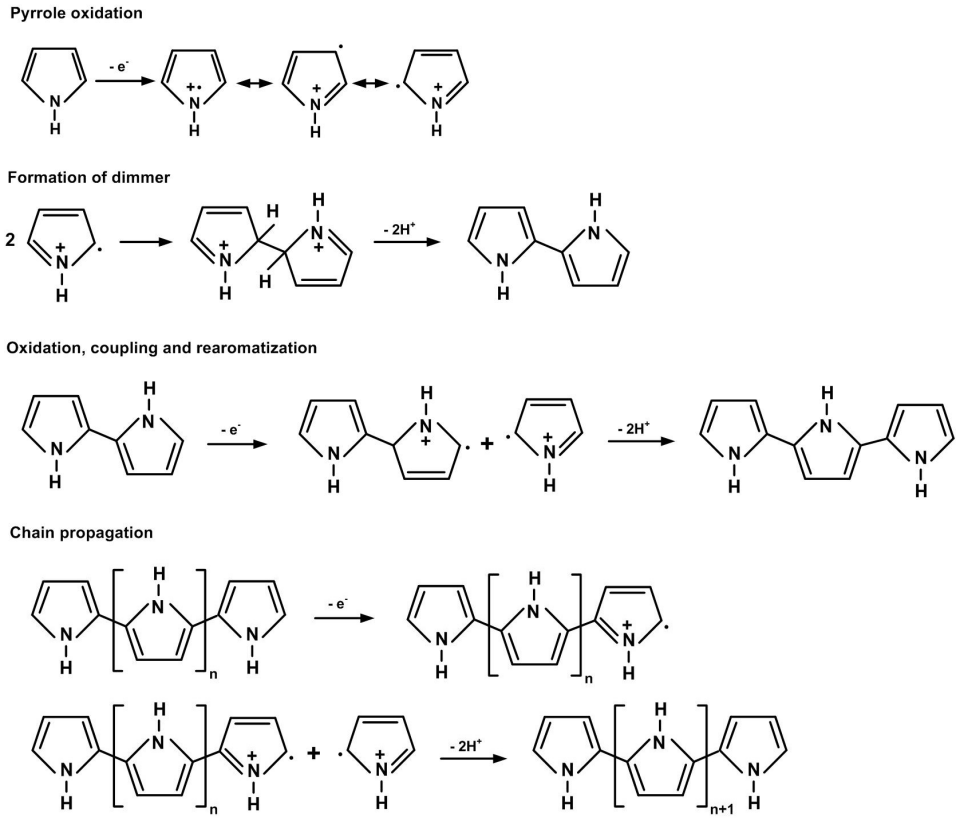

Fig. 4. Mechanism of polypyrrole electrochemical synthesis.

electron spin density is the greatest at *o*-positions, therefore they are the most reactive, so radical coupling takes place at these positions [28].

By coupling of two primary radical cations, positively charged dimer is formed. Since two protons of the positively charged dimer distort the conjugation, rearomatization is likely to occur through deprotonation leading to formation of energetically favorable neutral dimer [4]. According to alternative, but not accepted mechanism, radical cation can react with neutral pyrrole molecules leading to formation of a new radical cation [4]. Neutral dimer is, in further step, oxidized at anode giving new radical cation. As expected, oxidation of the dimer is easier comparing to neutral pyrrole, therefore occurring at the lower potential. In the forthcoming steps coupling of dimer radical cations (lately, oligomer radical cations) and primary radical cations occur, followed by a release of protons and rearomatization. Oxidation, coupling and rearomatization are repeated leading to formation of polypyrrole. Although the electron spin density is the largest at *o*-position, by development of the conjugation length, spin density is spreading over conjugating system, so the radicals might be coupled in other positions, resulting in disturbing of the linearity and branching [4].

Factors influencing electrochemical synthesis of polypyrrole

Nature of the electrochemical synthesis of polypyrrole is affected by similar factors as in the case of electrochemical synthesis of polyaniline.

Pyrrole, similarly to aniline, is easily electrochemically polymerized in both aqueous and organic based electrolytes containing pyrrole on inert anodes, including graphite, gold or platinum, according to above given mechanism. Figure 5 shows galvanostatic polymerization of pyrrole from aqueous electrolyte together with cyclic voltammogram obtained after galvanostatic synthsis in the same electrolyte in order to show characteristic doping/dedoping processes occurring during potentiodynamic synthesis (inset of Fig.5).

As seen in Fig. 5, chronoamperometric curve is characterized, by fast increase of the potential during which the electrode is covered with a layer of polypyrrole, the succeeding plateau of the potential although lower than in the case of polyniline, refers to further polymerization on already formed polymer. It can be noticed that after galvanostatic synthesis the polypyrrole is almost completely in its doped state which is reflected in rapid increase of the potential [6]. Cathodic part of the voltammogram is characterized by wide peak attributed to dedoping of ions from polypyrrole, after which anodic part of the voltammogram refers to

doping and further polymerization of pyrrole occurring simultaneously [84].

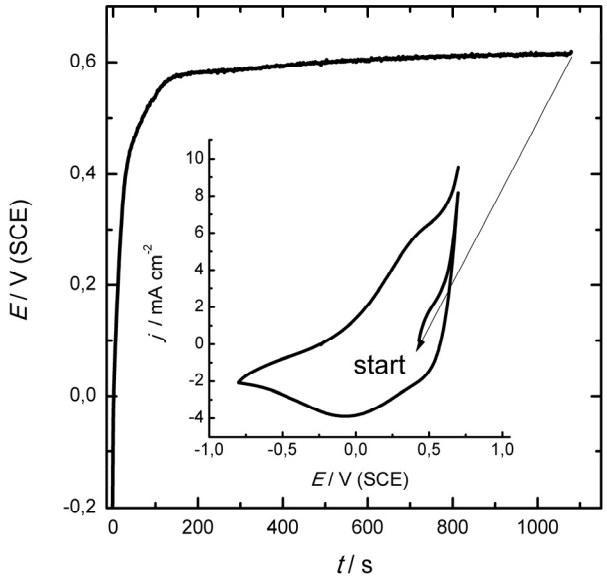

Figure 5. Chronoamperometric curve of electrochemical polymerization of pyrrole at graphite electrode (j = 2.0 mA cm^{-2}) from 0.1 mol dm^{-3} HCl and 0.2 mol dm^{-3} pyrrole. Inset: cyclic voltammogram (v = 20 mV s^{-1}) recorded after 1100 s of galvanostatic synthesis of polypyrrole from the same electrolyte.

Electrochemical synthesis of polypyrrole on active metals is faced to expected problems of the substrate dissolution owing to the high potential required for oxidation of the monomer [4,22,85–88].

Lot of efforts have been taken in order to find suitable conditions to passivate metal without hindering electrochemical synthesis of polypyrrole. Smooth and uniform polypyrrole coatings were deposited using lower current densities on low carbon steel and mild steel using oxalic acid based aqueous electrolyte [41,86,88,89]. In these cases, metal surface was shown to be firstly passivated by conductive interlayer of iron oxalate, on which uniform and protective film of polypyrrole was formed [90]. There are also evidence in literature that adherent polypyrrole might be formed on different oxidizable metals in aqueous electrolyte containing sodium salycilate. Sodium salycilate is capable of producing, together with metal ions, thin protective layer slowing substrate dissolution without impeding polymerization of pyrrole [86].

Beside oxalate based electrolytes, electrochemical synthesis of polypyrrole on aluminum was achieved in molybdate containing electrolytes [85,91,92].

Electrochemical polymerization of pyrrole was intensively studied in non-aqueous solutions, primarily in acetonitrile [4]. When polymerization is carried out in aqueous electrolytes it was assumed that water had role in the polymerization process. It was experimentally confirmed that polypyrrole maintained 2–4% of water which was impossible to remove [5,93]. When acetonitrile was used as solvent for electrochemical polymerization of pyrrole, obtained polypyrrole had lower porosity as a consequence of impossibility of hydratation of dopants (counter-ions), unlike aqueous solutions in which the dopants are hydrated resulting in increased porosity of the obtained polypyrrole. On the other hand, it was also observed that polypyrrole electrochemically synthesized from either acetonitrile or propylene carbonate, exhibited higher conductivity comparing to those obtained from aqueous electrolytes [4]. Recently ionic liquids were also used as both solvents and source of dopants in electrochemical synthesis of electroconducting polymers. It was shown that polypyrrole grown from ionic liquids had different morphology and conductivity [38,94].

The nature and concentration of dopants, *i.e*., counter ions, has influence on conductivity and polymerization rate of pyrrole, this effect was observed in both aqueous and non-aqueous solvents [4,82]. It was confirmed that doping by sulfonated aromatic ions, such as *p*-toulensulfonate led to higher conductivity of polypyrrole due to formation of crystalline structure [95,96]. Proteins and polyelectrolytes can also be incurporated as dopants during electrochemical formation of polypyrrole [4,97,98]. Besides pyrrole, the electrochemical polymerization of substituted pyrroles was also investigated, although these polymers were shown to be less conductive comparing to polypyrrole.

CONCLUSIONS

The existence of specific molecular structure that involves the system of conjugated double bonds leading to delocalization of electronic states is a key feature of electroconducting polymers, important representatives of synthetic metals. Electrical conductivity achieved by specific doping on stoichiometric level is, beside of the polymer type, dependent on the nature and amount of dopants, covering practically whole range from insulator, semiconductor to conductor regime. Since the presence of different amount of dopants makes conductivity adjustable, and bearing in mind that doping (oxidation) and dedoping (reduction) are reversible processes, electroconductive polymers are very promising materials for practical applications in various fields. Therefore not surprisingly, electroconducting polymers are still important subject of numerous researches. The application of electrochemical techniques of both synthesis and characterization has very important role in the science of electroconducting polymers, since it enables relatively simple and reproductive approach. From the very beginning and up to now, synthesis and characterization of polyaniline and polypyrrole are certainly the most investigated.

Acknowledgment

This work was supported by the Ministry of Education, Science and Technological Development, Republic of Serbia, under Contract No. 172046.

REFERENCES

[1] S. Jovanović, G. Nestorović, K. Jeremić, Elektroporovodni polimerni materijali, Hem. Ind. **57** (2003) 511–525.

[2] Conducting Polymers-Theory, Sinthesis, Properties and Characterization, T.A. Skotheim, J. Reynolds, Eds., CRC-Press, Teyor & Francis Group, New York, 2007.

[3] A.G. Macdiarmid, Synthetic Metals: A Novel Role for Organic Polymers, Nobel Lecture, 2001.

[4] G.G. Wallace, P.R. Teasdale, G.M. Spinks, L.A.P. Kane-Maguire, Conductive Electroactive Polymers, 3rd. ed. Telyor & Francis Group, Boca Raton, FL, 2009.

[5] J. Škodova, D. Kopecký. M. Vrňata, M. Varga,J. Prokeš, M. Cieslar, P. Bober, J. Stejskal, Polypyrrole-silver composites prepared by the reduction of silver ions with polypyrrole nanotubes, Polym. Chem. **4** (2014) 3610–3616.

[6] J. Heinze, B. Frontana-Uribe, S. Ludwigs, Electrochemistry of conducting polymers-persistent models and new concepts. Chem. Rev. **110** (2010) 4724–4771.

[7] B. Jugović, M. Gvozdenović, J. Stevanović, T. Trišović, B. Grgur, Characterization of electrochemically synthesized PANI on graphite electrode for potential use in electrochemical power sources, Mater. Chem. Phys. **114** (2009) 939–942.

[8] M.M. Gvozdenović, B.Z. Jugović, T.L. Trišović, J.S. Stevanović, B.N. Grgur, Electrochemical characterization of polyaniline electrode in ammonium citrate containing electrolyte, Mater. Chem. Phys. **125** (2011) 601–605.

[9] B.N. Grgur, M.M. Gvozdenović, J. Stevanović, B.Z. Jugović, V.M. Marinović, Polypyrrole as possible electrode materials for the aqueous-based rechargeable zinc batteries, Electrochim. Acta **53** (2008) 4627–4632.

[10] Y. Zhang, H. Feng, X. Wu, L. Wang, A. Zhang, T. Xia, H. Dong, X. Li, L. Zhang, Progress of electrochemical capacitor electrode materials: A review, Int. J. Hydrogen Energy **34** (2009) 4889–4899.

[11] H.R. Ghenaatian, M.F. Mousavi, S.H. Kazemi, M. Shamsipur, Electrochemical investigations of self-doped polyaniline nanofibers as a new electroactive material for high performance redox supercapacitor, Synth. Met. **159** (2009) 1717–1722.

[12] L. Zhang, G. Zhao, Y. Wang, Polyaniline nanowire electrodes with high capacitance synthesized by a simple approach, Mater. Sci. Eng., C **33** (2003) 2013.

[13] E.D.C. Rios, A. Viana Rosario, A. Flávia Nogueira, L. Micaroni, Electrochromic devices based on poly(3-methylthiophene) and various secondary electrochromic materials, Sol. Energy Mater. Sol. Cells **94** (2010) 1338–1345.

[14] P. Camurlu, C. Gültekin, A comprehensive study on utilization of *N*-substituted poly(2,5-dithienylpyrrole) derivatives in electrochromic devices, Sol. Energy Mater. Sol. Cells **107** (2012) 142–147.

[15] A.J.C. da Silva, F.A. Ribeiro Nogueira, J. Tonholo, A.S. Ribeiro, Dual-type electrochromic device based on polypyrrole and polythiophene derivatives, Sol. Energy Mater. Sol. Cells **95** (2011) 2255–2259.

[16] M.M. Gvozdenović, B.Z. Jugović, D.I. Bezbradica, M.G. Antov, Z.D. Knežević-Jugović, B.N. Grgur, Electrochemical determination of glucose using polyaniline electrode modified by glucose oxidase, Food Chem. **124** (2011) 396–400.

[17] D. Bezbradica, B. Jugović, M. Gvozdenović, S. Jakovetić, Z. Knežević-Jugović, Electrochemically synthesized polyaniline as support for lipase immobilization, J. Mol. Catal., B **70** (2011) 55–60.

[18] D. Jambrec, M. Gvozdenović, M. Antov, B. Jokić, J. Stevanović, B. Jugović, B. Grgur, Electrochemically deposited nanofibrous polyaniline for amperometric determination of glucose, Dig. J. Nanomater. Biostructures **7** (2012) 785–794.

[19] Ö. Yavuz, M.K. Ram, M. Aldissi, P. Poddar, H. Srikanth, Polypyrrole composites for shielding applications, Synth. Met. **151** (2005) 211–217.

[20] J.D. Sudha, S. Sivakala, R. Prasanth, V.L. Reena, P. Radhakrishnan Nair, Development of electromagnetic shielding materials from the conductive blends of polyaniline and polyaniline-clay nanocomposite-EVA: Preparation and properties, Compos. Sci. Technol. **69** (2009) 358–364.

[21] A. Kaur, S.K. Dhawan, Tuning of EMI shielding properties of polypyrrole nanoparticles with surfactant concentration, Synth. Met. **162** (2012) 1471–1477.

[22] S. Biallozor, A. Kupniewska, Conducting polymers electrodeposited on active metals, Synth. Met. **155** (2005) 443–449.

[23] M.M. Gvozdenović, B.N. Grgur, Electrochemical polymerization and initial corrosion properties of polyaniline-benzoate film on aluminum, Prog. Org. Coat. **65** (2009) 401–404.

[24] A. Elkais, M. Gvozdenović, B. Jugović, T. Trišović, M. Maksimović, B. Grgur, Electrochemical synthesis and corrosion behavior of thin polyaniline film on mild steel, copper and aluminum, Hem. Ind. **65** (2011) 15–21.

[25] M.M. Popović, B.N. Grgur, Electrochemical synthesis and corrosion behavior of thin polyaniline-benzoate film on mild steel, Synth. Met. **143** (2004) 191–195.

[26] M.M. Gvozdenović, B.Z. Jugović, J.S. Stevanović, B. Grgur, T.L. Trišović, Z.S. Jugović, Electrochemical synthesis and corrosion behavior of polyaniline-benzoate coating on copper, Synth. Met. **161** (2011) 1313–1318.

[27] S. Bhadra, D. Khastgir, N.K. Singha, J.H. Lee, Progress in preparation, processing and applications of polyaniline, Prog. Polym. Sci. **34** (2009) 783–810.

[28] J. Kankare, Conducting polymers: Basic Methods of Synthesis and Characterization, in: Electrical and Optical Polymer Systems: Fundamentals, Methods and Applications, D. Wise, G. Wnek D. Trantolo, J.Cooper, D. Gresser, Eds., CRC Press, New York, 1998, pp. 167–199.

[29] G. Inzelt, Temperature dependence of the voltammetric response of polyaniline film electrodes, J. Electroanal. Chem. Interfacial Electrochem. **279** (1990) 169–178.

[30] G. Inzelt, Conducting Polymers-A New Era in Eelctrochemistry, Springer-Verlag Berlin, 2008.

[31] H. Daifuku, T. Kawagoe, T. Matsunaga, N. Yamamoto, T. Ohsaka, N. Oyama, Quartz crystal microbalance study on redox reaction mechanism of polyaniline, Synth. Met. **43** (1991) 2897–2900.

[32] L. Arsov, W. Plieth, G. Koßmehl, Electrochemical and Raman spectroscopic study of polyaniline; influence of the potential on the degradation of polyaniline, J. Solid State Electrochem. **2** (1998) 355–361.

[33] A. Diaz, J. Crowley, J. Bargon, G. Gardini, J. Torrance, Electrooxidation of aromatic oligomers and conducting polymers, J. Electroanal. Chem. Interfacial Electrochem. **121** (1981) 355–361.

[34] R. Mažeikienė, A. Malinauskas, Electrochemical behaviour of polyaniline film polymerized by the use of a chemical oxidation step, Electrochim. Acta **41** (1996) 1587–1591.

[35] Z. Mandić, L. Dujić, F. Kovačiček, The influence of counter-ions on nucleation and growth of electrochemically synthesized polyaniline film, Electrochim. Acta **42** (1997) 389–1402.

[36] Handbook of Radical Polymerization, K. Matyjaszewski, T. Davys, Eds., John Wiley & Sons, Hoboken, NJ, 2002.

[37] P.C. Innis, Y.C. Chen, S. Ashraf, G.G. Wallace, Electrohydrodynamic polymerisation of water-soluble poly ((4--(3-pyrrolyl)) butane sulfonate), Polymer **41** (2000) 4065–4076.

[38] J.M. Pringle, J. Efthimiadis, P.C. Howlett, J. Efthimiadis, D.R. MacFarlane, A.B. Chaplin, S.B. Hall, D.L. Officer, G.G. Wallace, M. Forsyth, Electrochemical synthesis of polypyrrole in ionic liquids, Polymer **45** (2004) 1447–1453.

[39] Y. Pornputtkul, L.A.P. Kane-Maguire, G.G. Wallace, Influence of Electrochemical Polymerization Temperature on the Chiroptical Properties of (+)-Camphorsulfonic Acid-Doped Polyaniline, Macromolecules **39** (2006) 5604–5610.

[40] G. Inzelt, M. Pineri, J. Schultze, M. Vorotyntsev, Electron and proton conducting polymers: recent developments and prospects, Electrochim. Acta **45** (2000) 2403–2421.

[41] B.N. Grgur, P. Živković, M.M. Gvozdenović, Kinetics of the mild steel corrosion protection by polypyrrole-oxalate coating in sulfuric acid solution, Prog. Org. Coatings **56** (2006) 240–247.

[42] G. Ćirić-Marjanović, Recent advances in polyaniline research: Polymerization mechanisms, structural aspects, properties and applications, Synth. Met. **177** (2013) 1–47.

[43] B.N. Grgur, A. Žeradjanin, M.M. Gvozdenović, M.D. Maksimović, T.L. Trišović, B.Z. Jugović, Electrochemical characteristics of rechargeable polyaniline/lead dioxide cell, J. Power Sources **217** (2012) 193–198.

[44] D. Bhattacharjya, I. Mukhopadhyay, Controlled Growth of Polyaniline Fractals on HOPG through Potentiodynamic Electropolymerization, Langmir **28** (2012) 5893–5899.

[45] M.M. Gvozdenović, B.Z. Jugović, J.S. Stevanović, T.Lj. Trišović, B.N. Grgur, Electrochemical Polymerization of Aniline, in Electropolzmeriyation, E. Schab-Balcerzak, Ed., InTech, Rijeka, 2011.

[46] V. Gupta, N. Miura, Large-area network of polyaniline nanowires prepared by potentiostatic deposition process, Electrochem. Commun. **7** (2005) 995–999.

[47] Z. Tang, S. Liu, Z. Wang, S. Dong, E. Wang, Electrochemical synthesis of polyaniline nanoparticles, Electrochem. Commun. **2** (2000) 32–35.

[48] V. Tsakova, A. Milchev, J. Schulze, Growth of polyaniline films under pulse potentiostatic conditions, J. Electroanal. Chem. **346** (1993) 85–97.

[49] S. Mu, Y. Yang, Spectral characteristics of polyaniline nanostructures synthesized by using cyclic voltammetry at different scan rates, J. Phys. Chem., B **112** (2008) 11558–11563.

[50] V. Aboutanos, L.A.P. Kane-Maguire, G.G. Wallace, Electrosynthesis of polyurethane-based core-shell PAn (+)/-HCSA colloids, Synth. Met. **114** (2000) 313–320.

[51] P.C. Innis, I.D. Norris, L.A.P. Kane-Maguire, G.G. Wallace, Electrochemical Formation of Chiral Polyaniline Colloids Codoped with (+)- or (–)-10-Camphorsulfonic Acid and Polystyrene Sulfonate, Macromolecules **92** (1998) 6521––6528.

[52] A. Diaz, J. Crowley, J. Bargon, G. Gardini, J. Torrence, Electrooxidation of aromatic oligomers and conducting polymers, J. Electroanal. Chem. Interfacial Electrochem. **121** (1981) 355–361.

[53] S. Mu, Pronounced effect of the ionic liquid on the electrochromic property of the polyaniline film: Color changes in the wide wavelength range, Electrochim. Acta. **52** (2007) 7827–7834.

[54] Y. Sahin, A. Aydin, Y.A. Udum, K. Pekmez, A. Yildiz, Electrochemical synthesis of sulfonated polypyrrole in FSO3H/acetonitrile solution, J. Appl. Polym. Sci. (2004) 526–533.

[55] S. Perc, Electrochemical Synthesis of Poly(2-iodoaniline) and Poly(aniline-co-2-iodoaniline) in Acetonitrile, J. Appl. Polym. Sci. **89** (2003) 1652–1658.

[56] H. Okamoto, T. Kotaka, Structure and properties of polyaniline films prepared via electrochemical polymerization. I: Effect of pH in electrochemical polymerization media on the primary structure and acid dissociation constant of product polyaniline films, Polymer **39** (1998) 4349–4358.

[57] [H. Okamoto, T. Kotaka, Effect of counter ions in electrochemical polymerization media on the structure and responses of the product polyaniline films III . Structure and properties of polyaniline films prepared via electrochemical polymerization, Polymer **40** (1998) 407––417.

[58] A. Syed, M. Dinesan, Polyaniline—A novel polymeric material,Talanta **38** (1991) 815–837.

[59] A. Pron, P. Rannou, Processible conjugated polymers : from organic semiconductors to organic metals and superconductors, Prog. Polym. Sci. **27** (2002) 135–190.

[60] A. McDiarmid, J. Chiang, M. Halpern, W. Huang, S. Mu, N. Somasiri, W. Wu, S. Yaniger, Polyaniline: Interconversion of Metallic and Insulating Forms, Mol. Cryst. Liq. Cryst. **121** (1985) 173–180.

[61] H. Javadi, F. Zuo, M. Angelopoulus, A. McDiarmid, A. Epstein, Frequency Dependent Conductivity of Emeraldine: Absence of Protonic Conductivity, Mol. Cryst. Liq. Cryst. Inc. Nonlinear Opt. **160** (1988) 225–233.

[62] N. Gospodinova, L. Terlemezyan, Conducting polymers prepared by oxidative polymerization: polyaniline, Prog. Polym. Sci. **23** (1998) 1443–1484.

[63] J. Stejskal, I. Sapurina, Polyaniline: Thin films and colloidal dispersions (IUPAC Technical Report), Pure Appl. Chem. **77** (2005) 815–826.

[64] J. Stejskal, P. Kratochvíl, A. Jenkins, The formation of polyaniline and the nature of its structures, Polymer **37** (1996) 1420–1481.

[65] P. Fedorko, M. Trznadel, A. Pron, D. Djurado, J. Planès, J. P. Travers, New analytical approach to the insulator–metal transition in conductive polyaniline, Synth. Met. **160** (2010) 1668–1671.

[66] N.V. Blinova, J. Stejskal, M. Trchová, J. Prokeš, M. Omastová, Polyaniline and polypyrrole: A comparative study of the preparation, Eur. Polym. J. **43** (2007) 2331––2341.

[67] J. Stejskal, I. Sapurina, M. Trchová, Polyaniline nanostructures and the role of aniline oligomers in their formation, Prog. Polym. Sci. **35** (2010) 1420–1481.

[68] G. Zotti, S. Cattarin, N. Comisso, Electrodeposition of polythiophene, polypyrrole and polyaniline by the cyclic potential sweep method, J. Electroanal. Chem. Interfacial Electrochem. **235** (1987) 259–273.

[69] A. Hussain, A. Kumar, Electrochemical synthesis and characterization of chloride doped polyaniline, Bulettin Mater. Sci. **26** (2003) 329–334.

[70] G. Zotti, S. Cattarin, N. Comisso, Cyclic potential sweep electropolymerization of aniline: The role of anions in the polymerization mechanism, J. Electroanal. Chem. Interfacial Electrochem. **239** (1988) 387–396.

[71] S. Mu, J. Kan, Evidence for the autocatalytic polymerization of aniline, Electrochim. Acta **41** (1996) 1593––1599.

[72] S. Mu, C. Chen, J. Wan, The kinetic behavior for the electrochemical polymerization of aniline in aqueous solution, Synth. Met. **88** (1997) 249–254.

[73] L. Arsov, W. Plieth, G. Koßmehl, Electrochemical and Raman spectroscopic study of polyaniline; influence of the potential on the degradation of polyaniline, J. Solid State Electrochem. **2** (1998) 355–361.

[74] A.R. Elkais, M.M. Gvozdenović, B.Z. Jugović, B.N. Grgur, The influence of thin benzoate-doped polyaniline coatings on corrosion protection of mild steel in different environments, Prog. Org. Coat. **76** (2013) 670–676.

[75] D.E. Tallman, G. Spinks, A. Dominis, G.G. Wallace, Electroactive conducting polymers for corrosion control, J. Solid State Electrochem. **6** (2002) 73–84.

[76] L. Duić, Z. Mandić, Counter-ion and pH effect on the electrochemical synthesis of polyaniline, J. Electroanal. Chem. **335** (1992) 207–221.

[77] H. Tang, A. Kitani, M. Shiotani, Effects of anions on electrochemical formation and overoxidation of polyaniline, Electrochim. Acta **41** (1996) 1561–1567.

[78] J. Lippe, R. Holze, The anion-specific effect in the overoxidation of polyaniline and polyindoline, J. Electroanal. Chem. **339** (1992) 411–422.

[79] V. Kertez, G. Inzelt, S. Pruneanu, E. Csaho, È. Lora, Electrochemical quartz crystal microbalance study of the influence of the solution composition on the behaviour of poly(aniline) electrodes, Electrochem. Commun. **43** (1998) 2305–2323.

[80] L. Mattoso, R. Faria, L. Bulhoes, A. MacDiarmid, Influence of electropolymerization conditions on the molecular weight of polyaniline, Polymer **35** (1994) 5104––5108.

[81] S. Zhou, T. Wu, J. Kan, Effect of methanol on morphology of polyaniline, Eur. Polym. J. **43** (2007) 395–402.

[82] S.H. Cho, S.K. Tae, L.J. Ypoung, Recent Advances in Polypyrrole, in: Conducting Polymers-Theory, Synthesis, Properties and Characterization, T. Skotheim, J. Reynolds, Eds., Teyor & Francis Group, 2007, pp. 1–87.

[83] T. Vernitskaya, O. Efimov, Polypyrrole: a conducting polymer; its synthesis, properties and applications, Russ. Chem. Rev. **66** (1997) 443–457.

[84] S. Carquigny, O. Segut, B. Lakard, F. Lallemand, P. Fievet, Effect of electrolyte solvent on the morphology of polypyrrole films: Application to the use of polypyrrole in pH sensors, Synth. Met. **158** (2008) 453–461.

[85] G.S. Akundy, J.O. Iroh, Polypyrrole coatings on aluminum – synthesis and characterization, Polymer **42** (2001) 9665–9669.

[86] N. Krstajić, B. Grgur, S. Jovanović, M. Vojinović, Corrosion protection of mild steel by polypyrrole coatings in acid sulfate solutions, Electrochim. Acta **42** (1997) 1685–1691.

[87] J. Nie, D.E. Tallman, G.P. Bierwagen, The electrodeposition of polypyrrole on Al alloy from room temperature ionic liquids, J. Coatings Technol. Res. **5** (2008) 327–334.

[88] S. Jovanović, R. Stanković, V. Laninović, G. Nestorović, M. M. Popović, B. Vidić, O. Pavlović, N. Krstajić, B.N. Grgur, S. Stanković, Synthesis and electrochemical properties of polypyrrole, polyaniline and poly-3-methyl thiophene, Hem. Ind. **54** (2000) 417–427.

[89] W. Su, J.O. Iroh, Electropolymerization of pyrrole on steel substrate in the presence of oxalic acid and amines, Electrochim. Acta **44** (1999) 2173–2184.

[90] C. Ferreira, S. Aeiyach, J. Aaron, P.C. Lacaze, Electrosynthesis of strongly adherent polypyrrole coatings on iron and mild steel in aqueous media, Electrochim. Acta **41** (1996) 1801–1809.

[91] I.L. Lehr, S.B. Saidman, Characterisation and corrosion protection properties of polypyrrole electropolymerised onto aluminium in the presence of molybdate and nitrate, Electrochim. Acta **51** (2006) 3249–3255.

[92] S. Dong, J. Ding, Study on polypyrrole film by electrochemical polymerization in aqueous solution, Synth. Met. **20** (1987) 119–124.

[93] M. Deepa, S. Ahmad, Polypyrrole films electropolymerized from ionic liquids and in a traditional liquid elec-

trolyte: A comparison of morphology and electro–optical properties, Eur. Polym. J. **44** (2008) 3288–3299.

[94] M. Kiani, G. Mitchell, The role of the counter-ion in the preparation of polypyrrole films with enhanced properties using a pulsed electrochemical potential, Synth. Met. **48** (1992) 203–218.

[95] M. Kiani, N. Bhatt, F. Davis, G. Mitchell, Highly anisotropic electrically conducting films based on polypyrrole, Polymer **33** (1992) 4113–4120.

[96] T. Shimadzu, A. Ohtani, K. Honda, Charge-controllable poly pyrrole/poly electrolyte composite membranes: Part III. Electrochemical deionization system constructed by anion-exchangeable and cation-exchangeable polypyrrole electrodes, J. Electroanal. Chem. **251** (1988) 323-337.

[97] K. Zhong, K. Doblhofer, Polypyrrole-based electrode coatings switchable electrochemically between the anion- and cation-exchanger states, Electrochim. Acta **35** (1990) 1971–1976.

IZVOD

ELEKTROHEMIJSKA SINTEZA ELEKTROPROVODNIH POLIMERA

Milica M. Gvozdenović[1], Branimir Z. Jugović[2], Jasmina S. Stevanović[3], Branimir N. Grgur[1]

[1]*Tehnološko–metalurški fakultet, Univerzitet u Beogradu, Beograd, Srbija*
[2]*Institut tehničkih nauka Srpske akademije nauka i umetnosti, Beograd, Srbija*
[3]*Institut za hemiju tehnologiju i metalurgiju, Univerzitet u Beogradu, Beograd, Srbija*

(Pregledni rad)

Tradicionalno shvatanje o polimerima kao odličnim izolatorima izmenjeno je sedamdesetih godina prošlog veka kada su naučnici uspeli da sintetizuju poiliacetilen čija je provodljivost bila bliska metalnoj. Ova činjenica ukazala je na novo svojstvo polimernih materijala i lansirala potpuno novo multidisciplinarno naučno polje, popularno nazvano, sintetički metali. Iako je danas pojmom elektroprovodnih polimera obuhvaćena velika grupa jedinjenja koja su klasifikovana prema prirodi prenosioca naelektrisanja, naziv elektroprovodni polimeri se najčešće koristi u literaturi upravo za polimerne materijala iz grupe sintetičkih metala koji poseduju elektronsku provodljivost kao posledicu specifičnosti molekulske strukture. Pored zahteva molekulske structure, koja podrazumeva konjugovani sistem dvostrukih veza, za provodljivost elektroprovodnih polimera neophodno je dopovanje. Termin dopovanje, iako preuzet iz terminologije klasičnih neorganskih poluprovodnika, podrazumeva u mnogome drugačiji proces. Dopovanje elektroprovodnih polimera podrazumeva oksidaciju tokom koje se, u cilju održavanja elektroneutralnosti polimernog lanca, uvodi stehiometrijska količina jona (anjona). Terminom dopovanje obuhvaćena je i protonacija polimernog lanca kiselinom, u slučaju polianilina, a nedavno je potvrđena i u slučaju polipirola. Kako je, na ovaj način, uvedena velika količina jona izmenjenja je polazna struktura elektroprovodnog polimera, tako da svojstva nastalog materijala zavise u velikoj meri od svojstava dopanta. Iako su na početku razvoja ove oblasti, elektroprovodni polimeri bili sintetizovani hemijskim postupcima, sticanjem uvida u mehanizam hemijske sinteze koja podrazumeva oksidativnu radikalnu polimerizaciju, postalo je jasno da se ovi materijali mogu dobiti i elektrohemijskim postupcima. Elektrohemijska sinteza ima prednosti, pošto se polimer dobija oksidacijom na elektrodama (anodama), čime je izbegnuta upotreba oksidacinog sredstva i omogućena veća čistoća proizvoda. Sa druge strane, elektroprovodni polimer je u većini slučajeva dobijen u obliku prevlake na elektrodi, pa je njegova dalja karakterizacija elektrohemijskim tenikama olakšana. Interesovanje za oblst sinteze elektroprovodnih polimera ne jenjava, pa je ovaj tekst posvećen osnovnim principima elektrohemijskih postupaka sinteze sa posebnim osvrtom na najpopularnije elektroprovodne polimere, polianilin i polipirol.

Ključne reči: elektrohemijska sinteza • anoda • polanilin • polipirol

Glycidyl methacrylate macroporous copolymer grafted with diethylene triamine as sorbent for Reactive Black 5

Zvjezdana P. Sandić[1], Marija J. Žunić[2], Danijela D. Maksin[3], Aleksandra D. Milutinović-Nikolić[2], Aleksandar R. Popović[4], Dušan M. Jovanović[2], Aleksandra B. Nastasović[5]

[1]*University of Banja Luka, Faculty of Science, Banja Luka, Bosnia and Herzegovina (Republic of Srpska)*
[2]*University of Belgrade, ICTM – Department of Catalysis and Chemical Engineering, Belgrade, Serbia*
[3]*University of Belgrade, Vinča Institute of Nuclear Sciences, Department of Chemical Dynamics and Permanent Education, Belgrade, Serbia*
[4]*University of Belgrade, Faculty of Chemistry, Belgrade, Serbia*
[5]*University of Belgrade, ICTM – Department of Chemistry, Belgrade, Serbia*

Abstract

In this paper, macroporous glycidyl methacrylate and ethylene glycol dimethacrylate copolymer functionalized with diethylene triamine (PGME-deta), was evaluated as Reactive Black 5 (RB5) sorbent. Batch RB5 removal from aqueous solution by PGME-deta was investigated by varying pH, contact time, sorbent dosage, initial dye concentration and temperature. The sorption is pH sensitive having maximum at pH 2 (dye removal of 85%), decreasing with the increase of pH (dye removal of 24% at pH 11) after 60 min. Sorption kinetics was fitted to chemical-reaction and particle-diffusion models (pseudo-first-, pseudo-second-order, intraparticle diffusion and Mckay models). The pseudo-second-order kinetic model accurately predicted the RB5 amount sorbed under all investigated operating conditions, while the intraparticle diffusion was the dominant rate-limiting mechanism. The diffusion mechanism was more prevalent with the decrease in temperature and the increase in concentration. The isotherm data was best fitted with the Langmuir model, indicating homogeneous distribution of active sites on PGME-deta and monolayer sorption, with the maximum sorption capacity of 353 mg g^{-1}. The calculated sorption rates improved with increasing temperature and an activation energy close to 40 kJ mol^{-1} was determined, suggesting that chemisorption was also rate-controlling.

Keywords: Reactive Black 5, macroporous crosslinked copolymer, diethylene triamine, kinetic modeling, equilibrium study.

Available online at the Journal website: http://www.ache.org.rs/HI/

Polymers

SCIENTIFIC PAPER

UDC 677.027.4:678–13:547:66

Hem. Ind. **68** (6) 685–699 (2014)

doi: 10.2298/HEMIND140127023S

Surface and groundwater pollution by industrial waste is widespread in highly industrialized countries due to direct discharge of such effluents into water bodies or by precipitation of air-borne pollutants into surface waters [1]. In general, dyes are the most easily detected pollutants in the industrial effluents since they are innately highly visible, meaning that concentrations as low as 0.005 mg dm^{-3} will seize the attention of public [2]. There is a variety of synthetic dyes appearing in the effluents of wastewaters in numerous industries such as textiles, leather, paper-making, plastics, food, rubber, pharmaceuticals and cosmetics with annual production of 7×10^8 kg [3]. Reactive dyes, the most frequently used due to their bright colors, excellent colorfastness and ease of application pose a serious threat to human health due to their carcinogenic, mutagenic and toxicological effects on organisms [4]. The presence of small amounts of dyes in water blocks the passage of light and significantly affects photosynthetic activity in aquatic life [5]. The current estimation is that 2% of dyes are discharged directly in aqueous effluents during the production process of these dyes [6].

Methods for dye removal from dye-containing industrial effluents generally include chemical (oxidative processes, use of Fenton's reagent, ozonation, photochemical and electrochemical destruction), physical (sorption, membrane filtration and electrokinetic coagulation) and biological methods (decolorization by microbial cultures and sorption by living/dead microbial biomass) [6]. Sorption techniques have gained favor recently due to their efficiency for the removal of persistent pollutants unaffected by the conventional methods. Decolorization is the result of two mechanisms: sorption and ion exchange [7], influenced by dye/sorbent interaction, sorbent surface area, particle size, temperature, pH, and contact time [8]. A wide variety of sorbents, like activated carbon and bone char [6,9], beet pulp carbon [10], clay and peat [6], fly ash

Correspondence: A. Nastasović, University of Belgrade, Institute of Chemistry, Technology and Metallurgy, Center for Chemistry, Njegoševa 12, 11000 Belgrade, Serbia.
E-mail: anastaso@chem.bg.ac.rs; anastasovic@yahoo.com
Paper received: 27 January, 2014
Paper accepted: 18 March, 2014

[11], chitin/chitosan [12,13], synthetic polymers [3] and others have been suggested for textile dye removal from wastewaters. Polymeric sorbents have been increasingly investigated as a potential alternative to activated carbon due their controllable pore structure, stable physical and chemical properties, as well as their ability to be regenerated and reused [14]. Macroporous hydrophilic copolymers based on glycidyl methacrylate, GMA, produced by radical suspension copolymerization as regular beads of required size and porosity are very attractive, since the epoxy group can be easily transformed under mild reaction conditions into amino, iminodiacetate, thiol, azole and pyrazole, pyridine groups, etc. The porous structure of these copolymers can be controlled and optimized by adjusting the reaction mixture composition [15]. Amino-functionalized GMA-based macroporous copolymers proved to be very useful for sorption of heavy and precious metals [16], radionuclides [17] and textile dyes [3,18,19].

In this paper, macroporous copolymer of GMA and ethylene glycol dimethacrylate, EGDMA (PGME) additionally functionalized via ring-opening reaction of the pendant epoxy groups with diethylene triamine (PGME--deta), was tested as Reactive Black 5 (RB5) sorbent. The effects of the pH, sorbent dosage, contact time and temperature on the sorption properties of PGME-deta in RB5 removal from aqueous solutions were studied in order to evaluate this material as a potential dye wastewater sorbent. Sorption kinetic data were analyzed using four kinetic models (pseudo-first, pseudo-second--order, intraparticle diffusion and Mckay models) to determine the best fit equation for RB5 sorption by amino-functionalized PGME.

MATERIALS AND METHODS

Materials

All the chemicals used for copolymer synthesis were analytical grade products and used as received: glycidyl methacrylate (Aldrich, Germany), ethylene glycol dimethacrylate (Aldrich, Germany), diethylene triamine (Sigma-Aldrich Chemie GmbH, Germany), 2,2'-azobis-iso-butyronitrile, AIBN (Aldrich, Germany), poly(*N*-vinyl pyrrolidone) (Kolidon 90, BASF, Fine chemicals, Switzerland), cyclohexanol (Sigma-Aldrich Chemie GmbH, Germany) and dodecanol (Sigma-Aldrich Chemie GmbH, Germany). Synthetic textile dye, Reactive Black 5 (Alfa--Aesar, USA) having chemical purity of *ca*. 55% was used without further purification as test dye.

Methods

The epoxy group content in the synthesized PGME was determined by HCl–dioxane method [20]. The amino-functionalized sample was analyzed for carbon, hydrogen and nitrogen content using the Vario EL III device (GmbH Hanau Instruments, Germany). The degree of conversion of the epoxy groups and the amino group concentration in PGME-deta were calculated from elemental analysis data. The pore size distribution was determined by mercury porosimetry (Carlo Erba 2000, Milestone 200 software). The sample was dried at 323 K for 8 h and degassed at room temperature and pressure of 0.5 Pa for 2 h.

The pH drift method [21] was used to determine the pH at point zero charge (pH_{PZC}) of the PGME-deta surface using 20 cm^3 of 0.01 M NaCl in a series of Erlenmeyer flasks, where the pH values were adjusted using 0.1 M NaOH and 0.1 M HCl in the range between 2 and 12 with a Jenway 3320 pH meter. The initial pH of the solutions (pH_i) was determined and 50.0 mg of the polymer was added to each of the flasks. The mixtures were shaken for 24 h and the final pH values of the solutions (pH_f) were measured. pH_{PZC} was recorded as the pH value in which the initial pH equals the final pH [22].

Preparation of poly(GMA-co-EGDMA) and functionalization with diethylene triamine

Macroporous PGME sample was prepared by radical suspension copolymerization of GMA and EGDMA, in the presence of inert component (90 mass% of cyclohexanol and 10 mass% dodecanol) as described previously [23]. Particles with diameters in the range 0.15––0.30 mm were functionalized with diethylene triamine. A mixture of 3.6 g of PGME, 15.7 g of diethylene triamine and 100 cm^3 of toluene was left at room temperature for 24 h then heated at 353 K for 6 h. The modified sample was filtered, washed with ethanol, dried and labeled as PGME-deta (additional label -deta designates sample functionalized with diethylene triamine) [24].

Dye sorption experiments

The sorption of RB5 by PGME-deta was investigated in aqueous solutions in batch mode, either in a thermostated shaker (Memmert WNE 14 and SV 1422) or in a Pyrex beaker (thermostated by Julabo F 25 with circular heater and cooler) which was equipped with a magnetic stirrer. The same volume of the solution (50.0 cm^3) was used in all the experiments. The effects of pH and sorbent dosage were investigated at the initial dye concentration c_0 = 50 mg dm^{-3} and room temperature (298 K) using magnetic stirring. The pH value was adjusted by addition of the appropriate amounts of 1 M HCl or 1 M NaOH.

Magnetic stirring was also used for the investigation of the influence of the initial dye concentration (c_0, 30––150 mg dm^{-3}) at 298 K. For contact time studies the samples were taken at predetermined time intervals (10, 20, 30, 60, 120, 180 min and 24 h). The effect of temperature on the sorption was evaluated with the selected initial dye concentrations (c_0, 50–90 mg dm^{-3})

at four different temperatures (288, 298, 308 and 318 K), up to 24 h.

Sorption isotherms were obtained in the shaker, by placing 25.0 mg of copolymer in contact with a series of RB5 solutions in the concentration range 175–1500 mg dm^{-3}, at room temperature and unadjusted pH. Equilibrium time was 24 h.

The amount of dye sorbed by the sorbent at time *t*, Q_t (mg g^{-1}), was calculated by the following mass balance relationship:

$$Q_t = \frac{(c_0 - c_t)V}{m} \quad (1)$$

Where: c_t is dye solution concentrations (mg dm^{-3}) after sorption time *t*, *V* is the volume of the aqueous phase (dm^3) and *m* is the amount of the PGME amino-functionalized beads used for the experiment (g).

The solution samples were withdrawn at the specified time intervals, dye solution was centrifuged and the absorbance of the supernatant solution was measured. The spectra were obtained using Thermo Electron Nicolet Evolution 500 UV–Vis spectrophotometer and the absorption peak of RB5 at 597 nm was chosen for monitoring the sorption process.

Standard statistical methods were applied to calculate the mean values and standard deviations for each set of data. All experiments were repeated in triplicate or more if necessary. Relative standard deviations were less than or equal to 5%.

RESULTS AND DISCUSSION

Characterization of sorbents

Relevant physicochemical characteristics of amino-functionalized copolymer sample PGME-deta are given in Table 1. The degree of conversion of 40% was expected, since similar values were already obtained for reaction with ethylene diamine (50%), and triethylene tetramine (31%) [24].

Table 1. Relevant characteristics of amino-functionalized copolymer sample PGME-deta [18]

Property	Value
$S_{s,Hg}$ / m^2 g^{-1}	53
V_S / cm^3 g^{-1}	0.635
$D_{V/2}$ / nm	59
D_{av} / nm	50
Degree of conversion of epoxy groups, %	40
Ligand concentration, mmol g^{-1}	1.67
Amino group concentration, mmol g^{-1}	5.01

The porosity parameters, *i.e.*, the values of specific pore volume (V_s) average pore diameter (D_{av}) and pore diameter which corresponds to half of pore volume ($D_{V/2}$) were read from the pore size distribution curves, while the specific surface area ($S_{s,Hg}$) was calculated as the sum of incremental specific surface areas from the pore size distribution curves as described in the literature [25].

Effect of pH

The initial pH of the sorbate/sorbent system is a critical process parameter because the aqueous chemistry and the surface binding sites of the sorbent are dependent on the pH value of the mixture. The sorption of dye ions on the sorbent surface is primarily influenced by the surface charge of the sorbent, which in turn is influenced by the solution pH. The effect of the solution pH on the dye uptake can be rationalized on the basis of pH_{PZC} of the copolymer [26]. pH_{PZC} by definition is the value of pH when the overall charge on the sorbent surface is zero. This is a convenient indicator of either positive or negative charge of the sorbent surface as a function of pH. When the pH value of the mixture of PGME-deta and RB5 solution is lower than pH_{PZC}, it means that the sorbent surface is positively charged. If the pH of the mixture is higher than pH_{PZC}, the surface would be negatively charged.

The RB5 dye is an acidic dye with a complex molecule (Scheme 1) that consists of two benzene rings and one naphthalene ring, incorporating two azo (chromophore) groups, accountable for the coloring, and auxochrome and anti-auxochrome groups (sulpho, amino, hydroxyl, methyl, etc.), which contribute to the richness of the color [27]. Two sulfonate groups and another two sulfatoethylsulfone group are negatively charged even in very acidic solutions, as a result of their $pK_a < 0$ [28].

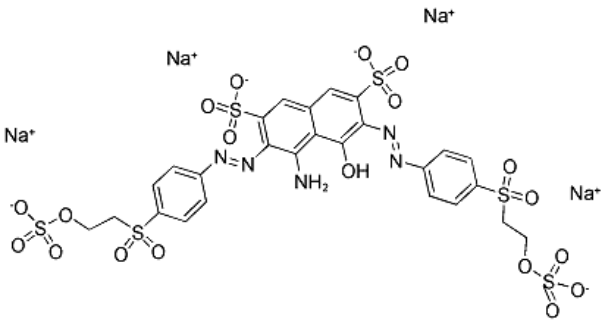

Scheme 1. Structure of RB5 dye in aqueous solution.

The effect of pH on the RB5 sorption by PGME-deta and the pH_{PZC} of PGME-deta is shown in Fig. 1. The size of the dye molecules and its ability to form negatively charged species have an effect on its sorption from solution onto the sorbent [1]. The pH values in this experiment were varied between 2 and 11, keeping other parameters constant. The pH_{PZC} of PGME-deta determined by the pH drift method was approximately 7.7

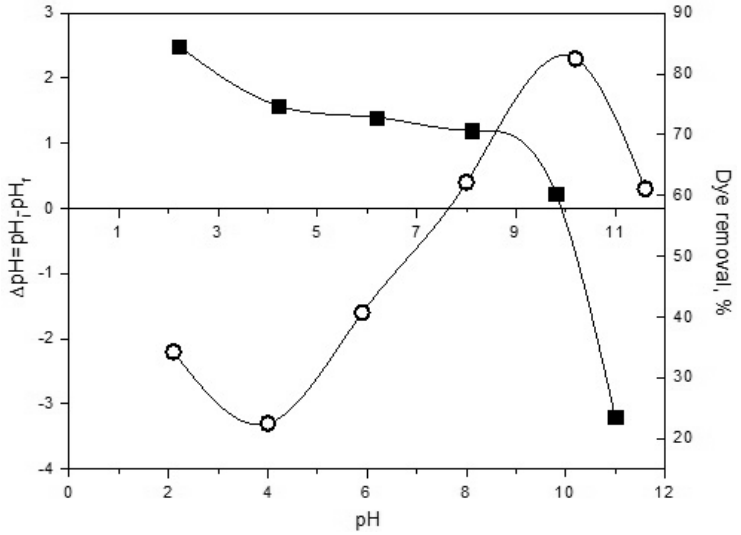

Figure 1. Effect of pH on the RB5 sorption by PGME-deta and pH_{PZC} measurement of PGME-deta (c_0 = 50 mg dm^{-3}, T = 298 K, t = 60 min); dye removal – black squares; ΔpH – white circles.

(Fig. 1). Consequently, at acidic pH values, there is attraction between the PGME-deta particle with its protonated amino groups and the negative RB5 dye ion. As long as the RB5 solution pH < pH_{PZC}, its surface would bring an overall positive charge. However, there is significant dye removal at pH < pH_{PZC}. Accordingly, electrostatic attraction mechanism must be included as a significant but not the only factor in RB5 sorption by PGME-deta. Özcan and Özcan previously established that at strongly acidic pH values exists a major electrostatic attraction between the positively charged sorbent surface and anionic dyes [29]. In contrast, negatively charged sorbent surface sites do not promote the sorption of dye anions, due to the electrostatic repulsion. In a highly acidic solution (pH 2), a high concentration of positively charged protonated amino groups exists on the surface of PGME-deta, and interaction occurs with four negatively charged sulfonic groups of RB5 (85% dye removal). At pH values around 11, negatively charged hydroxyl ions compete with the dye resulting in the inhibition of RB5 sorption on PGME-deta surface and a low percent removal was noted (24%). The exceptionally slow decrease in dye removal in the pH range of 4–8 (from 75 to 71%) might be associated with the fact that the sorption mechanisms above mentioned are affected indistinctively by a change of pH in this region [22]. The pK_a value of amine groups typically lies within the range 8–11 [30], implying that the amine groups are fully protonated at pH < 5 and that the extent of protonation slowly decreases with the increase in pH, accounting for the phenomenon. It is very likely that predominantly hydrogen bonds are being formed between dye molecules and neutral amino groups at pH values higher than 8 [17,30].

Considering that the main goal of this research was synthesis of a sorbent for purification of the dye production industry wastewaters which already have fluctuating pH values, pH adjustment of the working solution would mean an additional operation which would increase the procedure cost and cause an ecological problem. Therefore, the further sorption investigations were carried out at the unadjusted pH value of 5.5, being less efficient but satisfactory. The usual pH values in surface water systems fall between 6.5 and 8.5 and for groundwater systems between 6 and 8.5 [31], thus these conditions appear to be quite close to optimal for effluent treatment due to the near neutral pH of the final discharge after sorption.

Effect of sorbent dosage

In order to determine the optimal quantity of PGME-deta required for RB5 sorption, the influence of sorbent dosage and sorption capacity after 60 min (Q_{60}) on dye removal was investigated at room temperature and presented in Figure 2.

As can be seen, the RB5 removal was observed to be dependent on the PGME-deta dosage. The percent of dye removal sharply increased from 0.1 up to 1.0 g dm^{-3}, and for higher sorbent doses it reached the plateau of 100% dye removal. In contrast, as expected due to the variation in the concentration gradient, the sorption uptake increased with decreasing PGME-deta dosage, and the maximum sorption capacity of 86 mg g^{-1} was obtained for 0.1 g dm^{-3}. The increase of percent dye removal with the increased sorbent dosage can be ascribed to the enhanced sorbent surface area and the availability of more sorption sites with the increase of sorbent content, thus leading to a higher interaction between PGME-deta particles and RB5 molecules [32]. For further experiments, the mass of 25.0 mg, *i.e*., the dose of 0.5 g dm^{-3} of PGME-deta was chosen for the

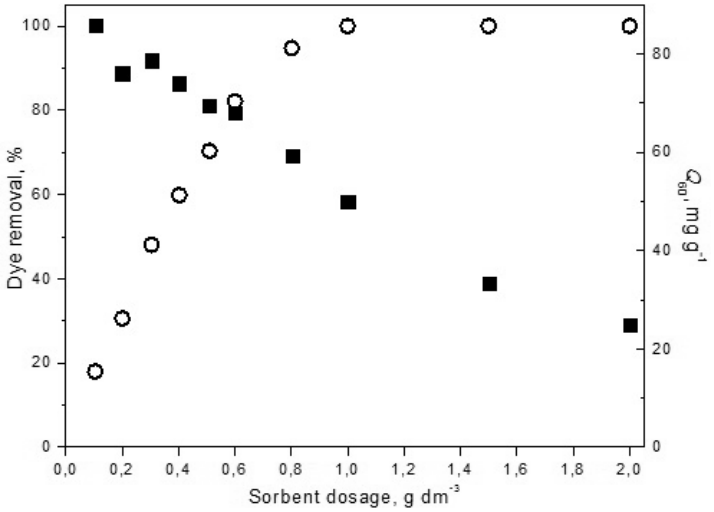

Figure 2. Effect of sorbent dosage on RB5 sorption by onto PGME-deta (pH 5.5, c_0 = 50 mg dm^{-3}, T = 298 K, t = 60 min); dye removal – white circles; Q_{60} – black squares.

purpose of comparison with previous results and reducing the cost of the potential practical application [18].

Effect of contact time

Since dye sorption is a time-dependent process, the effect of contact time on the amount of RB5 sorbed by PGME-deta (Figure 3) was investigated.

The rate of RB5 removal by PGME-deta was high initially and the process then gradually slowed down. The time profile of dye sorption by PGME-deta was a single continuous curve leading to saturation, suggesting the possible monolayer coverage of RB5 on the sorbent surface [33]. With the increased initial concentrations the saturation was reached at prolonged sorption times. For c_0 = 30 and 50 mg dm^{-3}, the sorption equilibrium was reached after 180 min, while for the higher initial concentrations the time necessary for equilibrium attainment was prolonged to 24 h.

As an illustration, in Table 2 are presented the data on removal efficiency (*RE*) for selected initial concentrations.

Table 2. Removal efficiency (%) for indicated RB5 initial concentrations at 298 K

t / min	c_0 / mg dm^{-3}			
	30	50	70	130
60	90	82	78	66
120	99	97	94	82
180	100	100	99	95

Effect of temperature

Kinetic studies were also carried out at different temperatures (288–318 K) and the sorption process was found to accelerate with increasing temperature

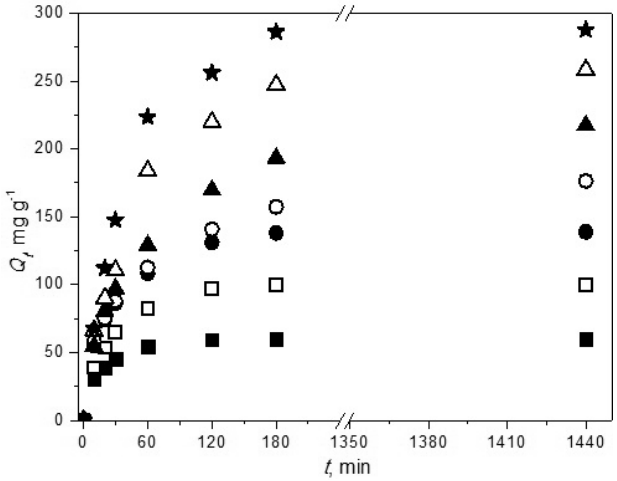

Figure 3. Effect of contact time on RB5 sorption by PGME-deta at different initial concentrations (0.5 g dm^{-3}, pH 5.5, T = 298 K); 30 mg dm^{-3} – black squares; 50 mg dm^{-3} – white squares; 70 mg dm^{-3} – black circles; 90 mg dm^{-3} – white circles; 110 mg dm^{-3} – black triangles; 130 mg dm^{-3} – white triangles; 150 mg dm^{-3} – black stars.

(Figure 4). It was also observable from the graphs that the half-life of each process decreased with increasing temperature, which verified that the continuing process was of endothermic nature.

As an illustration, the data on RE for the initial concentration of 90 mg dm^{-3} is presented in Table 3. The equilibrium sorption capacity of RB5 on PGME-deta was not at all affected by temperature in the investigated concentration range (50–90 mg dm^{-3}), inside the experimental error. However, for higher temperatures the equilibrium sorption capacity was achieved faster. It should be noted that 100% RE was achieved for all three initial concentrations at all four temperatures within 24 h.

Table 3. Removal efficiency (%) for RB5 at different temperatures for initial concentration of 90 mg dm^{-3}

t / min	T / K			
	288	298	308	318
60	60	64	79	80
120	79	80	97	97
180	93	89	100	100

Sorption dynamics

The sorption kinetics is essential for implementation since it controls the overall process efficiency and provides insight into sorption mechanism.

Surface reaction-based models

Since the pseudo-first (PFO) and the pseudo-second-order (PSO) kinetic models are the most commonly used to determine kinetic parameters of sorption processes for various solute/sorbent combinations, the kinetic data in this study were treated with both models [34,35]. The integrated rate laws for pseudo-first-order and pseudo-second-order reactions in linear form are presented in Eqs. (2) and (3), respectively:

$$\log\left(Q_\mathrm{e} - Q_t\right) = \log Q_\mathrm{e} - \frac{k_1 t}{\ln 10} \tag{2}$$

$$\frac{t}{Q_t} = \frac{1}{k_2 Q_\mathrm{e}^2} + \frac{1}{Q_\mathrm{e}} t \tag{3}$$

$$h = k_2 Q_\mathrm{e}^2 \tag{4}$$

where Q_t is the amount of sorbed dye (mg g^{-1}) at any time t, Q_e is the amount of sorbed dye at equilibrium (mg g^{-1}), k_1 is the PFO rate constant (min^{-1}), k_2 is the PSO rate constant (g mg^{-1} min^{-1}), h (defined by Eq. (4)) is initial sorption rate from PSO model (mg g^{-1} min^{-1}).

The values for Q_e, k_1 and k_2, h, as well as the corresponding coefficients of determination (R^2) for each initial dye concentration are presented in Table 4 and for each temperature in Table 5. The values for k_1 were calculated from the plots of $\log(Q_\mathrm{e} - Q_t)$ *vs*. t for each initial dye concentration, while k_2 and h were calculated from the t/Q_t *vs*. t plot. The compliance of experimental data with the model-predicted values was judged against the R^2 values. Also, the values of Q_e obtained from the experimental data were compared with those calculated from PFO and PSO reaction kinetic plots.

Table 4 illustrates that k_1 and k_2 changed with variation in concentration of the dye in solution. However, according to the Arrhenius equation the rate constant of a reaction changes only with change in temperature kinetics, and it never varies with differing concentrations of reactant species [36]. PSO generated higher R^2 values (≥0.999) than PFO model for all investigated concentrations and temperatures and the predicted values of $Q_\mathrm{e}^{\mathrm{calc}}$ agreed well with the experimental values. From this it can be inferred that the kinetics of this sorbate/sorbent system is accurately described by this model at all time intervals, indicating that the sorption rate is controlled by both the sorbent capacity and the sorbate concentration.

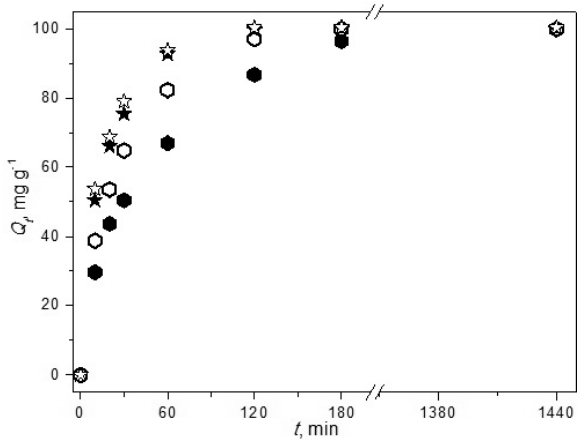

Figure 4. Effect of contact times of RB5 sorption by PGME-deta at different sorption temperatures (0.5 g dm^{-3}, pH 5.5, c_0 = 50 mg dm^{-3}); 288 K – black hexagons; 298 K – white hexagons; 308 K – black stars; 318 K – white stars.

Table 4. Kinetic parameters for RB5 sorption using PGME-deta at different initial dye concentration

c_i / mg L^{-1}	30	50	70	90	110	130	150
Q_e / mg g^{-1}	60.03	99.91	138.89	176.51	217.42	258.29	287.84
PFO							
k_1 / min^{-1}	0.03963	0.02549	0.02593	0.01123	0.01143	0.01663	0.02623
Q_e^{calc} / mg g^{-1}	51.41	80.97	124.66	137.27	184.20	237.59	316.542
R^2	0.9938	0.9908	0.9861	0.9731	0.9878	0.9903	0.9466
PSO							
$k_2 \times 10^3$ / g mg^{-1} min^{-1}	2.395	0.8254	0.5152	0.1898	0.1258	0.1230	0.2500
h / mg g^{-1} min^{-1}	8.723	8.397	10.15	6.156	6.247	9.054	21.14
$t_{1/2}$ / min	6.9	12.0	13.8	29.3	35.7	29.1	13.8
Q_e^{calc} / g g^{-1}	60.35	100.86	140.37	180.08	222.87	263.92	290.78
R^2	0.9999	0.9999	0.9999	0.9999	0.9990	0.9996	0.9999
Intraparticle							
k_{1id} / mg g^{-1} $min^{-0.5}$	7.806	11.28	13.56	13.16	15.52	22.01	27.12
c_{1id} / mg g^{-1}	0	0	0	0	0	0	0
R^2	0.9839	0.9953	0.9779	0.9789	0.9928	0.9918	0.9911
k_{2id} / mg g^{-1} $min^{-0.5}$	Not applicable	Not applicable	Not applicable	Not applicable	Not applicable	11.17	11.02
c_{2id} / mg g^{-1}	–	–	–	–	–	97.29	137.35
R^2	–	–	–	–	–	0.9999	0.9946
McKay							
S / min^{-1}	0.0397	0.0282	0.0259	0.0112	0.0114	0.0166	0.0262
R^2	0.9938	0.9947	0.9861	0.9731	0.9878	0.9903	0.9466

Table 5. Kinetic parameters for RB5 sorption using PGME-deta at different temperatures

T / K	288			298			308			318		
c_i / mg L^{-1}	50	70	90	50	70	90	50	70	90	50	70	90
Q_e / mg g^{-1}	100.00	139.94	179.76	99.91	138.89	176.51	99.97	140.50	179.64	100.25	137.65	177.11
PFO												
k_1 / min^{-1}	0.01719	0.014603	0.01359	0.02549	0.02593	0.01123	0.04609	0.03450	0.02817	0.04359	0.03632	0.03468
Q_e^{calc} / mg g^{-1}	88.65	125.94	160.62	80.97	124.66	137.27	92.82	119.50	168.21	82.46	121.01	190.35
R^2	0.9906	0.9917	0.9857	0.9908	0.9861	0.9731	0.9952	0.9794	0.9916	0.9824	0.9912	0.9825
PSO												
$k_2 \times 10^3$ g mg^{-1} min^{-1}	0.4051	0.2270	0.1625	0.8254	0.5152	0.1898	1.5564	0.8593	0.3925	1.8039	0.8696	0.4395
h / mg g^{-1} min^{-1}	4.197	4.653	5.508	8.397	10.15	6.156	15.71	17.19	12.95	18.29	16.70	14.06
$t_{1/2}$ / min	24.3	30.8	33.4	12.0	13.8	29.3	6.4	8.2	14.0	5.5	8.3	12.7
Q_e^{calc} / g g^{-1}	101.79	143.16	184.09	100.86	140.37	180.08	100.48	141.42	181.62	100.69	138.56	178.89
R^2	0.9998	0.9996	0.9998	0.9999	0.9999	0.9999	0.9999	0.9999	0.9998	0.9999	0.9999	0.9998
Intraparticle												
k_{1id} / mg g^{-1} $min^{-0.5}$	7.918	10.60	13.14	11.28	13.56	16.71	13.21	17.13	19.20	13.63	17.46	20.69
c_{1id} / mg g^{-1}	0	0	0	0	0	0	0	0	0	0	0	0
R^2	0.9880	0.9971	0.9730	0.9953	0.9779	0.8931	0.9858	0.9864	0.9684	0.9805	0.9904	0.9518
McKay												
S / min^{-1}	0.01719	0.01722	0.01359	0.0282	0.0259	0.0112	0.0418	0.0345	0.0282	0.0436	0.0363	0.0291
R^2	0.9906	0.9845	0.9857	0.9947	0.9861	0.9731	0.9864	0.9794	0.9916	0.9824	0.9912	0.9902

It was noted that the value of the rate constant k_2 decreases with increasing initial RB5 concentration (Table 4). With the increase in concentration, the trend becomes more obvious, but then levels of at approx. 110 mg dm^{-3}. The explanation for this behavior can be the lower competition of the dye species for the sorp-

tion surface sites at lower dye concentrations. Decreased sorption rates at higher concentrations result from the heightened competition for the surface active sites [22], except in the case of the formation of dye molecule aggregates, which reduces the effective concentration of the sorbate species in the solution.

Namely, dye ions tend do aggregate or to self-associate in aqueous solutions [37]. The almost complete formation of dimers occurs even at very low dye concentrations (10^{-4}–10^{-6} M) before subsequent aggregation takes place; it happens initially between dimeric units and then proceeds onto higher order aggregation [38]. Szyguła and associates established that the strongly acidic sulphonic groups reacted with the protonated amino groups of chitosan and that the dye removal was higher the greater the number of sulphonic groups in the dyes [27]. Their findings confirmed that in comparison with other sulphonic group-containing dyes, RB5 needed a lower number of amine functionalities for neutralizing sulphonic groups of the dye, in all probability as a result of dye aggregation.

Based on the PSO model the half-life of RB5 sorption by PGME-deta ($t_{1/2}$) is inversely related to the product of the sorption capacity of the sorbent and PSO constant, *i.e*., the initial sorption rate [39]:

$$t_{1/2} = \frac{1}{k_2 Q_e} \tag{5}$$

The $t_{1/2}$ gradually increased from 7 min for c_0 = 30 mg dm^{-3} to 35 min for 110 mg dm^{-3} and then decreased to 29 min for 130 mg dm^{-3} and 14 min for 150 mg dm^{-3} (Table 4), possibly due to dye aggregation at higher concentrations as stated above.

Raising temperature also led to a significant increase in the initial sorption rate (h) and considerable decrease in $t_{1/2}$, being the lowest (5 min) for 50 mg dm^{-3} at 318 K, which may indicate a kinetically controlled process. However, the sorption capacities at 180 min are nearly the same at 288 and 318 K for this concentration, implying the possible presence of other rate-governing processes (Table 5). It is furthermore noteworthy that for 90 mg dm^{-3}, $t_{1/2}$ decreased from 33 min for 288 K to only 13 min at 318 K.

The fitting of parameters of the sorption kinetic data to the PSO kinetic model allows exploration of the temperature effect on the values of the sorption rate constant (k_2). The values for R^2 for RB5 removal by PGME-deta were ≥0.999 indicating that the PSO model is appropriate for description of the effect of the solution temperature on the process kinetics (Table 5). This fact is an additional confirmation that chemisorption was the rate-limiting step, within the confines of the mass transfer in the sorption systems [40]. The k_2 values decreased with the decline in temperature and the half-life of the process was delayed for lower temperatures. This indicates that the RB5 surface sorption step is not the only rate-controlling in the sorption process and that the improvement in the rate of RB5 removal as the temperature increases may be due to the increased movement of the dye molecules as the solution temperature increases, which in turn enhances the RB5 diffusion from the bulk solution to the sorbent external and internal surface [41].

Apparent activation energy of sorption

The activation energy for the RB5/PGME-deta sorption system can be determined from the linearized Arrhenius equation:

$$\ln k_2 = \ln A - \frac{E_a}{RT} \tag{6}$$

where A is the temperature independent factor (frequency factor) (g mmol^{-1} min^{-1}), E_a is the activation energy (kJ mol^{-1}), T is the temperature (K) and R is the universal gas constant equal to 8.314 J mol^{-1} K^{-1}. The $\ln k_2$ *vs*. $1/T$ plot was observed to be linear with acceptable R^2 values for the investigated dye concentrations and E_a values for the studied sorption system were calculated from the slopes. These parameter's values may provide insights into the sorption mechanism. The calculated values of activation energy ranged from 28.3 to 39.2 kJ mol^{-1} for the investigated RB5 concentrations (50–90 mg dm^{-3}). These relatively small values of the activation energy (below 42 kJ mol^{-1}) corroborate the fact that the process of RB5 removal by use of amino-functionalized macroporous PGME is diffusion-controlled, *i.e*., the chemical step is faster in comparison with the mass transfer of RB5 molecules the inside the copolymer pores [42].

Particle diffusion-based models

Recognizing the mechanism of sorption, that is, the reaction at the surface (physical or chemical) as well as the rate controlling mechanism is significant. Generally, when microporous/mesoporous/macroporous sorbents are used, the rate controlling mechanism is strongly dependent on either pore or surface diffusion [9]. In order to determine whether the process rate in the studied sorption system is directed by film or pore diffusion, the intraparticle and Mckay's models were applied:

A classical approach to examine the influence of intraparticle diffusion is plotting the equation [29,43]:

$$Q_t = k_{id} t^{1/2} + c_{id} \tag{7}$$

where k_{id} is the intraparticle diffusion coefficient (mg g^{-1} min$^{-0.5}$), and c_{id} is a constant.

In the case of a linear Q_t *vs*. $t^{1/2}$ plot, and if the line passes through the origin, intraparticle diffusion is the

only rate-controlling step [33]. If not, some other mechanisms are also involved.

Weber and Morris model [43] allows interpretation of intraparticle diffusion (IPD) in 3 different forms [44]: 1) Q_t is plotted against $t^{1/2}$ to obtain a straight line that is forced to pass through the origin [45]; 2) multi-linearity in Q_t *vs*. $t^{1/2}$ plot is taken into account (*i.e.*, 2 or 3 steps are included to follow the whole process) [46]; and 3) Q_t is plotted against $t^{1/2}$ to get a straight line but does not automatically pass through the origin; *i.e*., there is an intercept [47]. In the literature, virtually all the described intercepts are positive, implying that rapid sorption takes place within a short period of time [44].

The first method was used to process the collected data in this study. The plot of the square root of time ($t^{1/2}$) vs. the uptake (Q_t) for the RB5 sorption (Figure 5) resulted in a linear relationship, implying that one of the rate-limiting steps of sorption may be intraparticle diffusion.

There are opinions in the literature that multi-linear Q–$t^{1/2}$ plots might be the consequence of the distinctive phases in intraparticle diffusion. Assorted studies considering sorbents with extensive pore size distribution demonstrated that multi-linear plots might represent the stages of intraparticle diffusion into the macro-, meso- and microporous structure of sorbent [48,49]. The first phase could be assigned to the sorption over the outer surface and in the macropores of polymeric sorbents, rendering it the fastest sorption stage. The second stage could be attributed to the intraparticle diffusion through mesopores, while the third could be regarded as the diffusion through micropores, and, of course, it is followed by the establishment of equilibrium. The third stage might be omitted or combined with the equilibrium attainment phase, if the sorbent in question is macroporous, as is the case with PGME-deta.

The sufficient macro- and mesopores of PGME-deta provided the effective diffusion channels for RB5 to sorption sites and enhanced the sorption kinetics. The diffusion resistance of sorbate in mesopores should be larger than in macropores.

From Figure 5 it can be appreciated that RB5 sorption tends to follow the following stages. The intraparticle diffusion model suggests that the film diffusion (stage 1) is absent from the plot due to completing before 10 min (the first recorded point), and that the final equilibrium sorption (stage 3) started after 120 to 180 min. The linear portion(s) included the intermediate sorption period, representing intraparticle diffusion and binding of RB5 by active sites in PGME-deta particles.

The intraparticle rate constants at different initial concentrations acquired from the slope of the plots were summarized in Table 4. Higher initial concentration gave larger slope. A number of investigations reported previously the variation of intraparticle diffusion rate constant as a normal phenomenon [44] due to the change in diffusion driving force which is strongly dependent on the availability of sorbate per unit mass of the sorbent [50]. High initial k_i values may be attributable to a large number of vacant sites available at the early stage with respect to initial dye concentrations, resulting in an increased concentration gradient between sorbate in solution and sorbate on the sorbent surface. Later on this concentration gradient diminishes due to accumulation of dye particles in the vacant sites, leading to a decrease in sorption rate.

The last portion (after 120–180 min, depending on the initial concentration and temperature, not shown

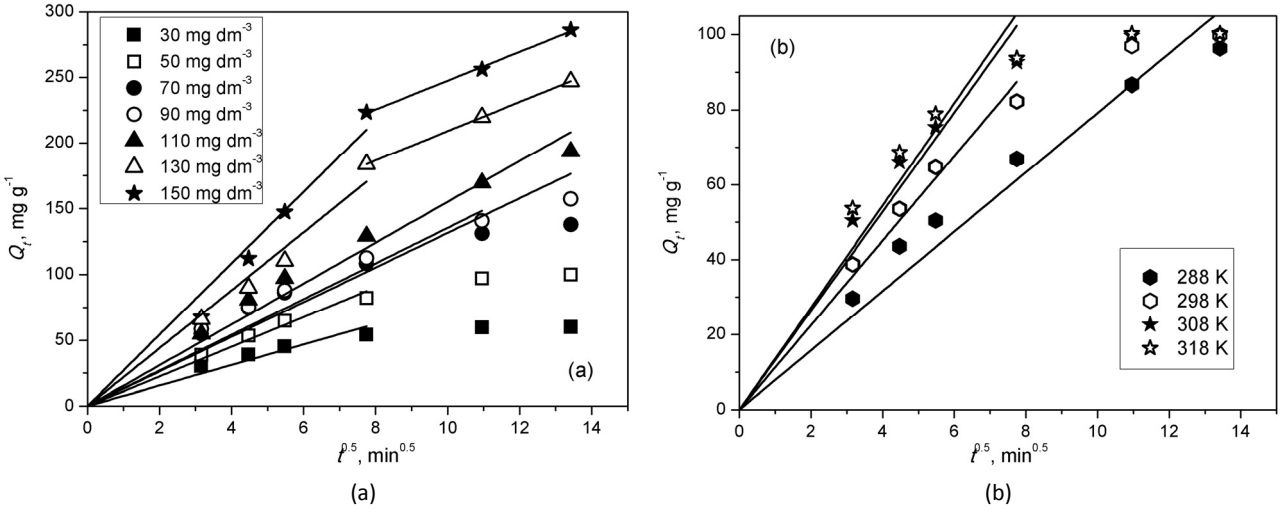

Figure 5. a) Plot of intraparticle diffusion model for sorption of RB5 on PGME-deta for different initial concentrations (30 mg dm^{-3} – black squares; 50 mg dm^{-3} – white squares; 70 mg dm^{-3} – black circles; 90 mg dm^{-3} – white circles; 110 mg dm^{-3} – black triangles; 130 mg dm^{-3} – white triangles; 150 mg dm^{-3} – black stars) and b) temperatures for 50 mg dm^{-3} (288 K – black hexagons; 298 K – white hexagons; 308 K – black stars; 318 K – white stars).

in Figure 5) is the final equilibrium stage where the intraparticle diffusion in micropores begins to decalerate due to the extremely low solute concentration in solution [49]. The calculated R^2 values were high; thus it could be deduced that intraparticle diffusion seemed to be the most significant rate process controlling sorption of RB5 on PGME-deta.

If the external resistance to mass transfer surrounding the particles is dismissed, as has been proposed for other sorbate/sorbent systems [51], the single plotted line will depict macropore and mesopore diffusion for concentrations 30–110 mg dm^{-3} (10–180 min); in the case of two discernible slopes (130 and 150 mg dm^{-3}), the first one will correspond to macropore and the second to mesopore diffusion. The equilibrium is achieved probably through micropore diffusion. For the two above mentioned concentrations, the results showed that the diffusion rates decreased with increasing the contact time. Over time, the pores for diffusion become smaller, because the molecules of the dye diffuse into the inner structure of the sorbents, causing the decrease of the free path for the molecules in the pore as well as pore blockage [9].

Cumulative pore distribution curve for PGME–deta determined by mercury porosimetry is presented in Figure 6. In the case of PGME–deta only two sections are discernible for high initial concentrations (130 and 150 mg dm^{-3}), since there are almost no micropores present in the sample; the fraction surface area of pores 7.5-50 nm in diameter is 46% and from 50–10000 nm is 54%. The fractional uptake of RB5 in the first linear region (macropore) is roughly 43%, and in the second linear region (mesopores) (53%). The remaining 4% can most likely be ascribed to the pores less than 7.5 nm in diameter which are not measurable by mercury porosimetry. Also, it needs to be taken into account that the cut-off value between macropore and mesopore diameter is merely arbitrary and does not reflect the pore size distribution shown in Figure 6.

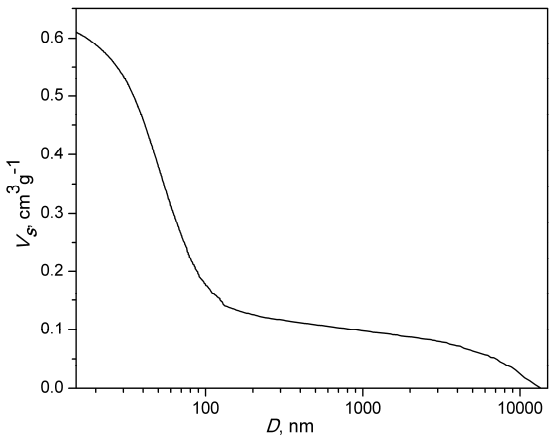

Figure 6 Cumulative pore size distribution curve for sample PGME–deta.

Li and associates determined that the sorption of solute molecules can happen in pore diameters of 1.3––1.8 times the solute molecular width [52]. If a value of 1.6 times the molecular width is presumed, this implies a minimum pore sorbing diameter of 1.37 nm for RB5 as illustrated by Ip and associates [9]. In the case of PGME-deta this threshold value is amply surpassed, seeing that the average pore diameter is 50 nm (Table 1). The specific surface area of PGME-deta is quite low (53 m^2/g, Table 1) in comparison with, *e.g.*, active charcole and zeolites. At lower concentrations, the effect of pore distribution is not pronounced enough to yield two slopes, since the available dye is well below the concentration that instigates aggregation of dye molecules. The findings of Caceres et al. supported the supposition that this result may be due to the magnitude of the sorbent surface area [51].

Further substantiation of the above remark was executed with the help of Mckay's graph based on the equation [53,54]:

$$\log(1-F) = -\left(\frac{S}{2.303}\right)t \tag{8}$$

where F is the fractional attainment of equilibrium at time t (min) and S is the rate parameter [53].

Figure 7 displays typical Mckay's plots at different RB5 concentration and at different temperatures. The log(1 – F) *vs*. t plots were linear ($R^2 \geq 0.97$). The S values calculated from their slopes and the intercepts are presented in Tables 4 and 5. It is remarkable that the linearity is maintained in the whole range of the time axis with intercepts close to 0 for most of the plots and thus can be deduced that the sorption rate of RB5 on PGME--deta is governed mainly by internal transport mechanism, *i.e.*, pore diffusion, with minor influence of film diffusion. Both processes were enhanced with the increase of initial concentration and temperature.

Sorption isotherms

Equilibrium sorption data were fitted into Freundlich and Langmuir equations in order to determine model that is most appropriate to describe obtained results.

The linear form of the Freundlich equation [55] is as follows:

$$\ln Q_e = \ln K_F + \frac{1}{n}\ln c_e \tag{9}$$

Where c_e is the equilibrium dye concentration in solution (mg dm^{-3}), while K_F (mg g^{-1})/(mg dm^{-3})$^{1/n}$) and n are the Freundlich sorption constants characteristic for the system.

The well-known linearized expression of the Langmuir model is [56,57]:

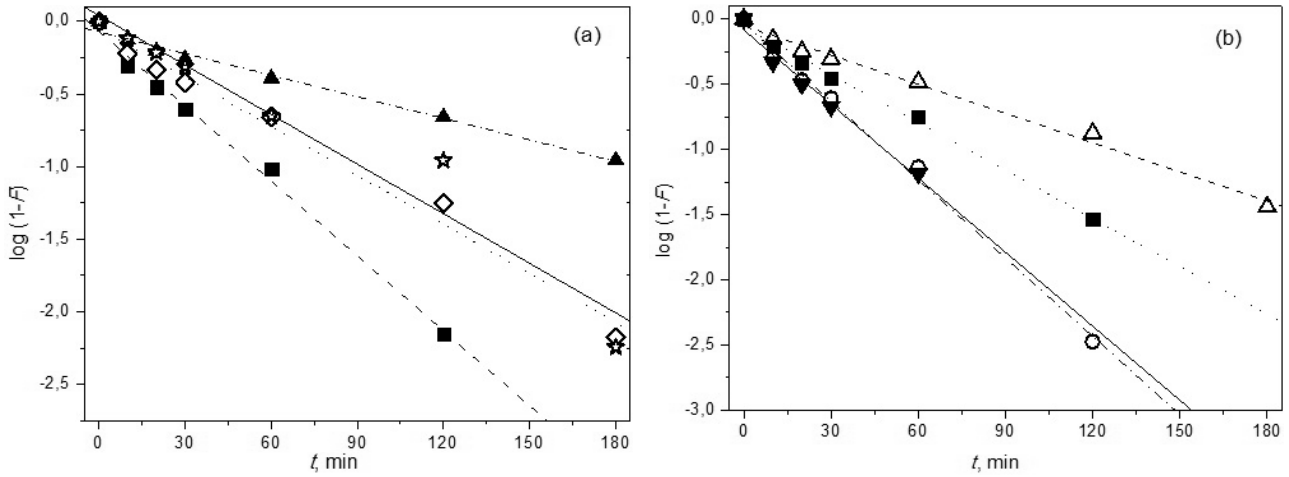

Figure 7. a) Mckay plots for RB5 sorption by PGME-deta at selected initial concentrations (30 mg dm^{-3} – black squares; 70 mg dm^{-3} – white rhombi; 110 mg dm^{-3} – black triangles; 150 mg dm^{-3} – white star) and b) at different temperatures (288 K – white triangles; 298 K – black squares; 308 K – white circles; 318 K – black triangles).

$$\frac{c_e}{Q_e} = \frac{1}{Q_{max} K_L} + \frac{c_e}{Q_{max}} \tag{10}$$

where Q_{max} is the monolayer capacity of the sorbent (mg g^{-1}) and K_L is the Langmuir sorption constant (dm^3 g^{-1}).

The characteristics of Langmuir isotherm can be expressed by dimensionless constant called Langmuir equilibrium parameter R_L given in Eq. 4 [57]:

$$R_L = \frac{1}{1 + K_L c_0} \tag{11}$$

The value of R_L indicates the type of the isotherm either to be unfavorable (R_L > 1), linear (R_L = 1), favorable (0 < R_L < 1) or irreversible (R_L = 0).

Table 6. Langmuir and Freundlich constants for RB5 sorption by PGME-deta

Model	Parameter	Value
Langmuir	Q_{max} / mg g^{-1}	353
	K_L / dm^3 g^{-1}	2317
	R_L×10^4	2.88
	R^2	0.9999
Freundlich	n	21.0
	1/n	0.048
	K_- / mg g^{-1}/(mg dm^{-3})$^{1/n}$	262.2
	R^2	0.6301

When the quantity of protonated amine groups was sufficient to completely neutralize the anionic charges on RB5, the removal of this dye reached a maximum [40].

According to the results for coefficients of determination presented in Table 6, Freundlich model is inapplicable in this case due to the very low R^2 value. This value for Langmuir model is very close to unity and therefore correct for this system. At the same time, the value of R_L = 2.88×10^{-4} designates that this sorption process of RB5 by PGME-deta lies well within the favorable limits, and close to the irreverisible. The fact that the Langmuir isotherm fits the experimental data more appropriately indicates that the distribution of active sites by PGME-deta is homogeneous and that RB5 is sorbed as a monolayer.

Comparison with other sorbents

The literature data on RB5 removal includes a variety of sorbents, some of them were listed in Table 7. However, diverse experimental conditions make direct comparison of the literature data difficult to achieve. Nevertheless, some of the results will be discussed.

The maximum sorption capacity, Q_{max} (experimental or Langmuir) has been extensively taken as an indicator of the efficiency of a sorbent. The maximum RB5 sorption capacities of various sorbents lie in a wide range between 793 mg g^{-1} reported for high lime fly ash [11] up to approximately 774 mg g^{-1} for chitosan with amino and quaternary ammonium chloride groups [12].

The maximum sorption capacity calculated from the Langmuir isotherm equation for sorption of RB5 on PGME-deta was 353 mg g^{-1} (Table 7). The maximum sorption capacities of analogous copolymers are as follows: 34.2 mg g^{-1} for chitosan [58], 201.90 mg g^{-1} for chitosan hydrogel beads formed by alkali gelation (CB) [13], 168.07 mg g^{-1} for chitosan hydrogel beads formed by sodium dodecyl sulphate gelation (CSB) [13], 625 mg g^{-1} for chitosan/amino resin [12] and 484 mg g^{-1} for glycidyl methacrylate/methelenebisacrylimide resin loaded with tetraethelenepentamine (GMA/MBA-TEPA) [3]. For all materials listed in the previous sentence, the Langmuir model was the best fit for the equilibrium data, and the kinetic data was best represented by the

Table 7. Overview of RB5 uptake with various adsorbents; L–F = Langmuir–Freundlich; R–P = Redlich–Peterson isotherm model

Sorbent	pH	T / K	c_i range, mg L^{-1}	c_i / mg L^{-1}	Isotherm model	Kinetic model	Q_{max} / mg g^{-1}	Ref.
Bone char	5.2	298	50–200	–	L–F	Pseudo-second	160	[9]
[a]F400	5.2	298	50–200	–	L–F	Pseudo-second	198	[9]
[a]BACX2	5.2	298	50–200	–	R–P	Pseudo-second	286	[9]
[a]BACX6	5.2	298	50–200	–	R–P	Pseudo-second	473	[9]
Beet pulp carbon (BPC)	1.0	298	20–500	400	L	Pseudo-second	80	[10]
High lime fly ash	5.64	293	0–30	27	F	Pseudo-second	7.93	[11]
Chitosan	4.0	306	45–100	35	L	Pseudo-second	34.2	[58]
[b]CB	6.0	303	0–1000	900	L	Pseudo-first	201.90	[13]
[b]CSB	6.0	303	0–1000	900	L	Pseudo-first	168.07	[13]
[b]PEI-CB	3.0	298	5–100	2000	L	Pseudo-first	709.27	[13]
[b]PEI-CSB	3.0	293	32–225	3000	L	Pseudo-first	413.23	[13]
Chitosan/amino resin	3.0	298	0–400	400	L	Pseudo-second	625	[12]
Chitosan with amino and quaternary ammonium chloride groups	3.0	298	0–200	200	L	Pseudo-second	774	[12]
[c]GMA/MBA-TEPA	3.0	298	600	500	L	Pseudo-second	484	[3]

[a]F400 – commercial active carbon and bamboo derived carbons, BACX2 and BACX6 with a high specific surface areas, *i.e.*, 2123 and 1400 m^2/g, respectively; [b]CB – chitosan hydrogel beads formed by alkali gelation, CSB – chitosan hydrogel beads formed by sodium dodecyl sulphate (SDS) gelation, PEI-CB – polyethyleneimine (PEI)-grafted CB; PEI-grafted CSB (PEI-CSB); [c]GMA/MBA-TEPA - glycidyl methacrylate/methelenebisacrylimide resin loaded with tetraethelenepentamine

pseudo-second-order model with the exception of CB and CSB where the pseudo-first-order model provided the most adequate representation. For GMA/MBA-TEPA [3], chitosan/amino resin [12] and CB and CSB [13] it was also shown that the intraparticle diffusion may play a significant role in those sorption systems.

CONCLUSION

Removal of textile dye Reactive Black 5 (RB5) from aqueous solutions was studied using macroporous crosslinked glycidyl methacrylate based copolymer additionally functionalized with diethylene triamine (PGME-deta). The capacity of PGME-deta for RB5 sorption was tested with respect to pH, sorbent dosage, contact time and initial concentration. The functionalized sample showed affinity for RB5 sorption due to the presence of protonated amino groups that attract anionic sulfonate groups in the dye molecule and the possibility of hydrogen bonds formation between the sorbent and the sorbate. The sorption is pH sensitive having maximum at pH 2 and decreasing with the increase of pH. A very high maximum dye sorption removal of 85% was observed at pH 2, while only 24% of dye was removed at pH 11 after 60 min. Sorption kinetics study demonstrated that the sorption of RB5 by PGME-deta obeyed the PSO kinetic model, suggesting that the sorption rate is controlled by both sorbent capacity and sorbate concentration. The process mechanism dominantly consisted of intraparticle diffusion, with minor involvement of film diffusion. These diffusion mechanisms were more prevalent with the decrease in temperature and the increase in concentration. The isotherm data was best fitted with the Langmuir model, indicating homogeneous distribution of active sites on the PGME-deta and monolayer sorption. The calculated sorption rates improved with increasing temperature and an activation energy close to 40 kJ mol^{-1} was determined, suggesting that chemisorption was also rate-controlling.

Abbreviations

A	Temperature independent factor (frequency factor) (g $mmol^{-1}$ min^{-1})
c_e	Equilibrium dye concentration in solution (mg dm^{-3})
c_0	Initial dye concentration
c_{id}	Constant in intraparticle diffusion model (intercept)
c_t	Dye solution concentrations (mg dm^{-3}) after sorption time t
D_{av}	Average pore diameter (nm)
$D_{V/2}$	Pore diameter which corresponds to half of pore volume
E_a	Activation energy (kJ mol^{-1})
F	Fractional attainment of equilibrium at time t (min)
h	Initial sorption rate from PSO model (mg g^{-1} min^{-1})
k_1	PFO rate constant (min^{-1})
k_2	PSO rate constant (g mg^{-1} min^{-1})

K_F	Freundlich sorption constant characteristic for the system
k_{id}	Intraparticle diffusion coefficient (mg g^{-1} $min^{-0.5}$)
K_L	Langmuir sorption constant (dm^3 g^{-1})
m	Amount of the copolymer beads used for the experiment (in g)
n	Freundlich sorption constant characteristic for the system
PFO	Pseudo–first kinetic model (PFO)
PGME	Glycidyl methacrylate and ethylene glycol dimethacrylate copolymer
PGME-deta	Glycidyl methacrylate and ethylene glycol dimethacrylate copolymer functionalized with diethylene triamine
pH_{PZC}	Value of pH when the overall charge on the sorbent surface is zero
PSO	Pseudo–second–order (PSO) kinetic model
Q_e	Amount of sorbed dye at equilibrium (mg g^{-1})
Q_e^{cal}	Amount of sorbed dye at equilibrium calculated from PSO (mg g^{-1})
Q_{max}	Maximum sorption capacity (mg g^{-1})
Q_{60}	Sorption capacity after 60 minutes (mg g^{-1})
Q_t	Amount of dye sorbed by the sorbent at time t (mg g^{-1})
R^2	Determination coefficient
RB5	Reactive Black 5
R_g	Universal gas constant equal to 8.314 J mol^{-1} K^{-1}
R_L	Dimensionless constant called Langmuir equilibrium parameter
S	Rate parameter
$S_{s,Hg}$	Specific surface area (m^2 g^{-1})
T	Temperature (K)
$t_{1/2}$	Sorption half–time; i.e. time required to reach 50% of the total sorption capacity
V	Volume of the aqueous phase (dm^3)
V_s	Specific pore volume (cm^3 g^{-1})

Acknowledgements

This work was supported by the Ministry of Education, Science and Technological Development of the Republic of Serbia (Projects III 43009, TR 37021 and III 45001).

REFERENCES

[1] A.E. Ofomaja, Kinetic study and sorption mechanism of methylene blue and methyl violet onto mansonia (*Mansonia altissima*) wood sawdust, Chem. Eng. J. **143** (2008) 85–95.

[2] J.J. Pierce, Colour in textile effluents—the origins of problem, J. Soc. Dyers Colour. **110** (2008) 131–133.

[3] K.Z. Elwakeel, M. Rekaby, Efficient removal of Reactive Black 5 from aqueous media using glycidyl methacrylate resin modified with tetraethelenepentamine, J. Hazard. Mater. **188** (2011) 10–18.

[4] M.A. Brown, S.C. De Uito Predicting azo dye toxicity, Crit. Rev. Env. Sci. Technol. **23** (1993) 249–324.

[5] A. Kuleyin, F. Aydin, Removal of reactive textile dyes dyes (Remazol Brillant Blue R and Remazol Yellow) by surfactant-modified natural zeolite, Environ. Prog. Sustainable Energy **30** (2011) 141–151.

[6] [6] T. Robinson, G. McMullan, R. Marchant, P. Nigam, Remediation of dyes in textile eluent: a critical review on current treatment technologies with a proposed alternative, Bioresour. Technol. 77 (2001) 247-255

[7] Y.M. Slokar, A.M. Le Marechal, Methods of decoloration of textile wastewaters, Dyes Pigments **37** (1997) 335––356.

[8] M.N.V.R. Kumar, T.R. Sridhari, K.D. Bhavani, P.K. Dutta, Trends in colour removal from textile mill effluents, Colorage **40** (1998) 25–34.

[9] A.W.M. Ip, J.P. Barford, G. McKay, A comparative study on the kinetics and mechanisms of removal of Reactive Black 5 by adsorption onto activated carbons and bone char, Chem. Eng. J. **157** (2010) 434–442.

[10] A.Y. Dursun, O. Tepe, G. Uslu, G. Dursun, Y. Saatci, Kinetics of Remazol Black B adsorption onto carbon prepared from sugar beet pulp, Environ. Sci. Pollut. Res. Int. **20** (2013) 2472–2483.

[11] Z. Eren, F.N. Acar, Equilibrium and kinetic mechanism for Reactive Black 5 sorption onto high lime Soma fly ash, J. Hazard. Mater. **143** (2007) 226–232.

[12] K.Z. Elwakeel, Removal of Reactive Black 5 from aqueous solutions using magnetic chitosan resins, J. Hazard. Mater. **167** (2009) 383–392.

[13] S. Chatterjee, T. Chatterjee, S.H. Woo, Influence of the polyethyleneimine grafting on the adsorption capacity of chitosan beads for Reactive Black 5 from aqueous solutions, Chem. Eng. J. **166** (2011) 168–175.

[14] Q. Liu, L. Wang, A. Xiao, J. Gao, W. Ding, H. Yu, J. Huo, M. Ericson, Templated preparation of porous magnetic microspheres and their application in removal of cationic dyes from wastewater, J. Hazard. Mater. **181** (2010) 586–592.

[15] S. Jovanović, A. Nastasović, N. Jovanović, K. Jeremić, Z. Savić, The influence of inert component composition on the porous structure of glycidyl methacrylate/ethylene glycol dimetacrylate copolymers, Angew. Makromol. Chem. **219** (1994)161–168.

[16] A. Nastasović, D. Jakovljević, Z. Sandić, D. Đorđević, Lj, Malović, S. Kljajević, J. Marković, A. Onjia, in: M.I. Barroso (Ed.), Reactive and Functional Polymers Research Advances, Nova Science Publishers, New York, 2008, pp. 79–112.

[17] R.V. Hercigonja, D.D. Maksin, A.B. Nastasović, S.S. Trifunović, P.B. Glodić, A.E. Onjia, Adsorptive removal of technetium-99 using macroporous poly(GMA-*co*-EGDMA) modified with diethylene triamine, J. Appl. Polym. Sci. **123** (2012) 1273–1282.

[18] Z. Sandić, A. Nastasović, N. Jović-Jovičić, A. Milutinović-Nikolić, D.J. Jovanović, Sorption of textile dye from

aqueous solution by macroporous amino functionalized copolymer. J. Appl. Polym. Sci. **121** (2011) 234–242.

[19] G. Bayramoglu, M.Y. Arica, Removal of reactive dyes from wastewater by acrylate polymer beads bearing amino groups: Isotherm and kinetic studies, Color. Technol. **129** (2013) 114–124.

[20] G.M. Kline, Analytical Chemistry of Polymers, Interscience, New York, 1959.

[21] B.H. Hameed, I.A.W. Tan, A.L. Ahmad, Adsorption isotherm, kinetic modeling and mechanism of 2,4,6-trichlorophenol on coconut husk-based activated carbon, Chem. Eng. J. **144** (2008) 235–244.

[22] H. Chen, G. Dai, J. Zhao, A. Zhong, J. Wu, H. Yan, Removal of copper(II) ions by a biosorbent—*Cinnamomum camphora* leaves powder, J. Hazard. Mater. **177** (2010) 228–236.

[23] S. Jovanović, A. Nastasović, N. Jovanović, K. Jeremić, Targeted porous structure of macroporous copolymers based on glycidyl methacrylate, Mater. Sci. Forum **214** (1996) 155–162.

[24] Lj. Malović, A. Nastasović, Z. Sandić, J. Marković, D. Đorđević, Z. Vuković, Surface modification of macroporous glycidyl methacrylate based copolymers for selective sorption of heavy metals, J. Mater. Sci. **42** (2007) 3326–3337.

[25] P.A. Webb, C. Orr, Analytical Methods in Fine Particle Technology. Micromeritics Instrument Corporation, Norcross, GA, 1997.

[26] V. Ponnusami, S. Vikram, S.N. Srivastava, Guava (*Psidium guajava*) leaf powder: novel adsorbent for removal of methylene blue from aqueous solutions, J. Hazard. Mater. **152** (2008) 276–286.

[27] A. Szyguła, E. Guibal, M. Ruiz, A.M. Sastre, The removal of sulphonated azo-dyes by coagulation with chitosan, Colloids Surfaces, A **330** (2008) 219–226.

[28] B. Royer, N.F. Cardoso, E.C. Lima, T.R. Macedo, C. Airoldi, A useful organofunctionalized layered silicate for textile dye removal, J. Hazard. Mater .**181** (2010) 366––374.

[29] A.S. Özcan, A. Özcan, Adsorption of acid dyes from aqueous solutions onto acid-activated bentonite, J. Colloid Interf. Sci. **276** (2004)39–46.

[30] C. Liu, Study of polyamines-functionalized PGMA beads as adsorbents for the removal of heavy metal ions from aqueous solutions, PhD. Thesis, National university of Singapore, Singapore, 2009.

[31] B. Oram, The pH of water, Water Research Center, http://www.water-research.net/ph.htm (accessed Dec, 2011).

[32] V.O. Arief, K. Trilestari, J. Sunarso, N. Indraswati, S. Ismadji, Recent progress on biosorption of heavy metals from liquid using low cost biosorbents: Characterization, biosorption parameters and mechanism studies, Clean-Soil Air Water **36** (2008) 937-962

[33] P.K. Malik, Use of activated carbons prepared from sawdust and rice-husk for adsorption of acid dyes: A case study of Acid Yellow 36, Dyes Pigments **56** (2003) 239–249.

[34] S. Lagergren About the theory of so-called adsorption of soluble substances, K Sven. Vetenskapsakad Handl. **24** (1898) 1–39.

[35] Y.S. Ho, Review of second-order models for adsorption systems, J. Hazard. Mater., B **136** (2006) 681–689.

[36] K.J. Laidler, The World of Physical Chemistry, Oxford University Press Inc., New York, 1993.

[37] E. Coates, Aggregation of dyes in aqueous solutions, J. Soc. Dyers Colour. **85** (1969) 355–368.

[38] G.M. Walker, L.R. Weatherley, Adsorption of dyes from aqueous solution-the effect of adsorbent pore size distribution and dye aggregation, Chem. Eng. J. **83** (2001) 201–206.

[39] A.E. Ofomaja, E.B. Naidoo, Biosorption of copper from aqueous solution by chemically activated pine cone: A kinetic study, Chem. Eng. J. **175** (2011) 260–270.

[40] M. Emine, Ni (II) removal from aqueous solutions using cone biomass of *Thuja orientalis*, J. Hazard. Mater. **137** (2006) 899–908.

[41] V.J. Inglezakis, M.D. Loizidou, H.P. Grigoropoulou, Ion exchange studies on natural and modified zeolites and the concept of exchange site accessibility, J. Colloid Interface Sci. **275** (2004) 570–576.

[42] G.S. Kirk, L.S. Donald, Temperature effect on nickel sorption kinetics at the mineral–water interface, Soil Sci. Soc. Am. J. **65** (2001) 719–728.

[43] W.J. Weber, Jr., J.C. Morris, Kinetics of adsorption on carbon from solution, J. Sanit. Eng. Div. Am. Soc. Civ. Eng. **89** (1963) 31–59.

[44] F.C. Wu, R.L. Tseng, R.S. Juang, Initial behavior of intraparticle diffusion model used in the description of adsorption kinetics, Chem. Eng. J. **153** (2009) 1–8.

[45] W. Zhang, Z. Xu, B. Pan, L. Lu, Q. Zhang, Q. Zhang, W. Du, B. Pan, Q. Zhang, Assessment on the removal of dimethyl phthalate from aqueous phase using a hydrophilic hypercrosslinked polymer resin NDA-702, J. Colloid Interface Sci. **311** (2007) 382–390.

[46] N. Dizge, C. Aydiner, E. Demirbas, M. Kobya, S. Kara, Adsorption of reactive dyes from aqueous solutions by fly ash: kinetic and equilibrium studies, J. Hazard. Mater. **150** (2008) 737–746.

[47] R. Dhodapkar, N.N. Rao, S.P. Pande, T. Nandy, S. Devotta, Adsorption of cationic dyes on Jalshakti, super absorbent polymer and photocatalytic regeneration of the adsorbent, React. Funct. Polym. **67** (2007) 540–548.

[48] C. Long, A. Li, H. Wub, Q. Zhang, Adsorption of naphthalene onto macroporous and hypercrosslinked polymeric adsorbent: Effect of pore structure of adsorbents on thermodynamic and kinetic properties, Colloids Surfaces, A **333** (2009) 150–155.

[49] Q. Sun, L. Yang, The adsorption of basic dyes from aqueous solution on modified peat-resin particle, Water. Res. **37** (2003) 1535–1544.

[50] D. Kumar, J.P. Gaur, Chemical reaction- and particle diffusion-based kinetic modeling of metal biosorption by a *Phormidium* sp.-dominated cyanobacterial mat, Bioresour. Technol. **102** (2011) 633–640.

[51] L. Caceres, M. Escudey, E. Fuentes, M.E. Baec, Modeling the sorption kinetic of metsulfuron-methyl on Andisols

and Ultisols volcanic ash-derived soils: Kinetics parameters and solute transport mechanisms, J. Hazard. Mater. **179** (2010) 795–803.

[52] L. Li, P.A. Quinlivan, D.R.U. Knappe, Effects of activated carbon surface chemistry and pore structure on the adsorption of organic contaminants from aqueous solution, Carbon **40** (2002) 2085–3000.

[53] B.S. Inbaraj, C.P. Chiu, G.H. Ho, J. Yang, B.H. Chen, Effects of temperature and pH on adsorption of basic brown 1 by the bacterial biopolymer poly(*γ*-glutamic acid), Bioresour. Technol. **99** (2008) 1026–1035.

[54] Y.S. Ho, Effect of pH on lead removal from water using tree fern as the sorbent, Bioresource Technol. **96** (2005) 1292–1296.

[55] H.M.F. Freundlich, Über die adsorption in lösungen, J. Phys. Chem. **57** (1906) 385–471.

[56] I.J. Langmuir, The adsorption of gases on plane surfaces of glass, mica and platinum, J. Am. Chem. Soc. **40** (1918) 1361–1403.

[57] G. McKay, H. Blair, J.R. Gardiner, The adsorption of dyes onto chitin in fixed bed column and batch adsorbers, J. Appl. Polym. Sci. **29** (1989) 499–508.

[58] T.K. Saha, N.C. Bhoumik, S. Karmaker, M.G. Ahmed, H. Ichikawa, Y. Fukumori, Adsorption characteristics of Reactive Black 5 from aqueous solution onto chitosan, Clean-Soil Air Water **39** (2011) 984–993.

IZVOD

MAKROPOROZNI KOPOLIMER NA BAZI GLICIDILMETAKRILATA FUNKCIONALIZOVAN SA DIETILENTRIAMINOM KAO SORBENT TEKSTILNE BOJE REACTIVE BLACK 5

Zvjezdana P. Sandić[1], Marija J. Žunić[2], Danijela D. Maksin[3], Aleksandra D. Milutinović-Nikolić[2], Aleksandar R. Popović[4], Dušan M. Jovanović[2], Aleksandra B. Nastasović[5]

[1]*Univerzitet u Banja Luci, Prirodno–matematički fakultet, Banja Luka, Bosna i Hercegovina (Republika Srpska)*
[2]*Univerzitet u Beogradu, IHTM – Centar za katalizu i hemijsko inženjerstvo, Beograd, Srbija*
[3]*Univerzitet u Beogradu, Institut za nuklearne nauke Vinča, Departman za hemijsku dinamiku i permanentno obrazovanje, Beograd, Srbija*
[4]*Univerzitet u Beogradu, Hemijski fakultet, Beograd, Srbija*
[5]*Univerzitet u Beogradu, IHTM – Centar za hemiju, Beograd, Srbija*

(Naučni rad)

U okviru ovog rada ispitana je mogućnost korišćenja makroporoznog kopolimera glicidilmetakrilata i etilenglikoldimetakrilata funkcionalizovanog reakcijom otvaranja epoksidnih grupa sa dietilentriaminom (PGME-deta) kao sorbenta reaktivne tekstilne boje Reactive Black 5 (RB5). U šaržnim uslovima je ispitano uklanjanje RB5 iz vodenog rastvora pomoću PGME-deta, variranjem pH, vremena kontakta, mase sorbenta, početne koncentracije boje i temperature. PGME-deta je pokazao afinitet za sorpciju RB5 zbog prisustva protonovanih amino grupa koje privlače anjonske sulfonatne grupe u molekulu boje i mogućnosti stvaranja vodoničnih veza između sorbenta i sorbata. Kinetika sorpcije je analizirana pomoću četiri kinetička modela (pseudo-prvog, pseudo-drugog reda, unutarčestične difuzije i Mekej) da bi se odredilo koji model najbolje opisuje sorpciju RB5. Zapažen je izrazit uticaj pH vrednosti na sorpciju RB5, sa maksimumom na pH 2 (pri čemu je efikasnost uklanjanja boje 85%), i smanjenjem količine sorbovane boje sa povećanjem pH (količina uklonjene boje na pH 11 posle 60 min iznosi samo 24%). Izučavanjem kinetike sorpcije pokazalo se da sorpcija RB5 pomoću PGME-deta sledi kinetički model pseudo-drugog reda (PSO), sugerišući da je brzina sorpcije kontrolisana kapacitetom sorbenta i koncentracijom sorbata. Mehanizam procesa dominantno čini unutarčestična difuzija, uz manji uticaj difuzije kroz film. Ovi mehanizmi difuzije su izraženiji pri nižim temperaturama i većim koncentracijama. Langmirov model najbolje opisuje ravnotežnu izotermu, ukazujući na homogenu raspodelu aktivnih mesta na površini PGME-deta i monoslojnu sorpciju. Maksimalni sorpcioni kapacitet izračunat iz Langmirove izoterme iznosi 353 mg g^{-1}. Zapaženo je da se brzina sorpcije povećava sa povećanjem temperature. Izračunata vrednost aktivacione energije od oko 40 kJ mol^{-1} potvrđuje da se radi o procesu koji dominantno kontroliše hemisorpcija.

Ključne reči: Reactive Black 5• Makroporozni Umreženi kopolimer • Dietilentriamin • Kinetički modeli • Ravnotežna sorpcija

Effect of PVC plastisol composition and processing conditions on foam expansion and tear strength

Rajko Radovanović[1], Vladislav Jašo[2], Branka Pilić[2], Dragoslav Stoiljković[2]

[1]*OOO JUTEKS RU, Kameshkovo, Russia*
[2]*Faculty of Technology, University of Novi Sad, Novi Sad, Serbia*

Abstract

The quality of vinyl floorings depends mainly on the right control of the formation of poly (vinyl chloride) (PVC) foam structure. Many process parameters influence the cellular structure and final properties of the PVC foam. In this paper the influence of concentration of blowing agent and calcium carbonate filler, as well as temperature and time of the blowing process on the expansion ratio and tear strength of the PVC foam, were studied. Moreover, regression analysis was performed in order to determine the significance of studied parameters influence on expansion ratio and tear strength of PVC foams. It was found that concentration of the blowing agent in the plastisol mixture had the principal influence on the expansion ratio of the PVC foam. Tear strength was found to depend more or less equally on all studied parameters. The study has also shown that the addition of calcium carbonate filler had insignificantly lowered the expansion ratio, but at the same time it could significantly lower the cost of the final product. This effect was practically employed to improve the economic efficiency of the PVC floorings production in JUTEKS plant in Russia.

Keywords: PVC plastisol; foam expansion, tear strength.

Available online at the Journal website: http://www.ache.org.rs/HI/

Polymers

SCIENTIFIC PAPER

UDC 678.743.22.01

Hem. Ind. **68** (6) 701–707 (2014)

doi: 10.2298/HEMIND140210028R

In the last decade of the previous century demand for polymeric foams has risen dramatically [1]. The growth in demand has been more dramatic in the United States than in Europe. In recent years, this trend of growth has continued at a rapid pace in the whole world. The cause of this are the numerous excellent properties that encompass light weight, excellent strength/weight ratio, superior insulating abilities, and energy absorbing performance and comfort features of polymeric foams [2]. The application possibilities of polymeric foams are very wide and include furniture, transportation, bedding, carpet underlay, packaging, textiles, toys, gasket, sport applications, and insulation appliances.

Early investigations about PVC foams dealt with the effect of viscosity regulators and how they can be used to control the process of foam formation [3]. Later, studies were concerned with how tensile and flexural properties, as well as toughness correlated to the density of foamed PVC [1]. It was found that as density decreases, so do all the mentioned properties [1]. Foam properties are also found to be dependent on and influenced by the cell structure [4]. A study which encompassed analysis of four different PVC types and eight different plasticizers, individually or as mixtures, on foam density, ratio of expansion and elasticity [5] showed that two-component plasticizer mixtures had better properties than single-component plasticizers. This study has shown that most appropriate mixtures are those of di-isoheptyl phthalate and butylbenzyl phthalate [5]. It was also shown that the precise timing of foam expansion and careful choice of temperature are critical for the foam properties. If the temperature is too high, the degradation of PVC becomes very rapid and decreases the quality of the product. At high temperatures, the melt viscosity is low so rapid gas expansion can cause cell rupture and collapse [6]. This results in non-uniform cell morphology, increased foam density and increased roughness. On the other hand, if the temperature is too low, decomposition of the blowing agent is too slow, which can considerably influence the productivity. Moreover, at low temperatures fusion between the PVC primary particles is insufficient. The plastisol is characterized by high viscosity in lower temperature range, so if the gas pressure is not high enough it may cause a decrease in cell size, increase in foam density, surface roughness and void formation.

Different studies have dealt with the influence of the stabilizer type [7], type and level of the acrylic processing aid [8], and processing conditions [9] on foam density and thus on the foam properties. Heat stabilizers such as Ca/Zn stearates or organotin compounds are added to the PVC to prevent dehydrochlorination by heating. The heat stabilizers also affect the rate of decomposition of chemical blowing agents [10,11].

Correspondence: R. Radovanović, OOO JUTEKS RU, Dorozhnaya Street 10, 601301 Kameshkovo, Russia.
E-mail: Rajko.Radovanovic@juteks.ru
Paper received: 10 February, 2014
Paper accepted: 2 April, 2014

The effect of the $CaCO_3$ particle size was studied in rigid PVC formulations [12–14]. Study of particle size effect in foam formulations [15] proved that smaller particle size enables efficient fusion of the compound. However, larger particle size fillers improve melt strength, giving foam with more homogeneous cell size distribution and smaller fraction of open cells. In that way, mechanical properties are improved [15]. It was observed that, samples containing zeolite, $CaCO_3$, cellulose or luffa flour had lower pore volume, but higher Young's modulus and stress values compared to unfilled samples [2]. Finally, at low filler concentration, filler acts as nucleating agent and increases the foam formation. The structure of PVC foams becomes rigid and strong at high filler concentration. It is observed that the properties of cellulose or luffa added foam are not suitable for practical foam applications such as thermal insulation and construction field, but can be used in plant watering equipment since they have high water uptake capacity [2].

In this study, we have investigated the effect of four process parameters on expansion ratio and tear strength of PVC foam. The parameters that were studied are temperature (in the stabile range of 180–196 °C), expansion time (in the range 90–150 s), calcium carbonate filler concentration, and azodicarbonamide blowing agent concentration. Multiple regression analysis was employed in order to determine the significance of the influence of the different parameters on the expansion ratio and tear strength.

EXPERIMENTAL

The plastisol consists of PVC powder (Solvic 367SF, Solvin, France), PVC extender (Solvic 266SF, Solvin, Belgium), dioctyl phthalate plasticizer (Roshalskiy Zavod Plastifikatorov, Roshaly, Russian Federation), azodicarbonamide blowing agent (MC-2, OOO Norteks, Moscow, Russian Federation), ZnO kicker (BC OM, Bellit, Saransk, Russian Federation), TiO_2 (R103, DuPont, Germany), calcium carbonate filler (Omycarb 40 UR, Omya Ural, Russian Federation, with particle size 26±5 μm), viscosity regulator (Viskobyk 4041, BYK Chemie, Germany) and dispersing agent (Dispersplast 1138, BYK Chemie Germany). Nine different formulations were prepared with three different calcium carbonate concentrations (40, 70 and 100 phr) and three different blowing agent concentrations (0.8, 1 and 1.2 wt.%). The ratio of blowing agent to kicker percent was 3:1 in all formulations. In total, there were nine different formulations (Table 1). One formulation was shown as an example in Table 2.

Table 2. PVC plastisol formulation (sample M1)

Ingredient	Concentration	
	phr	wt.%
PVC, Solvic 367NF	75.52	37.04
Ext. PVC, Solvic 266SF	24.48	12.00
DOP	55.94	27.44
$CaCO_3$	40.17	19.70
DOP (batch)	3.24	1.59
Viskobyk 4041	1.55	0.76
ADCA azodicarbonamide	1.64	0.80
ZnO	0.55	0.27
TiO_2	0.40	0.19
Disperplast 1138	0.40	0.19
Total	203.9	100.0

Poly (vinyl chloride) plastisols were prepared by mixing the appropriate components in a laboratory vacuum mixer (LPE, Werner Mathis AG, Switzerland). The prepared plastisols were coated on a silicon paper and were left to gel for 30 s at 150 °C in an oven (LTF, Werner Mathis AG, Switzerland). The samples were expanded into foam at five different temperatures (180, 184, 188, 192 and 196 °C) and in three different time periods (90, 120 and 150 s). The expansion of PVC foam was measured by comparing the height of the sample with the height of the control sample that was processed at 150 °C for 30 s and expressed as expansion ratio that shows how many times thickness has changed after expansion. The tear strength was measured by mechanical test machine (Zwick/Roell Z005) on samples 50 mm wide and 200 mm long with a longitudinal 100 mm slit along the middle at a tearing rate of 100 mm/min.

RESULTS

The main goal of this study was to determine which of the four studied parameters (concentration of calcium carbonate, concentration of blowing agent, tem-

Table 1. Plastisol samples designation and concentration of azodicarbamide blowing agent (ADCA), ZnO kicker and calcium carbonate filler (wt.%)

Ingredient	Sample								
	M1	M2	M3	M4	M5	M6	M7	M8	M9
ADCA	0.8	0.8	0.8	1.0	1.0	1.0	1.2	1.2	1.2
ZnO	0.27	0.27	0.27	0.33	0.33	0.33	0.4	0.4	0.4
$CaCO_3$	19.70	29.87	37.58	19.51	29.57	37.22	19.32	29.28	36.86

perature and foam expansion time) has the most significant influence on the expansion ratio and tear strength of the foam. Efforts were made to find the appropriate linear correlation with the least number of independent variables that would predict both of the mentioned properties with an acceptable level of accuracy. It is well known that with the increase of temperature, the rate of blowing agent decomposition increases thus allowing the greater expansion ratio. It should also rise with the time allowed for the foam formation, as well as with the higher concentration of blowing agent. Special attention was given to the influence of the calcium carbonate in the plastisol on the expansion ratio. The parameters that were studied were in the range used under normal production conditions, only the calcium carbonate percent was increased above the usual level. Temperatures were above the temperature which enables satisfactory rate of blowing gas evolution and beneath the level the degradation of PVC becomes considerable.

After the preparation of samples and measurements of foam properties, multiple linear regression was performed in order to study the effect of different parameters on the expansion ratio and tear strength. In the first step, linear correlation (1) between expansion ratio and each parameter was separately determined (Table 3):

$$E = a_i X_i, \quad i = 1,...,4 \tag{1}$$

The highest value of correlation coefficient (*R*) and the lowest root mean square error (*RMSE*) among four correlations indicates that azodicarbonamide blowing agent concentration (ADCA) has the biggest effect on the expansion ratio of PVC foam by far.

Table 3. Correlation factor (R) and root mean square error (RMSE) of correlations between expansion ratio and each single studied variables (Model E1)

Parameter	Variable designation	*R*	*RMSE*
ADCA, wt.%	*X*2	0.774	0.5041
Temperature, °C	*X*4	0.420	0.7226
$CaCO_3$, wt.%	*X*1	0.181	0.7831
Time, s	*X*3	0.236	0.7737

Further on, forward stepwise analysis was performed, introducing new parameters in the model in the order of their significance. Models are given below:

$$E = a_2 X_2 \tag{E1}$$

$$E = a_0 + a_2 X_2 + a_4 X_4 \tag{E2}$$

$$E = a_0 + a_2 X_2 + a_4 X_4 + a_3 X_3 \tag{E3}$$

$$E = a_0 + a_2 X_2 + a_4 X_4 + a_3 X_3 + a_1 X_1 \tag{E4}$$

The results of step two (two parameter model) and step three (three parameter model) are shown in Tables 4 and 5. First, we have tried to improve model E1 by including one more parameter. Effect of inclusion of each of the three remaining parameter was explored. The values of parameter coefficients (a_i), reduction in error sum of squares (*SS*), if the term is entered into the model and F ratio is given in the tables. *F* ratio is defined as the ratio of the explained variance to the unexplained variance and expresses the significance level of each parameter in F statistic. In our case it shows what would be the significance of the particular parameter in the model if it was included in the model. Higher value means higher significance.

Table 4. Model E2 coefficients reduction in sum of squares and F ratio after introduction of different parameters to the model (from Analysis of variance)

Parameter	Model coefficient	Sum of squares	*F* Ratio
Intercept	–10.3979	0	0
$CaCO_3$, wt.%	0	3.56	30.43
ADCA, wt.%	3.7464	50.52	352.54
Time, s	0	4.70	43.37
Temperature, °C	0.0586	14.87	103.79

Table 5. Model E3 coefficients, reduction in sum of squares and F ratio after introduction of different parameters to the model (from Analysis of variance)

Parameter	Model coefficient	Sum of squares	*F* Ratio
Intercept	-11.7544	0	0
$CaCO_3$, wt.%	0	3.56	43.54
ADCA, wt.%	3.7464	50.52	465.71
Time, s	0.0076	4.70	43.37
Temperature, °C	0.0586	14.87	137.11

If we look at correlation coefficients (*R*) and root mean square error (*RSME*, Table 6) for different correlations, we can see that introduction of the third and fourth term does not give much of an improvement. Because Model E2, with two parameters, is simpler, it was our model of choice. Comparison of the values of the expansion ratio predicted by the model and the experimental values were compared and the points that differed more than 2σ were disbanded (6 points from the total of 135 points) and calculation of the new improved model coefficients was performed (Table 7). All three models are shown in Figures 1 and 2.

Although analysis has indicated that concentration of the blowing agent (ADCA) is the most important factor that determines the expansion ratio, the processing parameters are very important as well. This is illustrated in Figures 3 and 4. The obtained results show

that foaming of PVC can be performed in a very narrow range of temperature and time. It is clear that foaming below 180 °C is difficult and insufficient. This can be explained by the fact that below 175 °C decay of the blowing agent does not take place and foaming does not start no matter how long the PVC plastisol is heated. On the other hand, at higher temperatures, longer time of heating does not give foam with much higher expansion ratio. Also worth mentioning is that above the temperature of 195 °C and 150 s, the degradation of the PVC starts and intensifies after reaching 200 °C and longer foaming times. Optimal processing conditions are in temperature range of 188–192 °C with a foaming time of 120 s.

Table 6. Correlation factor (R) and root mean square error (RMSE) for different correlation models for expansion ratio dependence on studied parameters

Model	Model parameters	*R*	*RMSE*
E2	*X*2, *X*4	0.881	0.3786
E3	*X*2, *X*4, *X*3	0.912	0.3294
E4	*X*2, *X*4, *X*3, *X*1	0.935	0.2862

Table 7. Model E2I coefficients, reduction in sum of squares and F ratio after introduction of different parameters to the model (from Analysis of variance)

Parameter	Model coefficient	Sum of squares	*F* Ratio
Intercept	–8.4382	0	0
ADCA, %	3.8195	50.75	544.39
Temperature, °C	0.0458	8.21	88.12

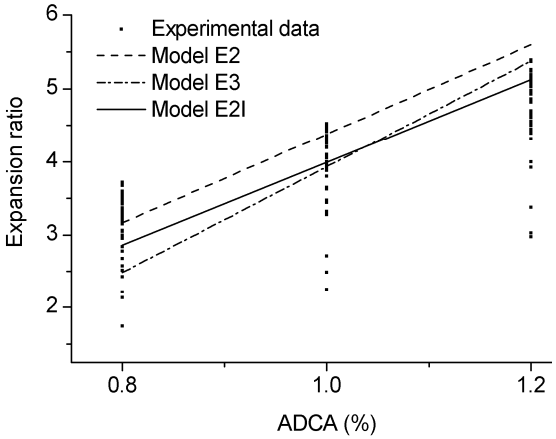

Figure 1. Experimental data of expansion ratio for different concentrations of blowing agent and different correlation models.

Adding calcium carbonate filler has negative effect on the expansion ratio, but significance of its effect (expressed as *F* ratio) is relatively low (Tables 3 and 4). This information is very important as it shows that with the addition of the filler, the price of the product can be lowered with an insignificant change of the expansion ratio.

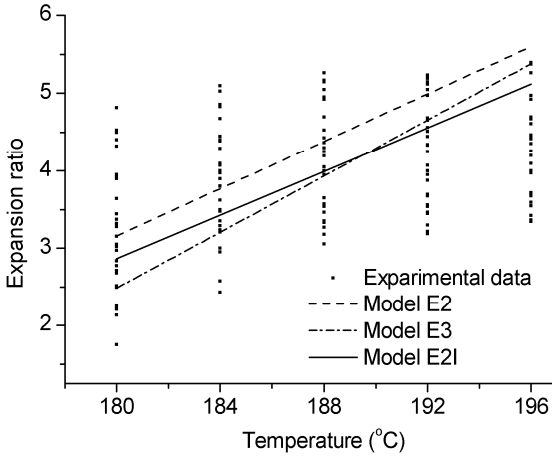

Figure 2. Experimental data of expansion ratio for different temperatures and different correlation models.

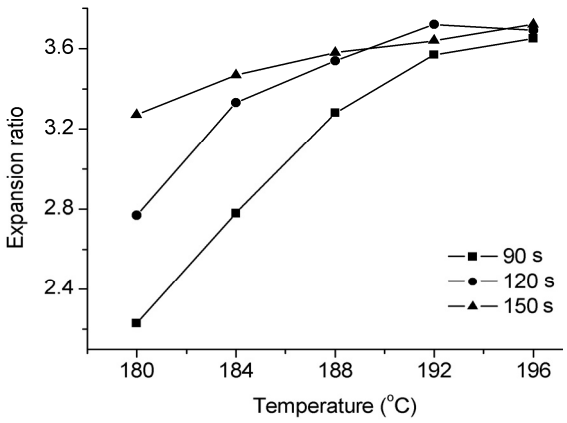

Figure 3. Experimentally obtained dependences of expansion ratio on temperature for different foaming time (Sample M3).

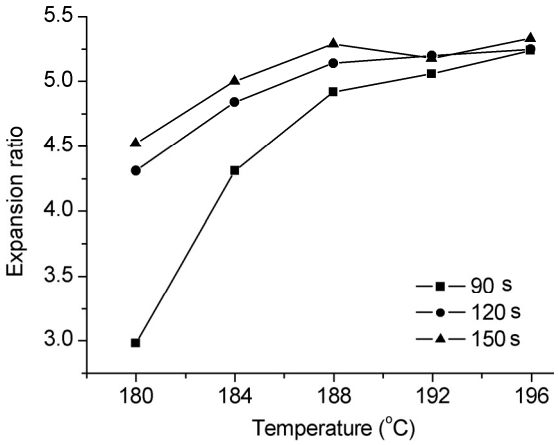

Figure 4. Experimentally obtained dependences of expansion ratio on temperature for different foaming time (Sample M9).

The effect of the studied factors on tear strength was also examined by statistical analysis. Correlation models are given below.

$$T = a_2 X_2 \quad \text{(T1)}$$

$$T = a_0 + a_2 X_2 + a_4 X_4 \quad \text{(T2)}$$

$$T = a_0 + a_2 X_2 + a_4 X_4 + a_3 X_3 \quad \text{(T3)}$$

$$T = a_0 + a_2 X_2 + a_4 X_4 + a_3 X_3 + a_1 X_1 \quad \text{(T4)}$$

Separate correlation between tear strength and each parameter was determined (Table 8). Again, concentration of the blowing agent (ADCA) and temperature are the most significant factors, but the calcium carbonate concentration also has a significant effect. The stepwise analysis routine was performed to find model coefficients (Tables 9 and 10). In the case of the model describing the effects of the studied factors on tear strength, it was decided that model with three parameters (Model T3) is more accurate than the model with two parameters (Model T2, Table 11). This model was then improved by recalculation of the model coefficients after the disbandment of experimental points outside the 2 σ region (Table 12).

Table 8. Correlation factor (R) and root mean square error (RMSE) for the correlations of tear strength and each single studied variables (Model T1)

Parameter name	Variable designation	*R*	*RMSE*
$CaCO_3$, wt.%	*X*1	0.421	2.925
Temperature, °C	*X*4	0.458	2.866
ADCA, %	*X*2	0.468	2.849
Time, s	*X*3	0.233	3.135

Table 9. Model T2 coefficients, reduction in sum of squares and F ratio after introduction of different parameters to the model (from Analysis of variance)

Parameter	Model coefficient	Sum of squares	*F* Ratio
Intercept	63.0125	0	0
$CaCO_3$, wt.%	0	262.02	65.04
ADCA, wt.%	–9.1645	302.36	50.53
Time, s	0	74.70	13.68
Temperature, °C	–0.2591	290.01	48.47

From the above analysis it may be concluded that all factors have negative effect on tear strength. This is understandable as the cellular structure weakens the strength of material to resist tearing. The tear strength decreases with increase of concentration of the calcium carbonate in the foam (Figures 5 and 6). Decrease of the tear strength is less dramatic if there is a higher concentration of blowing agent. At higher temperatures (Figure 6) all other factors have much less influence as the tear strength is low and could not be much increased by changing other factors.

Table 10. Model T3 coefficients, reduction in sum of squares and F ratio after introduction of different parameters to the model (from Analysis of variance)

Parameter	Model coefficient	Sum of squares	*F* Ratio
Intercept	68.8031	0	0
$CaCO_3$, wt.%	–0.1920	260.02	65.04
ADCA, wt.%	–9.4317	319.93	79.42
Time, s	0	74.70	21.44
Temperature, °C	–0.2591	290.01	71.99

Table 11. Correlation factor (R) and root mean square error (RMSE) for different correlation models for tear strength dependence on studied parameters

Model name	Model parameters	*R*	*RMSE*
Model T2	*X*2, *X*4	0.655	2.446
Model T3	*X*2, *X*4, *X*1	0.786	2.007
Model T4	*X*2, *X*4, *X*1, *X*3	0.819	1.867

Table 12. Model T3I coefficients, reduction in sum of squares and F ratio after introduction of different parameters to the model (from Analysis of variance)

Parameter	Model coefficient	Sum of squares	*F* Ratio
Intercept	50.6867	0	0
ADCA, wt.%	–7.7716	209.08	210.91
Temperature, °C	–0.1771	124.91	125.99
$CaCO_3$, wt.%	–0.1649	183.85	185.45

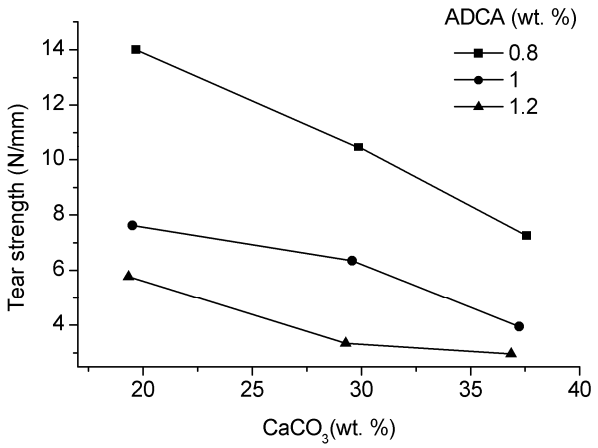

Figure 5. The dependence of tear strength on calcium carbonate concentrations for different blowing agent concentrations (184 °C, 90 s).

The correlation between experimental data of the tear strength and expansion ratio was also tested. This analysis (Figure 7) has shown that some correlation between the two properties exists although it is not

significant. This could be explained by the fact that tear strength depends only partially on expansion ratio or density of the foam, but more importantly on the cell structure and dimension of pores. This dependence will be studied in our further investigations.

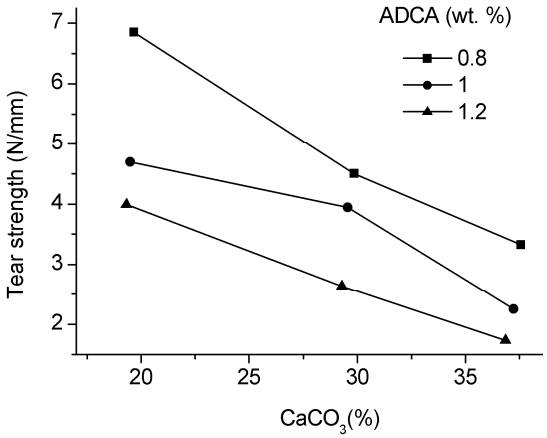

Figure 6. The dependence of tear strength on calcium carbonate concentrations for different blowing agent concentrations (196 ℃, 90 s).

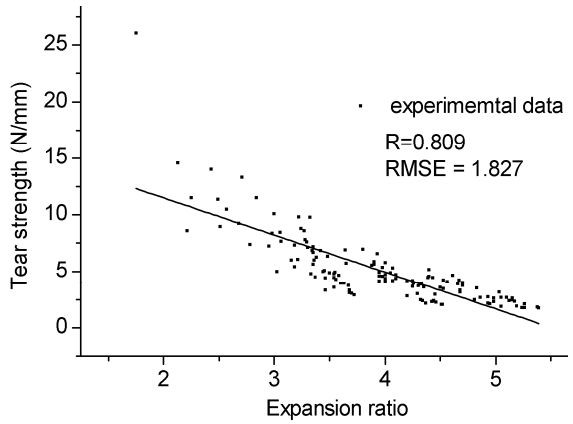

Figure 7. Correlation between tear strength and expansion ratio of the PVC foam (all 135 specimens: formulation M1–M9; time: 90, 120 and 150 sec; temperature: 180, 184, 188, 192 and 196 ℃).

CONCLUSIONS

In this study the effect of temperature, foaming time, calcium carbonate and blowing agent concentration on expansion ratio and tear strength was investigated. Statistical analysis was performed in order to study the significance of the influence of different factors on the expansion ratio and tear strength. Correlation models that describe these relations were developed. It was found that the expansion ratio of PVC foam is mostly dependent on the concentration of blowing agent and temperature. Both factors have a positive influence on the expansion ratio. Increase of the calcium carbonate concentration in the foam lowers the expansion ratio, but its influence was found to be the least significant among the four studied parameters. These findings confirm usefulness of calcium carbonate to lower the cost of the PVC foam products. In contrast to the influence of the expansion ratio, the increase of the concentration of calcium carbonate and ADCA, as well as temperature, has a negative impact on the tear strength. This means that the mixture formulation and the process conditions must be optimized in order to obtain the desired characteristics and sustainable cost.

Acknowledgments

This study was supported by the Ministry of Education, Science and Technological Development of the Republic of Serbia, Project No. III 45022. We specially thank associates working in Juteks DD development sector laboratories in Russia and Slovenia for their technical assistance.

REFERENCES

[1] J. Patterson, Vinyl foam: Effect of density on physical properties, J. Vinyl. Addit. Technol. **4** (1998) 26–29.

[2] H. Demir, M. Sipahioğlu, D. Balköse, S. Ülkü, Effect of additives on flexible PVC foam formation, J. Mater. Process. Technol. **195** (2008) 144–153.

[3] Lj. Čvorkov, I. Popović, S. Veličković, K. Brankov and V. Vukovljak, The Dependence of Plastisol Quality on the Type of Poly (Vinyl Chloride) and Viscosity Regulator, Acta Period Technol. **29–30** (1998) 97–104.

[4] J.L. Pfenning, M. Ross, Plastics Compounding, in: Proceeedings of PVC '90, PRI Brighton, UK, 1990, pp. 88–89.

[5] S. Veličković, D. Stojkov, I. G. Popović, K. Brankov, Lj. Čvorkov, The Effect of Plasticizers on the Properties of Poly(vinyl chloride) Foams, J. Vinyl. Addit. Technol. **8** (2002) 159–165.

[6] E.B. Rabinovitch, J.D. Isner, J.A. Sidor, D. J. Wiedel, Effect of extrusion conditions on rigid PVC foam, J. Vinyl. Addit. Technol. **3** (1997) 210–215.

[7] J. Patterson, G. Szamborski, Expanding PVC as a Building Material, J. Vinyl. Addit. Technol **1** (1995) 148–154.

[8] Y. Miki, N. Nakanishi, A. Takaki, and K. Yamazaki, Study of the Characteristics of Cellular PVC and Suitable Processing Aid, Proceedings SPE ANTEC (1999) 3592–3596.

[9] E. Rabinovitch, J. Isner, J. Sidor, D. Wiedl, Effect of Extrusion Conditions on Rigid PVC Foam, in: Technical papers of the Annual Technical Conference-Society of plastic Engineers Inc., **3** (1997) 3554–3559.

[10] E. Arkis, D. Balköse, Thermal stabilisation of poly(vinyl chloride) by organotin compounds, Polym. Degrad. Stab. **88** (2005) 46–51.

[11] D. Balköse, H.I. Gökcel, S.E. Göktepe, Synergism of Ca/Zn soaps in poly(vinyl chloride) thermal stability, Eur. Polym. J. **37** (2001) 1191–1197.

[12] L.G. Shaw, A.R. Diluciano, Effect of calcium carbonate and paraffin wax levels on the performance of PVC pipe, J. Vinyl. Addit. Technol. **5** (1983) 100–103.

[13] K.K. Mathur, D.B. Vanderheiden, Precipitated Calcium Carbonates as Ultraviolet Stabilizers and Impact Modifiers in Poly (Vinyl Chloride) Siding and Profiles, Polym. Sci. Technol. Polym. Addit. **6** (1984) 371–389.

[14] T.H. Ferrigno, E.J. Wickson, Handbook of PVC Formulating, John Wiley & Sons, Inc., New York, 1993, p. 426.

[15] B. Azimipour, F. Marchand, Effect of calcium carbonate particle size on PVC foam, J. Vinyl. Addit. Technol. **12** (2006) 55–57.

IZVOD

UTICAJ SASTAVA PVC PLASTISOLA I USLOVA PROIZVODNJE NA STEPEN EKSPANZIJE PENA I OTPORNOST NA CEPANJE

Rajko Radovanović[1], Vladislav Jašo[2], Branka Pilić[2], Dragoslav Stoiljković[2]

[1]OOO JUTEKS RU, Dorozhnaya street 10, 601301 Kameshkovo, Russia
[2]Tehnološki fakultet, Univerzitet u Novom Sadu, Novi Sad, Srbija

(Naučni rad)

Kvalitet PVC podova zavisi pre svega od kontrole nastanka ćelijske strukture polivinilhlorida (PVC) pena. Ćelijska struktura i krajnja svojstva PVC pene zavise od mnoštva proizvodnih prametara. U ovom radu izučavan je uticaj koncentracije sredstva za penjenje i kalcijum karbonata kao punila, kao i temperature i vremena penjenja na stepen ekspanzije i otpornosti na cepanje PVC pena. Osim toga, urađena je regresiona analiza u cilju utvrđivanja značaja navedenih parametara na stepen ekspanzije i otpornost na cepanja PVC pena. Utvrđeno je da koncentracija sredstva za penjenje u smeši za penjenje ima presudan uticaj na stepen ekspanzije PVC pena. Otpornost na cepanje, pokazalo se, zavisi podjednako od svih izučavanih parametara. Pokazano je da dodatak kalcijum karbonata kao punioca ima vrlo mali uticaj na smanjenje stepena ekspanzije ali zato, sa druge strane, značajno utiče na smanjenje cene krajnjeg proizvoda. Ovo je primenjeno u praksi radi povećanja ekonomske efikasnosti proizvodnje PVC podova u fabrici JUTEKS u Rusiji.

Ključne reči: PVC plastisol • Ekspanzija pena • Otpornost na cepanje

Capacitive properties of polypyrrole/activated carbon composite

Aleksandra Porjazoska Kujundziski[1], Dragica Chamovska[2], Toma Grchev[2]

[1]*International Balkan University, Faculty of engineering, Macedonia*
[2]*Faculty of Technology and Metallurgy, Sts. Cyril & Methodius University, Skopje, Macedonia*

Abstract

Electrochemical synthesis of polypyrrole (PPy) and polypyrrole/activated carbon (PPy/AC) – composite films, with a thickness between 0.5 and 15 μm were performed in a three electrode cell containing 0.1 mol dm^{-3} Py, 0.5 mol dm^{-3} $NaClO_4$ dissolved in ACN, and dispersed particles of AC (30 g dm^{-3}). Electrochemical characterization of PPy and PPy/AC composites was performed using cyclic voltammetry (CV) and electrochemical impedance spectroscopy (EIS) techniques. The linear dependences of the capacitance (q_C), redox capacitance (q_{red}), and limiting capacitance (C_L) of PPy and PPy/AC – composite films on their thickness (L), obtained by electrochemical and impedance analysis, indicate a nearly homogeneous distribution of the incorporated AC particles in the composite films (correlation coefficient between 0.991 and 0.998). The significant enhancement of q_C, q_{red} and C_L, was observed for composite films (for 40±5%) in respect to that of the "pure" PPy. The decreased values of a volume resistivity in the reduced state of the composite film, ρ = 1.3×10^6 Ω cm (for L = 7.5 μm), for two orders of magnitude, compared to that of PPy – film with the same thickness, $\rho \approx 10^8$ Ω cm, were also noticed.

Keywords: conducting polymers, composites, cyclic voltammetry, electrochemical impedance spectroscopy (EIS), electrical equivalent circuits (EECs).

Available online at the Journal website: http://www.ache.org.rs/HI/

Polymers

SCIENTIFIC PAPER

UDC 544.6:54–126:543.42

Hem. Ind. **68** (6) 709–719 (2014)

doi: 10.2298/HEMIND140305063P

Electrochemical capacitors (ECs) as power devices, with the possibility of completely charging or discharging in seconds, have an important role in complementing or substituting conventional batteries [1]. Depending on the charge storage mechanism, as well as the active material used, two types of ECs can be distinguished.

The first type is a double layer kind of capacitance that uses carbon-based active materials with a relatively high electronic conductivity, electrochemical stability and acceptable cost [2,3]. The power and energy-storage capabilities of these devices are closely linked to the physical and chemical characteristics of carbon electrodes. For example increases in specific surface area obtained through the activation of carbon, generally lead to an increased capacitance [3–5].

A second group of ECs, known as pseudocapacitors or redox supercapacitors, uses fast and reversible surface or near-surface reactions, Faradaic chemical processes. Transition metal oxides, as well as electrically conducting polymers (polyaniline, polypyrrole, polythiophene and their derivatives), have been tested in EC applications as pseudocapacitance materials [6].

In the case of the conducting polymer materials, it becomes somewhat difficult to distinguish whether the charging process is to be considered as the double layer type or a redox pseudocapacitance nature [1]. However, the capacitance developed on a conducting polymer holds a Faradaic origin with process of chemical/ /electronic changes like formation or removal of radical cation or radical anion centers indicating a pseudocapacitance character [6–9].

Among the conducting polymers known to date, ones based upon polypyrrole (PPy) have attracted great attention because of their excellent environmental stability, tuned electrical conductivity and biocompatibility [10,11], and potential technical application in various fields, such as in electronic and electrochromic devices [8], electrode material in supercapacitors [6,9], sensors [12], light-weight batteries [13], membrane separation [14], corrosion protection [15–17] or substrates for tissue engineering [10,11].

When used as bulk materials, conducting polymers suffer from a limited stability during cycling that reduces the initial performance [18]. The mechanical properties and electrochemical stability might be improved *via* preparation of graft and block copolymers [19], as well as systems comprising two electrochemically active components [3,6], one with a double layer capacitance, (carbon fibers or carbon black), and the other, with a pseudo-capacitance (Faradaic) features (electroconducting polymers, such as PPy) [20,21].

Thus, Kim *et al.* [3] prepared PPy/vapor grown carbon fibers/AC (PPy/VGCF/AC) composites characterized by both, pseudo and electric double layer capacitance. As observed by cyclic voltammetry, the specific capacitances of composites in 6 mol dm^{-3} KOH

Correspondence: T. Grchev, Faculty of Technology and Metallurgy, Sts. Cyril & Methodius University, Skopje, Macedonia.
E-mail: dragica@tmf.ukim.edu.mk
Paper received: 5 March, 2014
Paper accepted: 27 August, 2014

raises from ~165 F g^{-1} for 5 wt.% AC, to ~338 F g^{-1} for 60 wt.% AC in electrodes of 2 nm-thick PPy film deposited on a highly conductive carbon fiber.

One of the techniques of capacitance enhancement and supercapacitors life-cycles, nanocomposites based on electronically conductive polymers and carbon nanotubes [4] and / or conductive carbon powder have been prepared [5]. It was shown [4] that the specific capacitance of such systems increased with both, the nanotubes amount, and the PPy content in the composites.

Despite the advantages of carbon nanotubes concerning their mechanical, thermal, electrical properties, as well as their big specific area, very complex techniques for their synthesis, hence their high cost, and severe human's health impact especially during their handling, could be considered as their serious drawbacks [22,23].

Therefore, in our study as a component responsible for double layer capacitance of the composite material we have used activated carbon. We have shown [21] that incorporation of the AC particles in the PPy – matrix sharply increases the electronic conductivity from ~200 F g^{-1} for a neat PPy films to ~530 F g^{-1} for PPy/AC composites containing ~55 wt.% AC, results very similar to those elaborated in the literature for similar systems involving nanocomposites [4,24].

Our further research was concentrated on the synthesis of PPy and PPy/AC composite films with thicknesses ranging between 1.5 and 15 μm, from non-aqueous, acetonitrile (ACN) solution containing 0.1 mol dm^{-3} Py and dispersed particles of activated carbon (AC). The concentration of the AC particles in the solution for electrochemical polymerization was 30 g dm^{-3}. The obtained composites were investigated by cyclic voltammetry and electrochemical impedance spectroscopy (EIS).

The increased conductivity noticed among the "neat" PPy films with higher thicknesses, and also at PPy/AC composites over that of the "pure" PPy film, has been discussed in relation with the developed microporosity of composite films and facilitated diffusion of doping anions in the films bulk.

Different equivalent electrical circuits were used to fit the experimental impedance data at anodic (0.2 V/SHE) and cathodic potentials (–0.6 V/SHE) at which the PPy as a pure polymer film and in the composites as well, are in the conducting and insulating states, respectively. As proposed [24], the electrical circuit model parameters for the best fitting suggested by the simulation software, describe the behavior of the porous structure, anion diffusion, and charge transfer effect.

EXPERIMENTAL

High grade chemicals: pyrrole (Py, Merck), acetonitrile (ACN, Merck), sodium perchlorate (Aldrich), and activated carbon (AC, Merck) were used as received.

Specific area of activated carbon of ~ 540 m^2g^{-1} was determined using spectrophotometric method ($\lambda \approx 570$ nm) and methylene blue as an absorbate.

Electrochemical synthesis of PPy and PPy/AC composite films were carried out by Chronoamperostat CEAMD 6 – Tacussel, in the three electrode cell containing 0.1 mol dm^{-3} Py and 0.5 mol dm^{-3} $NaClO_4$ (used as doping agent) dissolved in ACN, and dispersed AC particles (30 g dm^{-3}). The sedimentation of AC particles during the process of electrochemical synthesis was efficiently prevented by the agitation of the solution with purified nitrogen (~120 bubbles min^{-1}).

Polymerization was performed with constant current of 2.0 mA cm^{-2} and the electrode potential of this process varied between 0.95 and 1.05 V/SHE. As shown previously [25] an anodic (polymerization) charge of 0.36 C cm^{-2} is necessary for deposition of 1 μm PPy film. The polymerization process was performed within suitable time period necessary to obtain the previously assigned thicknesses of PPy in the "pure" polymer and in the composite films as well. The content of AC in the composites was determined by elemental analysis (EA).

A thermostated glass cell (25 °C) with three electrode system, consisting of working, auxiliary and reference electrode was used during the synthesis and electrochemical characterization of the polymer and composite films. A platinum electrode with surface area, A = 1.7 cm^2, was used as working electrode; platinum foil (~20 cm^2) as an auxiliary electrode and saturated calomel electrode as reference electrode. All potentials were measured versus saturated calomel electrode (SCE) and are referred to the standard hydrogen electrode (SHE).

Polypyrrole (PPy) and the composite PPy/AC films were investigated using cyclic voltammetry and electrochemical impedance spectroscopy (EIS) at constant potentials in acetonitrile (ACN) solution containing 0.5 mol dm^{-3} $NaClO_4$.

The cyclic voltammetry measurements (potentiostat connected to function generator, Institut für Physikalische Chemie und Elektrochemie, Heinrich Heine – Universität Düseldorf) were performed in the potential window from 0.95 to –0.6 V/SHE, and sweep rates ranging from 2 to 30 mV s^{-1}.

EIS measurements (frequency response analyzer TF 2000, Institut für Physikalische Chemie und Elektrochemie, Heinrich Heine – Universität Düseldorf) were carried out in the frequency range from 100 kHz to 10 mHz at constant potential of 0.2 V/SHE, for the characterization of doped, and –0.6 V/SHE for the undoped state of PPy and/or PPy/AC composite films; with a.c.

signal of 5 mV. The experimental results were fitted using software developed by Boukamp [26].

RESULTS AND DISCUSSION

Cyclic voltammetry

Electrochemical synthesis of PPy and PPy/AC composite films was performed at constant current density (2.0 mA cm^{-2}) from ACN electrolyte containing 0.1 mol dm^{-3} pyrrole, 0.5 mol dm^{-3} $NaClO_4$ and dispersed AC particles (30 g dm^{-3}). The thicknesses of PPy (from 0.5 to 15 μm) as a "pure" polymer, and as a constituent in the composite films were regulated by parameter Q using the Eq. (1):

$$L_{PPy} = \frac{Q(M_{Py} + yM_{ClO_4^-})10^4}{(2+y)F\rho_{PPy}} \ (\mu m) \quad (1)$$

where Q is the anodic charge of formation (C cm^{-2}), and it was taken to be 0.36 C cm^{-2} μm^{-1} [25], while y is the doping level of the obtained PPy (usually 0.2–0.3), the density ρ_{PPy} = 1.51 g cm^{-3} [21], M_{Py} is the molar mass of the pyrrole repeating unit and $M_{ClO_4^-}$ the molar mass of the ClO_4^- doping anion, and F is the Faraday constant. As it was previously found the doping level of ClO_4^- in ACN solution was found to be 0.245 and 0.24 at the polymerization potentials of 0.95 and 1.05 V/SHE, respectively [25]. Regarding the thickness of polypyrrole (PPy) and composite (PPy/AC) films, as a first approximation, the same density of both has been taken ($\rho_{PPy} \approx \approx \rho_{PPy/AC} \approx 1.51$ g cm^{-3}).

Cyclic voltammograms of PPy and PPy/AC composite films in 0.5 mol dm^{-3} $NaClO_4$ obtained in potential range of –0.6 to 0.95 V/SHE, and scan rates of 2 to 30 mV s^{-1} are presented in Figure 1. The linear dependences of capacitance current (j_C) on sweep rates (dE/dt) for different thicknesses (5, 10 and 15 μm) of "neat" polymer and composite films are shown in Figure 2, while the corresponding voltammetric parameters are enclosed in Table 1.

Our observations of redox charge (q_{red}) and capacitance (q_C) enhancement for about 40% of PPy/AC – composites in respect to that of PPy-film confirm our previous observations [21] and literature data of similar systems [3,27]. Hence, q_{red} and q_C values from 283 C g^{-1} (216 F g^{-1}) for "pure" PPy-film increased to ~385 C g^{-1} (~318 F g^{-1}), for the PPy/AC composite films. q_{red} was calculated by the integration of an area under the voltammetric curves, Figure 1, and the values of the capacitance, q_C, were obtained according the Eq. (2) (as a slope of the linear j_C/(dE/dt) plots), Figure 2 [28,29]. The ratio q_C/q_{red} usually ranged about 0.8, for both, PPy and PPy/AC composite films, demonstrates a primary contribution of the capacitive component in the total current ($j_{total} = j_c + j_F$).

$$C = j_c \Big/ \mathrm{d}\left(\frac{\partial E}{\partial t}\right) \quad (2)$$

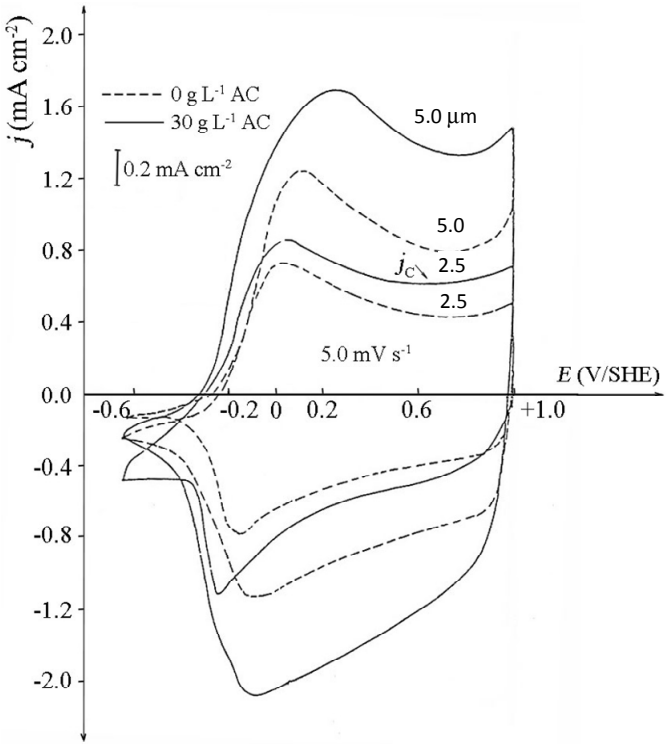

Figure 1. Voltamograms for PPy and PPy/AC – composite films synthesized from 0.1 mol dm^{-3} Py in 0.5 mol dm^{-3} $NaClO_4$; $Q_{pol.}$ = 0.36 C cm^{-2} μm^{-1}.

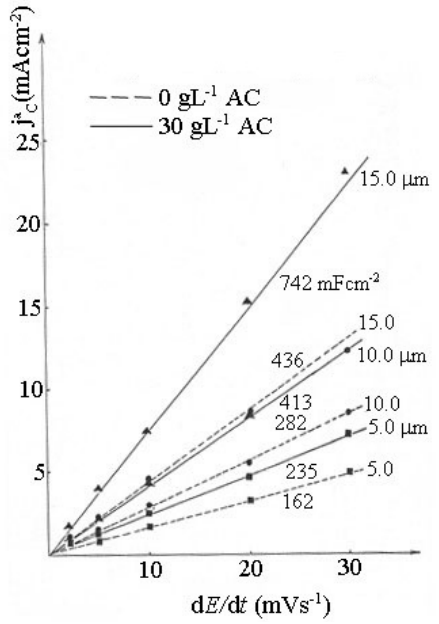

Figure 2. j_C/(dE/dt) dependences for composite PPy/AC films, with different thicknesses.

panied by the insertion and ejection of anions from a polymer film:

$$PPy + yClO_4^- \underset{\text{Reduction}}{\overset{\text{Oxidation}}{\rightleftharpoons}} [(PPy)^{y+} yClO_4^-] + ye^-$$

where ClO_4^- is a doping anion to compensate positive charges generated during oxidation processes, and *y* is the doping level.

The processes of doping (oxidation) of PPy films using the perchlorates are characteristic for the anodic potential range (0.9 – –0.2 V/SHE), while in the cathodic range (–0.2 – –0.6 V/SHE) PPy exists in its undoped (reduced) form.

The incorporated AC particles with their redox characteristics contribute to the redox behavior of the composite films. It is considered that the oxygen groups at the surface play the main role in the electrochemical behavior of activated carbon. The electronic conductivity of the activated carbon, mainly, does not depend on the potential, so as it was expected, their presence in the composite films provides a good conductivity, at

Table 1. Redox behavior of PPy and PPy/AC composite films obtained with dispersed particles of AC in the solution for electrochemical synthesis; C_{AC} = 30 g dm^{-3}. $j_{pol.}$ =2.0 mA cm^{-2}; $Q_{pol.}$ – anodic charge necessary for polymerization of PPy of a given thickness; τ_{pol} –time of polymerization of PPy and PPy/AC composites; L_{PPy} – the thicknes of the PPy film in the PPy/AC composite; $L_{PPy/AC}$ – the thickness of the composite PPy/AC film, values given in the parenthesis; assuming $\rho_{PPy} \approx \rho_{PPy/AC}$: 1.51 g cm^{-3}; m^f_{PPy} – mass of the polypyrrole in the composite film; $m^f_{PPy/AC}$ – mass of the composite film; m^f_{AC} – mass of activated carbon in the composite film; q_C – capacitance calculated from the voltammograms, by the relation:

$$C = j_C \Big/ \left(\frac{dE}{dt}\right);$$

q_{red} – redox capacitance, obtained by the graphical integration of the area under anodic and cathodic processes on the volatammograms

$Q_{pol.}$ / C cm^{-2}	τ_{pol} / s	L_{PPy}; $L_{PPy/AC}$ / μm	m^f_{PPy}	$m^f_{PPy/AC}$	m^f_{AC}	q_{red} / mC cm^{-2}		q_C / mF cm^{-2}	
				mg cm^{-2}		0	30 g dm^{-3} AC	0	30 g dm^{-3} AC
0.180	90	0.5 (~0.7)	0.075	0.105	0.030	22	–	16.8	–
0.540	270	1.5 (~2.43)	0.225	0.364	0.139	64.45	94.5	~58	62.5
0.900	450	2.5 (~4.55)	0.375	0.682	0.307	119	~142	92	108
1.800	900	5.0 (~8.85)	0.750	1.328	0.578	216	278	162	235
2.700	1350	7.5 (~13.43)	1.125	2.015	0.890	340	373	237	305
3.600	1800	10.0 (~18.13)	1.500	2.720	1.220	413	478	282	413
5.400	2700	15.0 (~27.07)	2.250	4.060	1.810	595	835	436	742

Significantly increased values of q_{red} and q_C for the composites are essentially attributed to the increased area of the solution / composite film interface and/or its capacitance similar to that shown for arrangements comprising electroconducting polymers and carbon based constituents [24,30,31]. Namely, in the case of the composite film mainly two processes take place: charging/discharging of the double layer AC particles/ /solution interface and the redox processes of the bulk PPy film [7,32,33]: it is known that the electrochemical behavior of PPy films is mainly based on their doping (oxidation)/undoping (reduction) processes, accom-

both oxidized and reduced state of polymer films. It was suggested that the synthesis of films with higher thicknesses and/or presence of AC particles increases the porosity of the composite films, which facilitate the ClO_4^- penetration in the films during doping, as well as their easier ejection during undoping processes [34].

The increased values of the capacitances of composite films in respect to those of "pure" PPy film, as well as, the linear q_{red}/L and q_C/L plots (correlation coefficient between 0.991 and 0.998), Figure 2 and Table 1, indicate a relatively homogenous distribution

of the AC particles irrespective to the thickness of the composite films.

Electrochemical impedance spectroscopy (EIS) study

The study performed by electrochemical impedance spectroscopy (EIS) confirms the electrochemical behavior of PPy and PPy/AC composite films shown in Figures 1 and 2, and Table 1.

Bode plots (log Z – log f, and φ – log f) of PPy/AC composite films with doped state of PPy (E = 0.2 V/SHE), are presented in Figure 3.

The impedance behavior of composite films indicates the existence of two regions:

The first one, between 100 kHz and ~10 Hz, with a small and almost constant values of the impedance, Z, and the values of the phase angle, φ, between 0 and –60°, is mainly attributed to the ohmic behavior of the electrolyte between the working and the reference electrode.

The second frequency range, $f \leq 10$ Hz, where Z and φ linearly increase in accordance with a "finite diffusion model" of Ho *et al*. [25,32], characterized by the existence of the diffusion controlled doping/undoping processes in the bulk of the composite films [32,33].

The impedance characteristics of the PPy/AC systems are summarized in Table 2, where R_{el} – resistance of the electrolyte ($Z' \approx R_{el}$ = ~13 Ω cm^2, determined at $f \rightarrow \infty$), R_L – limiting resistivity of the films, R_{total} – total resistance ($R_{total} = R_{el} + R_L$), extrapolated at very low frequencies ($Z' \approx R_{total}$, at $f \rightarrow 0$), C_L – limiting capacitance of the film, and D – diffusion constant of doping anions.

The values of the limiting capacitance, C_L, listed in the Table 2, are calculated from the linear plots: $-Z''/(1/\omega)$, shown in Figure 4, according the Eq. (3):

$$1 / C_L = \mathrm{d}(-Z'') / \mathrm{d}(1 / \omega) \quad (3)$$

where ω is an angular frequency ($\omega = 2\pi f$).

The linear dependences of C_L of polymer and composite films on their thicknesses are shown in Figure 5. Increasing values of the limiting capacitance, C_L, of the PPy/AC composite films compared to that of a "pure" PPy films, Figure 5, is in accordance to the previously calculated values of q_C. Namely, limiting capacitance (C_L) of the composite films, takes values of ~260 F g^{-1} (~73 A h kg^{-1}) compared to ~180 F g^{-1} (~50 A h kg^{-1}) for the PPy film, which is very close to those of similar sys–tems [35].

The diffusion coefficient, D, of the doping anions (ClO_4^-), for PPy/AC composite films, is calculated by equation: $D = L^2/3R_LC_L$, according to the diffusion model of Ho *at al*. [32]. It is obvious that for relatively small thicknesses, the diffusion coefficient takes values in the order of magnitude of 10^{-9} cm^2 s^{-1} (increasing with the thickness of the composite films, Table 2). This phenomenon is most probably result of the facilitated transport of the doping anions in the bulk of the composites, that could be ascribed, as it was shown in the literature, to the increased amount of both, PPy and AC particles in the films [19,36]. The values of the diffusion coefficients which depend on the thickness and morphology of the film, the synthesis condition, as well as the nature of the doping anion, are in accordance to the literature data [19,25,33,36]. Thus, Malviya *et al*.

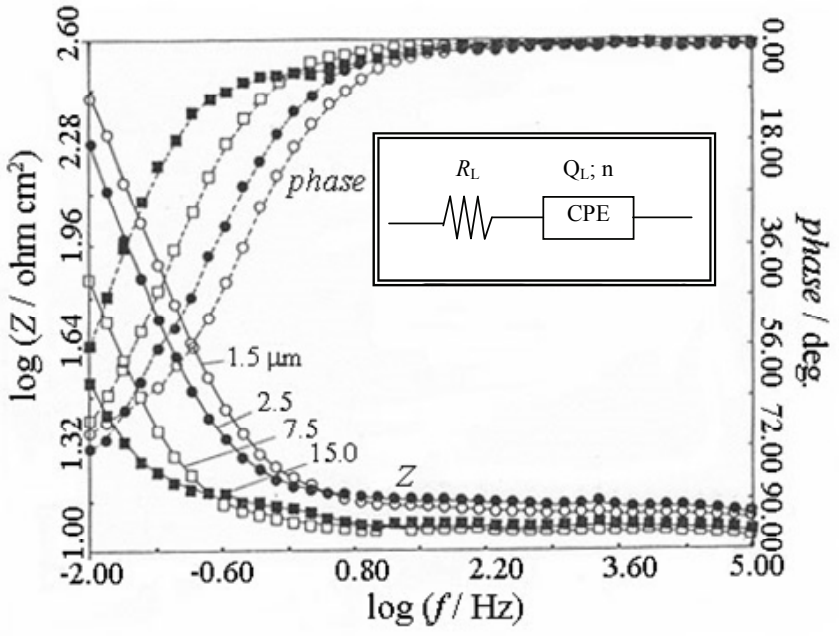

Figure 3. Bode plots (log Z – log f, and φ – log f) of PPy/AC composite films (30 g dm^{-3} AC) with different thicknesses, in doped (E = 0.2 V/SHE) state of PPy in the 0.5 mol dm^{-3} NaClO$_4$/ACN solution.

Table 2. Impedance characteristics of PPy/AC composite films in doped (oxidized) state of PPy; C_{AC} = 30 g dm^{-3}; E = 0.2 V/SHE

L_{Ppy} / μm (m^f_{PPy} / mg cm^{-2})	R_{el} / Ω cm^2	R_L / Ω cm^2	R_{total} / Ω cm^2	C_L / mF cm^{-2}	$D\times10^8$ / cm^2 s^{-1}
1.5 (0.225)	13±0.5	87	~100	~68	0.127
2.5 (0.375)		49	64	107	0.397
5.0 (0.750)		16.5	30	244	2.07
7.5 (1.125)		16.0	~28	360	3.26
10.0 (1.5)		12.0	~27	405	6.86
15.0 (2.25)		~5.5	~22	587	17

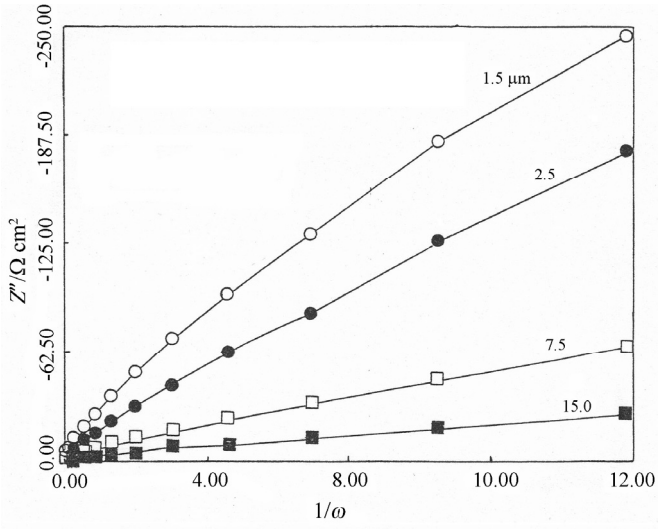

Figure 4. Z'' – 1/ω plots for PPy/AC composite films (30 g dm^{-3}) with different thicknesses, in the 0.5 mol dm^{-3} $NaClO_4$/ACN solution for the doped (E = 0.2 V/SHE) state of PPy.

found that the diffusion coefficient of a less voluminous chlorine anion in PPy system is of the order of magnitude of 10^{-7} cm^2 s^{-1} [36].

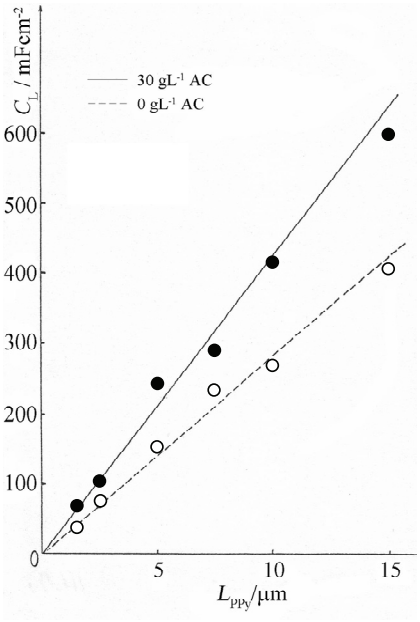

Figure 5. C_L/L_{PPy} plots (calculated from the –Z''/(1/ω)) for PPy and composite PPy/AC films in the doped (E = 0.2 V/SHE) state of PPy, in the solution of 0.5 mol dm^{-3} $NaClO_4$ (ACN).

Nyquist (–*Z*'' *vs. Z*') plots of PPy and composite PPy/AC films, for the conducting state of polymer component, are presented in Figure 6a and b.

The impedance behavior of "neat" PPy and/or PPy/AC composite films, for the best fit of the experimentally obtained data, in the conducting state of PPy (*E* = 0.2 V/SHE), as suggested by the simulation software developed by Boukamp [26], can be described by a simple RQ equivalent electrical circuit (EEC), presented in Figure 7a [31,37]. On the other hand, it appears that EEC presented in the Figure 7b [19,31,37] gives significantly better agreement to the –*Z*''/*Z*' plots, Figure 6a and b. Such a behavior has been observed mainly for composite films with the thicknesses higher than 2.5 μm.

The best fitting parameters of R(QR)Q equivalent electrical circuit (Figure7b) for PPy and composite PPy/AC films, as proposed by the software, are given in Table 3. R_{el} denotes the ohmic resistance of the electrolyte, R_{ct} is proportional to the charge transfer resistance, the element Q_1 (with the exponential coefficient n_1), known as constant phase element (CPE), correspond to the double layer capacitance, C_{dl} ($C_{dl} = Q^{1/n}$). For $L_{PPy} \geq 2.5$ μm the coefficients n_1 takes similar values for both, PPy and PPy/AC films, indicating diffusion or mixed (ohmic-diffusion) control at the film/solution

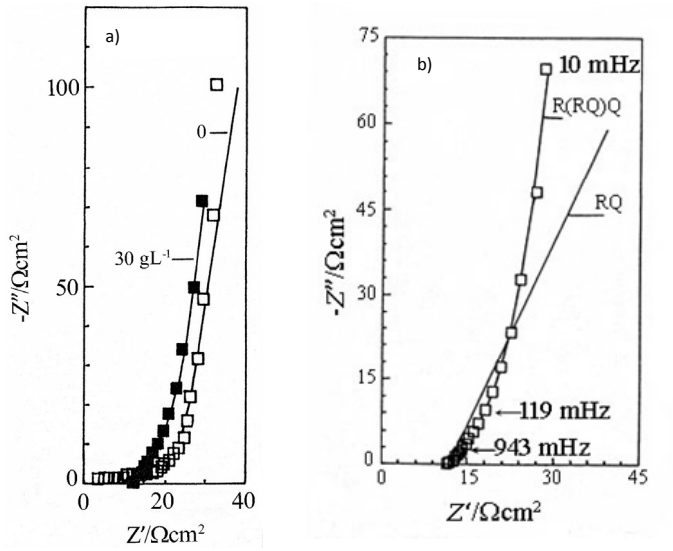

Figure 6. Nyquist plots for PPy (a) and composite PPy/AC film (a and b), L_{PPy}= 5 μm, in the oxidized (doped) state of PPy (E = 0.2 V/SHE) in 0.5 mol dm^{-3} $NaClO_4$/ACN solution for the RQ and R(QR)Q EEC; experimentally obtained values of "neat" PPy: (-□-) and PPy/AC composites: (-■-); simulation: (—).

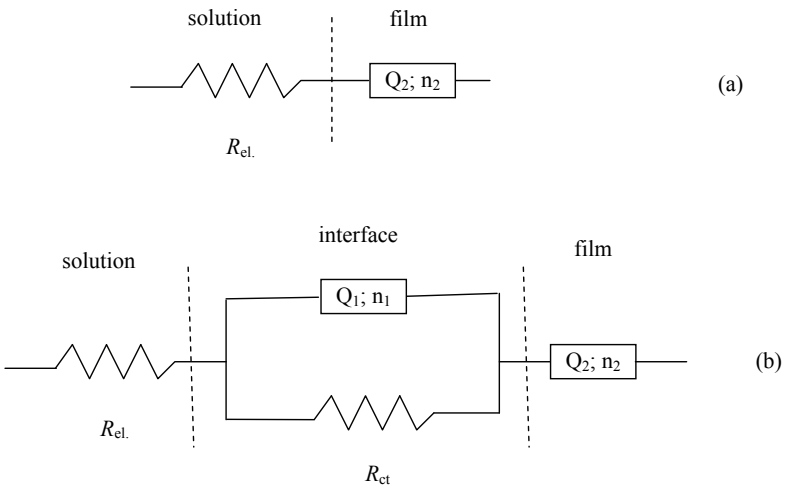

Figure 7. Electrical equivalent circuit for doped (E = 0.2 V/SHE) state of PPy (L_{PPy} = 5 μm) in the PPy/AC composite film.

Table 3. The best fitting impedance parameters of R(QR)Q equivalent electrical circuit (Figure 7b) for PPy (values given in the parenthesis) and composite PPy/AC films, C_{AC} = 30 g dm^{-3}, E = 0.2 V/SHE

L_{PPy} / μm	$R_{el.}$ / Ω cm^2	R_{ct} / Ω cm^2	Q_1/Ω^{-1} s^n cm^{-2}	n_1	Q_2/Ω^{-1} s^n cm^{-2}	n_2
0.5	–	–	–	–	–	–
	(4.1)	(46.0)	($7.23\cdot10^{-4}$)	(0.53)	($1.14\cdot10^{-2}$)	(0.907)
1.5	12.0	4.4	0.224	0.127	3.3×10^{-2}	0.783
	(3.0)	(36.0)	(5.22×10^{-4})	(0.485)	(3.27×10^{-2})	(0.917)
2.5	12.8	4.9×10^{18}	0.36	0.120	5.54×10^{-2}	0.82
	(3.2)	(131.0)	(5.94×10^{-5})	(0.735)	(2.25×10^{-2})	(0.735)
5.0	~12	23.5	0.123	0.517	0.235	0.977
	(~0)	(~33)	(1.11×10^{-2})	(0.226)	(0.119)	(0.921)
10.0	14.1	527	0.533	0.511	0.262	0.913
	(11.6)	(~9)	(1.445×10^{-2})	(0.525)	(0.207)	(0.88)
15.0	11.3	4.31	0.082	0.572	0.416	0.879
	(–)	(–)	(–)	(–)	(–)	(–)

interface [24,35]. The very slow processes in the bulk of the composite films are presented by a phase element Q_2 (with the exponent n_2), proportional to the limiting capacitance, C_L. The coefficient n_2 with a substantially higher values clearly shows a relatively close behavior to that of an ideal capacitor (n = 1). The difference in the values of the limiting capacitance Q_2 (28.4 mF cm^{-2} μm^{-1}), of PPy/AC composites, calculated by regression analysis (Q_2/L) of data in Table 3, and the limiting capacitance, C_L (39.4 mF cm^{-2} μm^{-1}), obtained using the $-Z''/(1/\omega)$ dependences, is most probably result of the different EECs considered. Namely, the simple RQ circuit, Fig. 7a, was applied during determination of C_L, while Q_2 values are obtained with the R(QR)Q EEC, more consistent with the experimentally obtained data (Fig. 7b).

Bode and Nyquist plots in Figures 8 and 9, respectively, concern the features of PPy film (5 μm) in doped (E = 0.2 V/SHE) and undoped (E = –0.6 V/SHE) states, indicating some qualitative and quantitative differences

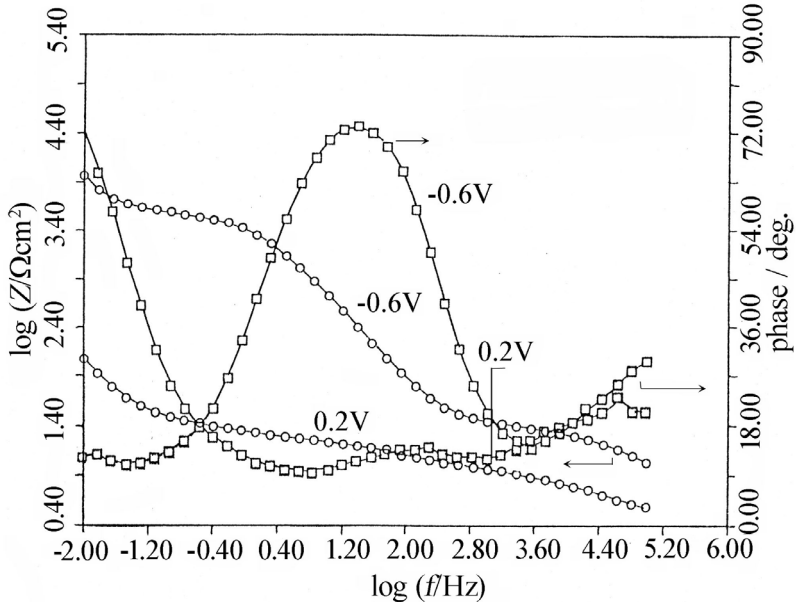

Figure 8. Bode plots (log Z – log f, and φ – log f) for PPy film (5 μm) in doped (E = 0.2 V/SHE) and undoped (E = –0.6 V/SHE) states, in 0.5 mol dm^{-3} NaClO$_4$/ACN solution.

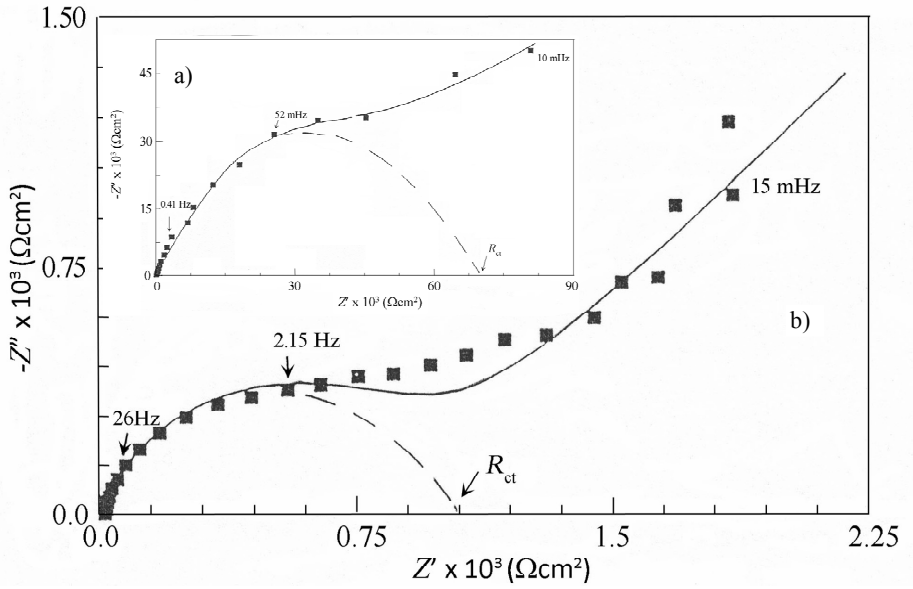

Figure 9. Nyquist plot (–Z''/Z') for a) PPy film and b) composite PPy/AC film (30 g dm^{-3} AC), L_{PPy} = 7.5 μm, in the undoped (E = –0.6 V/SHE) state of PPy, in 0.5 mol dm^{-3} NaClO$_4$/ACN) solution, for the best fitting R(QR)Q (a) and R[Q(RW)] (b) EEC; experimentally obtained values of "neat" PPy and PPy/AC composites: (-■-); simulation: (—).

in the impedance behavior of PPy and composite PPy/AC films in both, doped (conducting) and undoped (insulating) state of PPy.

When undoped state of PPy, "neat" and as a part of composite PPy/AC films is concerned, the dominant semicircles in $-Z''/Z'$ plots, Figure 9, attributed to the charge transfer processes at the polymer/solution interface, and the linear part of these dependences, at very low frequencies, characteristic for diffusion controlled processes, Warburg impedance [35], can be expressed by the EECs in Figure 10a and b. Namely, the simpler EEC, Figure 10a, has been used for fitting the data obtained for the films with lower thicknesses, while for the systems with higher thicknesses, a more complex EEC, Figure 10b, should be applied.

which mainly depends on the concentration of AC particles in the composites, and is almost independent on the given potential.

CONCLUSIONS

Polypyrrole (PPy) and composites based on polypyrrole/activated carbon (PPy/AC), with the thickness of PPy in both, the "neat" and the composite films ranged 1.5 and 15 μm, were synthesized electrochemically, from non-aqueous, acetonitrile (ACN) solution containing Py (0.1 mol dm^{-3}) and constant concentration of activated carbon (AC) (30 g dm^{-3}). The obtained composites were investigated by cyclic voltammetry and electrochemical impedance spectroscopy (EIS).

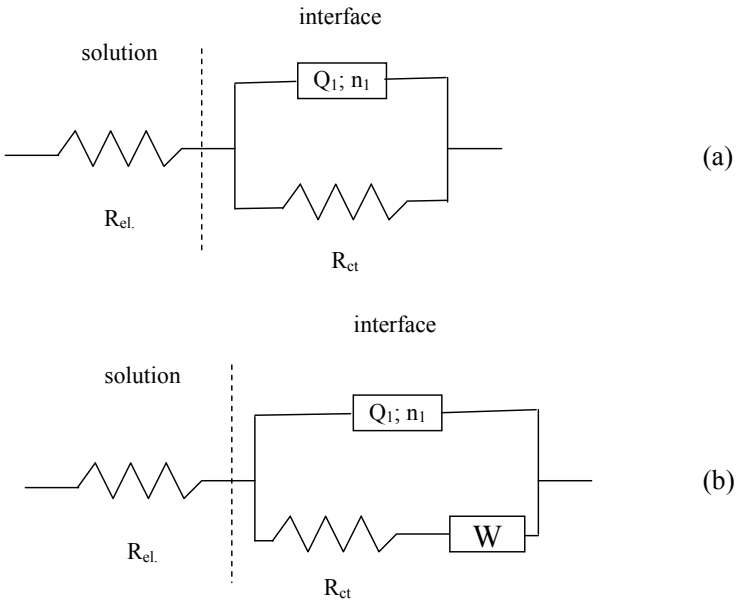

Figure 10. Equivalent electrical circuits R(QR) for PPy film (a) and R[Q(RQ)] for PPy/AC composite film (b), in undoped (E = –0.6 V/SHE) state of PPy.

The ohmic charge transfer resistance, R_{ct}, depends on both, the film thickness, and the quantity of AC particles in the composite film. The presence of the AC particles in composite film reduces the volume resistivity, ρ, for about two orders of magnitude in respect to that of the PPy-film. Thus, $\rho = 7\times10^{4}/7.5\times10^{-4} - 10^{8}$ Ω cm (the R_{ct} value is ~70 kΩ cm^2) for PPy film (Figure 9a), while ρ of the PPy/AC composite film, with the same thickness (Figure 9b), takes value of $1000/7.5\times10^{-4} = 1.3\times10^{6}$ Ω cm ($R_{ct} \approx 1$ kΩ cm^2). Such a behavior is most likely related to an increased conductivity and microporosity of these films. Two types of conductivities are characteristic for PPy/AC composites: ionic and electronic. Composites comprise two independent components: a polymer responsible for ionic conductivity, while AC with its physical and chemical properties provides the electronic conductivity of these systems,

It was shown that the best fitting EEC, for PPy and/or PPy/AC composite films in their conducting state is the R(QR)Q equivalent electrical circuit, and R[Q(RW)] equivalent electrical circuit for the insulating state.

The charge transfer resistance (R_{ct}) depends on both, the thickness of the films, as well as, the presence of the AC in the composites. A higher quantity of AC in the PPy/AC composites decreases the volume resistivity for two orders of magnitude in respect to a "pure" PPy films, in both, conducting and insulating states ($\rho = 1.3\times10^{6}$ Ω cm for the composite PPy/AC film, L = 7.5 μm, and $\rho \approx 10^{8}$ Ω cm for the PPy film with the same thickness).

Based on the previously presented results of the PPy/AC electroconducting composites comprising two electrochemically active components, such as DLC

(double layer capacitors)–active carbon and redox properties of PPy, can be effectively used in supercapacitors and/or batteries.

REFERENCES

[1] B.E. Conway, W.G. Pell, Double layer and pseudocapacitance types of electrochemical capacitor and their applications to the development of hybrid devices, J. Solid State Electrochem. **7** (2003) 637–644.

[2] E.D. Laird, M.A. Hood, C.Y. Li, in: Y. Gogotsi, V. Presser (Eds.), Carbon nanomaterials CRC Press, Taylor & Francis Group, Boca Raton, FL, 2006, pp. 135–187.

[3] J-H. Kim, Y-S. Lee, A.K. Sharma, C.G. Liu, Polypyrrole/carbon composite electrode for high-power electrochemical capacitors, Electrochim. Acta **52** (2006) 1727–1732.

[4] A. Imani, G. Farzi, A. Ltaief, Facile synthesis and characterization of polypyrrole-multiwalled carbon nanotubes by in situ oxidative polymerization, Int. Nano Lett. **52** (2013) 1–8.

[5] S. Paul, J-H. Kim, D-W. Kim, Cycling performance of supercapacitors assembled with polypyrrole/multiwalled carbon nanotube/conductive carbon composite electrodes, J. Electrochem. Sci. Techn. **2** (2011) 91–96.

[6] P. Simon, Y. Gogotsi, Materials for electrochemical capacitors, Nat. Mater. **7** (2008) 845–854.

[7] S.M. Jovanovic, R. Stankovic, V. Laninovic, G. Nestorovic, M. Popovic, B. Vidic, O. Pavlovic, N. Krstajic, B. Grgur, M. Vojnovic, S. Stankovic, Synthesis and electrochemical properties of polypyrrole, polyaniline and poly-3-methyl thiophene, Hem. Ind. **54** (2000) 417–427.

[8] M. Natalie, R.J. Mortimer, R.J. Mortimer, New Electrochromic Materials, Sci. Prog. **85** (2002) 243–262.

[9] J. Zhang, L-B. Kong, H. Li, Y-Ch. Luo, L. Kang, Synthesis of polypyrrole film by pulse galvanostatic method and its application as supercapacitor electrode materials, J. Mater. Sci. **45** (2010) 1947–1954.

[10] C. Mao, A. Zhu, Q. Wu, X. Chen, J. Kim, J. Shen, New biocompatible polypyrrole- based films with good blood compatibility and high electrical conductivity, Colloids Surfaces, B **67** (2008) 41–45.

[11] D. Beattie, K.H. Wong, C. Williams, L.A. Poole-Warren, T.P. Davis, C. Barner-Kowollik, M.H. Stenzel, Honeycomb-structured porous films from polypyrrole-containing block copolymers prepared *via* RAFT polymerization as a scaffold for cell growth, Biomacromolecules **7** (2006) 1072–1082.

[12] J. Zhang, S. Wang, M. Xu, Y. Wang, H. Xia, S. Zhang, X. Guo, S. Wu, Polypyrrole-coated SnO_2 hollow spheres and their application for ammonia sensor. J. Phys. Chem., C **113** (2009) 1662–1665.

[13] H.K. Song, G.T.R. Palmore, Redox-active polypyrrole: toward polymer-based batteries, Adv. Mater. **18** (2006) 1764–1768.

[14] Q. Ameer, S.B. Adeloju, Polypyrrole-based electronic noses for environmental and industrial analysis, Sens. Actuators, B **106** (2005) 541–552.

[15] N.V. Krstajić, B.N. Grgur, S.M. Jovanović, M.V. Vojnović, Corrosion protection of mild steel by polypyrrole coatings in acid sulfate solutions. Electrochim. Acta **42** (1997) 1685–1691.

[16] L. Koene, W.J. Hamer, J.H. De Wit, Electrochemical behavior of poly(pyrrole) coatings on steel, J. Appl. Electrochem. **36** (2006) 545–556.

[17] H. Shokry, Corrosion protection of mild steel electrode by electrochemical polymerization of acrylamide, Chem. Met. Alloys **2** (2009) 202–210.

[18] R. Kotz, M. Carlen, Principles and applications of electrochemical capacitors, Electrochim. Acta **45** (2000) 2483––2498.

[19] E. Kalaycioglu, L. Toppare, T. Grchev, M. Cvetkovska, Y. Yagci, Impedance characteristics of conducting polypyrrole-poly(ethylvinylether) graft films, Turk. J. Chem. **23** (1999) 1–7.

[20] M.Cvetkovska, T. Grchev, T. Obradovic, Electroconductive polymer composite: Fibrous carrier-polypyrrole, J. Appl. Polym. Sci. **60** (1996) 2049–2058.

[21] A. Porjazoska Kujundziski, D. Chamovska, M. Cvetkovska and T. Grchev, Electrochemical Study of Electroconducting Composite Material–Polypyrrole/Activated Carbon, Int. J. Electrochem. Sci. **7** (2012) 4099–4113.

[22] G. Tejral, N.R. Panyala, J. Havel, Carbon nanotubes: toxicological impact on human health and environment, J. Appl. Biomed. **7** (2009) 1–13.

[23] A. Helland, P. Wick, A. Koehler, K. Schmid, C. Som, Reviewing the environmental and human health knowledge base of carbon nanotubes, Environ. Health Perspect. **115** (2007) 1125–1131.

[24] B. Veeraraghavan, J. Paul, B. Haran, B. Popov, Study of polypyrrole graphite composite as anode material for secondary lithium-ion batteries, J. Power Sources **109** (2002) 377–387.

[25] T. Grcev, M. Cvetkovska, Z. Sekovska, Voltammetric study of the redox processes of polypyrrole films, J. Serb. Chem. Soc. **58** (1993) 781–790.

[26] B.A. Boukamp, A Nonlinear Least Squares Fit procedure for analysis of immittance data of electrochemical systems, Solid State Ionics **20** (1986) 31–44.

[27] V. Khomenko, E. Frackowiak, F. Béguin, Determination of the specific capacitance of conducting polymer/nanotubes composite electrodes using different cell configurations, Electrochim. Acta **50** (2005) 2499–2506.

[28] J.W. Schultze, A. Thyssen, The kinetics of electropolymerization, Synth. Met. **43** (1991) 2825–2830.

[29] T.F. Otero, E. Angulo, Comparative kinetic studies of polypyrrole electrogeneration from acetonitrile solutions, J. Appl. Electrochem. **22** (1992) 369–375.

[30] T. Grchev, M. Cvetkovska, T. Obradovic, Redox properties of an electrochemically activated (oxidized) carbon fibre electrode, J. Serb. Chem. Soc. **62** (1997) 157––164.

[31] M. Ates, Review study of electrochemical impedance spectroscopy and equivalent electrical circuits of conducting polymers on carbon surfaces, Prog. Org. Coat. **71** (2011) 1–10.

[32] C. Ho, I.D. Raistrick, R.A. Huggins, Application of A-C Techniques to the Study of Lithium Diffusion in Tungsten Trioxide Thin Films, J. Electrochem. Soc. **127** (1980) 343–350.

[33] J. Mostany, B.R. Scharifker, Impedance spectroscopy of undoped, doped and overoxidized polypyrrole films, Synth. Met. **87** (1997) 179–185.

[34] E. Frackowiak, F. Beguin, Carbon materials for the electrochemical storage of energy in capacitors, Carbon **39** (2001) 937–950.

[35] P.A. Basnayaka, M.K. Ram, L. Stefanakos, A. Kumar, Graphene/polypyrrole nanocomposite as electrochemical supercapacitor electrode: electrochemical impedance studies, Graphene **2** (2013) 81–87.

[36] M. Malviya, J.P. Singh, B. Lal, R.N. Singh, Transport behavior of Cl^- in composite films of polypyrrole and $CoFe_2O_4$ obtained for oxygen reduction, New J. Mat. Electrochem. Sys. **8** (2005) 223–228.

[37] M.M. Lohrengel, O. Genz, Mechanism of the redox process of conducting polymers, Ionics **4** (1995) 304–310.

IZVOD

KAPACITIVNA SVOJSTVA KOMPOZITNIH FILMOVA POLIPIROL/AKTIVNI UGALJ

Aleksandra Porjazoska Kujundžiski[1], Dragica Čamovska[2], Toma Grčev[2]

[1]*International Balkan University, Faculty of engineering, Macedonia*
[2]*Faculty of Technology and Metallurgy, Sts. Cyril & Methodius University, Skopje, Macedonia*

(Naučni rad)

Elektrohemijska sinteza polipirola (PPy) i kompozitnih filmova polipirol/aktivni ugalj (PPy/AU) različitih debljina od 0,5 do 15 μm, ostvarena je u uslovima konstante količine naelektrisanja, iz rastvora acetonitrila koji je sadržavao 0,5 mol dm^{-3} $NaClO_4$; 0,1 mol dm^{-3} pirola (Py) i dispergovane čestice aktivnog uglja (30 g dm^{-3}). Elektrohemijske karakteristike PPy i PPy/AU kompozitnih filmova određene su pomoću ciklične voltametrije i spektroskopije elektrohemijske impedancije. Linearne zavisnosti kapacitivnosti (q_C), redoks kapacitivnosti (q_{red}) i granične kapacitivnosti (C_L) od debljine polipirolnih i kompozitnih filmova (L) ukazuju na homogenu distribuciju inkorporiranih čestica aktivnog uglja u kompozitne filmove. Primećeno je znatno povećanje q_C, q_{red}, i C_L vrednosti za kompozitne filmove (~40±5%) u odnosu na iste veličine ″čistog″ PPy filma. Uočeno je da kompozitni filmovi u neprovodnom stanju imaju za oko dva reda veličine manje vrednosti za specifičnu otpornost, ρ = 1,3×10^6 Ω cm, (za L = 7,5 μm) u poređenju sa PPy filmovima iste debljine, $\rho \approx 10^8$ Ω cm.

Ključne reči: Elektroprovodni polimeri • kompoziti • Ciklična voltametrija • Spektroskopija elektrohemijske impedancije • Električna ekvivalentna kola

Preparation, characterization and antimicrobial activity of chitosan microparticles with thyme essential oil

Danijela Pecarski[1], Zorica Knežević-Jugović[2], Suzana Dimitrijević-Branković[2], Katarina Mihajilovski[2], Slobodan Janković[3]

[1]*Sanitary and Medical School of Professional Studies "Visan", Belgrade, Serbia*
[2]*University of Belgrade, Faculty of Technology and Metallurgy, Belgrade, Serbia*
[3]*University of Kragujevac, Faculty of Medical Science, Kragujevac, Serbia*

Abstract

Development of an available drug delivery system is of great interest considering the therapeutic effects of formulations with violate essential oils, especially assuming the fact that using essential oils as antimicrobial agents is a rather expanded in antimicrobial therapy nowadays. In this paper, the chitosan microparticles with encapsulated thyme essential oil were prepared in the emulsion by cross-linking method. The effect of thyme oil and glutaraldehyde initial concentrations on particle size, morphology, and particle size distribution was investigated. In addition, the influence of these parameters on the encapsulation of thyme oil in chitosan microparticles, concerning thyme oil loadings and encapsulation efficiency was also tested. The particles showed a spherical shape with an average diameter of 4.71±1.42 to 13.65±4.34 μm, depending on the concentration of the essential oil and glutaraldehyde that were used. The diameter of microparticles appeared to increase with increasing the thyme essential oil concentration, and decreased with the increase of glutaraldehyde concentration. It was shown that the concentration of glutaraldehyde did not affect the degree of encapsulation, but the increase in the initial concentration of thyme oil increased the degree of encapsulation of this essential oil in chitosan microparticles. All particles containing thyme essential oil, as well as essential oil of thyme itself showed significant antimicrobial activity against *Staphylococcus aureus* ATCC 25923*, Esherichia coli* ATCC 25922*, Candida albicans* ATCC 24433 and *Enterococcus faecalis* ATCC 25929. This study showed a great potential of the use of thyme essential oil as an antimicrobial agent, especially when encapsulated in a drug delivery system with controlled release of the active antimicrobial component.

Keywords: chitosan, thyme, antimicrobial activity, essential oil, microparticles.

Available online at the Journal website: http://www.ache.org.rs/HI/

Polymers

SCIENTIFIC PAPER

UDC
582.292.4:547.913:615.28:544.23

Hem. Ind. **68** (6) 721–729 (2014)

doi: 10.2298/HEMIND140415048P

The main purpose of the drug therapy of any disease is to maintain the desired therapeutic concentration of the drug for the entire duration of the treatment. Essential oils are secondary metabolites of plants with very complex structures based on the terpenoid substances, which show great antibacterial activity, especially from the plants belonging to *Lamiaceae* family, documented by number of studies [1,2]. Thyme essential oil shows very strong antimicrobial effect on large number of bacteria and fungi and it is very interesting in antimicrobial therapy in the era of antimicrobial resistance [3]. Essential oils, thyme oil as well, are volatile compounds which easily evaporate, and decompose during drug and cosmetics formulation, and direct exposure to heat, pressure, oxygen or light [4]. Their encapsulation inside the particles is very important to protect bioactive components that are consisted in essential oils, from the direct contact of the external factors that can change their biochemical properties. Encapsulation is, thus, the best way to retain functional properties of the essential oil and to reach promising therapeutic effect, that essential oils show in *in vitro* testing [5].

Chitosan is a biodegradable, biocompatible, mucoadhesive and nontoxic natural polymer and has great potential for pharmaceutical application as drug and therapeutic enzyme carriers [6,7]. The physical and chemical properties of chitosan make this polymer also a rather attractive for encapsulation of thyme essential oil. It is a natural linear polysaccharide, obtained by alkaline deacetylation of chitin, which is a component of the protective cuticles of crabs, shrimps and other crustaceans and fungal mycelia [8]. Chitosan is soluble in acid conditions, but it has poor solubility above pH 6.5. It is structurally a linear polysaccharide composed of repeating units of *β*-(1-4)-2-amino-2-deoxy-D-glucopyranose (D-glucosamine), and has free amino groups on its polymeric chains. These amino groups protonate

Correspondence: D. Pecarski, Sanitary and Medical School of Professional Studies "Visan", Tošin bunar 7/a, Belgrade, Serbia.
E-mail: pecarski@eunet.rs
Paper received: 15 April, 2014
Paper accepted: 6 June, 2014

and give chitosan its cationic character that determines its main properties: controlled drug release for anionic substances, mucoadhesive properties, *in situ* gelling properties, etc [9]. Based on the antimicrobial properties of chitosan itself [9], this would be a great choice for the preparation of particles with incorporated antimicrobial essential oils such as thyme, in order to design a potent antimicrobial formulation for therapeutic use. Biodegradable, nontoxic, mucoadhesive and biocompatible properties make chitosan a promising biopolymer for the preparation of microparticles by different techniques: cross-linking with different cross-linking agents (glytaraldehyde, formaldehyde or genipin), spray drying, ionotropic gelation, simple and complex coacervation [11]. Among all these techniques, the emulsion cross-linking method would be the method of choice for the preparation of chitosan particles with essential oil of thyme, because some other methods involve temperature, high pressure, etc. The cross-linking method is based on the reaction of the amino group of chitosan and the aldehyde group of the cross-linking agent [12,13].

The primary aim of this study was to explore the potential of chitosan as a carrier for encapsulation of thyme essential oil. For this purpose, the effects of thyme and glutaraldehyde concentrations on particle size and size distribution, morphology and encapsulation efficiency were investigated. The second objective was to test the *in vitro* antimicrobial activity of optimized chitosan microparticles and thyme oil itself, as well as to control empty chitosan microparticles and to compare results. Overall, the main objective of this study was to design an effective biodegradable antimicrobial drug delivery system which would be very useful in antimicrobial therapy.

MATERIALS AND METHODS

Materials

Medium molecular weight chitosan (75–85% degree of deacetylation, CAS #9012-76-4), were purchased from Sigma–Aldrich (St. Louis, MO, USA). Acetic acid, lactic acid, Tween 80 (polysorbate 80) and glutaraldehyde were purchased from Merck Chemicals Co. (Darmstadt, Germany). Thyme essential oil was purchased from Sanoflore (France).

Microorganisms

For the purpose of *in vitro* testing of antimicrobial activity of thyme essential oil and chitosan particles with thyme, the following standardized bacterial and fungi cultures were used (ATCC – American Type Culture Collection): *Staphylococcus aureus* ATCC 25923, *Esherichia coli* ATCC 25922, *Candida albicans* ATCC 24433 and *Enterococcus faecalis* ATCC 29212. These cultures of microorganisms were propagate in Tripton soya broth and agar and used in antimicrobial assays as freshly prepared overnight broth cultures.

Gas chromatography with mass spectrometry (GC–MS)

Gas-chromatographic analysis of essential oils was conducted with Hewlett Packard 5973-689 GC–MS system in EI mode on 70eV with spectrometric detection of masses. Initial temperature of capillary column HP 5MS (30 mm×0.25 mm; film thickness 0.25 μm) was 60 °C. Using the heating speed of 3 °C/min, it was heated to 280 °C. Helium was gas carrier for this purpose, and it had the flow of 1 ml/min. The amount of 1 μl of each investigated sample was injected in GC column in proportion of 1:10.

Identification of components was based on calculated retention indexes (*RI*) [14] and mass spectra compared with standard substances and/or with NIS/NBS Wiley library of mass spectra, including literature data or data from free database (http//www. flavornet.org/iowtv.pherobase.com) [15]. Experimental values of retention indexes are defined using calibrated automated mass spectral deconvolution and identification system software (AMDIS ver. 2.1, DTRA/ /NIST, 2002). Results are compared with retention indexes from literature data and via internet available database.

Preparation of chitosan microparticles

Chitosan microparticles with encapsulated essential oil were obtained by the emulsion cross-linking method. The two series of the particles were made: one with varied concentration of essential oils (3, 6, 12 and 15 μl/ml) and the other with varied concentration of the cross-linking agent glutaraldehyde (2, 3, 5 and 8%).

10 ml of 1% of chitosan solution in 1.65% lactic acid is added to 50 ml of liquid paraffin solution with thyme essential oil and 2% Tween 80, as a surfactant resulting in formulation of w/o emulsion. The phases were mixed on the magnetic stirrer (10 min at 8000 rpm), to become homogenous**.** After that glutaraldehyde, as a cross-linking agent, was added under condition of mixing 30 min at 10000 rpm (Yellowline, DI 25 basic, Ica Works Inc., Wilmington, 8000–24000 rpm), and the microparticles were spontaneously formed. The resultant microparticles were collected by centrifugation (Sigma 2-16, rotor 12141, Germany), for 10 min at 4000 rpm. The supernatant volume was separated and measured, as it will be later used in the calculation (to determine how much of thyme has not been incorporated into the microparticles). The remaining solid phase contained microparticles, and they were sequentially washed with 175 ml of 1% Tween solution, then with 80 ml of ethanol and finally with 75 ml of distilled water. Ethanol had the role of removing any

remaining polar compounds that were not encapsulated. The volume of the separated content is measured. The mass of the particles was measured on an analytical balance. The microparticles for microscopic imaging are stored in acetate buffer, pH 4.6, in a regular container. They are poured into it, and the container is filled up to the marker with acetate buffer.

Determination of thyme essential oil loading and encapsulation efficiency

Thyme essential oil loading, *TEOL* (mg/g), was determined from the following equation:

$$TEOL = \frac{\left[C_0V_0 - \left(C_1V_1 + C_2V_2\right)\right]}{w} \quad (1)$$

where C_0 is the thyme oil (polyphenols) concentration of the initial solution (mg/ml); V_0 its volume (ml); C_1 the thyme oil concentration in the supernatant (mg/ml); V_1 the volume of supernatant (ml); C_2 the thyme oil concentration in washing solutions (mg/ml) and V_2 their volumes (ml); w the weight of dry chitosan microparticles (g).

The efficiency of thyme encapsulation (*EE,* %) was measured as also the amount of thyme (polyphenols) encapsulated in microspheres (m_e), divided by the total amount of thyme (total polyphenols, m used for the preparation of microparticles, as shown in Eq. (2):

$$EE\% = \frac{m_e}{m} \quad (2)$$

The most reliable method for the determination of total polyphenols is the Folin–Ciocalteau (FC) method [16]. Reaction of polyphenols and FC reagent (mixture phosphor-wolfram and phosphor-molybdenum acids) in mild alkaline conditions leads to the formation of a relatively stable blue colored complex, which can be spectrophotometrically determined at 765 nm using UV–Vis spectrophotometer (Ultrospec 3300 pro, Amerischam Bioscience).

Microparticles characterization

Once made, microparticles are photographed and measured. Electronica microscope is used (Carl Zeiss GmbH, Wien). Suspension of microparticles is carefully placed on watch glass, and placed under a 200 times magnification lens, field of view is found, and the sample is photographed. For making the images, we used the program Axi Vision 4.6.

Methods of determination of antimicrobial activity

Agar well diffusion method was employed for the determination of antimicrobial activity of the thyme essential oil, as well as for chitosan microparticles. Tubules with diameter of 6 mm were placed on Petri plates with prepared sterile TSA (tryptone soya agar, Torlak, Serbia). After overlaying with soft TSA (0.60% of agar-agar) inoculated with the indicator microorganism, the tubules were removed and the obtained wells were filled with 20 µl of thyme essential oil. Plates are incubated at 37 °C during 24 h. The antimicrobial activity of thyme, lactic acid (20 µl), and of combined thyme oil and lactic acid (the compound included 50 ppm of lactic acid for 20 µl of essential oil) was investigated in order to determine their synergistic effect. Antibiogram tablets of clindamycin and nystatine (30 mg) were used as a positive control for the comparation of the antibacterial activity of essential oils.

Series of solutions of chitosan microparticles were made with various concentrations of essential thyme oil (0.3, 0.6, 1.2 and 1.5%) and have been kept in 0.5 M acetate buffer, pH 4.8. These solutions were prepared in the following manner: 0.31 g chitosan microparticles of various concentrations of thyme essential oil and 610 ml acetate buffer were mixed. For the antimicrobial analyses, 20 µl of dissolved chitosan microparticles were added in the agar wells, prepared as mentioned above.

Antimicrobial activity of thyme itself and chitosan micropaticles with encapsulated thyme oil are expressed by the inhibition zones which are measured and expressed in mm.

Statistical analysis

Data were summarized as mean ± standard deviation (*SD*). Data were analyzed by descriptive statistic using one way ANOVA test. Turkey test was used for comparing average values ($p > 0.01$).

RESULTS AND DISCUSSION

Chemical composition of thyme essential oil

Properties of essential oils can be changed, depending on their origin and composition. Thus, the chemical composition of thyme essential oil used in the current research has been investigated and the results are shown in Figures 1 and 2.

According to the results of the chemical analysis of thyme essential oil, 25 compounds were identified, which represented 94.53% of the oil content. It can be noted that the highest percentage of compounds includes three classes: monoterpene hydrocarbons, aromatic hydrocarbons and oxidized monoterpenes. Other groups of compounds are present in less than 1% (Figs. 1 and 2). More than half of total compounds of thyme essential oil include 6 dominant compounds. Among them, the most dominant is the oxidized monoterpene thymol (36.12%) and the monoterpene hydrocarbon *p*-cymene (21.15%). Other dominant components of this essential oil are the following: γ-terpinene

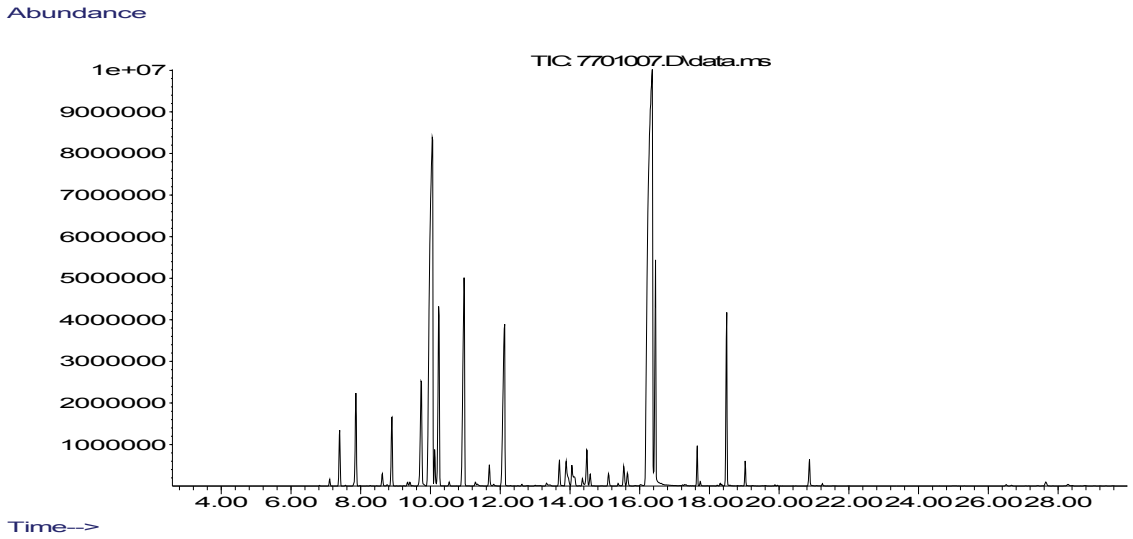

Figure 1. GC–MS chromatogram of thyme essential oil.

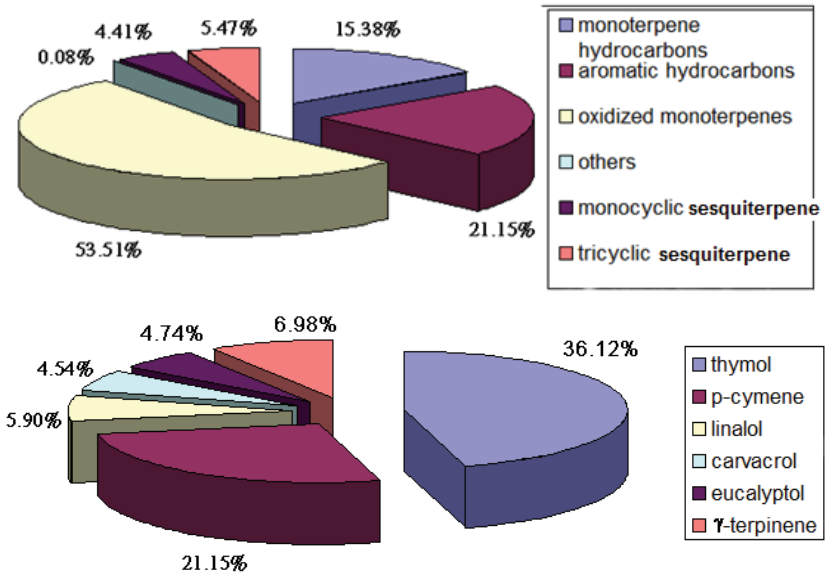

Figure 2. The basic compound classes in the thyme essential oil.

(6.98%), linalol (5.90%), carvacrol (4.54%) and eucalyptol (4.74%) (Figure 2).

These results are in accordance with previous published data about chemical composition of thyme essential oil [17]. The main components of essential oils determine the biological and pharmacological features of the oil itself. Therefore, the chemical composition of a certain essential oil will be important for its antibacterial activity.

Antimicrobial activity of thyme essential oil and chitosan microparticles

The *in vitro* antimicrobial activity of thyme oil and chitosan microparticles against aforementioned microorganisms, and their potential activities were assessed qualitatively and quantitatively by the presence or absence of inhibition zones, and the zone diameters were expressed in mm. According to the results represented in Table 1 and Fig. 3, thyme essential oil, as well as chitosan microparticles containing this oil, showed significant antibacterial and antifungal activity against all tested indicator strains. With increasing the initial concentration of essential oil from 0.3 to 1.5%, the inhibition zones increased from 4 to 6 mm against *S. aureus.* The same trend was observed for the inhibition zones against tested microorganisms: *E. faecalis, C. albicans and E. coli* (Table 1). Hence regardless of the tested bacteria and fungi the increase of the concentration of encapsulated essential oil in chitosan microparticles led to an increase of the inhibition zones.

Concerning Gram-positive bacteria, *S. aureus* (12 mm) was more sensitive than *E. faecalis* (8 mm) to

Table 1. Antimicrobial activity (Inhibition zone, mm) of chitosan microparticles containing different concentrations of thyme essential oil and chitosan itsef (data for 0.0%) against used bacteria and fungi

Initial concentration of thyme essential oil, vol.%	Bacterium			
	S. aureus	*E. coli*	*C. albicans*	*E. faecalis*
0.0	2.5	2.0	1.5	2.0
0.3	4.0	2.5	2.5	2.5
0.6	4.5	3.5	3.0	2.5
1.2	5.0	4.5	5.0	3.0
1.5	6.0	5.0	5.0	3.5

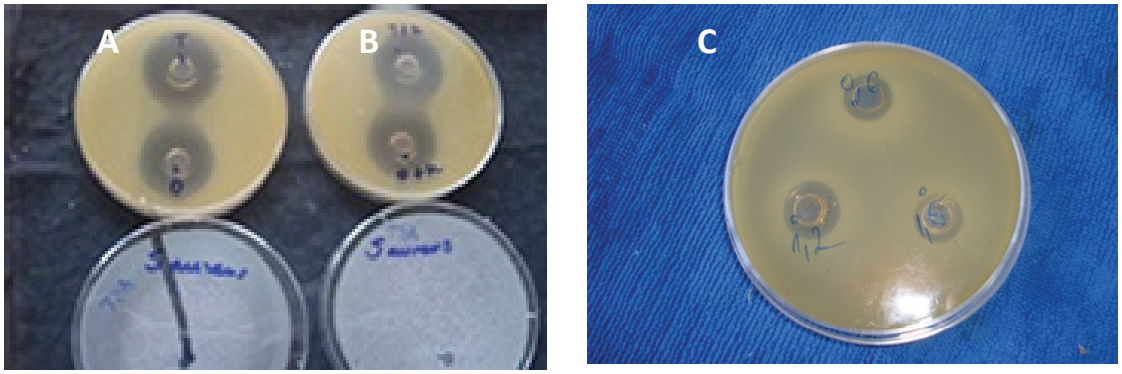

Figure 3. Antimicrobial activity of thyme and oregano essential oils and their combination with lactic acid against S. aureus, and of chitosan microparticles containing thyme essential oil against S. aureus. A) Inhibition zones of thyme and oregano essential oils; B) inhibition zones of combined thyme oil and lactic acid and oregano oil and lactic acid; C) inhibition zones of chitosan microparticles containing 0.6, 1.2 and 1.5% thyme essential oil.

thyme essential oil. Slightly less sensitive was Gram-negative bacteria *E. coli* (0.8 mm). The thyme oil also showed antifungal activity against *C. albicans* (2 mm). Low sensitivity of Gram-negative bacteria to essential oils can be the consequence of the construction of their cell wall which includes an external membrane around the peptidoglycan layer, which also inhibits diffusion of hydrophobic components through their lipopolysaccharide layer [18].

The antibacterial activity of essential oils with high content of thymol and carvacrol, such as thyme essential oil (thymol-36.12% and 4.54% carvacrol), is very well documented [19].

Also, chitosan microparticles containing thyme oil showed significant antimicrobial activity, as well as non-loaded chitosan microparticles, which was expected due to the known antimicrobial effect of chitosan itself [20].

Encapsulation of thyme essential oil in chitosan microparticles

Chitosan microparticles with different concentrations of thyme essential oil

In this study, thyme essential oil has been encapsulated in chitosan microparticles by the oil-in-water (o/w) emulsion cross-linking method. The effects of initial thyme essential oil concentration in the range from 0.3 to 1.5 vol.% on thyme essential oil loading and encapsulation efficiency were first investigated. The results are presented in Fig. 4.

The increase of the initial thyme concentration affected significantly its loading. Thyme essential oil loading increased rapidly with increasing concentration of thyme oil in the initial solution and then reached a maximum value of 58.85±1.32 mg/100 mg of microparticles. It seemed that the maximum loading for chitosan microparticles was not reached in this experiment. The encapsulation efficiency appeared to slightly increase with the thyme concentration, being in the range from 77.89±4.0 to 85.56±7.19%, for thyme concentration of 0.3 and 1.5 vol.%, respectively. This result is in accordance with previous published data [21,22].

Chitosan microparticles with different concentrations of glutaraldehyde

In order to study the effect of glutaraldehyde concentration on particle size and encapsulation efficiency, thyme oil concentration was fixed at 1.2 or 1.5%, while the glutaraldehyde concentration was varied in the range from 2 to 8%. The results are presented in Table 2 and Fig. 5. Optical microscopy images of the microcapsules are shown in Fig. 6.

According to the results presented in Fig. 5, the concentration of glutaraldehyde did not significantlly affect the degree of thyme oil encapsulation. However, an optimal glutaraldehyde concentration is required for

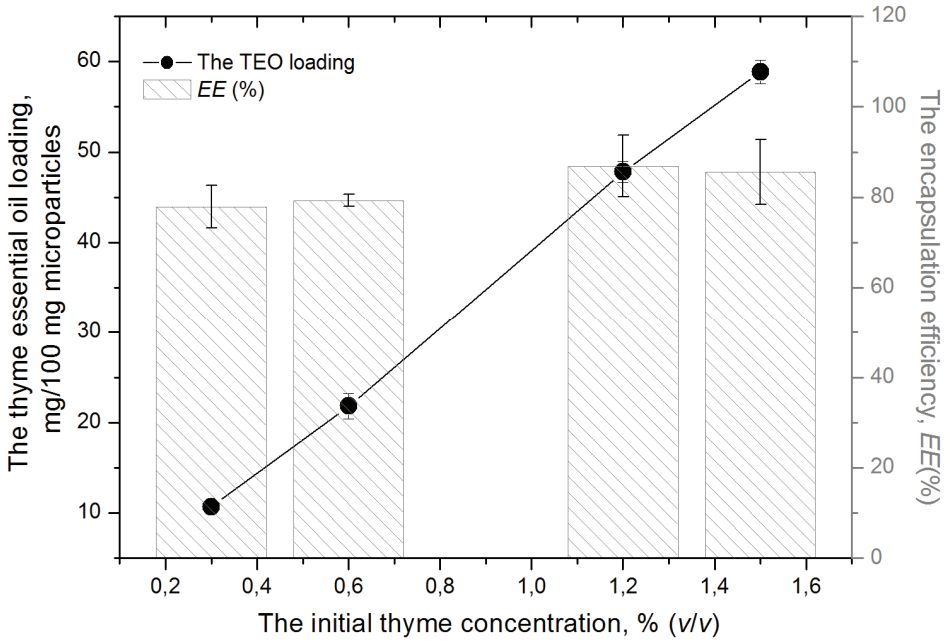

Figure 4. The effect of thyme essential oil concentration on the thyme oil loading and encapsulation efficiency.

Table 2. The effects of glutaraldehyde concentration on the thyme essential oil loading, TEOL, and encapsulation efficiency (EE, %) as well as on particle diameters with statistical analysis of chitosan microparticles diameter; TEOL – thyme essential oil loading; EE – encapsulation efficiency; ADS – average diameter size; STD – standard deviation; SE – standard error

Initial glutaraldehyde concentration, %	*TEOL*, mg/100mg	*EE*, %	*ADS*, μm	*STD*	*SE*
2	58.51	85.07	12.85	3.61935	0.80931
3	59.10	85.94	13.65	4.34231	0.97097
5	57.04	82.94	7.192	3.16752	0.70828
8	58.52	85.09	4.710	1.41743	0.31695

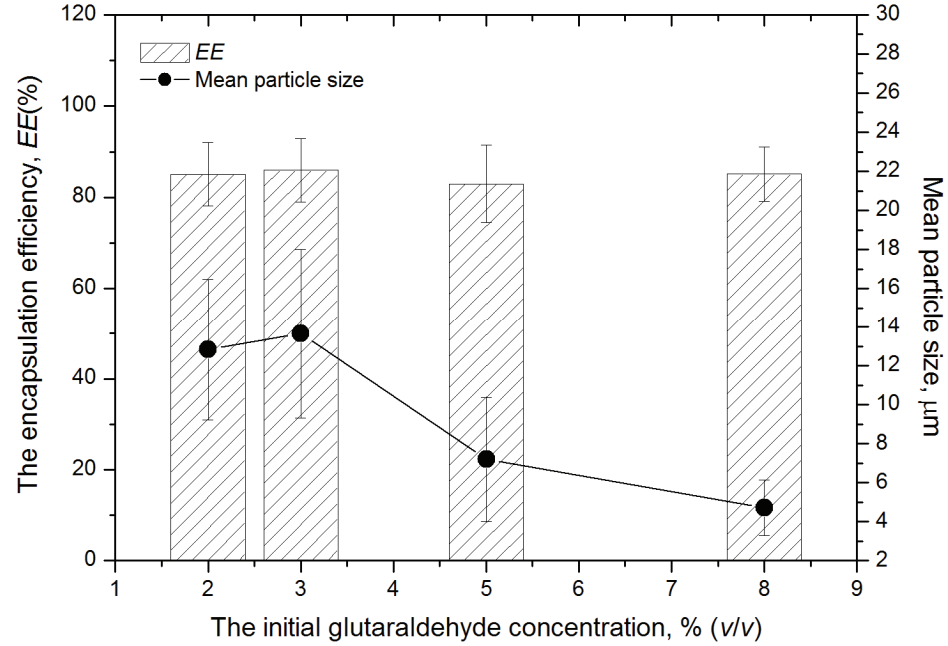

Figure 5. The effect of glutaraldehyde concentration on the thyme oil encapsulation efficiency (EE, %) and particle diameters.

chitosan microparticles formation regarding their shape, size and size distribution (Fig. 6). Namely, microparticles were spherical in shape with smooth surfaces. Except for few cases, the droplets of thyme oil appeared to be individually encapsulated as spherical particles with size distribution consistent with a microparticle size and one can notice also the absence of agglomerates.

The microspheres had a mean particle size in the range from 4.71±1.42 to 13.65±4.34 μm. Such particles were considered to be of the appropriate size suitable for several administrations. There was no significant difference in the particles size between microparticles with 2 and 3% glytaraldehyde used as cross-linking agent, neither in microparticles with 5 and 8% glytaraldehyde used. However, significant differences in particle size ($p < 0.01$) were found for particles with 2% glutaraldehyde compared to particles with 5 and 8% glytaraldehyde used as cross-linking agent, as well as for microparticles size with 3% glutaraldehyde compared with size of particles with 5 and 8% glutaraldehyde.

It appeared that the diameter of microparticles decreased with the increase of glutaraldehyde concentration. These results were similar to these reported in other studies [23–25], although there are not many reports about essential oils and their constituents being encapsulated.

In the present study, it was shown that the employed emulsion method was suitable for the preparation of chitosan microparticles for the purpose of thyme oil encapsulation.

CONCLUSIONS

The present work aimed to study the antimicrobial activity of thyme essential oil, as well as chitosan microparticles with encapsulated thyme oil on four tested microorganisms: *Staphylococcus aureus, Escherichia coli*, *Candida albicans* and *Enterococcus faecalis*. Gram-positive bacteria were more sensitive to microparticles with thyme essential oil, and thyme oil itself, than gram-negative bacteria.

The results revealed that essential oil concentration in microparticles had the most important influence on the diameter of the inhibition zone against tested microorganisms, as well on the diameter of chitosan microparticles that were made. The increase of the concentration of thyme essential oil in the chitosan microparticles induced an increase in the diameter of the inhibition zones of the tested microorganisms. On the other hand, the diameter of chitosan micropaticles decreased with increasing the concentration of the cross-linking agent glutaraldehyde, that was used for preparing microparticles. It is important to emphasize

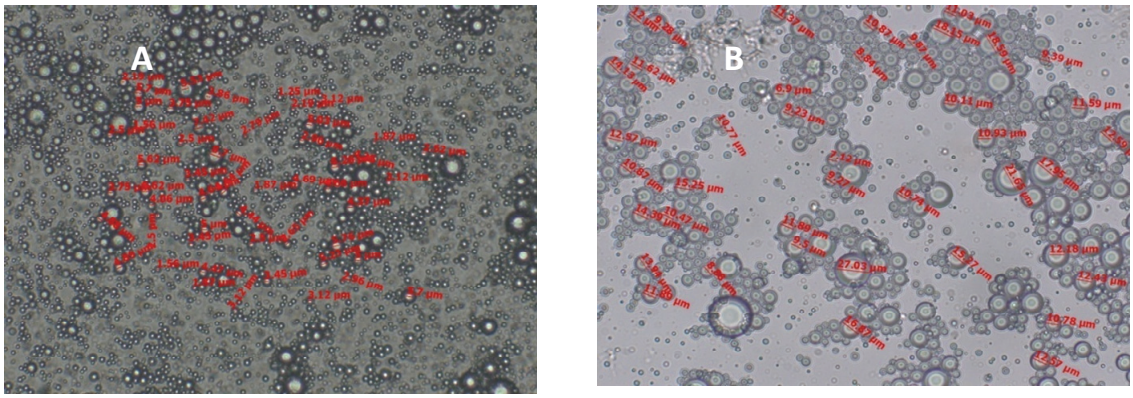

Figure 6. Electron microscopy of chitosan microparticles with encapsulated thyme essential oil and containing glutaraldehyde as the crosslinking agent. A) microparticles with encapsulated 1.5 % thyme essential oil and 8% glutaraldehyde (average size of microspheres was 4.71 μm); B) microparticles with encapsulated 1.5% thyme oil and 3% glutaraldehyde (average diameter of the particles is 13.64 μm).

that this research has not yet been reported in literature. Also the results of the determination of the influence of initial concentration of thyme essential oil on its encapsulation efficiency showed that the increase in the initial concentration of thyme increased its degree of encapsulation in chitosan microparticles. In the same experiment it was shown that the concentration of glutaraldehyde did not affect the degree of encapsulation.

These results of the study showed the potent antimicrobial effect of chitosan microparticles with thyme essential oil for future application in antimicrobial therapy.

REFERENCES

[1] N.C.C. Silva, A. Fernandes Júnior, Biological properties of medicinal plants: a review of their antimicrobial activity, J. Venom. Anim.Tox. Incl. Trop. Dis. **16** (2010) 402–413.

[2] M. Marino, C. Bersani, G. Comi, Impedance measurements to study the antimicrobial activity of essential oils from Lamiacea and Compositae, Int. J. Food Microbiol. **67** (2001) 187–195.

[3] S. Cosentino, C.I. G Tuberoso, B. Pisano, M. Satta, V. Mascia, E. Arzedi, *In vitro* antimicrobial activity and chemical composition of Sardinian Thymus essential oils, Lett. Appl. Microbiol., **29** (1999) 130–135.

[4] F. Bakkali, S. Averbeck, D. Averbeck, M. Idaomar, Biological effects of essential oils – A review, Food Chem. Toxicol. **46** (2008) 446–475.

[5] A. Sunil, N. Nadagouda, T. Mallikarjuna, M. Aminabhavi, Recent advances on chitosan-based micro- and nanoparticles in drug delivery, J. Control. Release **100** (2004) 5–28.

[6] A. Smelcerović, Z. Knežević-Jugović, Ž. Petronijević, Microbial polysaccharides and their derivatives as current and prospective pharmaceuticals, Curr. Pharm. Des. **14** (2008) 3168–3195.

[7] M.G. Žuža, B.M. Obradović, Z.D. Knežević-Jugović, Hydrolysis of Penicillin G by Penicillin G Acylase Immobilized on Chitosan Microbeads in Different Reactor Systems, Chem. Eng. Technol. **34** (2011) 1706–1714.

[8] V.R. Sinha, A.K. Singla, S. Wadhawan, R. Kaushik, R. Kumria, K. Bansal, S. Dhawan, Chitosan microspheres as a potential carrier for drugs, Int. J. Pharm. **274** (2004) 1–33.

[9] S.G. Kumbar, A.R. Kulkarni, T.M. Aminabhavi, Crosslinked chitosan microspheres for encapsulation of diclofenac sodium: effect of cross-linking agent, J. Microencapsulation **19** (2002) 173–180.

[10] F. Chellat, M. Tabrizian, S. Dumitriu, E. Chornet, C.H. Rivard, L Yahia, Study of biodegradation behavior of chitosan–xanthan microspheres in simulated physiological media, J. Biomed. Mater. Res. **53** (2000) 592–599.

[11] A.A. Al-Helw, A.A. Al-Angary, G.M. Mahrous, M.M. Al-Dardari, Preparation and evaluation of sustained release cross-linked chitosan microspheres containing phenobarbitone, J. Microencapsulation **15** (1998) 373–382.

[12] J. Meng, T.F. Sturgis, B.C. Youan, Engineering Tenofovir Loaded Chitosan Nanoparticles, Eur. J. Pharm. Sci. **44** (2011) 57–67.

[13] A. Groboillot , C. Champagne, G. Darling, D. Poncelet , R. Neufeld, Membrane formation by interfacial cross-linking of chitosan for microencapsulation of *Lactococcus lactis*, Biotechnol. Bioeng. **10** (1993) 1157–1163.

[14] H. Van den Dool, D.P. Kratz, A Generalisation of the Retention Index System Including Linear Temeprature Programmed Gas-Liquid Partition Chromatography, J. Chromatogr. **11** (1963) 463–471.

[15] R.P. Adams, Identification of Essential Oil Component by Gas Chromatography/Quadrupole Mass Spectrometry, Allured Publishing Corporation, Carol Stream, IL ,2007.

[16] A. Blainski, G.C. Lopes, J. C. Palazzo de Mello, Application and Analysis of the Folin Ciocalteu Method for the Determination of the Total Phenolic Content from *Limonium brasiliense* L., Molecules **18** (2013) 6852–6865.

[17] N. Chorianopoulos, E. Kalpoutzakis, N. Aligiannis, S. Mitaku, G.J. Nychas, S.A. Haroutounian, Essential Oils of Satureja, Origanum and Thymus Species: Chemical Composition and Antibacterial Activities Against Food borne Pathogens, J. Agric. Food Chem. **52** (2004) 8261–8267.

[18] I.M. Helander, H.L. Alakomi, K. Latva-Kala, T. Mattila-Sandholm, I Pol, E.J. Smid, L.G.M. Gorris, A. Von Wright, Characterization of the action of selected essential oil compnents on Gram-negative bacteria, J. Agric. Food Chem. **46** (1998) 3590–3595.

[19] L.P. Roldan, G.J. Diaz, J.M. Duringer, Composition and antibacterial activity of essential oils obtained from plants of the Lamiaceae family against pathogenic and beneficial bacteria, Revista Colombiana de Ciencias Pecuarias **23** (2010) 451–461.

[20] L.-Y. Zheng, J.-F. Zhu, Study on antimicrobal activity of chitosan with differnt molecular weights, Carbohydr. Polym. **54** (2003) 527–530.

[21] W.C. Hsieh, C.P. Chang, Y.L. Gao, Controlled release properties of chitosan encapsulated volatile citronella oil microcapsules by thermal treatments, Colloids Surfaces, B **53** (2006) 209–214.

[22] C. Anchisi, M.C. Meloni, A.M. Maccioni, Chitosan beads loaded with essential oils in cosmetic formulations, J. Cosmet. Sci. **57** (2006) 205–214.

[23] Y. Pranoto, S.K. Rakshit, V.M.Salokhe, Enhancing antimicrobial activity of chitosan films by incorporating garlic oil, potassium sorbate and nisin, LWT-Food Sci. Technol. **38** (2005) 859–865.

[24] S.F. Hosseini, M. Zandi, Two-step method for encapsulation of oregano essential oil in chitosan nanoparticles: Preparation, characterization and in vitrorelease study, Carbohydr. Polym. **95** (2013) 50–56.

[25] W. Lyeverton, C. Ribeiro, I.T.F. Macedo, J.M. Leite dos Santos, Activity of chitosan-encapsulated Eucalyptus staigeriana essential oil on *Haemonchus contortus*, Exp. Parasitol. **135** (2013) 24–29.

IZVOD

IZRADA, KARAKTERIZACIJA I ANTIMIKROBNA AKTIVNOST HITOZANSKIH MIKROČESTICA SA ETARSKIM ULJEM TIMIJANA

Danijela Pecarski[1], Zorica Knežević-Jugović[2], Suzana Dimitrijević-Branković[2], Katarina Mihajilovski[2], Slobodan Janković[3]

[1]*Visoka Zdravstveno–Sanitarna škola "Visan", Tošinbunar 7/a, Beograd*
[2]*Tehnološko–metalurški fakultet, Univerzitet u Beogradu, Karnegijeva 4, Beograd*
[3]*Medicinski fakultet, Univerzitet u Kragujevcu, Svetozara Markovića 69, Kragujevac*

(Naučni rad)

Etarska ulja kao antimikrobni agensi su sve više u upoterbi u antimikrobnoj terapiji, pa je i razvoj odgovarajućeg *drug delivery* sistema sa etarskim uljem od velikog terapijskog značaja. Inkapsulacija isparljivih etrskih ulja u odgovarajuće čestice je od velikog značaja da bi se žaštitile bioaktivne komponente, koje su sastavni deo etarskih ulja i koje su osetljive na direktno delovanje svetlosti, temperature i oksidacije jer ovi faktori menjaju njihove biohemijske osobine. Hitozan je biodegradibilan, biokompatibilan, mukoadhezivan i netoksičan prirodni polimer koji kao takav ima ogroman potencijal kao nosač aktivnih supstanci u farmaceutskim formulacijama. Hitozanske mikročestice sa inkapsuliranim etarskim uljem timijana su izrađene emulzionom metodom uz primenu umrežavajućeg agensa. Varirane su koncentracije etarskog ulja timijana i glutaraldehida kao umreživača, i praćen je njhov uticaj na veličinu čestica, količinu inkapsuliranog timijana i efikasnost inkapsulacije. Hitozanske mikročestice su imale sferičan oblik sa prosečnim prečnikom koji je bio u opsegu od 4.71±1.42 to 13.65±4.34 μm, u zavisnosti od koncentracije etarskog ulja i glutaraldehida koji su korišćeni pri izradi čestica. Prečnik čestica, odnosno veličina čestica, je rasla sa povećanjem koncentracije etarskog ulja timijana i smanjivala se sa povećanjem koncentracije glutaraldehida. Pokazano je da koncentracija glutaraldehida nema uticaja na stepen inkapsulacije etarskog ulja timijana u hitozanske mikročestice, dok sa porastom koncentracije etarskog ulja timijana raste količina inkapsuliranog ulja i efikasnost inkapsulacije. Sve mikročestice, uključujući i samo etarsko ulje timijana, su pokazali značajnu antimikrobnu aktivnost protiv *Staphylococcus aureus* ATCC 25923*, Esherichia coli* ATCC 25922*, Candida albicans* ATCC 24433 i *Enterococcus faecalis* ATCC 25929. Ova studija je pokazala veliki antimikrobni potencijal etarskog ulja timijana inkorporiranog u hitozanske mikročestice kao odgovarajuću farmaceutsku formulaciju sa kontrolisanim oslobađanjem aktivne antimikrobne komponente.

Ključne reči: Hitozan • Timijan • Antimikrobna aktivnost • Patogeni • Mikročestice • Etarsko ulje

Surface characterization, hemo- and cytocompatibility of segmented poly(dimethylsiloxane)-based polyurethanes

Marija V. Pergal[1], Jelena Nestorov[2], Gordana Tovilović-Kovačević[2], Petar Jovančić[3], Lato Pezo[4], Dana Vasiljević-Radović[1], Jasna Djonlagić[3]

[1]*Institute of Chemistry, Technology and Metallurgy, University of Belgrade, Belgrade, Serbia*
[2]*Department of Biochemistry, Institute for Biological Research "Siniša Stanković", University of Belgrade, Belgrade, Serbia*
[3]*Faculty of Technology and Metallurgy, University of Belgrade, Belgrade, Serbia*
[4]*Institute of General and Physical Chemistry, University of Belgrade, Belgrade, Serbia*

Abstract

Segmented polyurethanes based on poly(dimethylsiloxane), currently used for biomedical applications, have sub-optimal biocompatibility which reduces their efficacy. Improving the endothelial cell attachment and blood-contacting properties of PDMS-based copolymers would substantially improve their clinical applications. We have studied the surface properties and *in vitro* biocompatibility of two series of segmented poly(urethane-dimethylsiloxane)s (SPU-PDMS) based on hydroxypropyl- and hydroxyethoxypropyl-terminated PDMS with potential applications in blood-contacting medical devices. SPU-PDMS copolymers were characterized by contact angle measurements, surface free energy determination (calculated using the van Oss–Chaudhury–Good and Owens–Wendt methods), and atomic force microscopy. The biocompatibility of copolymers was evaluated using an endothelial EA.hy926 cell line by direct contact assay, before and after pre-treatment of copolymers with multicomponent protein mixture, as well as by a competitive blood-protein adsorption assay. The obtained results suggested good blood compatibility of synthesized copolymers. All copolymers exhibited good resistance to fibrinogen adsorption and all favored albumin adsorption. Copolymers based on hydroxyethoxypropyl-PDMS had lower hydrophobicity, higher surface free energy and better microphase separation in comparison with hydroxypropyl-PDMS-based copolymers, which promoted better endothelial cell attachment and growth on the surface of these polymers as compared to hydroxypropyl-PDMS-based copolymers. The results showed that SPU-PDMS copolymers display good surface properties, depending on the type of soft PDMS segments, which can be tailored for biomedical application requirements such as biomedical devices for short- and long-term uses.

Keywords: polyurethanes, siloxanes, surface free energy, cell adhesion, protein adsorption.

Available online at the Journal website: http://www.ache.org.rs/HI/

Polymers

SCIENTIFIC PAPER

UDC 678.13:678.664:544

Hem. Ind. **68** (6) 731–741 (2014)

doi: 10.2298/HEMIND141103082P

Thermoplastic segmented polyurethane elastomers (SPUs) are used extensively in cardiovascular devices such as heart valves and vein replacements, as an encapsulating material, for orthopedic and dermal application, and for transdermal drug delivery patches [1]. They possess relatively good biocompatibility, are easy to process, and have a wide range of tunable physical and mechanical properties [1,2]. The SPUs are known to exhibit a two-phase microstructure due to the thermodynamic incompatibility between the hard and soft segments.

In the last 10 years, the poly(dimethylsiloxane) (PDMS) has often been used to produce SPUs due to the fact that PDMS exhibits excellent thermal properties, hydrophobic properties and biostability [1,3,4]. PDMS is the non-polar oligomer, which hampers its conjunction with polar urethane matrix [5]. To overcome the difficulties, many approaches have been studied in order to synthesize the PDMS-based SPUs yielding high molecular weight and good mechanical properties. In line with these, the synthesis of high molecular weight SPU copolymers using hydroxybutyl-, hydroxyhexyl-, aminopropyl- and methylaminopropyl-terminated PDMS oligomers has been reported [6,7]. However, most of the research was focused on using hydroxyl-terminated PDMS or amino-terminated PDMS by cooperating with polyether macrodiol, in order to increase the compatibility of the reaction mixture and, thus, to achieve higher molecular weights and better mechanical properties of copolymers [7]. For instance, Adhikari *et al*. [8] studied the ability of hydroxyethoxypropyl terminated-PDMS to mix with the poly(hexa-

Correspondence: M.V. Pergal, Institute of Chemistry, Technology and Metallurgy – Center of Chemistry, University of Belgrade, Njegoševa 12, 11000 Belgrade, Serbia.
E-mail: marijav@chem.bg.ac.rs
Paper received: 3 November, 2014
Paper accepted: 13 November, 2014

methylene oxide) macrodiol (PHMO) as the soft segment of the SPUs, and the results indicated that about 20 wt.% PHMO in the soft segment produced SPUs with a combination of good biostability and mechanical properties. However, to further enhance the biostability of SPUs derived from hydroxyethoxypropyl terminated-PDMS, reduction of PHMO in the soft segment mixture is desirable [9–11].

Introduction of PDMS soft segment or siloxane based chain extenders into polyurethanes has led to the development of materials such as commercial polyether/PDMS based SPUs, *i.e*., Elast-Eon^{TM} 2 and 3, which comprise groups of very flexible high and low modulus SPU copolymers, respectively [1]. PDMS has been incorporated into these copolymers in order to obtain non-cytotoxic polymers with better microphase separation structures, and thus enhanced biostability and low thrombogenicity [11,12]. However, SPUs and PDMS in Elast-Eon^{TM} are inherently resistant to cell adhesion and support relatively poor endothelial cell growth. Bax *et al*. [12] found that Elast-Eon^{TM} exhibits low levels of human umbilical vein endothelial cell (HUVEC) adhesion and cell viability, but surface plasma modification and tropoelastin protein coating of Elast-Eon^{TM} enhanced endothelial cell attachment and reduced thrombogenicity.

SPUs possess blood-contacting properties that make them suitable for short and long-term biomedical applications, however their long-term thrombogenic nature can cause emboli occlusion [1]. Thrombosis is the major cause of short-term failure of heart valves, stents and vascular grafts. The investigation of protein adsorption, which is the first step in thrombus formation, is very important for understanding the molecular mechanisms underlying this process, and more importantly for engineering thromboresistant surfaces. Also, the structural conformation of the adsorbed protein appears to be crucial in influencing cell adhesion and growth [13], and studies on the behavior of protein adsorption and cell adhesion are important for improving the biocompatibility of SPU materials. *In vitro* cell culture in controlled conditions is one of the most often-used methods for evaluation of cytocompatibility, while the blood-based testing and plasma protein adsorption assays provide a good insight into the hemocompatible properties of the material [1]. The properties of SPUs surfaces are utmost important due to their role in thrombosis and inflammatory response. Namely, surface properties such as topography, surface free energy, surface composition, and chemistry of SPUs can greatly influence its protein adsorption, cell attachment and hence its biocompatibility [14–18]. In our previous works [16–18], we have found that microphase separation, surface roughness and soft segment content represent the most important properties influencing endothelial cell adhesion and protein adsorption.

The present work is focused on the surface properties, *in vitro* hemo- and cytocompatibility of two series of poly(urethane-dimethylsiloxane) copolymers (SPU-PDMS) based on hydroxypropyl- and hydroxyethoxypropyl-terminated PDMS. Therefore, the aim of this study is to investigate the influence of different soft PDMS segments on the water contact angle, surface free energy and its components, surface topography and biocompatibility of SPU-PDMS copolymers.

EXPERIMENTAL PART

Materials

α,ω-Dihydroxypropyl poly(dimethylsiloxane) (HP-PDMS, M_n = 960 g/mol) and *α,ω*-dihydroxyethoxypropyl poly(dimethylsiloxane) (EO-PDMS, M_n = 1000 g/mol) were purchased from ABCR. 4,4′-Methylenediphenyldiisocyanate (MDI), supplied by Aldrich, with an isocyanate content of 33.6 wt.%, was used without further purification. 1,4-Butanediol (BD, from Aldrich) used as a chain extender was purified by vacuum distillation. Stannous octanoate ($Sn(Oct)_2$) from Aldrich was used as a dilute solution in the anhydrous mixture of DMAc/THF (1/1, *V*/*V*). *N,N*-Dimethylacetamide (DMAc, from Acros) and tetrahydrofuran (THF, from J.T. Baker) were distilled before use. Formamide (analytically pure, Merck) and diiodomethane (analytically pure, UCB, Belgium) were used as received.

Synthesis of segmented polyurethanes

Two series of segmented polyurethanes were obtained by two-stage polymerization procedure in the solution (DMAc/THF, 1/1, *V*/*V*), using *α,ω*-dihydroxypropyl- or *α,ω*-dihydroxyethoxypropyl-PDMS, MDI and BD. Each series of the synthesized SPU-PDMS consisted of three samples of different hard segment content (20, 45 and 55 wt.%), which, in this study, is marked by the last two numbers in the name of prepared samples. The total molar ratio of –NCO and –OH groups was kept constant (NCO/OH = 1.05). Catalyst concentration was kept at 0.04 wt.%. The synthesis and characterization of SPU-PDMS copolymers have been described in details in our previously published papers [17,19]. SPU-PDMS samples were synthesized in 100 mL four-neck round-bottom flasks, placed in a silicone oil bath and connected to an inlet for dry argon, a mechanical stirrer, a dropping funnel and a reflux condenser. Calculated amounts of macrodiol and MDI were weighed into reaction flask at room temperature, dissolved in the mixture of DMAc/THF and then heated up to 80 (for the SPU-$PDMS_{HP}$ series) or 40 °C (for the SPU-$PDMS_{EO}$ series) under an argon atmosphere. The reaction started by the introduction of a solution of $Sn(Oct)_2$ in

DMAc/THF. The reaction mixture was stirred for 20 min (for the SPU-$PDMS_{HP}$ series) or 30 min (for the SPU--$PDMS_{EO}$ series) to prepare the NCO-terminated prepolymer, *i.e.*, until the theoretical NCO content was attained. The NCO content was controlled by the dibutylamine back-titration method [20]. In the second stage of the reaction, a dilute solution of BD in DMAc/THF was added dropwise to the NCO-terminated prepolymer and the reaction was continued for 24 h. Copolymers were precipitated into methanol/water (1/1, *V*/*V*) solution, filtered and dried to constant weight in a vacuum oven at 40 °C. The SPU-PDMS films (0.40–0.50 mm thickness) utilized for characterization and biocompatibility evaluation were cast from DMAc solution (10 wt.%) into Teflon® molds and were left for 48 h in a circulating air oven at 40 °C. Finally, the films were dried to constant weight under vacuum at 40 °C.

Characterization

Static contact angle was measured by a sessile drop method at 26 °C, using a contact angle analyzer (Krüss DSA100). Surface energy data were calculated from the contact angle values obtained by distilled water, formamide, and diiodomethane and the acid-base theory for solids according to the van Oss–Chaudhury–Good model [21]. Also, surface free energy and its components were obtained using the water and diiodomethane contact angles according to the Owens––Wendt model [22]. Single drops of tested liquid with a volume of 20 μL were deposited on the film surface and the contact angels were measured after 30 s. Contact angles for each polymer were calculated as the average value of five measurements.

The surface free energy can be calculated by the acid-base theory for solids according to the van Oss––Chaudhury–Good approach using the following equations [21]:

$$\begin{aligned}
\gamma_{LV1}(1+\cos\theta_1) &= 2\sqrt{\gamma_S^{LW}\gamma_{LV1}^{LW}} + \sqrt{\gamma_S^{+}\gamma_{LV1}^{-}} + \sqrt{\gamma_S^{-}\gamma_{LV1}^{+}} \\
\gamma_{LV2}(1+\cos\theta_2) &= 2\sqrt{\gamma_S^{LW}\gamma_{LV2}^{LW}} + \sqrt{\gamma_S^{+}\gamma_{LV2}^{-}} + \sqrt{\gamma_S^{-}\gamma_{LV2}^{+}} \\
\gamma_{LV3}(1+\cos\theta_3) &= 2\sqrt{\gamma_S^{LW}\gamma_{LV3}^{LW}} + \sqrt{\gamma_S^{+}\gamma_{LV3}^{-}} + \sqrt{\gamma_S^{-}\gamma_{LV3}^{+}} \\
\gamma_S &= \gamma_S^{LW} + \gamma_S^{AB} = \gamma_S^{LW} + 2\sqrt{\gamma_S^{+}\gamma_S^{-}}
\end{aligned} \quad (1)$$

where θ is the experimentally found contact angle between a liquid drop and a solid surface under investigation; γ_S is the total surface free energy of copolymers and composed of the dispersive (γ_S^{LW}) and the polar (γ_S^{AB}) components; γ^{+} and γ^{-} are the Lewis acid parameter and the Lewis base parameter of the surface free energy, respectively; γ_{LV} represents the surface tension of the corresponding testing liquids, and it is also divided into the dispersive and the polar components. In this way, if the values of γ_{LV}^{LW}, γ_{LV}^{+}, γ_{LV}^{-} for three testing liquids are known, γ_S^{LW} and γ_S^{AB} can be calculated according to Eq. (1) by measuring contact angles θ_1, θ_2 and θ_3 of three testing liquids on the SPU--PDMS surface, which can further give the surface free energy of solid film. Here the three testing liquids are distilled water (γ_{LV} = 72.8 mJ/m^2; γ_{LV}^{LW} = 21.8 mJ/m^2; γ_{LV}^{+} = 25.5 mJ/m^2; γ_{LV}^{-} = 25.5 mJ/m^2), formamide (γ_{LV} = 58.0 mJ/m^2; γ_{LV}^{LW} = 39.0 mJ/m^2; γ_{LV}^{+} = 2.28 mJ/m^2; γ_{LV}^{-} = 39.6 mJ/m^2), and diiodomethane (γ_{LV} = 50.8 mJ/m^2; γ_{LV}^{LW} = 50.8 mJ/m^2; γ_{LV}^{+} = 0 mJ/m^2; γ_{LV}^{-} = 0 mJ/m^2) [23].

The surface free energy can be calculated according to the Owens-Wendt model using the following equations [22]:

$$\begin{aligned}
\gamma_{LV1}(1+\cos\theta_1) &= 2\sqrt{\gamma_S^{d}\gamma_{LV1}^{d}} + \sqrt{\gamma_S^{p}\gamma_{LV1}^{p}} \\
\gamma_{LV3}(1+\cos\theta_3) &= 2\sqrt{\gamma_S^{d}\gamma_{LV3}^{d}} + \sqrt{\gamma_S^{p}\gamma_{LV3}^{p}} \\
\gamma_S &= \gamma_S^{d} + \gamma_S^{p}
\end{aligned} \quad (2)$$

where γ_S^{d} is the surface free energy connected with dispersion interactions; γ_S^{p} is the surface free energy connected with polar interactions.

Atomic force microscopy (AFM) characterizations were performed with an AutoProbe CP-Research SPM (TM Microscopes, Veeco) instrument. Measurements were performed under ambient conditions using the non-contact mode AFM technique. Veeco Phosphorus (n)-doped silicon contact metrology probes model MPP-31123-10 with Al-reflective coating and symmetric tip were used.

Differential scanning calorimetry (DSC) was carried out on a DSC Q1000V9.0 Build 275 thermal analyzer. The DSC scans were recorded under a dynamic nitrogen atmosphere (the flow rate of nitrogen was 50 mL/min), in the temperature range from –90 to 230 °C, at a heating and cooling rate of 10 and 5 °C/min, respectively. The total degree of crystallinity (X_{cDSC}) was calculated by following equation:

$$X_{cDSC} = \Delta H_m/\Delta H_m^{\circ} \quad (3)$$

where ΔH_m is the enthalpy of melting of sample, and ΔH_m° is the theoretical value of the enthalpy of the melting of perfectly crystalline MDI-BD homopolymer, based on the group contribution method (ΔH_m° = 91.2 J/g) [24].

Assessment of cytocompatibility

EA.hy926 cells were a kind gift from Dr. Cora Jean Edgell, University of North Carolina, USA. The cells were cultured in Dulbecco's Modified Eagle Media supplemented with 10% fetal bovine serum, 2 mM L-glutamine, 100 μg/cm^3 streptomycin, 100 U/cm^3 penicillin, and HAT media supplement and maintained in a humidified atmosphere containing 5% CO_2 at 37 °C. Prior to cell seeding, SPU-PDMS copolymers films were sterilized by ultraviolet irradiation for 30 min and placed into 96 well polystyrene microplates (Sarstedt, Ger-

many). The cells were seeded at a density of 30000 cells per well for all experiments. All tests were performed in triplicates.

The influence of SPU-PDMS copolymers on cell viability was evaluated using (MTT) assay, which was performed 96 hours post-seeding [16]. Absorbance was measured spectrophotometrically at 570 nm. The cell viability was expressed relative to control sample (cells grown without sample film), taken as 100%.

Cell adhesion onto the SPU-PDMS copolymers films was examined and photographed by a light microscopy using a computer based Carl Zeiss Axiovision microscope, 96 h after seeding. Cells were fixated with 3% glutaraldehyde solution. The samples were rinsed with PBS in order to remove detached cells. SPU-PDMS copolymers films were placed on microscope slides, stained with 0.4% nigrosin solution and photographed.

To assess the possible influence of surface preconditioning with the most abundant plasma proteins on cell adhesion, the samples were pre-incubated for 2 h at 37 °C in the mixture of bovine serum albumin (BSA, 40 mg/cm^3), bovine γ-globulins (BGG, 10 mg/cm^3) and bovine fibrinogen (FBG, 3 mg/cm^3) prior to cell seeding. Protein concentrations are chosen as to reflect the actual physiological concentration. After incubation, the SPU-PDMS films were rinsed two times with PBS. The cells were seeded in specified density of 30000 cells per well and SPU-PDMS copolymers films were photographed 96 hours after as indicated above.

Assessment of hemocompatibility

SPU-PDMS copolymer films were incubated (2 h, 37 °C) with a three-component mixture comprised of BSA (40 mg/cm^3), BGG (10 mg/cm^3) and FBG (3 mg/cm^3). Adsorbed proteins were resolved on 7.5% SDS–poly(acrylamide) gels under non-reducing conditions and quantified as previously reported [16]. The protein concentrations were calculated from the standard curves and expressed as μg of protein per cm^2 of the film.

Statistical analysis

Biocompatibility data were evaluated statistically by one way ANOVA, followed by post comparison Bonferroni's test: * indicates $p < 0.05$; ** $p < 0.01$; *** $p < 0.001$. For surface free energy data, descriptive statistical analyses for calculating the means and the standard error of the mean were performed using Microsoft Excel software (Microsoft Office 2007). All obtained results were expressed as the mean ± standard deviation (*SD*). The significant differences between specific samples are calculated according to post-hoc Tukey's HSD test at $p < 0.05$ significance level, 95% confidence limit, using StatSoft Statistica 10 software.

RESULTS AND DISCUSSION

Two series of SPU-PDMS copolymers containing different soft segment structures were synthesized by two-step polymerization in solution. These SPU-PDMS copolymers were used to study the effect of surface properties on hemo- and cytocompatibility. The chemical structure of two kinds of PDMS prepolymer used for preparation of SPU-PDMS copolymers are presented in Figure 1. The molar ratio of PDMS, MDI and BD in both series was 1:2:1, 1:4:3 and 1:6:5, which resulted in following of predetermined content of the hard MDI-BD segments: 20, 45 and 55 wt.%. The compositions and some DSC data of the examined copolymers are given in Table 1.

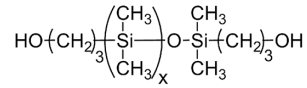

α,ω-dihydroxypropyl poly(dimethylsiloxane)

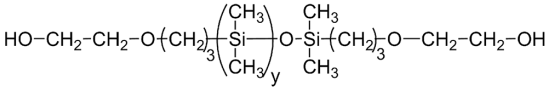

α,ω-dihydroxyethoxypropyl poly(dimethylsiloxane)

Figure 1. Chemical structures of poly(dimethylsiloxane) prepolymers.

Table 1. Composition, degree of crystallinity and contact angles of the SPU-PDMS copolymers

Sample	Molar ratio[a]	Content of hard segment, wt.% (in feed)[b]	X_{cDSC} / %[c]	θ_1 / ° (water)[d]	θ_2 / ° (formamide)[d]	θ_3 / ° (diiodomethane)[d]
SPU-PDMS$_{HP}$-20	1:2:1	21.9	0.9	96.2±1.2[e]	84.3±2.6[d]	71.4±1.2[e]
SPU-PDMS$_{HP}$-45	1:4:3	45.7	18.9	88.5±0.9[a]	78.4±1.2[b]	66.0±0.7[d]
SPU-PDMS$_{HP}$-55	1:6:5	58.4	27.2	83.3±1.0[c]	70.5±0.4[a]	56.8±0.4[c]
SPU-PDMS$_{EO}$-20	1:2:1	21.4	4.3	92.7±0.4[d]	77.8±1.2[b]	62.4±1.2[a]
SPU-PDMS$_{EO}$-45	1:4:3	44.9	19.6	87.0±0.4[a]	71.6±1.5[a]	59.9±0.4[a]
SPU-PDMS$_{EO}$-55	1:6:5	57.6	28.5	80.8±0.6[b]	63.5±1.9[c]	43.5±1.4[b]

[a] PDMS prepolymer:MDI:BD in the reaction mixture; at a 1.05 mole ratio of NCO/OH groups; [b] predetermined by the composition of the reaction mixtures; [c] determined by DSC results from the second heating run. The degree of crystallinity of SPU-PDMS$_{HP}$-20 sample is 2.6% in the first heating run; [d] a,b,c,d,e – values with the same letter are not statistically different at the p < 0.05 level (according to post-hoc Tukey's HSD test)

Since the synthesized SPU-PDMS copolymers prepared from the soft PDMS and hard MDI-BD segments were designed to obtain materials for biomedical applications, their surface energy and hydrophobicity/hydrophilicity play a key role. In the present study, the surface free energy of SPU-PDMS copolymers was calculated according to the van Oss–Chaudhury–Good [21] and Owens–Wendt methods [22]. In order to find and to validate the values of surface free energy those two methods were applied. Post-hoc Tukey's HSD test at 95% confidence limit was calculated to show any significant differences between samples. Moreover, in van Oss–Chaudhury–Good or Owens–Wendt methods, three (distilled water, formamide and diiodomethane) or two (distilled water and diiodomethane) liquids for the SPU-PDMS surface investigation were used.

The measurement of the contact angle represents well-known and very useful technique for characterization of solid surface. Tables 1 and 2 show the contact angles of the SPU-PDMS copolymers by using the three liquids as well as surface free energy and its components, respectively. The contact angles of SPU-PDMS$_{HP}$ and SPU-PDMS$_{EO}$ samples with water (θ_1) increased from 83.3 to 96.2° and from 80.8 to 92.7°, respectively, with increasing content of PDMS in the samples. In both series, the copolymers with higher PDMS content were more hydrophobic. These results may be explained by the migration tendency of PDMS on the surface of the copolymers, caused by very low surface energy of PDMS [4]. The hydrophobicity for SPU-PDMS copolymers based on HP-PDMS prepolymer is higher in comparison with copolymers based on EO-PDMS prepolymer with terminal hydrophilic ethylene oxide units. Furthermore, the values of the formamide (θ_2) and diiodomethane (θ_3) contact angle are higher for the samples of SPU-PDMS$_{HP}$ series in comparison with the samples of SPU-PDMS$_{EO}$ series. As shown in Table 2, the surface free energy of copolymers based on HP-PDMS is lower than that of copolymers based on EO-PDMS. Surface free energy of SPU-PDMS$_{HP}$ copolymers decreased due to the higher surface activity of HP-PDMS prepolymer incorporated into the soft segment in comparison with EO-PDMS prepolymer containing terminal hydrophilic ethylene oxide units. It was found that the decrease in the surface energy for SPU-PDMS$_{HP}$ samples in comparison with SPU-PDMS$_{EO}$ samples could be mainly attributed to decreasing values of the dispersive component γ_S^{LW} or γ_S^d. There was a very small change in the polar component γ_S^{AB} or γ_S^p with changing type of PDMS prepolymer. The surface energy values of the synthesized SPU-PDMS samples were higher than values obtained for the other poly(urethane-siloxane)s (around 20 mJ/m^2) [25,26] and silicone control sample (18 mJ/m^2) [26] presented in the literature. The results of the current study showed that the synthesized copolymers possess slightly amphiphilic character, implying the existence of both, hydrophobic PDMS and hydrophilic urethane groups at the surface.

AFM Analysis was carried out in order to understand the influence of the type of PDMS soft segments on the surface topography and heterogeneity relief of SPU-PDMS copolymers. The height and phase AFM images for SPU-PDMS copolymers are shown in Figure 2. Based on prior studies, it is known that the bright regions represent the hard phase, while the darker regions represent the soft PDMS phase. Height images show different surface topography for the synthesized copolymers. The topographies of SPU-PDMS$_{HP}$-20, SPU-PDMS$_{EO}$-20 and SPU-PDMS$_{EO}$-45 samples display spherullite particulate formations of tens of nm in size, SPU-PDMS$_{HP}$-45, SPU-PDMS$_{HP}$-55, SPU-PDMS$_{EO}$-55 show agglomerates of μm in size. Phase images (*i.e.*, maps of tip-sample interactions) enable qualitative insight into the homogeneity relief of samples. The synthesized copolymers based on EO-PDMS are characterized by two-phase morphology consisting of a hard segment-rich phase and a soft segment-rich phase. Therefore, the EO-PDMS based copolymers are distinguished by heterogeneous character, apparently connected with the good microphase separation. On the contrary, the copolymers based on HP-PDMS do not have sharp interfaces between the two phases, *i.e.*, they have mostly homogeneous character, apparently connected with the weak microphase separation.

Table 2. Results of surface free energy (mJ/m^2), its components and parameters for the SPU-PDMS copolymers calculated according to van Oss-Chaudhury-Good and Owens-Wendt methods; values with the same letter are not statistically different at the p < 0.05 level (according to post-hoc Tukey's HSD test)

Sample	van Oss-Chaudhury-Good method					Owens-Wendt method (water–diiodomethane liquids)		
	γ_S^{LW}	γ_S^+	γ_S^-	γ_S^{AB}	γ_S	γ_S^d	γ_S^p	γ_S
SPU-PDMS$_{HP}$-20	22.1±0.7^b	1.5±0.3^a	1.9±0.4^c	3.3±0.6^b	25.4±1.1^c	24.3±0.1^a	1.2±0.0^b	25.5±0.2^a
SPU-PDMS$_{HP}$-45	25.1±0.5^c	1.6±0.2^{ab}	2.8±0.1^{ab}	4.3±0.2^{ac}	29.4±0.7^{ab}	29.8±0.1^c	1.3±0.0^c	31.0±0.2^c
SPU-PDMS$_{HP}$-55	30.4±0.2^d	1.8±0.1^{ab}	3.0±0.4^b	4.6±0.3^a	35.0±0.3^d	27.2±0.2^b	2.0±0.0^e	29.1±0.3^b
SPU-PDMS$_{EO}$-20	27.3±0.8^a	1.9±0.3^{ab}	1.8±0.2^c	3.7±0.4^{bc}	31.1±1.0^{ab}	30.5±0.3^d	1.7±0.0^a	32.2±0.1^d
SPU-PDMS$_{EO}$-45	28.6±0.3^a	1.6±0.1^a	2.4±0.0^{ab}	3.9±0.2^{abc}	32.5±0.4^b	33.0±0.3^e	1.7±0.0^a	34.7±0.3^e
SPU-PDMS$_{EO}$-55	37.4±0.7^e	2.2±0.1^b	2.6±0.3^{ab}	4.8±0.4^a	42.2±0.3^e	40.8±0.2^f	1.6±0.0^d	42.3±0.2^f

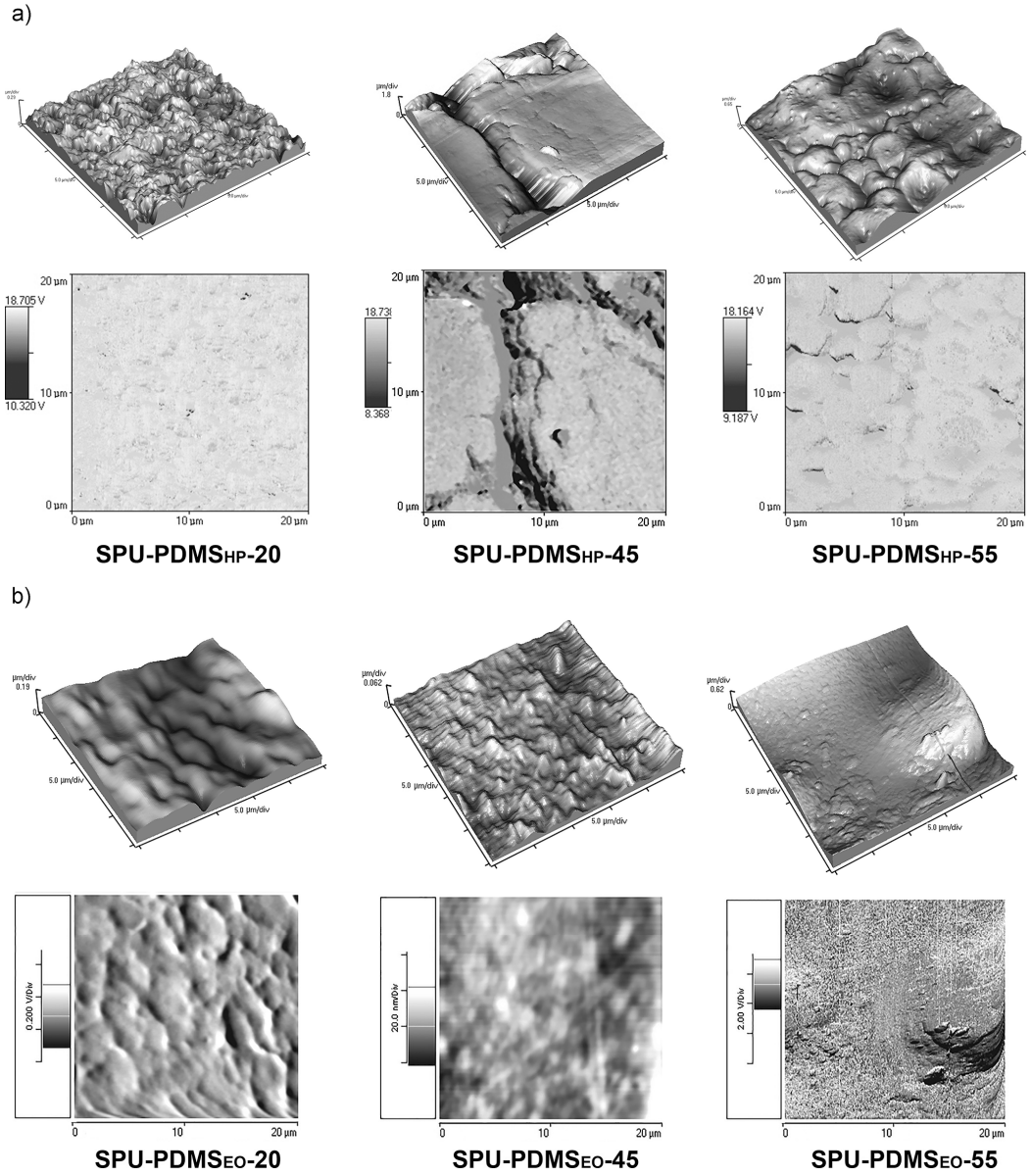

Figure 2. 3D AFM height and 2D AFM phase images of the surface of SPU-PDMS$_{HP}$ (a) and SPU-PDMS$_{EO}$ (b) copolymers (scan area 20 µm×20 µm).

Investigation of biocompatibility using endothelial cells and protein adsorption assays is paramount for further development of non-toxic, thromboresistant surfaces, given that almost all currently available biomaterials (*e.g.*, commercial PDMS/polyether based SPUs Elast-Eon^{TM}) have biocompatibility that is limited by inflammatory responses contributing to thrombosis formation, as well as low level of cell attachment [1,12]. In our study, the biocompatibility of copolymers was evaluated using endothelial EA.hy926 cell line by direct contact assay, before and after pre-treatment of copolymers with multicomponent protein mixture, as well as by a competitive blood-protein adsorption assay. Namely, in our research, we used EA.hy926 endothelial cell line to investigate cytocompatibility of the synthesized copolymers. Endothelial cells are the major cell type of the microvasculature, and they play a role in regulation of vascular tone and permeability, coagulation, inflammation and angiogenesis [1]. The response of these cells to a material is of great importance, and the endothelial cells are often used in *in vitro* evaluation of cytocompatibility of materials that might be used as medical devices, in particular, for the devices designed for cardiovascular applications aimed to have long-term close contacts with blood vessels.

The results of MTT assay showed that SPU-PDMS$_{HP}$ samples significantly inhibited attachment and growth of EA.hy926 cells, while SPU-PDMS$_{EO}$ samples supported the attachment and subsequent growth of endothelial cells on their surface without restriction

(Figure 3). The obtained results showed that the surfaces of SPU-PDMS$_{EO}$ samples might be favorable for the cell growth in comparison with the surface of SPU-PDMS$_{HP}$ copolymers, probably due to the better microphase separation and greater hydrophilic properties of surfaces of EO-PDMS-based copolymers.

Cell attachment to the SPU-PDMS copolymers was investigated by light microscopy 96 h post seeding. The representative photographs of EA.hy926 cells on the surface of copolymers are shown in Figure 4. In this study, the cell attachment appeared to depend on the type of PDMS soft segments, microphase separation, as well as surface hydrophilicity. Namely, the surface of SPU-PDMS$_{EO}$ samples favoured cell attachment, while a reduced cell attachment was observed in SPU-PDMS$_{HP}$ samples. Consequently, cell morphology was preserved on the surface of SPU-PDMS$_{EO}$ samples, while cells seeded onto SPU-PDMS$_{HP}$ samples could not spread to adopt the characteristic shape. As a result, cell attachment on the SPU-PDMS$_{EO}$ surface was much higher than on the SPU-PDMS$_{HP}$ surface due to higher hydrophilicity of SPU-PDMS$_{EO}$ copolymers. Again the amount of cells attached to the SPU-PDMS$_{EO}$ surface after a protein-preconditioning of their surface was much higher than on SPU-PDMS$_{HP}$ surface (Figure 5). Similar situation was observed after preconditioning of SPU-PDMS$_{HP}$ and SPU-PDMS$_{EO}$ copolymers surface with the three-component protein mixture (Figure 5), implying

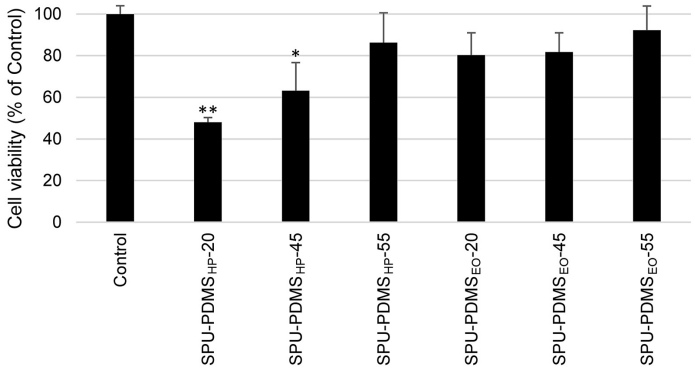

Figure 3. Ea.hy926 cell viability 96 h post seeding onto SPU-PDMS copolymers.

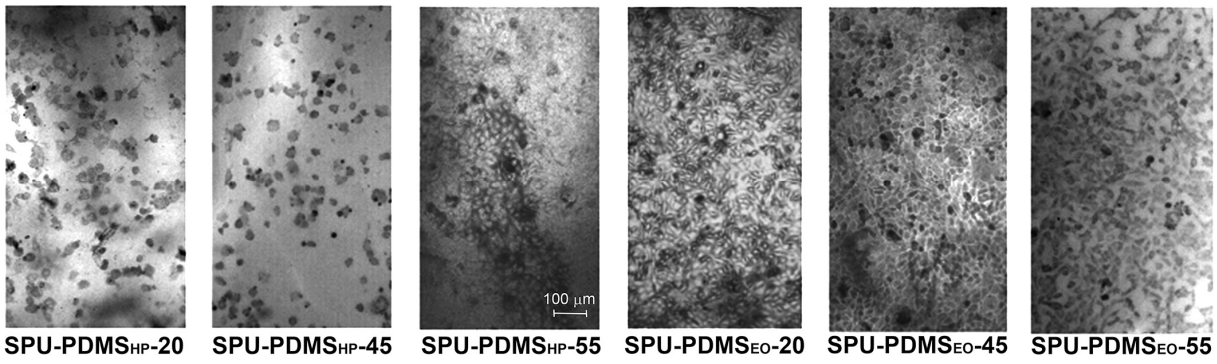

Figure 4. Photographs of SPU-PDMS copolymers with EA.hy926 cells adhered on their surface.

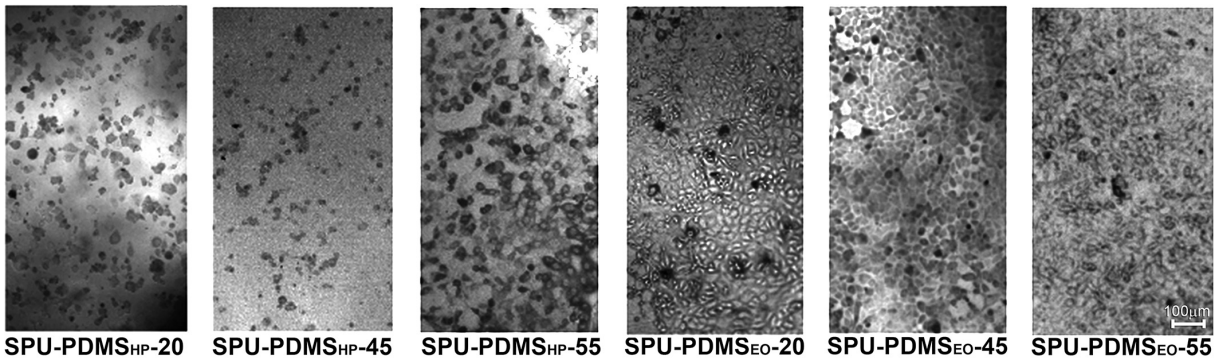

Figure 5. Photographs of SPU-PDMS copolymers pre-adsorbed with proteins mixture and adhered with EA.hy926 cells.

that pretreatment with blood proteins did not influence further cell attachment on the SPU-PDMS copolymers in both series. These results could be explained by limited FBG (*i.e*., cell adhesion-promoting protein) binding to all copolymers in both series. Namely, in this study the FBG/BSA adsorption ratio (Figure 6) did not affect cell attachment on the surface of proteins of pretreated copolymers. The obtained results suggested that endothelial cell attachment on the SPU-$PDMS_{EO}$ copolymer surface (81.4±6.0% for SPU-$PDMS_{EO}$-20, 81.0±9.4 for SPU-$PDMS_{EO}$-45, and 86.4±9.9% for SPU-$PDMS_{EO}$-55) was higher than on the Elast-Eon^{TM} (31.4±3.8%) [12], suggesting good biocompatibility of copolymers, which were derived only from EO-PDMS as soft segment.

Our *in vitro* measurements of plasma protein adsorption suggested good blood compatibility of all synthesized copolymers. All copolymers exhibited good resistance to fibrinogen adsorption and all favoured albumin adsorption (Table 3). Albumin adsorption is shown to passivate and protect the biomaterial surface from thrombosis, whereas fibrinogen promotes platelet adhesion on the polymer surface [1]. The adsorption ratio of FBG/BSA for the SPU-$PDMS_{HP}$ and SPU-$PDMS_{EO}$ copolymers from competitive experiments was in the range from 0.0320 to 0.0501 and from 0.0092 to 0.0208, respectively (Figure 6). The obtained results indicate that all copolymers preferentially adsorbed BSA, which is an indicator of good hemocompatibility [27]. It was suggested that polymers which show improved blood compatibility and less platelet adhesion have a smaller ratio of FBG/BSA [28], which was observed in our study. Nevertheless, in addition to blood–protein adsorption, other hemocompatibility investigations such as hemolysis and platelet adsorption, as well as *in vivo* testing are needed to confirm our preliminary results.

In this study, SPU-$PDMS_{EO}$ with a greater degree of microphase separation demonstrated a lower FBG/BSA adsorption ratio in competitive experiment and therefore better hemocompatibility in comparison with SPU-$PDMS_{HP}$ copolymers. This is in agreement with previous studies on SPUs based on polyether and PDMS soft segments and SPUs based on PCL-PDMS-PCL soft segments, where higher microphase separation of samples showed lower FBG adsorption levels [16,29]. Our results also suggest that the higher surface energy may be responsible for lower FBG adsorption of SPU-$PDMS_{EO}$ copolymers as compared to SPU-$PDMS_{HP}$ copolymers. Therefore, in this study we show that the hemocompatibility of the SPU-PDMS copolymers depends on the degree of microphase separation and surface free energy. Furthermore, the FBG interactions with SPU-$PDMS_{EO}$ are similar to those with commercial polyether/PDMS based SPUs, *i.e*., Elast-Eon^{TM} (adsorbed amount of FBG is 0.19 μg/cm^2 in competitive adsorption experiment) [30], suggesting good biocompatibility of SPU-$PDMS_{EO}$ copolymers and great promise for use in long-term blood-contacting biomaterials.

Table 3. Results of competitive adsorption of proteins on SPU-PDMS copolymers (μg/cm^2)

Sample	BSA	BGG	FBG
SPU-$PDMS_{HP}$-20	20.150±0.631	13.222±1.589	0.645±0.023
SPU-$PDMS_{HP}$-45	25.052±0.096	13.798±0.944	0.711±0.011
SPU-$PDMS_{HP}$-55	39.622±2.343	16.460±1.336	1.466±0.033
SPU-$PDMS_{EO}$-20	17.050±0.953	9.835±2.071	0.157±0.009
SPU-$PDMS_{EO}$-45	32.26±0.702	10.688±0.734	0.313±0.053
SPU-$PDMS_{EO}$-55	42.45±1.815	10.727±0.829	0.884±0.281

Our results indicate that SPU-PDMS copolymers have good surface properties, depending on the type of soft PDMS segments, which can be tailored for biomedical application requirements such as biomedical devices for short- and long-term uses. Copolymers based on EO-PDMS are less hydrophobic and have higher crystallinity (Table 1), as well as good microphase separation, which promoted better cell attachment and growth on polymer surface. EO-PDMS-based copolymers due to an excellent resistance to fibrinogen and stimulated endothelial cell adhesion properties

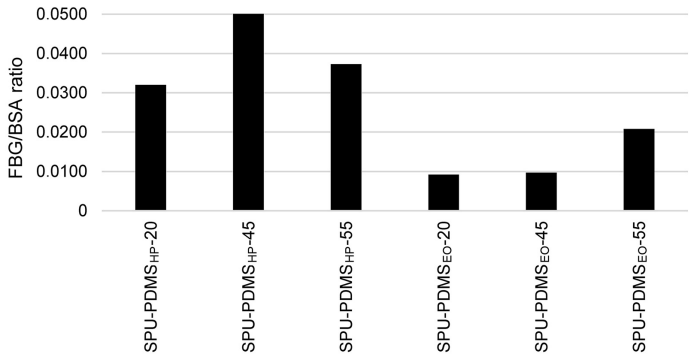

Figure 6. Fibrinogen/albumin ratio for SPU-PDMS copolymers from competitive adsorption experiments.

might be found suitable for long-term biomedical application such as in cardiovascular devices that particularly require good blood compatibility and stimulated attachment of endothelial cells. However, the obtained results showed that HP-PDMS-based copolymers have good hemocompatibility due to the excellent resistance to fibrinogen adsorption, but show low endothelial cell adhesion. These results are consistent with previous studies [31] reporting that PDMS imparted a hydrophobic character to the surface of PDMS polyether polyurethanes that may have resulted in lower cell density and cell coverage, but enhanced biostability as compared to polyether polyurethanes. Our results on endothelial cell line prompt us to propose that HP-PDMS-based copolymers might be found suitable for transient devices such as blood contacting portion of blood pumps and catheters. However, a further investigation (using different cell lines as well as blood-based tastings) is needed to clarify their potential for use in short-term biomedical devices.

CONCLUSION

The results of the current study show that the type of soft PDMS segments in the copolymers plays an important role in protein adsorption and endothelial cell adhesion onto the copolymer surfaces. The obtained results confirm good blood compatibility of synthesized copolymers since all copolymers exhibit good resistance to fibrinogen adsorption and all favor albumin adsorption. However, the higher surface energy and good microphase separation may partially account for a better hemocompatibility of copolymers based on EO-PDMS compared to HP-PDMS based copolymers. Our results imply that the surface of EO--PDMS based copolymers is more favourable for the cell attachment and growth than the surface of HP-PDMS based copolymers, probably due to the greater hydrophilic properties of surfaces of these materials. Copolymers based on HP-PDMS significantly inhibit attachment and growth of EA.hy926 cells, as demonstrated through the decrease in viability of cells grown in the presence of these copolymer films, which could be a consequence of the restricted ability of cells to attach on their surface. Therefore, the synthesized SPUs based on HP-PDMS due to good hemocompatibilty and cells non-adherent properties should be further investigated as potential materials that might be used in biomedical devices for short-term use. Furthermore, our results show that SPUs based on the EO-PDMS soft segment favor the adhesion of endothelial cells on their surface as compared to HP-PDMS based SPUs, due to the presence of hydrophilic ethylene oxide terminal units in the soft segment, implying that these copolymers might be used in long-term biomedical application.

Acknowledgements

This work was financially supported by the Ministry of Education, Science and Technological Development of the Republic of Serbia (Project No. 172062).

REFERENCES

[1] R. Vermette, H.J. Griesser, G. Laroche, R. Guidoin, Biomedical Appliactions of Polyurethanes, Landes Bioscience, Austin, TX, 2001.

[2] S. Gogolewski, Selected topics in biomedical polyurethanes. A review, Colloid Polym. Sci. **267** (1989) 757––785.

[3] P.R. Dvornic, R.W. Lenz, High Temperature Siloxane Elastomers, Hüthing & Wepf, Heidelberg and New York 1990.

[4] İ. Yilgör, J. McGrath. Polysiloxane containing copolymers: A survey of recent developments. Polysiloxane Copolymers/Anionic Polymerization, Adv. Polym. Sci. **86** (1988) 1–86.

[5] D.K. Chattopadhyay, K.V.S.N. Raju, Structural engineering of polyurethane coatings for high performance applications, Prog. Polym. Sci. **32** (2007) 352–418.

[6] R.W. Hergenrother, Y. Xue-Hai, S.L. Cooper, Blood-contacting properties of polydimethylsiloxane polyurea-urethanes, Biomaterials **15** (1994) 635–640.

[7] J.P. Sheth, A. Aneja, G.L. Wilkes, E. Yilgor, G.E. Atilla, I. Yilgor, F.L. Beyer, Influence of system variables on the morphological and dynamic mechanical behavior of polydimethylsiloxane based segmented polyurethane and polyurea copolymers: a comparative perspective, Polymer **45** (2004) 6919–6932.

[8] P.A. Gunatillake, G.F. Meijs, S.J. Mccarthy, R. Adhikari, Poly(dimethylsiloxane)/poly(hexamethylene oxide) mixed macrodiol based polyurethane elastomers. I. Synthesis and properties, J. Appl. Polym. Sci. **76** (2000) 2026–2040.

[9] T. Choi, J. Weksler, A. Padsalgikar, J. Runt, Microstructural organization of polydimethylsiloxane soft segment polyurethanes derived from a single macrodiol, Polymer **51** (2010) 4375–4382.

[10] R. Hernandez, J. Weksler, A. Padsalgikar, T. Choi, E. Angelo, J.S. Lin, L.-C. Xu, C.A. Siedlecki, J. Runt, A Comparison of Phase Organization of Model Segmented Polyurethanes with Different Intersegment Compatibilities, Macromolecules **41** (2008) 9767–9776.

[11] R. Hernandez, J. Weksler, A. Padsalgikar, J. Runt, In vitro oxidation of high polydimethylsiloxane content biomedical polyurethanes: Correlation with the microstructure, J. Biomed. Mater. Res., A **87** (2008) 546–556.

[12] D.V. Bax, A. Kondyurin, A. Waterhouse, D.R. McKenzie, A.S. Weiss, M.M.M. Bilek, Surface plasma modification and tropoelastin coating of a polyurethane co-polymer for enhanced cell attachment and reduced thrombogenicity, Biomaterials **35** (2014) 6797–6809.

[13] M. Yaseen, X. Zhao, A. Freund, A.M. Seifalian, J.R. Lu, Surface structural conformations of fibrinogen polypeptides for improved biocompatibility, Biomaterials **31** (2010) 3781–3792.

[14] M. Bil, J. Ryszkowska, P. Woźniak, K.J. Kurzydłowski, M. Lewandowska-Szumieł, Optimization of the structure of polyurethanes for bone tissue engineering applications, Acta Biomat. **6** (2010) 2501–2510.

[15] D. Spiller, C. Mirtelli, P. Losi, E. Briganti, S. Sbrana, C. Counoupas, S. Kull, S. Tonlorenzi, G. Soldani, *In vitro* evaluation of the PEtU-PDMS material immunocompatibility: the influence of surface topography and PDMS content, J. Mater. Sci. Mater. Med. **20** (2009) 2511–2520.

[16] M.V. Pergal, V.V. Antic, G. Tovilovic, J. Nestorov, D. Vasiljevic-Radovic, J. Djonlagic, In Vitro Biocompatibility Evaluation of Novel Urethane–Siloxane Co-Polymers Based on Poly(ε-Caprolactone)-block-Poly(Dimethylsiloxane)-block-Poly(ε-Caprolactone), J. Biomat. Sci., Polym. Edn. **23** (2012) 1629–1657.

[17] M.V. Pergal, J. Nestorov, G. Tovilovic, S. Ostojic, D. Gođevac, D. Vasiljevic-Radovic, J. Djonlagic, Structure and properties of thermoplastic polyurethanes based on poly(dimethylsiloxane): assessment of biocompatibility, J. Biomed. Mater. Res., A **102** (2014) 3951–3964.

[18] I.S. Stefanović, J. Djonlagić, G. Tovilović, J. Nestorov, V.V. Antić, S. Ostojić, M.V. Pergal, Poly(urethane-dimethylsiloxane) copolymers displaying a range of soft segment contents, noncytotoxic chemistry, and nonadherent properties toward endothelial cells, J. Biomed. Mater. Res., A (2014), DOI: 10.1002/jbm.a.35285.

[19] M.V. Pergal, i.S. Stefanovic, D. Gođevac, V.V. Antic, V. Milacic, S. Ostojic, J. Rogan, J. Djonlagic, Structural, thermal and surface characterization of thermoplastic polyurethanes based on poly(dimethylsiloxane), J. Serb. Chem. Soc. **79** (2014) 843–866.

[20] A. Marand, J. Dahlin, D. Karlsson, G. Skarping, M. Dalene, Determination of technical grade isocyanates used in the production of polyurethane plastics, J. Environ. Monit. **6** (2004) 606–614.

[21] C.J. Van Oss, R.J. Good, M.K. Chaudhury, Additive and nonadditive surface tension components and the interpretation of contact angles, Langmuir **4** (1988) 884–891.

[22] D.K. Owens, R.C. Wendt, Estimation of the surface free energy of polymers, J. Appl. Polym. Sci. **13** (1969) 1741––1747.

[23] J. Vince, B. Orel, A. Vilčnik, M. Fir, A. Šurca Vuk, V. Jovanovski, B. Simončič, Structural and Water-Repellent Properties of a Urea/Poly(dimethylsiloxane) Sol−Gel Hybrid and Its Bonding to Cotton Fabric, Langmuir **22** (2006) 6489–6497.

[24] D.W. Van Krevelen, Properties of Polymers, Elsevier, Amsterdam, 1990.

[25] Ł. Byczyński, Effect of different polyethers on surface and thermal properties of poly(urethane-siloxane) copolymers modified with side-chain siloxane, J. Therm. Anal. Calorim. **114** (2013) 397–408.

[26] P. Majumdar, S. Stafslien, J. Daniels, D. Webster, High throughput combinatorial characterization of thermosetting siloxane–urethane coatings having spontaneously formed microtopographical surfaces, J. Coat. Technol. Res. **4** (2007) 131–138.

[27] S.P. Victor, C.P. Sharma, Development and evaluation of cyclodextrin complexed hydroxyapatite nanoparticles for preferential albumin adsorption, Colloids Surfaces, B **85** (2011) 221–228.

[28] S.-L. Huang, M.-S. Chao, R.-C. Ruaan, J.-Y. Lai, Microphase separated structure and protein adsorption of polyurethanes with butadiene soft segment, Eur. Polym. J. **36** (2000) 285–294.

[29] T.G. Grasel, S.L. Cooper, Surface properties and blood compatibility of polyurethaneureas, Biomaterials **7** (1986) 315–328.

[30] D. Cozzens, A. Luk, U. Ojha, M. Ruths, R. Faust, Surface Characterization and Protein Interactions of Segmented Polyisobutylene-Based Thermoplastic Polyurethanes, Langmuir **27** (2011) 14160–14168.

[31] A.B. Mathur, T.O. Collier, W.J. Kao, M. Wiggins, M.A. Schubert, A. Hiltner, J.M. Anderson, *In vivo* biocompatibility and biostability of modified polyurethanes, J. Biomed. Mater. Res., A **36** (1997) 246–257.

IZVOD

POVRŠINSKA KARAKTERIZACIJA, HEMO- I CITOKOMPATIBILNOST SEGMENTIRANIH POLIURETANA NA BAZI POLI(DIMETILSILOKSANA)

Marija V. Pergal[1], Jelena Nestorov[2], Gordana Tovilović-Kovačević[2], Petar Jovančić[3], Lato Pezo[4], Dana Vasiljević-Radović[1], Jasna Djonlagić[3]

[1]*Institut za hemiju, tehnologiju i metalurgiju, Univerzitet u Beogradu, Beograd, Srbija*
[2]*Odeljenje za biohemiju, Institut za biološka istraživanja"Siniša Stanković", Univerzitet u Beogradu, Beograd, Srbija*
[3]*Fakultet za tehnologiju i metalurgiju, Univerzitet u Beogradu, Beograd, Srbija*
[4]*Institut za opštu i fizičku hemiju, Univerzitet u Beogradu, Beograd, Srbija*

(Naučni rad)

Segmentirani poliuretani na bazi poli(dimetilsiloksana), koji se trenutno koriste u biomedicini, imaju biokompatibilnost ispod optimalne što smanjuje njihovu efikasnost. Poboljšavajući vezivanje endotelnih ćelija i svojstva kopolimera na bazi PDMS u dodiru sa krvlju značajno bi se poboljšala i proširila njihova klinička primena. U ovom radu su proučavana površinska svojstva i *in vitro* biokompatibilnost dve serije segmentiranih poli(uretan-dimetilsiloksana) (SPU-PDMS) na bazi hidroksipropil- i hidroksietoksipropil- PDMS pretpolimera sa potencijalnim primenama u medicinskim uredjajima u kontaktu sa krvlju. SPU-PDMS kopolimeri su karakterisani merenjem kontaktnih uglova, određivanjem površinske energije (izračunate prema van Oss-Chaudhury-Good i Owens-Wendt metodama), i mikroskopijom atomskih sila. Biokompatibilnost kopolimera je ispitivana primenom endotelnih EA.hy926 ćelija u direktnom kontaktu, pre i nakon pretretiranja kopolimera sa višekomponentnom smešom proteina, kao i pomoću kompetitivne adsorpcije proteina. Dobijeni rezultati su potvrdili da sintetisani kopolimeri imaju dobru kompatibilnost prema krvi. Svi sintetisani kopolimeri pokazivali su dobru otpornost prema adsorpciji fibrinogena i svi kopolimeri su favorizovali adsorpciju albumina. Kopolimeri na bazi hidroksietoksipropil-PDMS imali su manju hidrofobnost, veću površinsku energiju, i bolju mikrofaznu separaciju u poređenju sa kopolimerima na bazi hidroksipropil-PDMS, što je dovelo do boljeg vezivanja i rasta endotelnih ćelija na površini ovih polimera u poređenju sa kopolimerima na bazi hidroksipropil-PDMS. Rezultati su pokazali da SPU-PDMS kopolimeri prikazuju dobra površinska svojstva, zavisno od vrste mekih PDMS segmenata, koja se mogu prilagođavati zahtevima u biomedicini, kao što su biomedicinski uređaji za kratkoročnu i dugoročnu upotrebu.

Ključne reči: Poliuretani • Siloksani • Površinska energija • Vezivanje ćelija • Adsorpcija proteina

Physicochemical characteristics of gamma irradiation crosslinked poly(vinyl alcohol)/magnetite ferrogel composite

Milena T. Marinović-Cincović, Aleksandra N. Radosavljević, Jelena I. Krstić, Jelena P. Spasojević, Nataša M. Bibić, Miodrag N. Mitrić, Zorica M. Kačarević-Popović

Vinča Institute of Nuclear Sciences, University of Belgrade, Belgrade, Serbia

Abstract

Magnetic field sensitive gels, ferrogels, are new promising class of hydrogels. The coupling of hydrogels and magnetic particles has potential application in soft actuators, such as artificial muscles, or for hyperthermia application. In this study, the composite of magnetite particles (Fe_3O_4) and poly(vinyl alcohol) (PVA) hydrogel is developed using gamma irradiation as a crosslinking agent. PVA and Fe_3O_4 were chosen due to their well-established biocompatibility, radiation crosslinking potential (PVA), mild magnetic properties and the Curie point near desired heating temperature range (Fe_3O_4). Physicochemical characteristics of these systems show the effect of the presence of particles in the process of radiation-induced crosslinking. Obtained PVA/Fe_3O_4 ferrogel composite has greater swelling capacity, activation energy of dehydration and dehydration rate compared to PVA hydrogel, crosslinked under the same conditions.

Keywords: gamma irradiation, PVA hydrogel, magnetite particles, ferrogel, swelling properties, dehydration properties.

Available online at the Journal website: http://www.ache.org.rs/HI/

Polymers

SCIENTIFIC PAPER

UDC 544.773.43:66:53

Hem. Ind. **68** (6) 743–753 (2014)

doi: 10.2298/HEMIND141104081M

One of the goals of material research is to create new materials with properties tailored to a particular application and to understand the physical and chemical mechanisms that determine these properties. Hydrogels are crosslinked polymeric networks that are capable of imbibing water and swelling. New promising class of these materials is ferrogel, the magnetic field sensitive gel. Zrinyi *at al*. developed magnetic field sensitive gels in which magnetic particles of colloidal size are dispersed and incorporated into the gels [1]. These ferrogels combine the magnetic properties of magnetic fillers and the elastic properties of gels. When the gels were placed into a spatially non-uniform magnetic field, forces act on the magnetic particles and as result of strong interaction between magnetic particles and polymer chains, they all move together as a single unit. The coupling of hydrogels and magnetic particles has potential application in soft actuators such as artificial muscles [2]. On the other hand, the use of magnetic sensitive hydrogels has been recently explored for hyperthermia applications. The polymer networks have properties which make the hydrogels suitable for applications in controlled drug delivery systems, while the magnetic particles, with ferromagnetic or superparamagnetic properties are used for magnetic hyperthermia [3].

Correspondence: Z. Kačarević-Popović, Vinča Institute of Nuclear Sciences, University of Belgrade, P.O. Box 522, 11001 Belgrade, Serbia.
E-mail: zkacar@vinca.rs
Paper received: 4 November, 2014
Paper accepted: 17 November, 2014

The purpose of this work was to develop magnetically responsive polymer network based on composites of magnetic particles and hydrogels using gamma irradiation as a crosslinking agent, and to investigate its physico-chemical characteristics, such as swelling behavior and kinetics of dehydration of equilibrium swollen ferrogel.

The feasibility of this idea was explored by using poly(vinyl alcohol) ferrogel system (PVA/Fe_3O_4). PVA and Fe_3O_4 were chosen due to their well-established biocompatibility and history of clinical usage. Iron oxide is chemically stable, non-toxic and non-carcinogenic with mild magnetic properties and the Curie point near desired heating temperature range [3].

Moreover, PVA as a matrix component is selected because it is radiation crosslinking type polymer.

Mechanism of radiation chemical crosslinking is as follow:

a) When dilute aqueous solution of polymer is subjected to gamma irradiation, most of the energy of ionizing radiation is absorbed by water. As a result, short-lived reactive species are formed, mainly hydrated electrons (e_{aq}^-), hydroxyl radicals ($OH^\bullet$) and hydrogen atoms ($H^\bullet$):

$$H_2O \xrightarrow{\gamma\text{-Irradiation}} e_{aq}^-, OH^\bullet, H^\bullet, H_3O^+, H_2, H_2O_2 \quad (1)$$

Out of these, hydroxyl radicals and hydrogen atoms are of interest in the present context, since they are capable to generate polymer radicals.

b) Both species ($OH^\bullet$ and $H^\bullet$) abstract preferentially hydrogen atoms in α-position to the hydroxyl group (–CH(OH)–) forming the tertiary radical (~70%), but

also from methylene group (–CH_2–) forming secondary radical (~30%), Scheme 1, paths a and b, respectively. The C–H bond dissociation energy of the secondary hydrogen is somewhat higher than that of the tertiary hydrogen and thus the some secondary radicals undergo the H-abstraction reaction (Scheme 1, path c) [4,5].

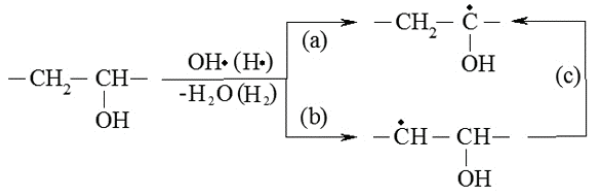

Scheme 1. Possible reaction pathways.

c) These PVA radicals may interact with one another by recombination, disproportionation, and chain scission (by β-fragmentation) [6]. In the case of PVA, the degradation cannot be totally avoided, but its yield is low and formation of polymer network occurs without any difficulty.

To construct three-dimensional polymer networks, the radiation chemistry method is offering advantages over conventional physical or chemical methods of network formation: mild reaction conditions, negligible formation of by-products, fast gelation, no need for catalysts and finally sterilization. Physicochemical properties of the radiation-crosslinked polymer network and the swelling ability of radiation-crosslinked hydrogels can be easily tailored by changing the irradiation time.

Preparation of ferrogels is similar to that of other filled elastomeric networks. One can precipitate well-dispersed particles in the polymeric material. *In situ* precipitation can be made before, during or after the crosslinking reaction. According to another method, the preparation and characterization of colloidal particles is made separately from the crosslinking reaction. In this paper, we report preparation of later type.

EXPERIMENTAL

Materials

All chemicals were of analytical grade and used as received, without further purification. Poly(vinyl alcohol) (PVA) with molecular weight 72000 and min. 99% degree of hydrolysis, and perchloric acid ($HClO_4$) were purchased from Merck. Iron(II) chloride ($FeCl_2$) and iron(III) chloride hexahydrate ($FeCl_3 \cdot 6H_2O$) were products of Sigma Aldrich and Polskie Odczynniki Chemiczne S.A., respectively. Deionized water was obtained from a Millipore Milli-Q system and used for solutions preparation and swelling experiments. High purity argon gas (99.5%) was used for bubbling of solutions.

Synthesis of PVA/Fe_3O_4 ferrogel composite

Iron oxide dispersion was prepared using the method already described, based on the coprecipitation of $FeCl_2$ and $FeCl_3$ by adding a concentrated solution of base into the mixture of iron salts [1]. The overall reaction can be written as:

$$Fe^{2+} + 2Fe^{3+} + 8OH^- \rightarrow Fe_3O_4 + 4H_2O \quad (2)$$

Obtained ferrofluid was black, which is the characteristic color of the magnetite. In order to counterbalance the Van der Waals attraction and the attractive part of magnetic dipole interactions, additional repulsion between the grains was achieved by electrostatic repulsion due to peptization (with $HClO_4$).

The 5 wt% PVA aqueous solution was prepared by dissolving polymer at 80 °C under the stirring for 6 h and then magnetic particles (20 wt.% Fe_3O_4 with respect to PVA) were added, and the solution was under the ultrasonication for 3 h. Although it is known that polymer chains can be broken under the influence of ultra sound, irreversible aggregation as one of the major concerns during the preparation of magnetic ferrofluid cannot be avoided or resolved with standard mixing or homogenization. Therefore, the sonication method becomes the preferred choice to overcome the attractive forces holding the clumped particles together and to break apart irreversible aggregates that have formed. Both, the PVA solution and PVA/Fe_3O_4 dispersion were aerated for 30 min with argon, in order to remove oxygen, and placed between two glass plates sealed with PVC spacer. The gamma irradiation was performed at ^{60}Co radiation source, under ambient condition, at a dose rate of 0.5 kGy/h, to absorbed dose of 25 kGy (our previous results confirmed that this is optimal irradiation dose for crosslinking [7]). The obtained ferrogels were immersed in deionized water, which was change every day, for one week, to remove uncrosslinked PVA, and dried at room temperature to constant mass. The masses of uncrosslinked PVA which were extracted from the PVA and PVA/magnetite composite hydrogel samples after crosslinking were 0.0021 and 0.0063 g, respectively. In relation to the initial mass of PVA sample before extraction, or PVA in PVA/Fe_3O_4 before extraction, it gives approximately 0.117 (11.8%) and 0.348 (34.8%) of sol fraction.

Structural characterization

The morphology of the as-prepared magnetite particles (Fe_3O_4) was examined by transmission electron microscopy (TEM) using Philips EM 400 microscope operated at an accelerating voltage of 120 kV. Samples for TEM studies were prepared by placing a drop of the dispersion of Fe_3O_4 particles onto a carbon-coated copper grid, followed by evaporating the solvent at room temperature. Moreover, the morphology of

PVA/Fe_3O_4 xerogel composite surface was observed by scanning electron microscopy (SEM) using JEOL JSM--6460 LV microscope operated at an accelerating voltage of 25 kV. Before observation, the sample of xerogel was coated with carbon.

The X-ray diffraction (XRD) analysis of investigated PVA/Fe_3O_4 xerogel composite was performed on Bruker D8 Advance diffractometer (CuKα1 radiation, λ = = 0.1546 nm).

FTIR spectra of xerogels, PVA and PVA/Fe_3O_4 composite, were recorded using Thermo Electron Corporation Nicolet 380 FTIR spectrophotometer, with the addition for work in the attenuated total reflection (ATR) mode.

Swelling experiments

Dynamic swelling experiments were performed in deionized water at 37±0.2 °C. Swollen gels, removed from the water at regular intervals, were dried superficially with filter paper, weighed and placed in the same bath. The swelling degree (*SD*) was calculated using the following equation:

$$SD = 100\left(m_t - m_0\right)/m_0 \quad (4)$$

where m_0 and m_t are the weights of the dry hydrogel (xerogel) at initial time (t = 0) and of the swollen hydrogel at time t, respectively.

The amount of absorbed water was measured until a constant weight of swollen hydrogel was reached (m_{eq}). Substituting the m_t by m_{eq} in Eq. (4), the equilibrium swelling degree (SD_{eq}) was calculated [8]. All swelling experiments were performed in triplicate and the average values were reported.

The normalized swelling degree (α) was defined as the ratio between the swelling degree at time t (SD_t) and equilibrium swelling degree:

$$\alpha = SD_t / SD_{eq} \quad (5)$$

Dehydration and thermal stability

Dehydration of PVA hydrogel and PVA/Fe_3O_4 ferrogel composite, were analyzed by thermogravimetric method. Thermogravimetric curves were recorded by a Setaram's SETSYS Evolution 1750 thermogravimetry analyzer. Dehydration analyses were performed with 20±0.1 mg of equilibrium swollen hydrogel, in platinum pans, under argon atmosphere (flow rate 16 mL/min). Measurements were carried out at heating rates (β) of 2.5, 5, 10 and 20 °C/min in the temperature range from 25 to 250 °C. Moreover, the thermal stability of xerogels was investigated in the temperature range from 25 to 750 °C, under the argon atmosphere at heating rate of 10 °C/min.

RESULTS AND DISCUSSION

Morphology and structural characterization

The typical TEM micrograph of as-prepared magnetite particles is shown in Fig. 1. It can be seen that the most part of Fe_3O_4 particles have spherical shape, with the size up to about 20 nm. Also, it can be observed that particles tend to aggregate into larger agglomerates, probably due to their extremely small sizes, high surface energies and magnetic properties.

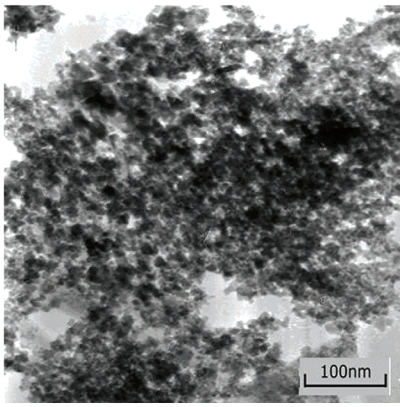

Fig. 1. TEM Micrograph of as-prepared magnetite particles.

In an attempt to explore the composite morphology, SEM micrographs were obtained. Figure 2 corresponds to PVA/Fe_3O_4 xerogel composite surface. It can be seen that the magnetic particles agglomerate, probably due to reduced stabilization ability of polymer network on the surface, as well as due to heating of

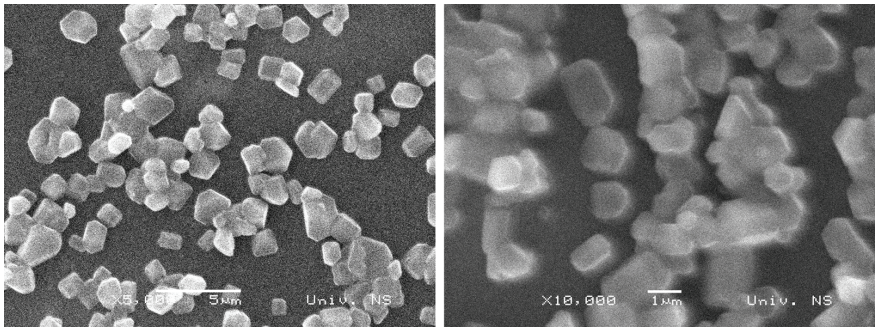

Fig. 2. SEM Micrographs of PVA/Fe_3O_4 xerogel composite surface.

system in consequence of energy absorption during gamma irradiation. Formed agglomerates have different shape and size in the range up to about 2 μm.

XRD technique was used to identify the desired particles prepared with ferric and ferrous salts, over 2θ range from 10 to 70°. In general, particles can be crystalline, amorphous or quasi-crystalline [9].

Crystalline magnetite structure is an inverse spinel with a face center cubic unit based on 32 O^{2-} ions. There are eight formula units per unit cell. Magnetite differs from other iron oxides in that it contains both divalent and trivalent iron. Its formula is written as $Fe^{III}[Fe^{II}Fe^{III}]O_4$ and the brackets denote octahedral sites. Tetrahedral Fe spins are directed antiparallel to octahedral Fe^{3+} and Fe^{2+} spins, so that the Fe^{3+} moments cancel, leaving a spontaneous magnetization equivalent to one Fe^{2+} moment per molecule. Eight tetrahedral sites are occupied by trivalent iron, and the divalent and trivalent cations occupied the sixteen octahedral sites. Although, X-ray diffraction is the most widely used technique to determine the crystalline structure of a material, in the case of magnetite it can be confusing because the magnetite has the same crystalline structure as maghemite, but this one has a interstitial voids, therefore by using XRD is not conclusive [10]. The diffraction peaks (Fig. 3) corresponding (220), (400) and (511) are characteristic peaks of the Fe_3O_4 crystal. Diffraction peaks corresponding to (024) and (300) are characteristic peaks of α-Fe_2O_3. The obtained XRD pattern suggests that the final product was a mixture of Fe_3O_4 and α-Fe_2O_3. The existence of α-Fe_2O_3 is common and occurs because of the oxidation of Fe_3O_4 during synthesis. In this case it is probably caused due to the heating of system in consequence of energy absorption during gamma irradiation.

Moreover, in the case of magnetite, the infrared spectroscopy is useful because this technique arises as a result of divalent and trivalent cations interaction with electromagnetic radiation. This interaction involves excitation for vibration or rotation of molecules in their ground electronic state, and they are associated with stretching deformation of the interatomic bonds and bending deformation of the interbond angles. In general, infrared spectra of the magnetite show the characteristic bands at 590 cm^{-1} due to the Fe−O bond. It was observed that this characteristic absorption band of bulk Fe_3O_4 was shifted from 573 to 656 cm^{-1} in the case of particles. It is caused by the breaking of a large number of bonds of surface atoms, resulting in the rearrangement of unlocalized electrons on the particle surface. In general the band at 600 cm^{-1} approximately is broadening when the particle size decreases. The existence of this characteristic absorption band, as shown in Fig. 4, confirms the presence of spinel structure Fe_3O_4 [11]. In addition, the peak at 1594 cm^{-1} observed in xerogel of PVA/Fe_3O_4 composite curve probably indicates a complex interaction between hydroxyl groups and oxygen containing groups emerged during sonication, on the surface of magnetic particles [12]. Since there are large surface-to-volume atomic ratio, the high surface activity and amount of dangling bonds on nanoparticle surface, the atoms on the surface are apt to adsorb ions or molecules. For Fe_3O_4 particles dispersed in a PVA xerogel, the atoms of Fe and O on the particle surface would adsorb OH groups and oxygen containing groups (carbonyl or carboxyl) causing their hydrogen bonding and a red shift of aliphatic oxygen groups adsorption from 1680–1750 cm^{-1} to 1594 cm^{-1}.

Swelling studies

When a xerogel is brought into contact with water, the water diffuses into the network and volume phase transition occurs, resulting in the expansion of the hydrogel, *e.g.*, hydrogel swells. Diffusion involves the migration of water into pre-existing or dynamically formed spaces among hydrogel chains. The capacity of

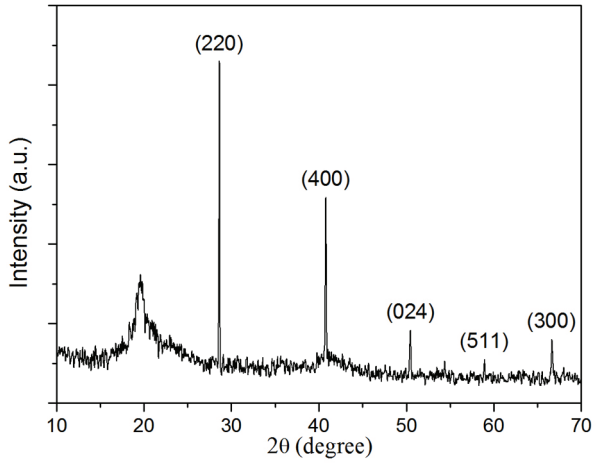

Fig. 3. XRD Pattern of the PVA/Fe_3O_4 xerogel composite.

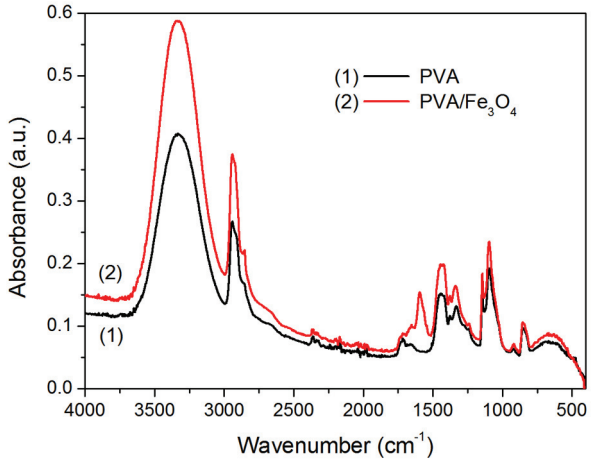

Fig. 4. FTIR Spectra of xerogels: PVA and PVA/Fe_3O_4 composite.

swelling is one of the most important parameters for evaluation the physicochemical properties of hydrogels. Many structural factors (charge and concentration of ionizable groups, degree of ionization, crosslinking density and hydrophilicity) influence the swelling degree of hydrogels, and the properties of swelling medium (the pH, ionic strength, counterion and its valence) affect the swelling characteristics [13].

PVA is hydrophilic polymer with a large number of hydrophilic –OH groups, which can easily form hydrogen bonds with free water molecules [14]. So, H_2O and other small molecules, easily penetrate into the space between the PVA chains, giving swelled polymer network. Figure 5 depicts the swelling curves of the PVA hydrogel (control sample) and PVA/Fe_3O_4 ferrogel composite in distilled water at 37 °C. As can be seen from the presented results, the swelling isotherms are similar in shape, but crosslinking of PVA in the presence of Fe_3O_4 particles has significant influence on the swelling properties in comparison to pure PVA hydrogel.

Three characteristic regions may be distinguished in swelling curves presented in Fig. 5: a linear part, a nonlinear part and a saturation range or plateau. In order to analyze the influence of xerogel structure on the swelling isotherm shape, specific parameters of the swelling isotherms are defined: period of linearity, initial swelling rate and swelling equilibrium degree. The period of linearity *e.g.*, range of applicability (P) presents the region of the normalized swelling degree, within which the kinetic swelling curves are linear. The initial swelling rate (v_{in}) is defined as the ratio of the swelling degree in the final point of the linear part of the swelling curve (SD_{in}) to the swelling time that corresponds to the linear part of the swelling curve (t_{in}) [15,16]:

$$v_{in} = SD_{in} / t_{in} \quad (6)$$

Table 1 presents the changes of the equilibrium swelling degree (SD_{eq}), the initial swelling rate (v_{in}) and range of applicability (P) for the PVA hydrogel and

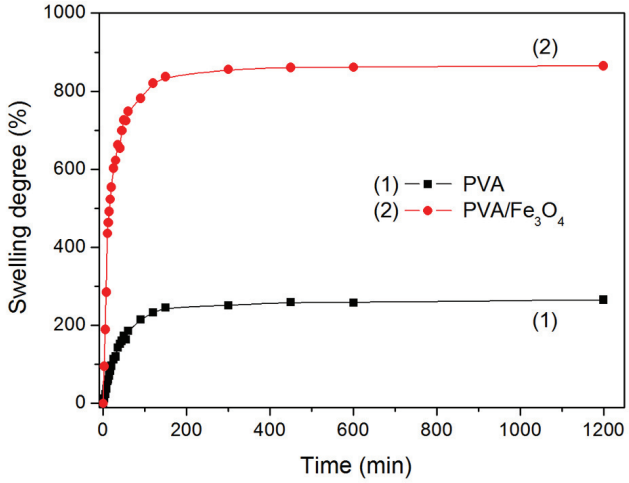

Fig. 5. Swelling isoterms of PVA hydrogel and PVA/Fe_3O_4 ferrogel composite in distilled water at 37 °C.

PVA/Fe_3O_4 ferrogel composite in distilled water at 37 °C. The obtained values show that with incorporation of Fe_3O_4 particles in PVA hydrogel all specific parameters of the swelling isotherms are increased. The swelling capacity and initial swelling rate of PVA/Fe_3O_4 ferrogel composite is found to be about 3.3 and 8.1 times, respectively, higher in comparison with control PVA hydrogel, which directly indicated that the crosslinking of PVA in the presence of Fe_3O_4 particles caused decreasing of crosslinking density. In general, it is well known that swelling is directly related to the structure of the crosslinked polymer and/or the density of the hydrogel.

Table 1. Specific parameters of swelling isotherms for PVA hydrogel and PVA/Fe_3O_{41}

Sample	SD_{eq} / %	v_{in} / % min^{-1}	P / %
PVA	261	4.1	0–55
PVA/Fe3O4	863	33.4	0–57

Swelling of the hydrogels involves large segmental motion, resulting ultimately in an increase in the separation distance among the hydrogel chains, and occurs until thermodynamic equilibrium was reached. The swelling equilibrium occurs when the values of the osmotic force driving the solvent into the network and when the elastic forces of the stretched sub-chains become equal. To analyze the model of water diffusion into the polymer network, the water sorption data was used. When the mass of water absorbed by the polymer, as a function of time (M_t), is normalized to the mass of water absorbed by the polymer at its equilibrium hydration level (M_∞), the time-dependent swelling of the polymer was determined according to the following equation:

$$M_t / M_\infty = kt^n \quad (7)$$

where k is a characteristic constant of the hydrogel, t is time and n is a characteristic exponent of the swelling (also noted as diffusion exponent) which represents solvent diffusion modes inside hydrogels, and provides information about the mechanism of swelling kinetics. The constants n and k can be calculated from a plot ln (M_t/M_∞) *vs*. ln t, from the slope and intercept, respectively. This equation is applicable to the initial stages of swelling, where a linear fit of the data was observed ($M_t/M_\infty \leq 0.6$) [17,18]. The graphical representation of ln (M_t/M_∞) *vs*. ln t is shown in Fig. 6.

The characteristic constants n and k can be related to the specific transport mechanism. It is generally accepted that the diverse responses of hydrophilic polymer networks to the presence of water can be described with three models, based on the relative rates of diffusion and polymer chain relaxation: *i*) Fickian or Case I diffusion ($n \leq 0.5$), occurs when the rate of diffusion is significantly slower than the rate of the polymer chains relaxation; *ii*) Case II diffusion (n = = 1) arises when the rate of diffusion is greater than the rate of the polymer chains relaxation. The main feature of this second limiting model is the establishment of a sharp boundary between the glassy core and the swollen shell, which advances at a constant velocity; *iii*) non-Fickian or anomalous diffusion ($0.5 < n < 1$) occurs when the rates of diffusion and polymer chain relaxation are comparable, and is connected with the transition region between the two limiting cases of Case I and Case II [19,20]. The characteristic constants n and k, calculated from parameters of straight line, Fig. 6, are given in Table 2. It is evident that in the case of considered condition (distilled water at 37 °C), the diffusion is non-Fickian for PVA hydrogel (n = 0.9050), as well as for PVA/Fe_3O_4 ferrogel composite (n = = 0.9117). The obtained results unambiguously indicate that the transport of water molecules into the polymer

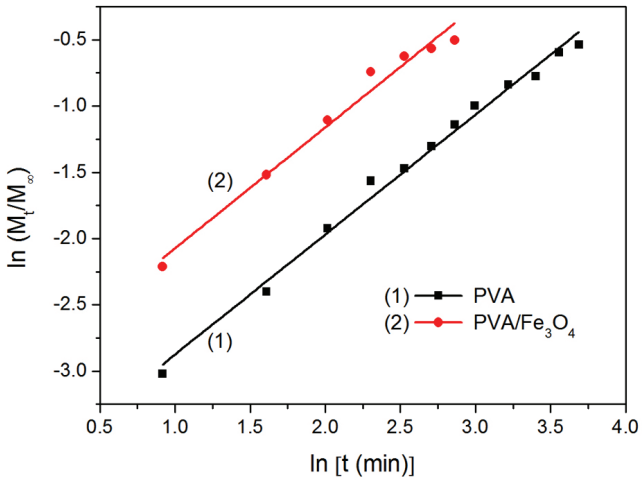

Fig. 6. The plots of ln (M_t/M_∞) vs. ln t for PVA hydrogel and PVA/Fe_3O_4 ferrogel composite in distilled water at 37 °C.

network is controlled by both diffusion and polymer chain relaxation.

Table 2. Swelling parameters k and n, and correlation coefficients for PVA hydrogel and PVA/Fe_3O_4 ferrogel composite in distilled water at 37 °C

Sample	*k*	*n*	R^2	$DE\times10^8$ cm^2/s	$DL\times10^9$ cm^2/s
PVA	0.0229	0.9050	0.9904	1.02	2.27
PVA/Fe_3O_4	0.0506	0.9117	0.9757	2.65	3.17

The initial swelling process exhibits a non-Fikian behavior, while the extensive swelling process follows the Schott kinetics:

$$\mathrm{d}SD/\mathrm{d}t = k_S\left(SD_{eq} - SD\right)^2 \quad (8)$$

A rearrangement of Eq. (8):

$$t/SD = A + Bt \quad (9)$$

gives constants $A = 1/v_0$ ($v_0 = k_S SD_\infty^2$) and $B = 1/SD_\infty$ [19–21].

The Eq. (9) represents second order kinetics and a function relation of *t/SD versus t* gives the straight line (Fig. 7).

Equilibrium swelling (or as usually used, theoretical equilibrium swelling), initial rate of swelling and swelling rate constant for PVA hydrogel and PVA/Fe_3O_4 ferrogel composite are calculated from the slope and intercept of the lines, and given in Table 3. The values of theoretical equilibrium swelling of the hydrogels are in good agreement with the experimentally obtained values (presented in Table 1). The swelling kinetic equations of PVA hydrogel and PVA/Fe_3O_4 ferrogel composite are also presented in Table 3. All the R^2 are greater than 0.99, indicating a small estimated standard error and a highly precise linear regression equation. The obtained results indicate that swelling process of PVA/Fe_3O_4 ferrogel composite is quicker than the swelling rate of PVA hydrogel (Table 3).

Table 3. Swelling kinetic equation, theoretical equilibrium swelling degree (SD_∞), swelling rate constant (k_S) and initial swelling rate (v_0) for PVA hydrogel and PVA/Fe_3O_4 ferrogel composite in distilled water at 37 °C

Sample	Swelling kinetic equation (Eq. (9))	R^2	SD_∞ %	v_0 %/min	$ks\times10^4$ 1/% min
PVA	$t/SD = 0.1288 + 0.0037t$	0.9988	273	7.76	1.04
PVA/Fe_3O_4	$t/SD = 0.0135 + 0.0011t$	0.9998	876	74.07	0.96

As already stated, the Eq. (7) represents the time-dependent swelling of the polymer network and can be related to the diffusion coefficient [17,18]. The early-time approximation method for calculating diffusion coefficients of water into the hydrogel, which is generally valid only for the first 60% of the swelling, is given as:

$$M_t/M_\infty = 4\left(D_E t/\pi\delta\right)^{1/2} \quad (10)$$

where D_E is the coefficient of water diffusion for the early stage of swelling, t is the time and the δ is thickness of the xerogel. The diffusion coefficients were also calculated from the late-time approximation which is presented as:

$$M_t/M_\infty = 1 - \left(8/\pi^2\right)\exp\left(-\pi^2 D_L t/\delta^2\right) \quad (11)$$

where D_L is the coefficient of water diffusion for the longer diffusion times.

The values of the coefficients of water diffusion for early- and late-time approximations are presented in Table 2. The value of the coefficient of diffusion

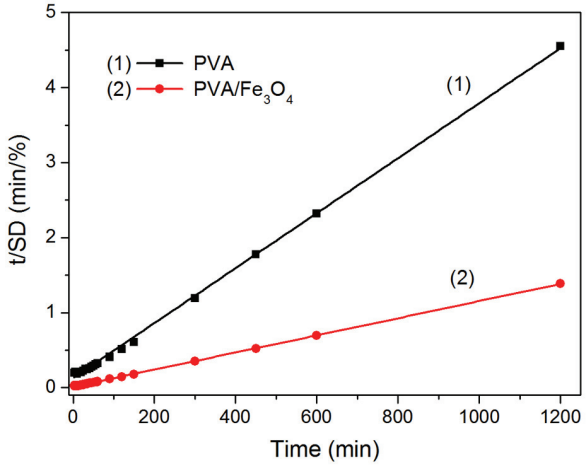

Fig. 7. The plots of t/SD vs. t for PVA hydrogel and PVA/Fe_3O_4 ferrogel composite in distilled water at 37 °C.

increases in the case when the crosslinking of PVA occurred in the presence of Fe_3O_4 particles, compared to control PVA hydrogel crosslinked under the same conditions. Also, it can be noticed, that the D_L is higher than the D_E value, as can be expected bearing in mind the higher water absorption values. According to the theory of Reinhart and Peppas [22] the large swelling ratios lead to higher coefficients of water diffusion.

Kinetic of non-isothermal dehydration and thermal stability

Beside the swelling capacity, another important physicochemical characteristic of hydrogels (and ferrogels), which may affect its usability in various applications, is dehydration. Conversion curves of dehydration of PVA hydrogel and PVA/Fe_3O_4 ferrogel composite obtained at different heating rates (2.5, 5, 10 and 20 °C/min) are shown in Fig. 8.

All the curves are asymmetric and were moved to higher temperatures with increase of heating rate. From Fig. 8 it can be seen that for the same value of conversion (for example 50%), at the same heating rate, the dehydration temperatures are higher for the PVA hydrogel in comparison with the PVA/Fe_3O_4 ferrogel composite. The activation energy of dehydration was determined using the model-free kinetics method, which is based on calculation of the effective activation energy (E_a) as a function of the conversion (α) [23,24]. The respective conversion curves are calculated out of the TG measured curves. For each conversion, the plot ln (β/T^2) *versus* $1/T\alpha$ (β is the heating rate, T is the temperature) giving rise to a straight line with slope $-E_a\alpha/R$, therefore providing the activation energy as a function of conversion.

The activation energy for the thermal dehydration process of PVA hydrogel and the PVA/Fe_3O_4 ferrogel composite is shown in Fig. 9. The standard deviation was in the range from 0.03 for PVA hydrogel to 0.09 to PVA/Fe_3O_4 ferrogel composite. Note that the activation energy for pure PVA hydrogel is lower than that for the dehydration of PVA/Fe_3O_4 ferrogel composite, which means that magnetite filler increases the energy barrier of the thermal dehydration process.

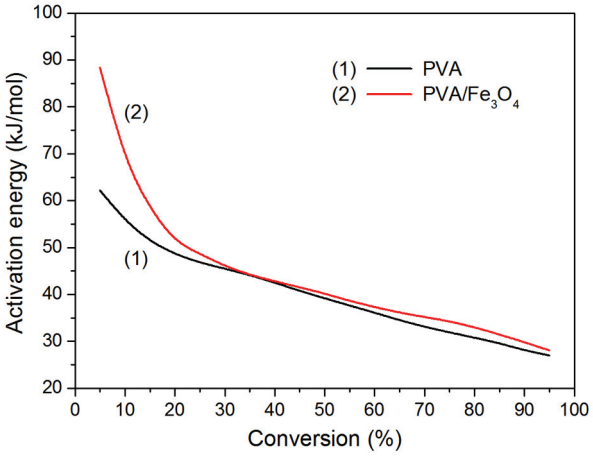

Fig. 9. Dependence of dehydration activation energy on conversion for PVA hydrogel and PVA/Fe_3O_4 ferrogel composite under non-isothermal conditions.

The observation made from conversion curves in Fig. 8 is more evident when examining the plots of conversion versus time, as it is shown in Fig. 10 that was obtained from the model-free data. These graphs show comparative curves between PVA hydrogel and PVA/Fe_3O_4 ferrogel composite at several set temperatures. One can see clearly that the time for the dehydration of PVA hydrogel and PVA/Fe_3O_4 ferrogel composite decreases considerably as a function of temperature. The PVA/Fe_3O_4 ferrogel composite dehydrates faster than pure PVA hydrogel at all temperatures and all heating rates, except for 10 °C/min (Fig. 10C).

Moreover, the thermal stability of the investigated xerogels was studied by thermogravimetry analysis and the obtained TGA curves are presented in Fig. 11. The

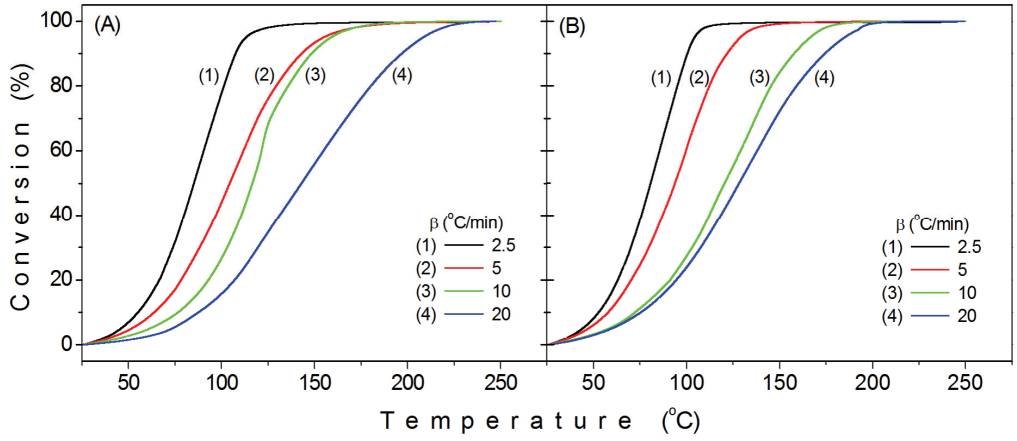

Fig. 8. Conversion curves of dehydration of PVA hydrogel (A) and PVA/Fe_3O_4 ferrogel composite (B).

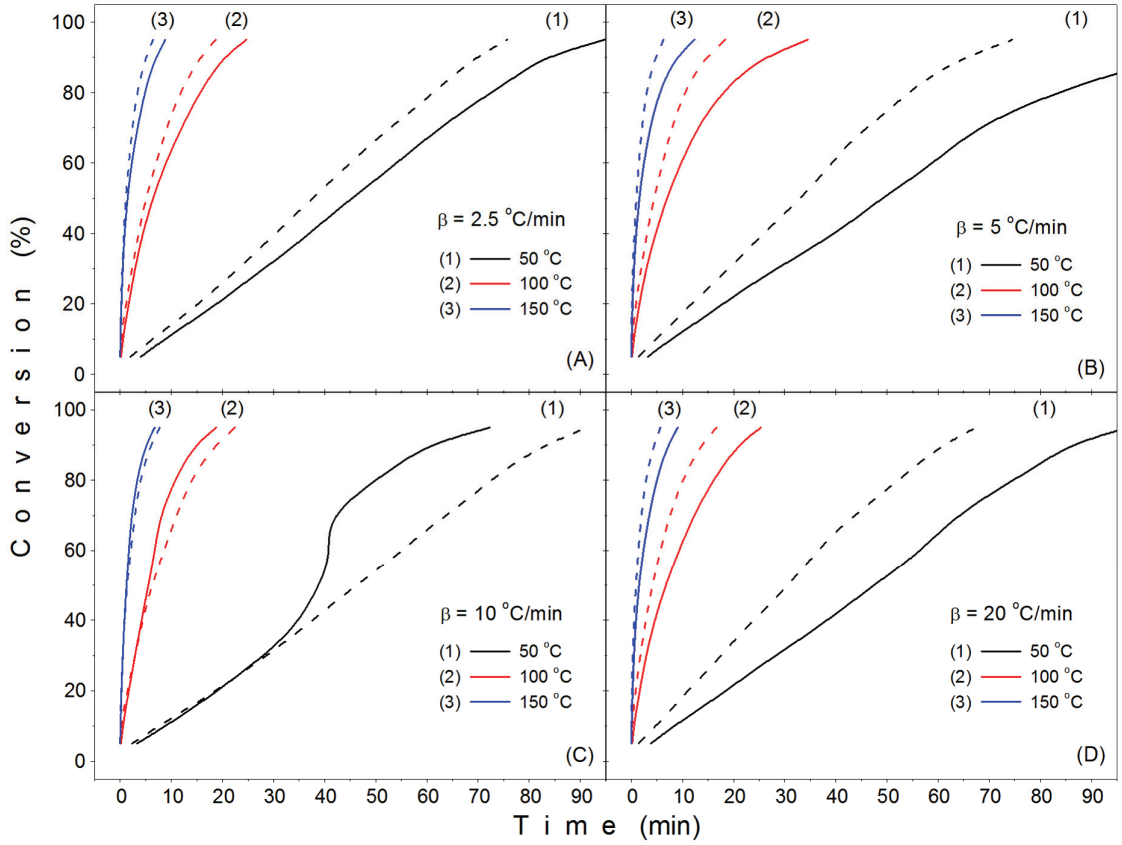

Fig. 10. Dehydration conversion of PVA hydrogel (solid line) and PVA/Fe_3O_4 ferrogel composite (dashed line) as a function of time, for different heating rates.

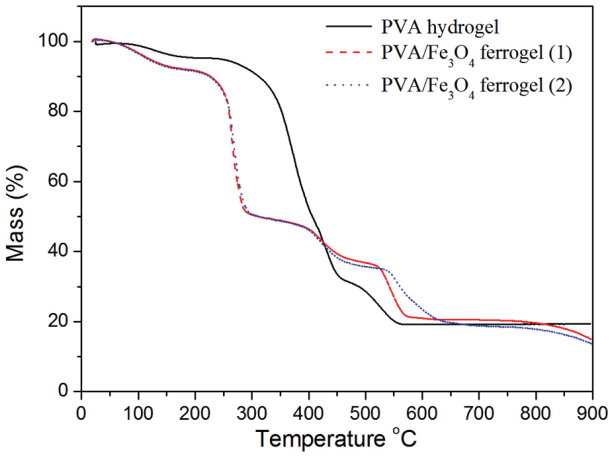

Fig. 11. TGA curves of PVA hydrogel and PVA/Fe_3O_4 ferrogel composite.

TGA curve of PVA/Fe_3O_4 xerogel composite exhibits a steeper slope between 100 and 450 °C, indicating a lower thermal stability in comparison to the pure PVA xerogel. It is probably caused by the change of the network structure, mainly due to the decrease in the crosslink density.

CONCLUSION

This study shows that gamma irradiation crosslinking of polymer in the presence of particles does not interrupt processes of intra- and/or intermolecular crosslinking of PVA chains, giving PVA/Fe_3O_4 ferrogel composite. Thus obtained crosslinked structure has an influence on the physicochemical characteristics of ferrogels. An increase in the values of swelling kinetic parameters, dehydration rate as well as the activation energy of dehydration is noticed for ferrogel compared to pure PVA hydrogel crosslinked under the same conditions.

Acknowledgement

This work is financed by the Ministry of Education, Science and Technological Development of the Republic of Serbia, projects III 45005 and 172056.

REFERENCES

[1] M. Zrínyi, L. Barsi, A. Büki, Ferrogel: a new magneto-controlled elastic medium, Polym. Gels Netw. **5** (1997) 415–427.

[2] R.V. Ramanujan, L.L. Lao, The mechanical behavior of smart magnet–hydrogel composites, Smart Mater. Struct. **15** (2006) 952−956.

[3] L.L. Lao, R.V. Ramanujan, Magnetic and hydrogel composite materials for hyperthermia applications, J. Mater. Sci. Mater. Med. **15** (2004) 1061−1064.

[4] B. Wang, S. Mukataka, E. Kokufuta, M. Kodama, The influence of polymer concentration on the radiation-chemical yield of intermolecular crosslinking of poly-(vinyl alcohol) by γ-rays in deoxygenated aqueous solution, Radiat. Phys. Chem. **59** (2000) 91–95.

[5] C. von Sonntag, Free-Radical-Induced DNA Damage and Its Repair: A Chemical Perspective, Springer−Verlag Berlin, 2006.

[6] S. Kadlubowski, J. Grobelny, W. Olejniczak, M. Cichomski, P. Ulanski, Pulses of Fast Electrons as a Tool To Synthesize Poly(acrylic acid) Nanogels. Intramolecular Cross-Linking of Linear Polymer Chains in Additive-Free Aqueous Solution, Macromolecules **36** (2003) 2484––2492.

[7] A. Krklješ, J. Nedeljković, Z. Kačarević-Popović, Fabrication of Ag-PVA hydrogel nanocomposite by gamma irradiation, Polym. Bull. **58** (2007) 271–279.

[8] C.L. Bell, N.A. Peppas, Biomedical membranes from hydrogels and interpolymer complexes, Adv. Polym. Sci. **122** (1995) 125–175.

[9] S. Wu, A. Sun, F. Zhai, J. Wang, W. Xu, Q. Zhang, A. Volinsky, Fe_3O_4 magnetic nanoparticles synthesis from tailings by ultrasonic chemical co-precipitation, Mater. Lett. **65** (2011) 1882–1884.

[10] P.G. Casillas, C.R. Gonzales, C.M. Perez, Infrared Spectroscopy of Functionalized Magnetic Nanoparticles, Infrared Spectroscopy−Materials Science, Engineering and Technology, InTech, Shanghai, 2012.

[11] T.H. Ngo, D.L. Tran, H.M. Do, V.H. Tran, V.H. Le, X.P. Nguyen, Facile and solvent-free routes for the synthesis of size-controllable Fe3O4 nanoparticles, Adv. Nat. Sci.: Nanosci. Nanotechnol. **1** (2010) 035001.

[12] L. Hoa, T. Dung, T. Danh, N. Duc, D. Chien, Preparation and characterization of magnetic nanoparticles coated with polyethylene glycol, Journal of Physics: Conference Series **187** (2009) 012048.

[13] T. Çaykara, İ. Akçakaya, Swelling Behaviors of Ionic Poly(N,N-dimethylacrylamideco-acrylamide) Hydrogels in Various Media, J. Appl. Polym. Sci. **104** (2007) 2140––2145.

[14] M. Ru-yin, X. Dang-sheng, Synthesis and properties of physically crosslinked poly (vinyl alcohol) hydrogels, J. China Univ. Mining Technol. **18** (2008) 271–274.

[15] J. Jovanović, B. Adnađević, Influence of poly(acrylic acid) xerogel structure on swelling kinetics in distilled water, Polym. Bull. **58** (2007) 243–252.

[16] B. Adnađević, J. Jovanović, Novel approach in investigation of the poly(acrylic acid) hydrogel swelling kinetics in water, J. Appl. Polym. Sci. **107** (2008) 3579––3587.

[17] V. Kumar, C.V. Chaudhari, Y.K. Bhardwaj, N.K. Goel, S. Sabharwal, Radiation induced synthesis and swelling characterization of thermo-responsive N-isopropylacrylamide-co-ionic hydrogels, Eur. Polym. J. **42** (2006) 235––246.

[18] S.Lj. Tomić, M.M. Mićić, J.M. Filipović, E.H. Suljovrujić, Swelling and drug release behavior of poly(2-hydroxyethyl methacrylate/itaconic acid) copolymeric hydrogels obtained by gamma irradiation, Radiat. Phys. Chem. **76** (2007) 801–810.

[19] Y.L. Luo, Q.B. Wei, F. Xu, Y.S. Chen, L.H. Fan, C.H. Zhang, Assembly, characterization and swelling kinetics of Ag nanoparticles in PDMMA-g-PVA hydrogel networks, Mater. Chem. Phys. **118** (2009) 329–336.

[20] H.K. Can, B.K. Denizli, S. Kavlak, A. Guner, Preparation and swelling studies of biocompatible hydrogel systems by using gamma radiation-induced polymerization, Radiat. Phys. Chem. **72** (2005) 483–488.

[21] I. Katime, J.L. Velada, R. Novoa, E.D. de Apodaca, Swelling kinetics of poly(acrylamide)/poly(mono-n-alkyl itaconates) hydrogels, Polym. Int. **40** (1996) 281–286.

[22] C.T. Reinhart, N.A. Peppas, Solute diffusion in swollen membranes. Part II: Influence of crosslinking on diffusive properties, J. Membrane. Sci. **18** (1984) 227–239.

[23] .N. Krklješ, M.T. Marinović-Cincović, Z.M. Kačarević-Popović, J.M. Nedeljković, Dynamic thermogravimetric degradation of gamma radiolytically synthesized Ag-PVA nanocomposites, Thermochim. Acta **460** (2007) 28–34.

[24] J. Kuljanin-Jakovljević, M. Marinović-Cincović, Z. Stojanović, A. Krklješ, N.D. Abazović, M.I. Čomor, Polystyrene/hematite composites: thermal degradation kinetics, J. Compos. Mater. **45** (2010) 839–847.

IZVOD

FIZIČKO–HEMIJSKA SVOJSTVA POLI(VINIL ALCOHOL)/MAGNETIT FERROGEL KOMPOZITA UMREŽENOG GAMA ZRAČENJEM

Milena T. Marinović-Cincović, Aleksandra N. Radosavljević, Jelena I. Krstić, Jelena P. Spasojević, Nataša M. Bibić, Miodrag N. Mitrić, Zorica M. Kačarević-Popović

Institut za nuklearne nauke "Vinča", Univerzitet u Beogradu, Beograd,Srbija

(Naučni rad)

Gelovi osetljivi na magnetno polje su nova klasa hidrogelova. Oni kombinuju magnetna svojstva magnetnih punioca sa elastičnim svojstvima gelova. Ovakvi sistemi imaju potencijalnu primenu u mekim aktuatorima, kao što su veštački mišići. S druge strane, od skora se magnetno osetljivi gelovi ispituju za hipertermijske primene. Naime, polimerne mreže imaju svojstva pogodna za primene kod kontrolisane dostave lekova, dok su magnetne čestice sa feromagnetnim i superparamagnetnim svojstvima pogodne za magnetnu hipertermiju. Cilj rada je bio sinteza magnetno osetljivih materijala, baziranih na kompozitu magnetnih čestica i hidrogela, korišćenjem gama zračenja kao agensa za umrežavanje, i ispitivanje fizičko-hemijskih karakteristika kao što su bubrenje i kinetika dehidratacije ravnotežno nabubrelog ferogela. U tom cilju je korišćen poli(vinil alkohol)/magnetit ferogel (PVA/Fe_3O_4). PVA i Fe_3O_4 su izabrani zbog svojih biokompatibilnih svojstava. Gvožđe-oksid je hemijski stabilan, netoksičan, sa blagim magnetnim svojstvima i Kiri tačkom koja je bliska fiziološkom temperaturnom opsegu. PVA je izabran zato što je radijaciono umrežavajući polimer. Naime, radijaciono–hemijska metoda ima prednosti u odnosu na konvencionalne fizičke ili hemijske metode umrežavanja: blage reakcione uslove, zanemarljivo formiranje nusprodukata, brzo umrežavanje bez katalizatora i na kraju sterilizaciju. Gvožđe-oksid disperzija je dobijena metodom koprecipitacije $FeCl_2$ i $FeCl_3$ prereakcije umrežavanja. Strukturna karakterizacija sintetisanih sistema je izvrsena TEM, SEM, XRD i FTIR metodama. Iz tipičnih TEM mikrografa se može videti da čestice imaju sferičan oblik, veličine do 20 nm. Dobijeni difraktogrami X-zračenja ukazuju da je krajnji produkt sinteze čestica smeša Fe_3O_4 i α-Fe_2O_3 nastala oksidacijom Fe_3O_4 tokom sinteze. Infracrveni spektri potvrđuju spinelnu strukturu Fe_3O_4 kao i kompleksnu interakciju između hidroksilnih grupa polimera na površini čestica. Studija bubrenja ukazije na porast kapaciteta bubrenja kao i kinetičkih parametara bubrenja kod PVA/Fe_3O_4 ferogel kompozita u odnosu na PVA hidrogel. Dinamička TG analiza dehidratacije ukazuje takođe na veću brzinu dehidratacije ferogela, ali i veću energiju aktivacije dehidratacije ovih sistema. Umanjena termička stabilnost PVA/Fe_3O_4 ferogel kompozita je verovatno prouzrokovana izmenjenom strukturom mreže tj. manjom gustinom umreženja.

Ključne reči: Gama zračenje • PVA hidrogel • Čestice magnetita • Ferogel • Bubrenje • Dehidratacija

Modifikacija epoksidnih smola termoplastičnim segmentiranim poliuretanima na osnovu polikarbonatnog diola

Jelena Pavličević[1], Mirjana Jovičić[1], Vesna Simendić[1], Oskar Bera[1], Radmila Radičević[1], Milena Špírková[2]

[1]*Univerzitet u Novom Sadu, Tehnološki fakultet, Novi Sad, Srbija*
[2]*Institute of Macromolecular Chemistry AS CR v.v.i., Prague, Czech Republic*

Izvod

Sintetisani su epoksidni hibridi dodavanjem različitog udela termoplastičnih poliuretana u cilju dobijanja epoksidnog materijala sa poboljšanim mehaničkim i toplotnim svojstvima. Proučavan je uticaj masenog udela sintetisanih poliuretana na osnovu polikarbonatnog diola, kao i udela tvrdih segmenata elastomera na proces umrežavanja epoksidnih kompozita, kao i na toplotna i mehanička svojstva umreženih uzoraka. Kinetički modeli izokonverzije: dva integralna (Ozawa–Flynn–Wall i Kissinger–Akahira–Sunose) i jedan diferencijalni (Friedman) su primenjeni za analizu DSC podataka dobijenih programiranim zagrevanjem uzoraka od 30 do 300 °C, pri tri različite brzine zagrevanja (5, 10 i 20 °C/min). Utvrđeno je da dodatak poliuretana utiče na mehanička svojstva modifikovanih epoksidnih uzoraka (zateznu čvrstoću, tvrdoću i prekidno izduženje).

Ključne reči: *epoksid, segmentirani poliuretani, DSC, kinetika umrežavanja, mehanička svojstva*.

Dostupno na Internetu sa adrese časopisa: http://www.ache.org.rs/HI/

NAUČNI RAD

UDK 678.686.017:678.664:66.018:544

Hem. Ind. **68** (6) 755–765 (2014)

doi: 10.2298/HEMIND130904086P

Veliki broj istraživanja posvećen je modifikovanju epoksidnih smola radi poboljšanja njihovih mehaničkih i toplotnih svojstava. Nađeno je da pomenuta svojstva, kao i adhezija smole mogu biti poboljšani dodatkom različitih neorganskih nanočestica [1,2], modifikacijom epoksidne smole neorganskim punilima mikro dimenzija [3], različitim vrstama guma [4], kao i modifikacijom termoplastičnim polimerima kao punilima [5–9]. Radi poboljšavanja mehaničkih svojstava, Wang i Chen [10] su modifikovali epoksidnu bisfenol A smolu sa poliuretanima čiji je prepolimer imao krajnje aromatske aminske grupe, kao i krajnje fenolne hidroksilne grupe. Rezultati ovog načina modifikacije su pokazali da epoksidne smole modifikovane sa poliuretanima čiji prepolimer sadrži fenolne hidroksilne grupe imaju poboljšana mehanička svojstva u odnosu na smole modifikovane sa prepolimerima sa amino grupama na krajevima. Poliuretanski lanci se mogu ugraditi u epoksidne mreže preko fizičkih i hemijskih veza, obrazujući interpenetrirajuću strukturu. Hsieh i Hanh [11] su ispitivali mehanička svojstva epoksidnih smola modifikovanih poliuretanima na osnovu diola različitih dužina. Harani i saradnici [12] su dokazali da dodatak poliuretana poboljšava mehaničke karakteristike epoksida. Reakcija produživača lanca sa poliuretanskim prepolimerom koji sadrži krajnje izocijanatne grupe uticala je na značajno povećanje otpornosti na udar modifikovanih epoksidnih materijala u odnosu na nemodifikovane. Park i Jin [13] su ispitivali termomehanička svojstva, kao i slobodnu površinsku energiju smeše epoksid/poliuretan. Polarne komponente slobodne površinske energije su znatno zavisile od dodatka poliuretana, koji je izazvao povećanje otpornosti na udar pri niskim temperaturama. Poboljšanje mehaničkih svojstava je nastalo kao rezultat ostvarenih vodoničnih veza između epoksidne smole i uretanskih grupa u poliuretanu. Istraživan je uticaj dodatka poliuretana sa različitim izocijanatnim indeksom na mehanička i toplotna svojstva epoksidnih smola [14]. Najveće poboljšanje mehaničkih svojstava modifikovanih epoksida je postignuto dodavanjem poliuretana sa viškom izocijanatnih grupa, koji je omogućio reakciju kalemljenja modifikatora i epoksidne matrice, i na taj način uticao na dobijanje epoksidnog hibridnog materijala sa boljim mehaničkim karakteristikama.

Jedan od načina poboljšanja mehaničkih svojstava epoksidnih smola jeste njihova modifikacija termoplastičnim poliuretanskim elastomerima dobijenim na osnovu polikarbonatnog diola. Zbog biodegradabilnosti, biokompatibilnosti i jedinstvenog hemijskog sastava, kao i dobrih mehaničkih karakteristika [15] u širokom opsegu temperatura i deformacije ovi poliuretani služe za specijalne namene, a njihova najznačajnija primena je u oblasti medicine [16–20]. Neobična elastičnost poliuretanskih materijala potiče od termodinamičke nekompatibilnosti segmenata, a mehanička svojstva veoma zavise od stepena mikrofaznog razdvajanja, koji ne zavisi samo od sposobnosti tvrdih segmenata da obrazuju vodonične veze, nego i od hemijske strukture i sastava poliuretanskih materijala [21,22].

Poznato je da fizička svojstva umreženih epoksidnih smola zavise od stepena umreženosti [23], uslova

Prepiska: J. Pavličević, Tehnološki fakultet, Bulevar cara Lazara 1, Novi Sad, Srbija.
E-pošta: jelenapavlicevic@gmail.com
Rad primljen: 4. septembar, 2013
Rad prihvaćen: 26. novembar, 2013

umrežavanja [24,25], kao i vremena i temperature umrežavanja [26]. Iz tog razloga, diferencijalna skenirajuća kalorimetrija (DSC) [27] je našla široku primenu za ispitivanje veze između procesa umrežavanja i krajnjih svojstava nemodifikovanih i modifikovanih epoksidnih smola, u cilju dobijanja materijala visokih performansi [28,29].

U ovom istraživanju, vršena je modifikacija epoksidne smole dodatkom alifatskih termoplastičnih poliuretana na osnovu polikarbonatnog diola. Primenom kinetičkih modela izokonverzije: dva integralna (Ozawa––Flynn–Wall i Kissinger–Akahira–Sunose) i jednog diferencijalnog (Friedman) za analizu DSC podataka, proučavan je uticaj udela sintetisanih poliuretana (5, 10 i 15 mas.% u odnosu na epoksid), kao i udela tvrdih segmenata elastomera (20, 25 i 30 mas.%) na proces umrežavanja epoksidnih materijala, kao i na mehanička svojstva dobijenih epoksidnih hibrida.

EKSPERIMENTALNI DEO

Materijali

Za sintezu termoplastičnih poliuretana korišćene su sve alifatske polazne komponente. Polikarbonatni diol oznake 5651, molske mase oko 1000 g/mol, je dobijen od proizvođača Asahi Kasei korporacija. Ovaj polikarbonatni diol u lancu sadrži isti broj pentanskih i heksanskih jedinica, i njegove karakteristike su: hidroksilni broj, 111,4 mg KOH/g; sadržaj vode, 0,0052 mas.%, viskoznost na 5 °C, 1619 Pa s. Produživač lanca, 1,4-butandiol (BD), heksametilen-diizocijanat (HDI), i katalizator, dibutil-kalaj-dilaurat (DBTDL), su korišćeni od proizvođača Fluka. Za pripremu epoksidne komponente hibridnih materijala korišćene su sledeće sirovine: diglicidiletar bisfenola A (DGEBA, Sigma-Aldrich Chemie GmbH) i poli(oksipropilen)diamin (Jeffamine D-2000, Huntsman International LLC), čije su hemijske strukture prikazane na slici 1a i b, redom.

Postupak modifikacije epoksidnih smola

Za dobijanje hibridnih epoksidnih materijala, korišćeni su termoplastični poliuretanski materijali u obliku filmova (slika 1c) sa različitim udelom tvrdih segmenata (20, 25 i 30 mas.%), koji su određeni kao odnos zbira mase diizocijanata HDI i produživača lanca i ukupne mase reaktivne smeše kod dobijanja poliuretana. Detaljan opis jednostepenog postupka sinteze poliuretanskih materijala je prikazan u prethodnom radu [15].

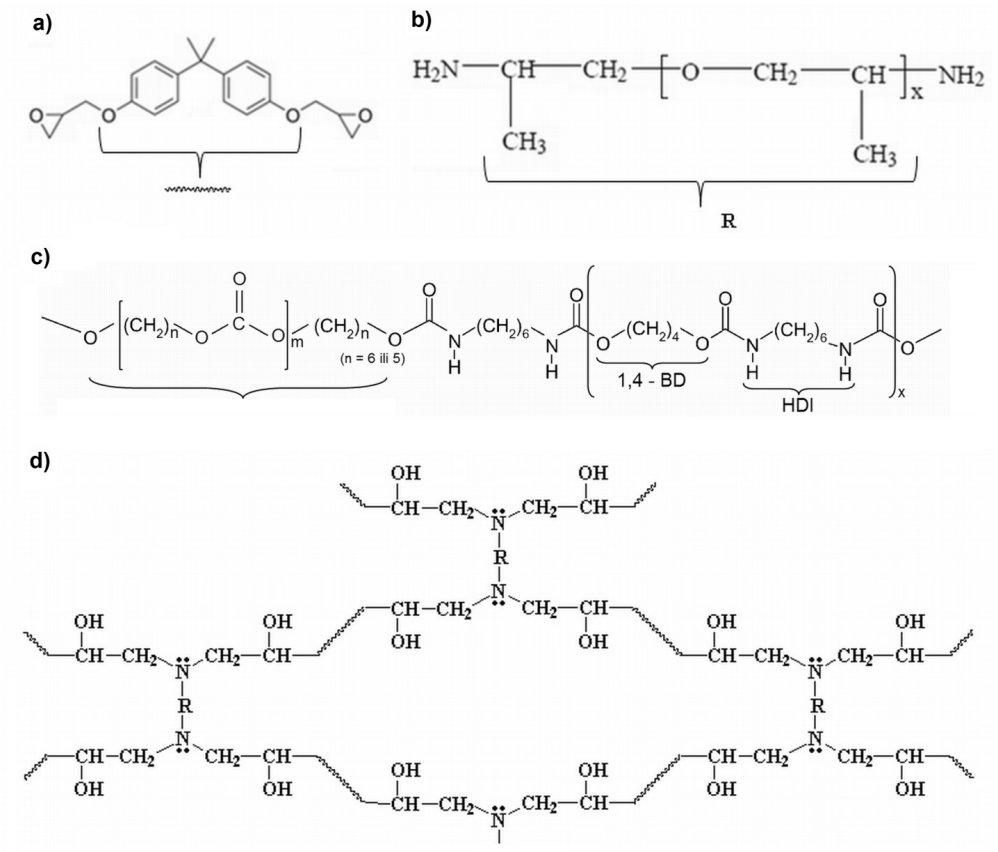

Slika 1. Hemijske strukture: a) diglicidiletra bisfenola A (DGEBA), b) poli(oksipropilen)diamina (Jeffamine D-2000) i c) poliuretana na osnovu polikarbonatnog diola i d) umrežene epoksidne smole.
Figure 1. Chemical structures of: a) diglycidyl ether bisphenol A (DGEBA), b) poly(oxypropylene)diamine (Jeffamine D-2000) and c) polycarbonate-based polyurethane and d) cured epoxy resin.

Dobijeni poliuretanski elastomeri stepena kristaličnosti između 11 i 13% [15], su dodavani u epoksid u različitim masenim udelima u odnosu na smolu (5, 10 i 15 mas.%). Pre dodatka u epoksid, poliuretanski materijal je zagrevan na temperaturi topljenja od 110 °C [30] 20 min, u cilju dobijanja rastopa elastomera. Nakon toga, radi umešavanja pripremljenog rastopa poliuretana i epoksida, vršeno je mešanje smeše pomoću magnetne mešalice 2 h na 40 °C. Zatim je, zbog bolje homogenizacije, smeša dodatno mešana 20 min u ultrazvučnom kupatilu. Nakon toga, u tako pripremljenu dvokomponentnu smešu dodavan je umreživač Jeffamine D-2000. Nova reakciona smeša je zatim postavljena 1 h u vakuum sušnicu radi otklanjanja zaostalih mehurova zarobljenog vazduha. U cilju dobijanja epoksidnih uzoraka u obliku standardnih epruveta za ispitivanje mehaničkih svojstava, reakciona smeša je izlivana u kalupe (SRPS G. S2. 612 standard). Nakon 24 h na sobnoj temperaturi, kalupi su stavljeni u sušnicu, gde je proces umrežavanja trajao dodatnih 4 h na temperaturi od 140 °C.

Praćenje umrežavanja primenom diferencijalno skenirajuće metode

Umrežavanje modifikovanih epoksidnih smola je praćeno diferencijalnim skenirajućim kalorimetrom (DSC Q20, TA Instruments), programiranim zagrevanjem od 30 do 300 °C, sa tri različite brzine zagrevanja: 5, 10 i 20 °C/min. Merenja su vršena u atmosferi azota sa protokom od 50 cm^3/min. Masa ispitivanih uzoraka je iznosila oko 7 mg. Prividni stepen umreženosti (α), srazmeran oslobođenoj toploti tokom reakcije, je izračunat preko površine egzotermnog pika.

Modeli izokonverzije [27]

Najčešće korišćena jednačina za opis brzine reakcije umrežavanja pri neizotermnim uslovima je:

$$\beta\frac{\mathrm{d}\alpha}{\mathrm{d}T}=k_0e^{-E_\mathrm{a}/RT}f(\alpha) \tag{1}$$

gde je β brzina reakcije (β = dT/dt (K/s)), α je stepen reagovanja, k_0 je predeksponencijalni faktor, E_a je energija aktivacije (J/mol), R je univerzalna gasna konstanta (8,314 J/(mol K)), t je vreme reakcije (s) i T je temperatura reakcije (K), dok funkcija $f(\alpha)$ zavisi od odabranog kinetičkog modela. Za izračunavanje kinetičkih parametara reakcije umrežavanja na osnovu neizotermnih DSC krivih korišćeni su modeli izokonverzije (Ozawa–Flynn–Wall (OFW), Kissinger–Akahira––Sunose (KAS) i Friedman (FR)) koji se zasnivaju na pretpostavci da brzina reakcije za dati stepen konverzije zavisi samo od temperature.

Ozawa–Flynn–Wall [31] model izokonverzije je opisan sledećom jednačinom:

$$\log\beta=\log\left[\frac{k_0E_\mathrm{a}}{Rg(\alpha)}\right]-2{,}315-0{,}4567\frac{E_\mathrm{a}}{RT} \tag{2}$$

gde je $g(\alpha)$ funkcija stepena reagovanja:

$$g(\alpha)=\int_0^\alpha\frac{\mathrm{d}\alpha}{f(\alpha)} \tag{3}$$

Kissinger–Akahira–Sunose [32,33] model na osnovu Coats–Redfern aproksimacije [34] je opisan jednačinom:

$$\ln\left(\frac{\beta}{T^2}\right)=\ln\left(\frac{RA}{E_\mathrm{a}g(\alpha)}\right)-\frac{E_\mathrm{a}}{RT} \tag{4}$$

Kao diferencijalni model izokonverzije odabran je Friedman [35] model koji je opisan jednačinom:

$$\ln\beta\frac{d\alpha}{dT}=\ln A+\ln f(\alpha)-\frac{E_\mathrm{a}}{RT} \tag{5}$$

Mehanička ispitivanja

Mehanička ispitivanja epoksidnih materijala (zatezna čvrstoća i izduženje pri kidanju) su rađena na instrumentu Instron 1122 prema SRPS G. S2. 612 standardu (ASTM D882). Veličina uzorka je merena mikrometrom, a brzina pri istezanju je iznosila 100 mm/min. Dobijene vrednosti predstavljaju srednje vrednosti pet merenja. Relativne greške merenja su se kretale u granicama od 2 do 5%. Tvrdoća je određena pomoću Zvik 3100 durometra na šor A skali.

REZULTATI I DISKUSIJA

Umrežavanje epoksidnih smola poli(oksipropilen)diaminom (DGEBA/Jeffamine D-2000) je veoma složeno i može da obuhvata nekoliko različitih hemijskih reakcija, ali se može pretpostaviti da se proces umrežavanja prvenstveno odigrava reakcijom između epoksidne grupe DGEBA i amino grupe Jeffamine D-2000 (slika 1d). Do sada nema mnogo podataka o uticaju dodatka termoplastičnih poliuretana na proces umrežavanja modifikovanih epoksidnih smola. Pretpostavlja se da dolazi do stvaranja fizičkih veza, odnosno, vodoničnih veza između atoma kiseonika iz OH grupa umrežene epoksidne smole i atoma vodonika iz NH grupa tvrdih segmenata termoplastičnih poliuretanskih elastomera. Na slici 2a date su DSC krive umrežavanja nemodifikovanih sistema DEGBA/Jeffamine D-2000, a na slici 2b prikazane su DSC krive umrežavanja hibrida modifikovanih sa 15 mas.% termoplastičnih poliuretana sa 20 mas.% tvrdih segmenata, za sve tri brzine zagrevanja.

Za sve ispitane nemodifikovane i modifikovane epoksidne uzorke dobijen je širok egzotermni pik na DSC krivoj koji predstavlja reakciju umrežavanja. Sa slike 2 može se uočiti da brzina zagrevanja ima veliki uticaj na

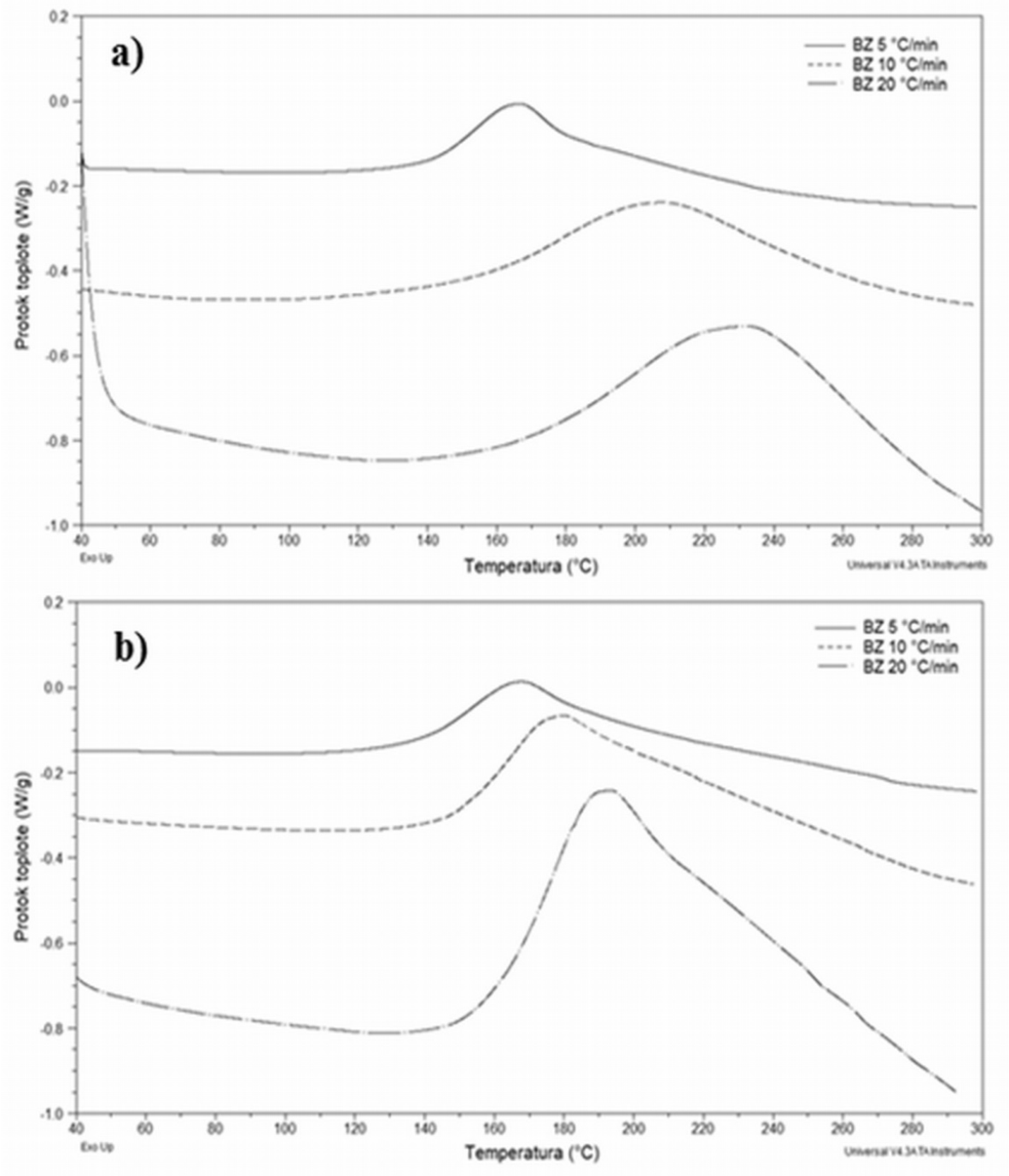

Slika 2. DSC krive umrežavanja epoksidnih sistema pri brzinama zagrevanja od 5, 10 i 20 ℃/min: a) DGEBA/Jeffamine D-2000 i b) hibrida koji sadrži 15 mas.% termoplastičnih poliuretana sa 20 mas.% tvrdih segmenata.
Figure 2. DSC Curves of the curing of epoxy systems at different heating rates (5, 10 and 20 ℃/min): a) DGEBA/Jeffamine D-2000 and b) hybrid with 15 wt.% of thermoplastic polyurethanes with 20 wt.% of hard segments.

umrežavanje. Sa porastom brzine zagrevanja površina egzotermnog pika raste i pikovi se pomeraju ka višim temperaturama. Na osnovu dobijenih DSC termograma izračunata je zavisnost stepena reagovanja od temperature (slika 3), sa koje se, takođe, zapaža da umrežavanje zavisi od brzine zagrevanja.

Na slici 4 je prikazan uticaj udela tvrdih segmenata u poliuretanu pri konstantnom masenom sadržaju poliuretana od 5 (slika 4a), 10 (slika 4b) i 15 mas.% (slika 4c), na umrežavanje epoksidnih uzoraka, pri brzini zagrevanja od 10 °C/min.

Pri dodatku malog sadržaja (5 mas.%) poliuretana, uticaj udela tvrdih segmenata (20, 25 i 30 mas.%) na pomeranje temperature maksimalne brzine reakcije umrežavanja nije uočen (slika 4a), i ona iznosi za sve modifikovane uzorke 179 °C. Na slici 4b i c može se

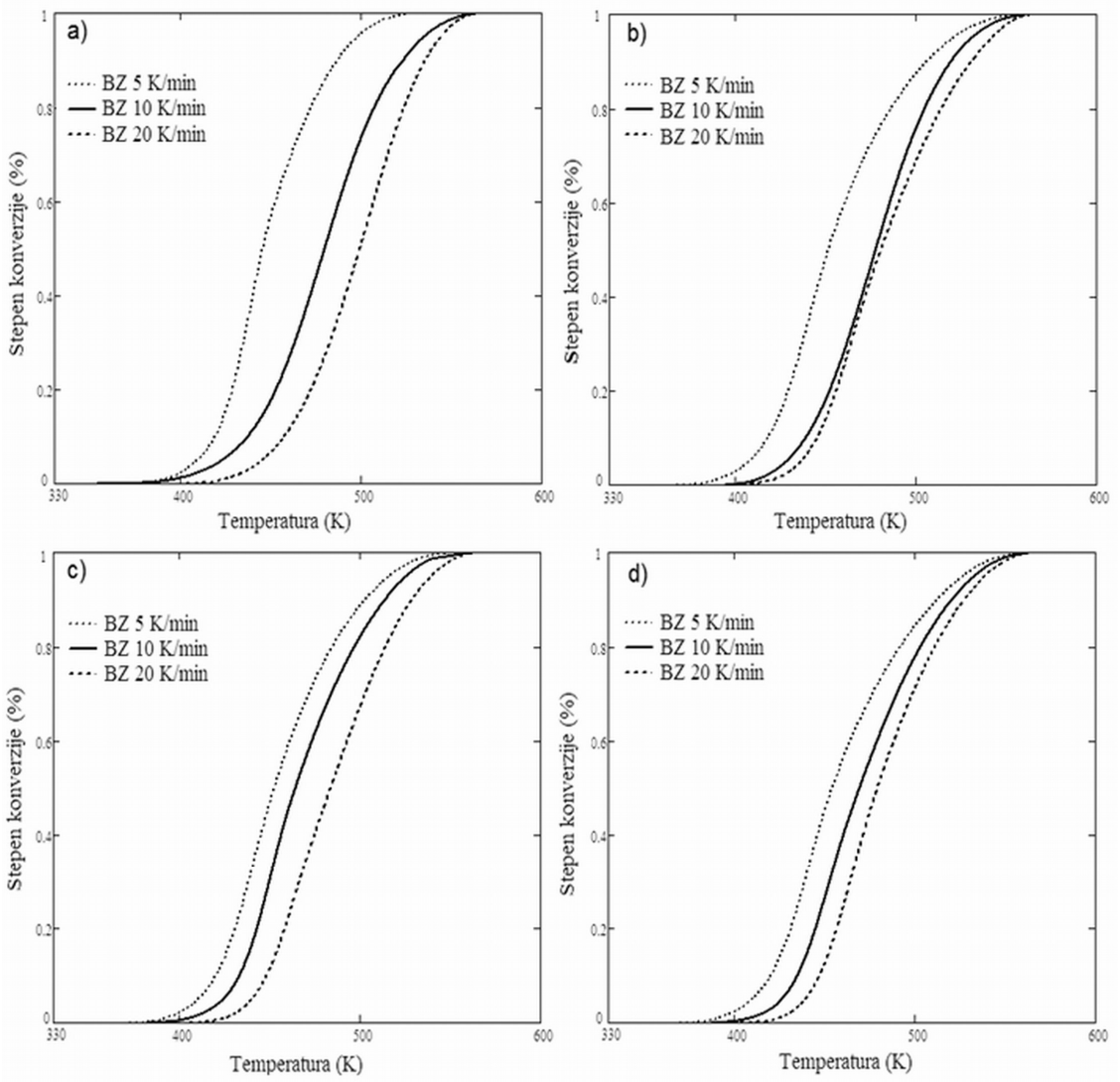

Slika 3. Zavisnost stepena reagovanja od temperature pri različitim brzinama zagrevanja: a) DGEBA/Jeffamin D-2000; b) DGEBA/ /Jeffamine D-2000/PU20-5 mas.%; c) DGEBA/Jeffamine D-2000/PU20-10 mas.% ;d) DGEBA/Jeffamine D-2000/PU20-15 mas.%.
Figure 3. The conversion degree dependence on temperature recorded at different heating rates; a) DGEBA/Jeffamine D-2000; b) DGEBA/ Jeffamine D-2000/PU20-5 wt.%; c) DGEBA/Jeffamine D-2000/PU20-10 wt.% and d) DGEBA/Jeffamine D-2000/PU20-15 wt.%.

videti da se sa porastom udela tvrdih segmenata pri većem sadržaju poliuretana (10 i 15 mas.%) u reakcionoj smeši, temperatura maksimalne brzine reakcije umrežavanja pomera ka nižim vrednostima (od 205 do 179 °C). Ovaj efekat se može pripisati uticaju vodoničnih veza između epoksidnih i uretanskih grupa na reakciju umrežavanja epoksidnih hibridnih materijala [13]. Na osnovu slike 4 može se uočiti da pored toga što se sa porastom udela tvrdih segmenata (od 20 do 30 mas.%) u reakcionoj smeši reakcija umrežavanja pomera na niže temperature, menja se i oblik DSC kriva, na osnovu čega se može pretpostaviti da se menjaju i kinetički parametri, tj. sam mehanizam umrežavanja.

Nagib prvog dela krive umrežavanja, koji je proporcionalan brzini reakcije i samim tim utiče na celu kinetiku umrežavanja, raste sa povećanjem udela tvrdih segmenata poliuretana. To znači da u prisustvu poliuretana sa najmanjim udelom tvrdih segmentata (20 mas.%) reakcija započinje ranije, ali traje duže, jer je brzina reakcije manja.

U tabeli 1 date su izračunate vrednosti promena entalpije reakcija umrežavanja, ΔH, čistog epoksida i reakcione smeše epoksida koja sadrži poliuretan (serije DGEBA/Jeffamine D-2000/PU20, DGEBA/Jeffamine D-2000/PU25 i DGEBA/Jeffamine D-2000/PU30), dobijene pri različitim brzinama zagrevanja reakcione smeše. Na osnovu datih podataka za sve ispitivane serije, uočava se da se sa porastom brzine zagrevanja povećava vrednost ΔH. Nije utvrđena zavisnost promene entalpije reakcije umrežavanja od sadržaja dodatih poliuretana (5, 10 i 15 mas.%), a najveća vrednost ΔH je određena za uzorak sa 30 mas.% tvrdih segmenata poliuretana, pri brzini zagrevanja od 15 °C/min.

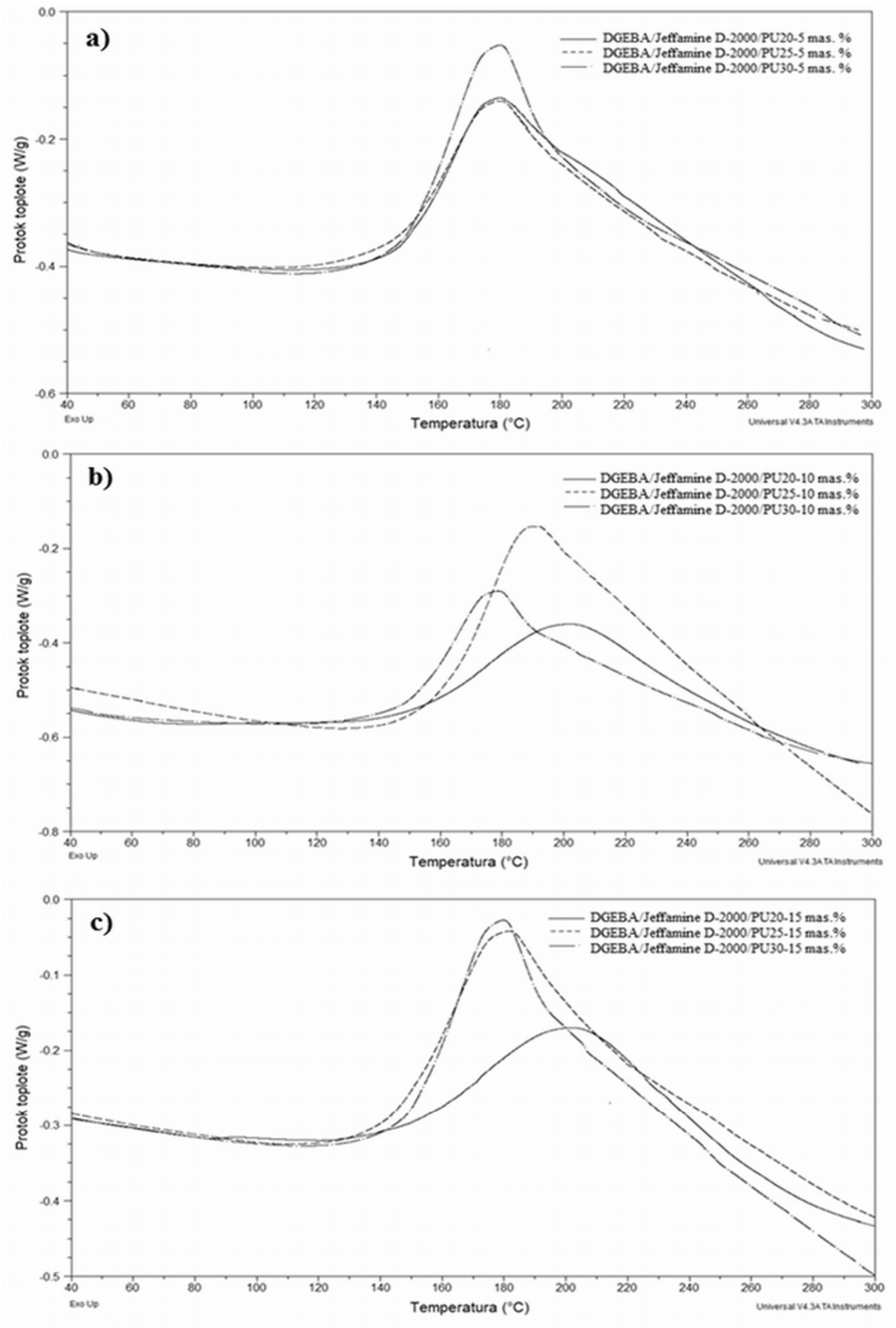

Slika 4. DSC krive umrežavanja epoksidnih uzoraka modifikovanih sa a) 5 mas.% poliuretana, b) 10 mas.% poliuretana i c) 15 mas.% poliuretana koji sadrže 20, 25 i 30 mas.% tvrdih segmenata. Brzina zagrevanja je 10 °C/min.
Figure 4. DSC Curves of the curing of epoxy samples modified with a) 5 wt.% of polyurethanes, b) 10 wt.% of polyurethanes and c) 15 wt.% of polyurethanes with 20, 25 and 30 wt.% of hard segments. Heating rate was 10 °C/min.

Na osnovu DSC podataka za tri brzine zagrevanja, primenjeni su modeli izokonverzije da se razjasni uticaj prisustva poliuretana sa različitim udelima tvrdih segmenata na mehanizam složene reakcije umrežavanja epoksidnih smola. Korišćena su tri modela izokonverzije: dva integralna (Ozawa–Flynn–Wall i Kissinger––Akahira–Sunose) i jedan diferencijalni (Friedman). Primenom ovih modela izračunati su kinetički parametri

Tabela 1. Vrednosti promena entalpije reakcija umrežavanja nemodifikovanih epoksidnih smola, kao i modifikovanih DGEBA uzoraka dodatkom 5, 10 i 15 mas.% poliuretana sa 20 i 30 mas.% tvrdih segmenata, pri različitim brzinama zagrevanja
Table 1. The values of curing enthalpy of unmodified epoxy resins, as well as modified DGEBA samples with addition of 5, 10 and 15 wt.% of poliurethanes with 20 and 30 wt.% of hard segments, at different heating rates

Naziv uzorka	Brzina zagrevanja, °C/min								
	5			10			15		
DGEBA/Jeffamine D-2000	Entalpija, ΔH / J g^{-1}								
	80,4			105,5			103,1		
	Udeo PU, mas.%								
	5	10	15	5	10	15	5	10	15
	Entalpija, ΔH / J g^{-1}								
DGEBA/Jeffamine D-2000/PU20	106,8	109,8	107,1	111,6	123,1	115,3	117,8	135,1	119,4
DGEBA/Jeffamine D-2000/PU25	111,2	114,6	117,8	119, 7	127,0	143,2	124,5	148,0	152,7
DGEBA/Jeffamine D-2000/PU30	128,7	115,8	119,3	140,4	129,1	149,9	167,7	161,4	168,3

umrežavanja u opsegu stepena reagovanja od 5 do 95%. Na slikama 5 i 6 prikazane su zavisnosti energije aktivacije, E_a, od stepena reagovanja izračunate primenom sva tri modela izokonverzije, za nemodifikovani sistem DGEBA/Jeffamine D-2000, i za sistem modifikovan poliuretanima sa 20 mas.% tvrdih segmenata. Ozawa–Flynn–Wall i Kissinger–Akahira–Sunose modeli opisuju sličnu promenu energije aktivacije umrežavanja smola sa stepenom reagovanja (slike 5 i 6), dok je Friedman metod zasnovan na numeričkom diferenciranju, i zbog toga dolazi do odstupanja vrednosti kinetičkih parametara u odnosu na one dobijene primenom Ozawa–Flynn–Wall i Kissinger–Akahira–Sunose metoda.

Kod epoksidnih hibrida zapaža se da na početku reakcije za α < 0,6 vrednosti E_a za definisane stepene reagovanja su veoma bliske vrednostima energija aktivacije dobijenim za nemodifikovani DGEBA/Jeffamine. Značajne razlike su uočene u drugom delu reakcije, za stepene reagovanja iznad 60%, energije aktivacije znatno rastu sa porastom stepena reagovanja, jer je tada zbog velike viskoznosti reakcione smeše reakcija umrežavanja usporena i otežana je pokretljivost molekula reaktanata. Analizom kinetičkih parametara je zaključeno da je uticaj otežane difuzije izraženiji u prisustvu termoplastičnih poliuretana, čime je pokazano da njihovo prisustvo utiče na ceo mehanizam umrežavanja.

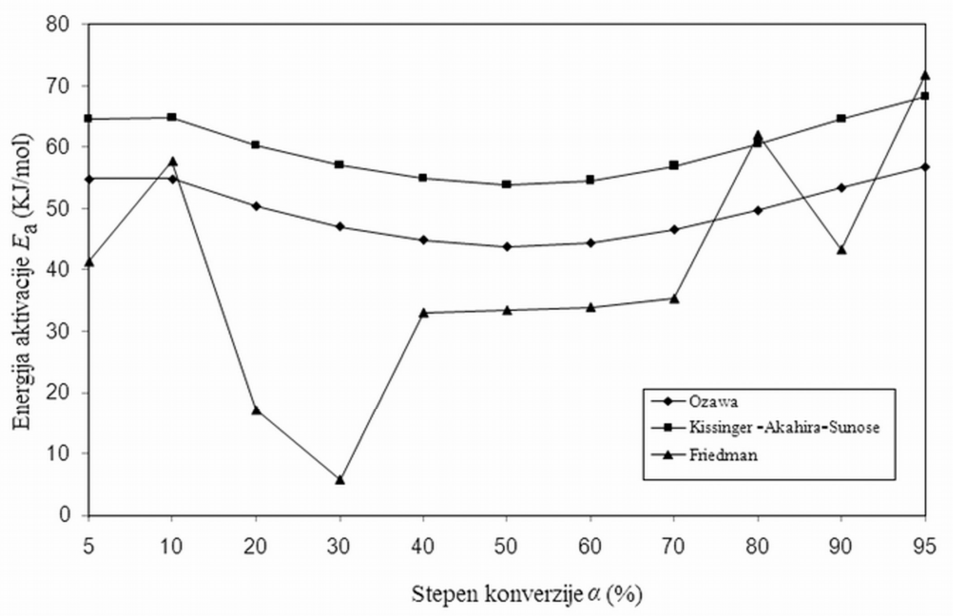

Slika 5. Zavisnost prividne energije aktivacije umrežavanja hibrida od stepena reagovanja dobijena Ozawa–Flynn–Wall, Kissinger–Akahira–Sunose i Friedman metodom izokonverzije, za nemodifikovani sistem DGEBA/Jeffamine D-2000.
Figure 5. The activation energy dependence on the curing degree of hybrids, obtained by applying Ozawa–Flynn–Wall, Kissinger–Akahira–Sunose and Friedman isoconversional model, for unmodified system DGEBA/Jeffamine D-2000.

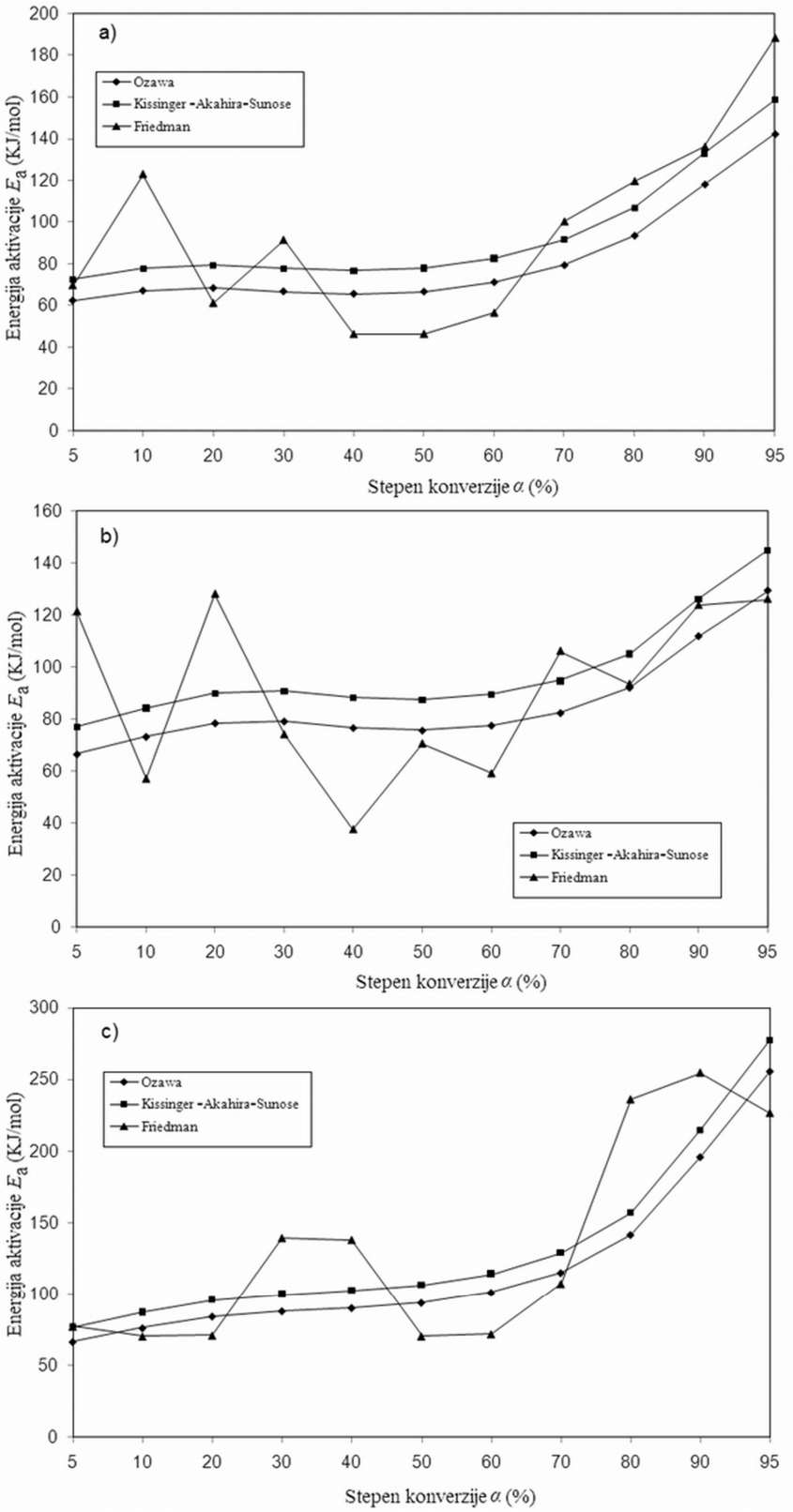

Slika 6. Zavisnost prividne energije aktivacije umrežavanja hibrida od stepena reagovanja dobijena Ozawa–Flynn–Wall, Kissinger–Akahira–Sunose i Friedman metodom izokonverzije, za DGEBA/Jeffamine D-2000 modifikovan sa poliuretanom koji sadrži 20 mas.% tvrdih segmenta čiji je udeo: a) 5, b) 10 i c) 15 mas.%.
Figure 6. The activation energy dependence on the curing degree of hybrids, obtained by applying Ozawa–Flynn–Wall, Kissinger–Akahira–Sunose and Friedman isoconversional model, for DGEBA/Jeffamine D-2000 modified with different content: a) 5, b) 10 and c) 15 wt.% of polyurethane with 20 wt.% of hard segments.

Uticaj dodatka segmentiranih poliuretana na mehanička svojstva modifikovanih epoksida

U cilju praćenja uticaja dodatka poliuretana sa različitim udelom tvrdih segmenata (20, 25 i 30 mas.%), kao i uticaja masenog udela poliuretana (5, 10 i 15 mas.%) u odnosu na čist epoksid, određena su mehanička svojstva (vrednosti zatezne čvrstoće, prekidnog izduženja i tvrdoće na Šoru A skali) odabranih uzoraka i rezultati su prikazani u tabeli 2. Na osnovu specifikacija SRPS G. S2. 612 standarda, za ispitivanje zatezne čvrstoće (σ) i prekidnog izduženja (ε) pripremljenih uzoraka u obliku epruveta, vrednosti su dobijene primenom jednačina:

$$\sigma = \frac{F}{A_0} \tag{6}$$

Tabela 2. Mehanička svojstva epoksidnih materijala
Table 2. Mechanical properties of epoxy materials

Oznaka uzorka	Udeo PU, mas.%	Zatezna čvrstoća, σ / MPa	Prekidno izduženje, ε / %	Tvrdoća, Šor A
DGEBA/Jeffamine D-2000	–	0,41	36	75
DGEBA/Jeffamine D-2000/PU20	5	0,40	239	48
DGEBA/Jeffamine D-2000/PU20	10	0,42	232	50
DGEBA/Jeffamine D-2000/PU20	15	0,44	227	51
DGEBA/Jeffamine D-2000/PU25	5	0,43	232	50
DGEBA/Jeffamine D-2000/PU25	10	0,45	229	53
DGEBA/Jeffamine D-2000/PU25	15	0,56	107	56
DGEBA/Jeffamine D-2000/PU30	5	0,45	214	52
DGEBA/Jeffamine D-2000/PU30	10	0,48	201	58
DGEBA/Jeffamine D-2000/PU30	15	0,59	102	63

$$\varepsilon\,[\%] = 100\frac{\Delta l}{l_0} \tag{7}$$

gde je: F - sila izmerena kod kidanja (N); A_0 – površina poprečnog preseka (mm^2); Δl – promena dužine (mm); l_0 – početna dužina uzorka pre istezanja (mm).

Na osnovu rezultata datih u tabeli 2, može se uočiti da zatezna čvrstoća modifikovanih epoksidnih uzoraka raste sa porastom udela tvrdih segmenata poliuretana, kao i sa porastom masenog udela elastomera u odnosu na čist epoksid. Najveća vrednost zatezne čvrstoće (0,59 MPa) je dobijena za uzorak modifikovan sa 15 mas.% poliuretana koji sadrži 30 mas.% tvrdih segmenata. Modifikacijom termoplastičnim segmentiranim poliuretanima na osnovu polikarbonatnog diola značajno je povećano prekidno izduženje epoksidnih smola što je i očekivano zbog fleksibilnosti mekih segmenata elastomera. Epoksidi modifikovani sa najmanjim udelom tvrdih segmenata (najvećim udelom mekih segmenata), kao i epoksidi modifikovani sa najmanjim masenim udelom pri istom sadržaju tvrdih segmenata poliuretana od 25 mas.%, imaju najveće vrednosti prekidnog izduženja (227 i 232%, redom) u odnosu na epoksid bez poliuretana čije vrednost za ε iznosi 36%. Dobijeni rezultati su u skladu sa vrednostima pronađenim u literaturi za slične epoksidne sisteme [36]. Dodatkom poliuretana tvrdoća po Šoru A se smanjuje (za nemodifikovani epoksid iznosi 75 Šor A). Sa porastom udela tvrdih segmenata poliuretana dodatih u istom masenom procentu u epoksidnu matricu, tvrdoća raste. Takođe, porast tvrdoće modifikovanih epoksida je uočen i dodatkom većeg masenog sadržaja poliuretana pri istom udelu tvrdih segmenata (Tabela 2).

ZAKLJUČCI

Sintetisana je serija epoksidnih smola modifikovanih poliuretanima na osnovu polikarbonatnog diola i ispitan je uticaj masenog udela sintetisanih poliuretana na osnovu polikarbonatnog diola (5, 10 i 15 mas.% u odnosu na epoksid), kao i udela tvrdih segmenata elastomera (20, 25 i 30 mas.%) na proces umrežavanja epoksidnih kompozita. Sa porastom udela tvrdih segmenata pri većem sadržaju poliuretana (10 i 15 mas.%) u reakcionoj smeši, temperatura maksimalne brzine reakcije umrežavanja se pomera ka nižim vrednostima (od 205 do 179 °C). Primenom tri modela izokonverzije: dva integralna (Ozawa–Flynn–Wall i Kissinger–Akahira–Sunose) i jednog diferencijalnog (Friedman) izračunate su vrednosti za energije aktivacije umrežavanja epoksidnih hibridnih materijala. Značajne razlike su uočene u drugom delu reakcije umrežavanja epoksida, za stepene reagovanja iznad 60%, energije aktivacije znatno rastu sa porastom stepena reagovanja, jer je tada zbog velike viskoznosti reakcione smeše reakcija usporena i otežana je pokretljivost molekula reaktanata. Analizom kinetičkih parametara je zaključeno da je uticaj otežane difuzije izraženiji u prisustvu termoplastičnih poliuretana na osnovu polikarbonatnih diola, čime je pokazano da njihovo prisustvo utiče na ceo mehanizam umreža-

vanja. Epoksid sa najvećim sadržajem tvrdih segmenata poliuretana ima najveću vrednost zatezne čvrstoće (0,59 MPa) što je i očekivano usled prisustva najveće koncentracije čvorova fizičkih mreža. Dodatkom termoplastičnih segmentiranih poliuretana na osnovu polikarbonatnog diola značajno je povećano prekidno izduženje epoksidnih smola, usled velike fleksibilnosti mekih segmenata elastomera.

Zahvalnica

Autori se zahvaljuju Ministarstvu prosvete, nauke i tehnološkog razvoja Republike Srbije za finansijsku podršku (projekat III 45022), i Pokrajinskom sekretarijatu za nauku i tehnološki razvoj (projekat 114-451-2396/ /2011-01). M. Š. duguje zahvalnost „*the Grant Agency of the Czech Republic*“ (*Czech Science Foundation, project No*. P108/10/0195).

LITERATURA

[1] C. Basara, U. Yilmazer, G. Bayram, Synthesis and characterization of epoxy based nanocomposites, Appl. Polym. Sci. **98** (2005) 1081–1086.

[2] X. Kornmann, H. Lindberg, L.A. Berglund, Synthesis of epoxy-clay nanocomposites: influence of the nature of the clay on structure, Polymer **42** (2001) 1303–1310.

[3] N. Chikhi, S. Fellahi, M. Bakar, Modification of Epoxy Resin with Kaolin as a Toughening Agent, J. Appl. Polym. Sci. **82** (2001) 861–878.

[4] N. Chikhi, S. Fellahi, M. Bakar, Modification of epoxy resin using reactive liquid (ATBN) rubber, Eur. Polym. J. **38** (2002) 251–264.

[5] J.L. Hedrick, I. Yilgor, G.L Wilkes, J.E. McGrath, Chemical modification of matrix Resin networks with engineering thermoplastics, Polym. Bull. **13** (1985) 201–208.

[6] M. Frigione, D. Acierno, L.Mascia, Miscibilization of low molecular weight functionalized polyethylenes in epoxy resins: Part 2. Effects of curing on morphological features and mechanical properties, Adv. Polym. Technol. **18** (1999) 237–253.

[7] D.J. Hourston, J.M. Lane, N.A. MacBeath, Toughening of Epoxy Resins with Thermoplastics II. Tetrafunctional Epoxy-polyetherimide Blends, Polym. Inter. **26** (1991) 17–21.

[8] M. Rong, H. Zeng, Polycarbonate-epoxy semi-interpenetrating polymer network: 2. Phase separation and morphology, Polymer **38** (1997) 269–277.

[9] M. Bakar, I. Wojtania, I. Legocka, J. Gospodarczyk, Property enhancement of epoxy resins by using a combination of polyamide and montmorillonite, J. Adv. Polym. Technol. **26** (2007) 223–231.

[10] H.H. Wang, J.C. Chen, Modification and compatibility of epoxy resin with hydroxyl-terminated or amine-terminated polyurethanes, Polym. Eng. Sci. **35** (1995) 1468––1475.

[11] K.H. Hsieh, J.L. Han, Graft interpenetrating polymer networks of polyurethane and epoxy. I. mechanical behavior, J. Polym. Sci. **28** (1990) 623–630.

[12] H. Harani, S. Fellahi, M. Bakar, Toughening of epoxy resin using synthesized polyurethane prepolymer based on hydroxyl-terminated polyesters, J. Appl. Polym. Sci. **70** (1998) 2603–2618.

[13] S.J. Park, J.S. Jin, Energetic studies on epoxy–polyurethane interpenetrating polymer networks, Appl. Polym. Sci. **82** (2001) 775–780.

[14] M. Bakar, R. Duk, M. Przybylek, M. Kostrzewa, Mechanical and thermal properties of epoxy resin modified with polyurethane, J. Reinf. Plast. Compos. **28** (2009) 2107–2118.

[15] M. Špírková, J. Pavličević, A. Strachota, R. Poreba, O. Bera, L. Kaprálková, J. Baldrian, M. Šlouf, N. Lazić, J. Budinski-Simendić, Novel polycarbonate-based polyurethane elastomers: Composition–property relationship, Eur. Polym. J. **47** (2011) 959–972.

[16] J.W. Boretos, W.S. Pierce, A new elastomer for biomedical applications, Science **158** (1967) 1481–1482.

[17] E.M. Christenson, J.M. Anderson, A. Hiltner, Biodegradation Mechanisms of Polyurethane Elastomers, Corros. Eng. Sci. Technol. **42** (2007) 312–323.

[18] K.D. Andrews, P. Feugier, R.A. Black, J.A. Hunt, Vascular prostheses: Performance related to cell-shear responses, J. Surg. Res. **149** (2008) 39–46.

[19] J. Urbano, F. Manzarbetia, C. Caramelo, Cholesterol embolism evaluated by polarized light microscopy after primary renal artery stent placement with filter protection, J. Vasc. and Interv. Radiol. **19** (2008) 189–194.

[20] K.B. Chandran, S.H. Kim, G. Han, Stress distribution on the cusps of a polyurethane trileaflet heart valve prosthesis in the closed position, J. Biomech. **24** (1991) 385–395.

[21] Y.S. Kim, J.S. Lee, Q. Ji, J.E. McGrath, Surface properties of fluorinated oxetane polyol modified polyurethane block copolymers, Polymer **43** (2002) 7161–7170.

[22] S. Velankar, S.L. Cooper, Microphase Separation and Rheological Properties of Polyurethane Melts. 1. Effect of Block Length, Macromolecules **31** (1998) 9181–9192.

[23] S. Montserrat, J. Málek, A kinetic analysis of the curing reaction of an epoxy resin, Thermochim. Acta **228** (1993) 47–60.

[24] D. Rosu, F. Mustata, C.N. Cascaval, Investigation of the curing reactions of some multifunctional epoxy resins using differential scanning calorimetry, Thermochim. Acta **370** (2001) 105–110.

[25] S. Montserrat, Calorimetric measurement of the maximum glass transition temperature in a thermosetting resin, J. Thermal. Anal. **40** (1993) 553–563.

[26] C.N Cascaval, D. Rosu, A. Stoleriu, Curing of some epoxy-acrylate glycidyl ethers based on para-alkyl substituted phenols, Polym. Deg. Stab. **55** (1997) 281–285.

[27] M.C. Jovičić, O.J. Bera, J.M. Pavličević, V.B. Simendić, R. Ž. Radičević, The influence of montmorillonite content on the kinetics of curing of epoxy nanocomposites, Hem. Ind. **66** (2012) 863–870.

[28] R. Thiagarajan, P.V. Reddy, S. Sridhar, M.C. Ratra, Determination of cure schedules of epoxies by differential scanning calorimetry, J. Thermal. Anal. **36** (1990) 277––287.

[29] D. Roşu, C.N. Caşcaval, F. Mustată, C. Ciobanu, Cure kinetics of epoxy resins studied by non-isothermal DSC data, Thermochim. Acta **383** (2002) 119–127.

[30] O. Bera, B. Pilić, J. Pavličević, M. Jovičić, B. Holló, K. Mészáros Szécsényi, M. Špirkova, Preparation and thermal properties of polystyrene/silica nanocomposites, Thermochim. Acta **515** (2011) 1–5.

[31] T. Ozawa, Kinetic analysis of derivative curves in thermal analysis, J. Therm. Anal. Calorim. **2** (1970) 301–324.

[32] H.E. Kissinger, Reaction kinetics in differential thermal analysis, Anal. Chem. **29** (1957) 1702–1706.

[33] T. Akahira, T. Sunose, Trans. Joint convention of four electrical institutes, Research Report, Chiba Institute of Technology Sci. Technol. **16** (1971) 22–31.

[34] A.W. Coats, J.P. Redfern, Kinetic parameters from thermogravimetric data, Nature **201** (1964) 68–69.

[35] H.L. Friedman, Kinetics of thermal degradation of char-forming plastics from thermogravimetry. Application to a phenolic plastic, J. Polym. Sci. **6** (1964) 183–195.

[36] L. Liu, H. D. Wagner, Rubbery and glassy epoxy resins reinforced with carbon nanotubes, Compos. Sci. Technol. **65** (2005) 1861–1868.

SUMMARY

MODIFICATION OF EPOXY RESINS WITH THERMOPLASTIC SEGMENTED POLYCARBONATE-BASED POLYURETHANES

Jelena Pavličević[1], Mirjana Jovičić[1], Vesna Simendić[1], Oskar Bera[1], Radmila Radičević[1], Milena Špírková[2]

[1]*University of Novi Sad, Faculty of Technology, Novi Sad, Serbia*
[2]*Institute of Macromolecular Chemistry AS CR v.v.i., Prague, Czech Republic*

(Scientific paper)

In this paper, the epoxy hybrid materials were synthesized by addition of thermoplastic segmented aliphatic polyurethanes with good elastic properties. The modified epoxy samples were obtained by curing of previously homogenized mixture of prepared polyurethane melts, epoxy resin and crosslinking agent Jeffamine D-2000. The influence of different weight content of polyurethanes (5, 10 and 15 wt.% compared to pure epoxy resin), as well the influence of different hard segments of elastomers (20, 25 and 30 wt.%), on the curing of modified epoxy systems was studied. The curing was followed by differential scanning calorimetry (DSC), in dynamic regime from 30 to 300 °C, at three heating rates (5, 10 and 20 °C/min). With the increase of hard segments in content of polyurethanes added in higher concentration (10 and 15 wt.%) into epoxy matrix, the temperature of maximum ratio of curing was shifted to lower values (from 205 to 179 °C). Obtained DSC data were analysed using two integral methods (Ozawa––Flynn–Wall and Kissinger–Akahira–Sunose) and one differential kinetic model (Friedman). The significant differences were observed in the second part of the epoxy curing (for the reaction degrees higher than 60%), where the values of activation energies remarkably increase. The addition of polyurethane elastomers retarded the curing process due to decreased mobility of reactant molecules caused by higher viscosity of reaction mixture. By detailed analysis of determined kinetic parameters, it is concluded that the influence of slow diffusion is more pronounced in the presence of thermoplastic polycarbonate-based polyurethanes, which confirmed their effect on the mechanism of epoxy curing. The highest tensile strength and hardness showed the DGEBA modified with the polyurethane with the highest hard segment content. The tensile strength of modified epoxy was increased by increasing the hard segment in content of polyurethane and its concentration in matrix. The elongation at break of modified epoxy samples was significantly improved by addition of polycarbonate-based polyurethanes with low hard segment content, due to higher content of flexible soft segment chains.

Keywords: Epoxy • Segmented polyurethanes • DSC • Curing kinetics • Mechanical properties

Aromatic compound in different peach cultivars and effect of preservatives on the final aroma of cooked fruits

Mojca Bavcon Kralj[1], Tjaša Jug[1], Erika Komel[1], Nikita Fajt[1], Kristjan Jarni[2], Jelena Živković[3], Ibrahim Mujić[4]

[1]*Chamber for Agriculture and Forestry of Slovenia, Agricultural and Forestry Institute Nova Gorica, Nova Gorica, Slovenia*
[2]*Department of Forestry and Renewable Forest Resources, Biotechnical Faculty, University of Ljubljana, Ljubljana, Slovenia*
[3]*Department of Chemistry, Faculty of Medicine, University of Niš, Niš, Serbia*
[4]*Collegium Fluminense Polytechnic of Rijeka, Rijeka, Croatia*

Abstract

Four yellow-fleshed peach cultivars („Royal Glory", „Redhaven", „Maria Marta" and „Norman") were used during two-year period in this study. The characterization of aromatic constituents of investigated cultivars was done using headspace solid phase micro-extraction (HS-SPME). The intention was to make implicit discrimination between cultivars by analysis of components present in all cultivars during two-year period. Also, the impact of added preservatives (Na-benzoate and citric acid) on the final aroma of cooked peaches was studied. The cultivars' differences and the impact of preservatives (Na-benzoate and citric acid) were statistically evaluated. Multiple discriminant analysis of peaches' aromatic profile was used to segregate investigated peach cultivars. Although they were very similar, the cultivars were segregated by two discriminant functions, function 1 (which accounted for 56.9% of this peach model) and function 2 (31.7%). The use of preservatives had also an important impact on the aromatic profile of cooked peaches. The statistical analysis indicated that from 57 identified volatiles, 40 volatiles showed statistically significant difference regarding the way of preservation. The main negative impact had Na-benzoate compared to control or samples preserved with citric acid.

Keywords: peach aroma, peach volatile compounds, discriminant analysis, food preservatives, solid phase micro-extraction.

Available online at the Journal website: http://www.ache.org.rs/HI/

SCIENTIFIC PAPER

UDC 634.25.076:54:66

Hem. Ind. **68** (6) 767–779 (2014)

doi: 10.2298/HEMIND130913003B

Peaches and apricots are among the most delectable fruits available and they are cultivated for family consumption or for sale on local markets. The tree ripe fruit can reach the consumer only in local markets, while regarding to market needs they are mostly picked immature. An earlier survey conducted by UC Davis researchers indicated that the main reasons why consumers do not eat more stone fruits are their lack of taste, failure to ripen, fruit is hard and mealy [1]. Peaches, nectarines, plums and apricots, are all members of the *Prunus* genus and therefore are closely related. They commonly are referred to as "stone fruits" because the seed is very large and hard. Thus, it is useful to determine the main volatilities which correspond directly to different maturity stage, accumulated either in the case when fruits were exposed to injuries or they could be indicative for rotten fruit. There is a lack of research about peach aroma development and aroma stability, as well as a suitable classification among cultivars and their label on the market.

The evaluation of the flavour ranged on scales is usually done by panellists, and to all advanced research-oriented growers the sensory evaluation is certainly helpful [2–4]. Careful evaluation of single aromatic compound and a group of compounds that have a specific impact on the overall fruit aroma are certainly useful. Within components which defining peach aroma, we recognize (*E*)-2-hexenol and (*E*)-2--hexenal, as representatives of "green aroma". On the other hand, as representatives of fruity, ripe aroma, γ-decalactone and γ-dodecalactone are detected [5]. During ripening the amount of C6 compounds decreases, while the concentration of lactones increases [6,7]. Peach ripening and the development of typical peach aroma are strongly dependent on the content of the lasts (δ- and γ-decalactones) [8]. Regarding to this remark, they are commonly used as markers in electronic transducers (e-nose) in fruit cool chambers [9––11]. Comparison of fresh and canned Halford peaches resulted in differences more due to the relative concentration of esters and monoterpenes than to γ-lactones [12]. Another study of chemical composition evaluation, firmness and variations in the colours of the

Correspondence: J. Živković, Department of Chemistry, Faculty of Medicine, University of Niš, 18000 Niš, Serbia.
E-mail: jelenazi2003@yahoo.com
Paper received: 13 September, 2013
Paper accepted: 27 December, 2013

fresh and canned peaches showed that picking the fruit more matured resulted in higher colour and flavour quality of products [13].

The contents of organic acids and sugars in foods and their relative ratio can provide precious information on food wholesomeness or to show how to optimize some selected technological processes [14]. Furthermore, the nature and concentration of the organic acids in fruits influence on their sensory characteristics, particularly on flavour, colour and aroma, and stability of fruit juices [15]. Sucrose, glucose, fructose and sorbitol are the main sugars or sugar alcohols encountered in the fruit of most plants from Rosaceae family. The edible quality of peaches (*Prunus persica* L. Batsch) depends to a great extent on their sweetness, which is related to sugar composition [16].

The relation between peach aromatic compounds, their evolution or/and masking effects on the one side and impact of temperature and preservatives on the other has not been much experimentally studied. Cooking during simultaneous steam distillation has an impact on the aromatic profile of the peaches generated an overall more intensive flavour extract [17]. Generally, in the industrial conditions, the high temperatures and times are applied, but they are specific for each procedure and purpose. There is a huge group of chemical preservatives too, which could be used to preserve the storage stability of juices, nectars and jams [18–20]. Citric acid has been widely used as an effective preservative due to its ability to reduce the superficial pH of cut fruits such as orange [21], peach, apricot and kiwifruit [22]. The use of another preservative sodium benzoate is highly disputable, since its application is connected with side health effects including increased hyperactivity [23], and asthma seemingly due to food allergy [24]. In the animal study it was shown that chronic exposure and use of benzoic acid and sodium benzoate can lead to reduced feed intake and reduced growth [25]. Moreover, very high doses of benzoic acid cause adverse effects such as metabolic acidosis, convulsions and hyperpnoea [26]. The EU directives on food additives other than colours and sweeteners (94/35/EC, 94/36/EC and 95/2/EC) regulate the use of permitted food additives. In subsidiary legislation 449.48 a limited number of additives are permitted for use in foodstuffs. For jams and similar products, the citric acid (E330) is allowed in *quantum satis* (as much as suffices) maximum level, whereas the maximum level for fruit juices and nectars is 5 g/L. Conditionally permitted preservative, such as sodium benzoate (Na benzoate) (E211) and benzoic acid, is allowed from 150 to 500 mg/kg. On the other hand, the US Code of Federal regulations (number 184.1021) regulates the use of benzoic acid in a concentration of 0.1% in food.

The principal component analysis (PCA) is a simple, chemometric, linear, unsupervised, and pattern recognition technique used for analysing, classifying, and reducing the dimensionality of numerical datasets in a multivariate problem [27]. Multivariate statistical analyses, employing PCA, were effective in describing chemical (pH, sugars and acids) and sensory (sweetness, fruity, sourness) variables in order to characterize peach quality [28,29]. The PCA was used in order to discriminate the optimum maturity date for harvesting peaches (model cultivar “Royal Glory”) and nectarines (“Big Top”) [30]. Also, peach juices (cv. “Redhaven”, “Suncrest” and “Maria Marta”) were clearly distinguished by PCA, with the most relevant variables, such as glucose, fructose, sorbitol, malic acid and colour parameters [31]. Further, PCA was used to segregate cultivars into different organoleptic groups [28], and 4 typical volatility groups (the groups with higher content of lactones, terpenes, esters and linalool) [32]. Discriminative analysis (DA), on the other hand, is one of the most widely used classification procedure. This method maximizes the variance between categories and minimizes the variance within specific category. DA was efficiently applied in order to discriminate apricot, pear and peach nectars according to their production, organic, conventional or/and flavoured characteristics [33]. According to our knowledge, discrimination of cultivars using the same volatile substances present in all examined cultivars, by exclusion of those which are typical only for one cultivar that has not yet been fully investigated.

The aim of the present work was to create the volatility profile, and to determine acids and sugars’ content of four peach cultivars, “Royal Glory”, “Redhaven”, “Maria Marta” and “Norman”. We also tried to make discrimination of peach cultivars by the analysis of commonly found substances present in all cultivars under investigations, with the simultaneous exclusion of those, which are typical only for one cultivar, during two seasons (2009 and 2010). Further, the impact of added preservatives (chelating agents, citric acid and sodium-benzoate) on volatiles and their evolution and/or masking effect in cooked peaches were studied.

EXPERIMENTAL PROCEDURE

Plant material and sampling

The trial was performed during 2009 and 2010 at the Fruit Growing Centre of Bilje near Nova Gorica (N 450 53.528; E 0130 38.606), Slovenia. Four yellow-fleshed peach cultivars: “Royal Glory”, “Redhaven”, “Maria Marta” and “Norman” were sampled at three stages of ripening: pre-technological maturity, commercially ripe and tree-ripe in July 2009 (monthly rainfall 122.8 L/m^2) and July 2010 (monthly rainfall

200.3 L/m^2). The trees were irrigated and hail net was used to protect them from bad weather. The orchard was managed according to standard integrated pest management plan approved in 2007 by the Ministry of Agriculture, Forestry and Food of Slovenia. Chosen cultivars are freestone types, they have melting flesh that becomes soft and juicy as it ripens. This type of peaches usually is preferred for eating fresh or for processing, and commonly grown in southern EU. Approximately 30 undamaged peaches (~4-5 kg) randomly sampled (east, west, north, south, top and bottom) from 5–7 trees of each cultivar (rootstocks were planted in a permanent place in spring 2005 and grafted with cultivars in August 2005) were harvested in the period ranged from 7 to 10 days in seasons 2009 and 2010. From each fruit three longitudinal slices (from stem end to calyx-end) are taken. Then the slices were put in the blender. The blender was equipped with a tube, through which a gentle stream of nitrogen was passing in order to prevent oxidation during mixing. The peach pulp was then immediately analysed, a part of it was immersed into liquid nitrogen (for volatile analysis) and the other part was transferred into the freezer at -16°C (for acids and sugars analysis).

Analytical procedure

Chemicals

Chemicals: 1-octanol (the internal standard), lactones components (γ-hexalactone, γ-heptalactone, γ-octalactone, γ-nonalactone, γ-decalactone and δ-decalactone), terpenes (α-terpineol, β-citronell, geraniol, and nerol), (*E*)-2-hexenal, (*Z*)-3-hexenol and 2-nonenol were purchased from Sigma Aldrich, Germany. Further, 1-hexanol, hexanal, 1-heptanol, linalool, octanal, (*E*)-2-hexenyl acetate, n-hexyl acetate and 2-nonenol were obtained from Alfa Aesar, Germany. Most standards were analytical grade or at least of 95% purity. Citric acid was obtained from Sigma Aldrich, and the analytical grade was >99.7%. Sodium benzoate was purchased from Alfa Aesar and was 99% pure.

Analysis of volatiles

20 g (in flask) of peach pulp (frozen in liquid nitrogen) was spiked with internal standard 1-octanol (0.23 mg/kg final concentration in pulp) and placed into the gas-tight 50 mL artisan made single-necked round-bottom flask. The flask was then put in the magnetic stirrer water bath (Ecorototherm from Dinkelberg analytics GmbH) at 40 °C for 10 min for thermal equilibration, and left for 20 min for solid phase micro-extraction (SPME). SPME device (manual holder, Supelco, Bellefonte, PA, USA) with a 10 mm fibre coated with 50/30 μm carboxen/polydimethylsiloxane/divinylbenzene – DVB/CAR/PDMS, was used for the extraction. After extraction, the SPME device was introduced in a gas chromatograph with mass selective detector (GC–MS – Agilent 6890 Series GC System with Agilent 5973 mass selective detector) in the splitless injector 270 °C for 10 min. Daily, prior analysis, the fibre was conditioned and activated by inserting it into the GC injector at 270 °C for 30 min. The volatiles were separated on Rtx-20 column (60 m, 0.25 mmID, 1μm, Restek, USA). The temperature program was as follows: initial temperature 50 °C (2 min) – 10 °C min^{-1} – 150 °C (for 3 min) – 10 °C min^{-1} – 250 °C (for 5 min). Total run time was 30 min. The mass spectrometer was operated in the electron ionisation mode at a voltage of 70 eV, the temperature of the MS Quad was set at 150 °C and the ion source at 230 °C. Compounds were identified on the basis of their retention times (comparison with standards) and spectra using the searchable EI-MS spectra library (NIST02). The peak areas needed for qualification and quantification were measured either in TIC chromatogram or in an extracted ion chromatogram in the case of co-elution with other compounds. The average *RSD* of the method applied was 13%.

Analysis of sugars and acids

10 g of peach pulp was diluted with 40 mL of deionised water. In order to achieve the best resolution and precision, two procedures were compared, direct injection and sample clean-up with Bond Elute® Sax cartridge (Varian, Harbor City, CA). Diluted samples were filtered through a 0.45 μm cellulose acetate membrane before direct injection.

In comparison with this simplified procedure, pretreatment with Sax cartridge, following the procedure (with some modifications) according to Chinnici *et al.* was applied. The solid phase extraction (SPE) employing Sax cartridges offered the separation of neutral compounds (*e.g.*, sugars and alcohols) from the acidic ones. The cartridge (3 mL/500 mg) was preliminarily conditioned with methanol (3 mL) and deionised water (3 mL). Then the diluted sample (5 mL, corrected to pH 7.0) was slowly passed through the cartridge (less than 0.2 mL/min). The neutral compounds were not retained, whereas the acidic ones were afterwards eluted with 2.5 mL of acid and washed with 2.5 mL of deionised water. The two fractions (the first containing neutral compounds – sugars and sorbitol and the second containing acids) were injected in the HPLC apparatus. The HPLC system (Agilent 1100) was equipped with quaternary pump (G1311A), a variable wavelength detector (G1314A) set at 210 nm (for the analysis of organic acids) connected in series with a refractive index detector (G1362A) (for sugar analysis), and an injection valve fitted with a 20 μL loop. The samples were isocratically separated at 0.6 mL/min, using a Bio-Rad Ami-/nex HPX 87H column (300 mm×7.8 mm i.d.) at 30 °C. Diluted sulphuric acid (0.005 M) was used as a mobile phase. Quantification was carried out using the external standard method, with the $R^2 \geq 0.9999$ in all cases.

Addition of preservatives

According to EU directives on food additives other than colours and sweeteners (94/35/ES, 94/36/ES, 95/2/ES) and the US Code of Federal regulations (number 184.1021), which regulates the use of benzoic acid and its salt, the added concentration of citric acid and sodium benzoate was in all cases of 0.1% of peach pulp weight. Thus, 20 g of peach pulp (individually made of four yellow-fleshed peach cultivars: "Royal Glory", "Redhaven", "Maria Marta" and "Norman" sampled in year 2010 frozen in liquid nitrogen) was spiked with internal standard 1-octanol (0.23 mg/kg final concentration in pulp) and 20 mg of either citric, or sodium benzoate and placed into the flask, capped and put in the water bath (Julabo TWB22) at 95 °C for 30 min for imitating the cooking process. Then the flask was transferred into the magnetic stirrer water bath (Ecorototherm from Dinkelberg analytics GmbH) at 40 °C for 10 min for thermal equilibration, and left for 20 min for solid phase micro-extraction. The procedure followed steps was previously described under *Analysis of volatiles* Section.

Data treatment

Descriptive statistics, such as arithmetic mean and range, were used to describe the main features (comparison) of four yellow-fleshed peach cultivars. Analysis of variance was used to determine the differences between individual cultivars, as well as the impact of different preservatives on volatile profile. For this purpose two factorial ANOVA was carried out to test the main effect of cultivars (C), preservative method (P) and their interaction. Tukey's multiple comparison tests were performed to determine the differences between group means.

Forward stepwise discriminant analysis with Wilks' lambda method was used to determine the differences between the individual cultivars. By using a stepwise selection procedure, only the most significant discriminant variable was identified. The scatter plot of discriminant scores corresponding to each sample (regardless of the season and maturity) in the multivariate space defined by the first two discriminant functions was introduced to present a multivariate volatile profile variation between examined groups. All computations were carried out with SPSS Statistics 18.0 and Statistica for Windows software.

RESULTS AND DISCUSSION

Differences in peach volatiles regarding the season and variety

The analysis of volatile components in investigating cultivars during seasons 2009 (monthly rainfall 122.8 L/m^2) and 2010 (monthly rainfall 200.3 L/m^2) was presented in Table 1. On the basis of gained results we found that the influence of external factors, like monthly rainfall on the overall amount of volatiles identified in the specific cultivar, is very important. The influence of seasonal differences was confirmed for the particular components in all 4 cultivars, and that results are pointed out (marked **bold**). In the group of alcohols, the seasonal difference was observed in the case of 1-nonanol, which was present in 3 cultivars only in year 2010 (in Norman it was absent both years), whereas in the year 2009 was not detected. Higher concentrations of hexanal, (*E*)-2-hexane, heptanes (except for Redhaven) and 2,5-furandicarboxaldehyde were found in all 4 cultivars in the year 2009. The C6 compounds (hexanal and (*E*)-2-hexenal) are the representatives of peach green aroma and are directly proportional to the stage of peach ripeness [34–36]. Besides that, aldehydes are for most varieties the most abundant compounds. Esters, which were found to be susceptible to monthly rainfall, were ethyl acetate, pentyl acetate, 3-hexenyl acetate, ethyl-2(*5H*)-furanone, octyl acetate and all identified lactones. However, lactones are known to increase with maturity [37,38].

The season had the most pronounced effect in the group of terpenes, since their concentration was significantly higher in all cases in season 2009. In fact, obtained results are in accordance with the observation, that terpenes synthesis increases considerably at high temperatures resulting in high concentrations in tissues, which led to the hypothesis that emitted terpenes may protect plants from high temperature [39]. Similarly, it was found that water deficit increased the concentrations of several individual monoterpenes and resin acids in conifers [40]. There are some assumptions that carbon fixed in photosynthesis could be used for the formation of secondary metabolites. However, our study is the first report indicating the negative effect of rainfall on the concentration of terpenes in fruit.

On the basis of the obtained results from Table 1, beside seasonal also cultivars' differences could be observed. (*E*)-2-nonenal (tallowy, fatty) and 2-methylhexyl propanoate (fruity, green, ripe, sweet) were detected only in "Royal Glory", (*Z*)-2-heptenal (fatty), (*E*)-2-octenal (green, fatty) were found in "Maria Marta" and "Norman", 3(2H)-benzofuranone, octyl acetate (orange) and (*E*)-2-hexenyl hexanoate (green, fruity, cheesy) in "Royal Glory" and "Redhaven" and *cis*-geraniol (rose-like odor) was found only in "Redhaven".

Discriminant analysis

Considering we followed the evolution of peach volatiles during 2009 and 2010 at three stages of ripening: pre-technological maturity, commercially ripe and tree-ripe on four yellow-fleshed peach cultivars: "Royal Glory", "Redhaven", "Maria Marta" and "Nor-

*Table 1. Minimum-maximum range and arithmetic means of identified volatiles; main seasonal differences are marked **bold**; RT – retention time; n.d. - not detected*

Compound	Identification ions/*RT*	Royal Glory 2009	Royal Glory 2010	Redhaven 2009	Redhaven 2010	Maria Marta 2009	Maria Marta 2010	Norman 2009	Norman 2010
					Alcohols				
3-Hexen-1-ol	41, 67, 55, 39, 82 / 12.99	0.003 (0.002 – 0.005)	0.003 (0.003 – 0.003)	n.d.	0.006 (0.004 – 0.009)	0.003 (0.002 – 0.004)	0.003 (0.002 – 0.004)	n.d.	0.006 (0.004 – 0.007)
*1-Hexanol	56, 43, 41, 55, 42 / 13.18	0.611 (0.393 – 1.083)	0.361 (0.298 – 0.405)	0.387 (0.274 – 0.467)	0.635 (0.542 – 0.709)	0.510 (0.429 – 0.583)	0.417 (0.332 – 0.527)	0.417 (0.254 – 0.596)	0.305 (0.294 – 0.313)
*(*E*)-2-Hexen--1-ol	57, 41, 67, 39, 82 / 13.27	0.331 (0.265 – 0.467)	0.342 (0.300 – 0.370)	0.283 (0.140 – 0.528)	0.431 (0.340 – 0.569)	0.343 (0.269-0.438)	0.330 (0.238 – 0.477)	0.262 (0.122 – 0.353)	0.211 (0.193 – 0.226)
1-Nonanol	41, 55, 43, 56, 70 / 20.31	n.d.	0.003 (0.003 – 0.003)	n.d.	0.005 (0.005 – 0.005)	n.d.	0.003 (0.003 – 0.003)	n.d.	n.d.
					Aldehydes				
*Hexanal	44, 56, 41, 43, 57 / 12.00	3.924 (2.840 – 5.209)	2.296 (2.181 – 2.406)	4.754 (3.400 – 6.068)	4.497 (3.978 – 4.800)	5.137 (4.953 – 5.364)	3.177 (2.605 – 4.266)	4.245 (2.341 – 5.104)	2.551 (2.544 – 2.560)
*(*E*)-2-Hexenal	41, 55, 69, 39, 83 / 13.42	4.690 (2.655 – 5.688)	3.686 (3.660 – 3.711)	4.761 (2.720 – 5.989)	4.207 (3.716 – 4.642)	5.669 (4.878 – 5.992)	3.515 (2.577 – 4.942)	5.355 (2.310 – 6.991)	3.168 (2.982 – 3.470)
Heptanal	44, 43, 41, 70, 29/ 14.21	0.008 (0.007 – 0.008)	0.004 (0.003 – 0.005)	0.008 (0.008 – 0.010)	0.010 (0.009 – 0.011)	0.009 (0.007 – 0.010)	0.007 (0.005 – 0.008)	0.012 (0.011 – 0.014)	0.005 (0.004 – 0.005)
*(*E,E*)-2,4-Hex-adienal	81, 39, 41, 53, 67 / 15.14	0.409 (0.241 – 0.491)	0.432 (0.424 – 0.438)	0.415 (0.202 – 0.523)	0.546 (0.461 – 0.597)	0.494 (0.412 – 0.561)	0.432 (0.320 – 0.605)	0.486 (0.191 – 0.656)	0.402 (0.366 – 0.474)
(*Z*)-2-Heptenal	41, 27, 55, 83, 57 / 15.94	n.d.	n.d.	n.d.	n.d.	n.d.	0.007 (0.006 – 0.008)	0.023 (0.003 – 0.034)	0.012 (0.010 – 0.014)
(*E*)-2-Nonenal	41, 27, 43, 29, 55 / 15.28	0.009 (0.009 – 0.009)	0.014 (0.013 – 0.015)	n.d.	n.d.	n.d.	n.d.	n.d.	n.d.
*Benzalde-hyde	106, 77, 105, 51, 50 / 17.18	0.094 (0.063 – 0.168)	0.114 (0.099 – 0.137)	0.355 (0.294 – 0.405)	0.407 (0.350 – 0.496)	0.252 (0.201 – 0.285)	0.159 (0.126 – 0.192)	0.444 (0.324 – 0.601)	0.240 (0.209 – 0.303)
(*E*)-2-Octenal	41, 29, 55, 70, 27 / 18.38	n.d.	n.d.	n.d.	n.d.	0.005 (0.005-0.005)	0.006 (0.006-0.006)	0.008 (0.007-0.009)	0.004 (0.003-0.004)
Nonanal	57, 41, 43, 56, 44 / 19.10	0.021 (0.013 – 0.029)	0.017 (0.015 – 0.019)	0.027 (0.022 – 0.031)	0.030 (0.029 – 0.032)	0.022 (0.019 – 0.025)	0.019 (0.016 – 0.024)	0.028 (0.017 – 0.038)	0.022 (0.018 – 0.025)
2,5-Furandi-carb-oxalde-hyde	124, 123, 95, 67, 125 / 20.4	0.006 (0.005 – 0.008)	n.d.	0.058 (0.058 – 0.058)	n.d.	0.011 (0.002 – 0.020)	n.d.	0.007 (0.003 – 0.014)	0.004 (0.002 – 0.005)
*Decanal	41, 43, 57, 29, 55 / 21.20	0.002 (0.002 – 0.003)	0.005 (0.004 – 0.005)	0.004 (0.004 – 0.005)	0.008 (0.006 – 0.008)	0.003 (0.003 – 0.004)	0.003 (0.002 – 0.005)	0.005 (0.002 – 0.007)	0.002 (0.002 – 0.003)

Table 1. Continued

Compound	Identifications/*RT*	Royal Glory 2009	Royal Glory 2010	Redhaven 2009	Redhaven 2010	Maria Marta 2009	Maria Marta 2010	Norman 2009	Norman 2010
				Ketones					
3-Methyl-2--cyclopenten--1-one	96, 67, 53, 39, 81 / 15.55	0.005 (0.005 – 0.005)	0.009 (0.007 – 0.010)	n.d.	n.d.	0.005 (0.005 – 0.005)	0.009 (0.008 – 0.009)	n.d.	0.007 (0.006 – 0.009)
2,3-Octanedione	43, 99, 71, 41, 55 / 16.13	n.d.	n.d.	n.d.	n.d.	n.d.	n.d.	0.007 (0.004-0.009)	0.004 (0.003-0.005)
3(2*H*)-Benzofuranone	134, 105, 76, 77 / 21.69	0.002 (0.001 – 0.003)	n.d.	n.d.	0.003 (0.002 – 0.004)	n.d.	n.d.	n.d.	n.d.
				Esters					
Ethyl acetate	**43, 29, 45, 61, 27 / 7.86**	**n.d.**	**n.d.**	**0.144 (0.144 – 0.144)**	**0.029 (0.029 – 0.029)**	**0.137 (0.137 – 0.137)**	**n.d.**	**0.491 (0.491 – 0.491)**	**n.d.**
Pentyl acetate	**43, 70, 42, 55, 61 / 14.17**	**0.018 (0.018 – 0.018)**	**n.d.**	**0.017 (0.006 – 0.028)**	**0.005 (0.005 – 0.005)**	**0.010 (0.010 – 0.010)**	**n.d.**	**0.011 (0.011 – 0.011)**	**n.d.**
*Hexyl acetate	43, 56, 61, 55, 41 / 16.60	1.425 (1.146 – 2.153)	1.230 (0.833 – 1.635)	1.695 (0.985 – 3.405)	1.919 (0.750 – 3.622)	1.615 (0.929 – 2.638)	0.993 (0.841 – 1.269)	1.266 (0.607 – 1.766)	0.930 (0.837 – 1.059)
***3-Hexenyl acetate**	**43, 67, 82, 41, 39 / 16.69**	**1.160 (0.918 – 1.497)**	**1.018 (0.697 – 1.189)**	**0.546 (0.304 – 0.950)**	**0.543 (0.474 – 0.657)**	**0.769 (0.613 – 1.093)**	**0.712 (0.527 – 0.928)**	**1.108 (0.405 – 1.587)**	**0.889 (0.867 – 0.901)**
*2-Hexenyl acetate	43, 67, 41, 82, 27 / 16.88	0.764 (0.678 – 0.874)	0.859 (0.693 – 1.056)	1.213 (0.494 – 2.745)	1.470 (0.491 – 2.765)	1.051 (0.477 – 1.737)	0.746 (0.521 – 1.158)	0.891 (0.207 – 1.488)	0.677 (0.626 – 0.729)
Methyl octanoate	74, 87, 43, 41, 55 / 19.29	0.012 (0.007 – 0.023)	0.009 (0.009 – 0.009)	0.017 (0.009 – 0.030)	0.021 (0.021 – 0.021)	0.014 (0.014 – 0.014)	n.d.	0.014 (0.014 – 0.014)	n.d.
***5-Ethyl--2(5*H*)-furanone**	**83, 55, 27, 29, 17 / 19.37**	**0.012 (0.010 – 0.014)**	**0.009 (0.009 – 0.010)**	**0.021 (0.020 – 0.022)**	**0.017 (0.016 – 0.019)**	**0.016 (0.014 – 0.019)**	**0.010 (0.005 – 0.018)**	**0.015 (0.005 – 0.022)**	**0.006 (0.005 – 0.007)**
***γ-Caprolactone**	**85, 29, 42, 27, 56 / 19.76**	**0.008 (0.004 – 0.015)**	**0.002 (0.002 – 0.003)**	**0.016 (0.011 – 0.019)**	**0.014 (0.011 – 0.021)**	**0.014 (0.008 – 0.022)**	**0.006 (0.005 – 0.008)**	**0.012 (0.007 – 0.015)**	**0.007 (0.006 – 0.009)**
2-Methylhexyl propanoate	43, 71, 89, 56, 41 / 20.61	0.002 (0.002 – 0.002)	0.004 (0.003 – 0.004)	n.d.	n.d.	n.d.	n.d.	n.d.	n.d.
Ethyl octanoate	88, 29, 57, 41, 60 / 20.70	0.002 (0.002 – 0.003)	0.003 (0.002 – 0.003)	0.005 (0.001 – 0.017)	0.010 (0.010 – 0.010)	0.007 (0.007 – 0.007)	n.d.	0.010 (0.010 – 0.010)	n.d.
*2-Hexenyl butanoate	71, 67, 43, 41, 27 / 20.85	0.003 (0.002 – 0.005)	0.013 (0.012 – 0.014)	0.047 (0.001 – 0.179)	0.008 (0.003 – 0.017)	0.004 (0.003 – 0.005)	0.004 (0.002 – 0.007)	0.007 (0.003 – 0.010)	0.004 (0.002 – 0.007)
Octyl acetate	**43, 56, 70, 55, 84 / 20.99**	**n.d.**	**0.047 (0.032 – 0.062)**	**n.d.**	**0.020 (0.005 – 0.044)**	**n.d.**	**n.d.**	**n.d.**	**n.d.**
(*E*)-2-Hexenyl hexanoate	99, 43, 41, 55, 71 / 24.32	n.d.	0.006 (0.004 – 0.010)	0.005 (0.004 – 0.006)	n.d.	n.d.	n.d.	n.d.	n.d.

Table 1. Continued

Compound	Identification ions/*RT*	Royal Glory 2009	Royal Glory 2010	Redhaven 2009	Redhaven 2010	Maria Marta 2009	Maria Marta 2010	Norman 2009	Norman 2010
				Esters					
γ-Octalactone	**85, 29, 57, 56, 41 / 23.67**	**n.d.**	**n.d.**	**n.d.**	**n.d.**	**0.002 (0.002-0.002)**	**n.d.**	**0.002 (0.002-0.002)**	**n.d.**
***γ-Decalact-one**	**85, 29, 128, 43, 41 / 27.03**	**0.007 (0.002 – 0.017)**	**0.002 (0.002 – 0.003)**	**0.019 (0.002 – 0.050)**	**0.007 (0.003 – 0.015)**	**0.010 (0.002 – 0.027)**	**0.006 (0.004 – 0.008)**	**0.010 (0.002 – 0.031)**	**0.003 (0.001 – 0.004)**
δ-Octalactone	**99, 42, 71, 70, 55 / 27.83**	**0.004 (0.004 – 0.004)**	**n.d.**	**0.010 (0.005 – 0.016)**	**n.d.**	**n.d.**	**–**	**n.d.**	**n.d.**
				Terpenic compounds					
α-Pinene	**93, 41, 69, 39, 77 / 15.91**	**0.007 (0.006 – 0.008)**	**n.d.**	**0.020 (0.011 – 0.037)**	**n.d.**	**n.d.**	**n.d.**	**0.003 (0.003 – 0.003)**	**n.d.**
***cis*-Geraniol**	**69, 93, 41, 68, 67 / 15.92**	**n.d.**	**n.d.**	**0.013 (0.010-0.017)**	**n.d.**	**n.d.**	**n.d.**	**n.d.**	**n.d.**
Limonene	**68, 67, 93, 39, 41 / 17.33**	**0.032 (0.021 – 0.049)**	**n.d.**	**0.080 (0.030 – 0.134)**	**0.017 (0.017 – 0.017)**	**0.063 (0.021 – 0.105)**	**n.d.**	**0.032 (0.020 – 0.044)**	**0.010 (0.010 – 0.010)**
α-Cymene	**119, 134, 91, 120/ 17.54**	**0.010 (0.007 – 0.013)**	**n.d.**	**0.028 (0.018 – 0.045)**	**0.014 (0.014 – 0.014)**	**0.009 (0.009 – 0.009)**	**n.d.**	**0.014 (0.008 – 0.018)**	**n.d.**
***Linalool**	**71, 93, 41, 69, 43 / 18.91**	**0.125 (0.046 – 0.205)**	**0.029 (0.023 – 0.038)**	**0.389 (0.250 – 0.493)**	**0.064 (0.043 – 0.095)**	**0.048 (0.031 – 0.081)**	**0.007 (0.003 – 0.013)**	**0.104 (0.030 – 0.211)**	**0.020 (0.009 – 0.030)**
α-Terpineol	**59, 93, 121, 136 / 21.62**	**0.002 (0.002 – 0.002)**	**n.d.**	**0.003 (0.002 – 0.003)**	**n.d.**	**n.d.**	**n.d.**	**0.003 (0.003 – 0.003)**	**n.d.**
				Other					
Hexanoic acid	60, 73, 41, 27, 43 / 15.4	0.008 (0.008 – 0.008)	0.014 (0.013 – 0.015)	0.019 (0.008 – 0.030)	0.029 (0.025 – 0.032)	0.012 (0.008 – 0.019)	0.016 (0.009 – 0.023)	0.010 (0.003 – 0.014)	0.011 (0.010 – 0.012)
2-Ethylfuran	81, 53, 96, 39, 41 / 9.64	0.021 (0.014 – 0.031)	0.058 (0.055 – 0.062)	0.025 (0.016 – 0.029)	0.060 (0.054 – 0.069)	0.030 (0.024 – 0.035)	0.047 (0.024 – 0.074)	0.039 (0.016 – 0.079)	0.053 (0.040 – 0.072)
***2-Pentylfuran**	81, 82, 27, 53, 95 / 16.25	0.010 (0.006 – 0.015)	0.011 (0.010 – 0.011)	0.014 (0.012 – 0.020)	0.016 (0.014 – 0.018)	0.013 (0.009 – 0.016)	0.007 (0.005 – 0.010)	0.017 (0.011 – 0.021)	0.010 (0.008 – 0.012)
5-(Hydroxy-methyl)-2--furan-carb-oxaldehyde	97, 126, 41, 39, 69 / 23.3	n.d.	n.d.	0.120 (0.001 – 0.238)	n.d.	0.028 (0.028 – 0.028)	n.d.	0.006 (0.001 – 0.011)	n.d.

man", our predominant task was to perform the analysis, which would offer us a discrimination of cultivars using the same compounds present in all peach cultivars during two completely different seasons (the amount of rainfall). For this purpose we applied the discriminant analysis using the compositional data marked with stars (*) in Table 1 and the data regarding the composition of sugars (glucose, fructose, sucrose and sorbitol) and acids (citric and malic) in peaches. By applying the multiple group discriminant analysis, it is not necessary to specify how to combine groups so as to form different discriminant functions. The first function provides the most overall discrimination between groups; the second provides second most,

and so on. Moreover, the functions will be independent or orthogonal, and their contributions to the discrimination between groups will not overlap. The analysis included three discriminant functions, of which all three have significant contribution to group differentiation.

Function 1, which accounts for 56.9% of the variance explained by the model, is more heavily weighted by citric acid, linalool, (*E*)-2-hexenal and benzaldehyde (Table 2). Thus, function 1 separates "Royal Glory" cultivar with its sweet fruits from "Redhaven" cultivar which has much sour and aromatic fruits (Fig. 1). In fact, the most discriminative component in "Royal Glory" peaches is glucose, whereas in "Redhaven" peaches is linalool, with its floral, fresh note and benzaldehyde with almond-like odor. Both classifications of peach cultivars are in complete accordance with sensory evaluations.

Table 2. Standardized canonical discriminant function coefficients for the first three functions

Compound	Function 1	Function 2	Function 3
1-Hexanol	0.369	0.986	0.398
(*E*)-2-Hexenal	–1.212	–0.872	–0.925
(*Z*)-3-Hexenyl acetate	–0.560	–1.019	0.362
Benzaldehyde	1.083	0.119	1354
α-Linalool	1.350	1.047	1.244
γ-Caprolactone	0.237	0.392	–1.194
Citric acid	1.706	–1.127	–0.322
Sucrose	0.631	–1.250	0.803
Glucose	–0.797	1.870	0.359
Eigenvalue	18.83	10.48	3.79
% Of explained variance	56.9	31.7	11.5

The second function accounts for another 31.7% of the explained variance and seems to be associated mostly with glucose and to a less extent by sucrose, citric acid, linalool, 1-hexanol, (*E*)-2-hexenal and (*Z*)-3-hexenyl acetate. Hence function 2 separates sensorial similar cultivars "Norman" and "Maria Marta" from "Redhaven" and "Royal Glory" cultivars, but this separation is not as strong as the separation caused by function 1 (Fig. 1). The most discriminative coefficients were for both cultivars lower values of glucose and higher values of sucrose and citric acid.

Function 3 also significantly contributes to group differentiation (data not shown). Its contribution to the explained variance is 11.5% but the relatively low value of eigenvalue shows weak discriminant ability, so its interpretation is less important.

The impact of preservatives (citric acid *vs*. sodium benzoate) on the aromatic profile of cooked peaches

Cooking by itself has an important impact on the aromatic profile of the peaches and it has been studied in details also by other authors [12,13,17]. Cooking of peaches at 95 °C for 30 min is one of many procedures which could be applied, but it is maybe one of the most applicable for household scale, and that was the reason why we have chosen it. In the first place, we were interested in the promoting or/and the masking effect of preservatives on the overall aroma of peaches used as canned peaches, jams or other products. In our study we used two common preservatives citric acid and sodium benzoate.

The statistical analysis indicated that from 57 identified volatiles (Table 3), 40 volatiles showed statistically significant difference regarding the way of preser-

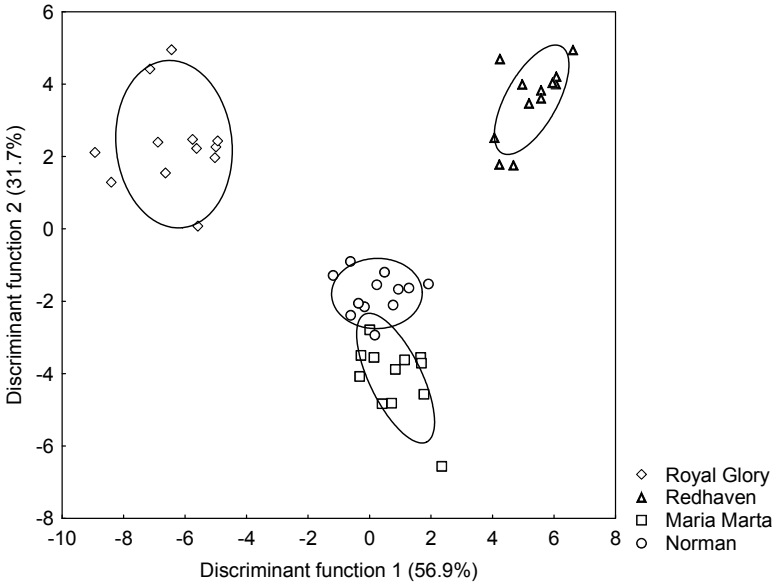

Figure 1. Distribution of the first two discriminant functions according to the stepwise discriminant analysis of peach aromatic profile. The ellipses delimit the space that represents a particular peach cultivar (p = 0.95).

*Table 3. Arithmetic means of identified volatiles expressed as concentration of internal standard 1-octanol (mg/kg); means followed by the same letter in the same row are not significantly different at p > 0.05 according to Tukey's test; * 0.01 < p < 0.05; ** 0.001 < p< 0.01; *** p < 0.001*

Compound	Peach variety	Control		Citric acid		Na benzoate		Interaction
				Alcohols				
4-Methyl-cyclohex-anol	***	0.0057	A	0.0053	A	0.0032	B[b]	*
3-Hexen-1-ol	**	0.0030	B	0.0023	A	0.0024	AB	***
1-Hexanol		0.1888	A	0.1796	A	0.1374	B	
(*E*)-2-Hexen-1-ol	*	0.1843	B	0.1654	AB	0.1365	A	
1-Nonanol	***	0.0011		0.0010		0.0011		***
				Aldehydes				
(*E*)-2-Pentenal	***	0.0020	A	0.0020	A	0.0016	B	
Hexanal		1.1799	AB	1.3580	B	1.0874	A	
(*E*)-2-Hexenal	*	1.6761		1.7045		1.5955		
Heptanal	***	0.0179	B	0.0166	AB	0.0136	A	
(*E,E*)-2,4-Hexadienal		0.2078	A	0.1973	A	0.1653	B	
(*Z*)-2-Heptenal	**	0.0326	A	0.0295	A	0.0177	B	
(*E,E*)-2,4-Heptadienal	***	0.0020		0.0018		0.0017		*
Benzaldehyde	***	0.1569	A	0.1490	A	0.1776	B	
Octanal	***	0.0493	A	0.0496	A	0.0345	B	***
(*E*)-2-Octenal		0.0214		0.0203		0.0190		
Benzeneacetaldehyde	***	0.0042		0.0038		0.0036		
Nonanal	***	0.4163	B	0.3592	A	0.3199	A	
(*E*)-2-Nonenal		0.0103		0.0102		0.0092		
Decanal		0.0342	A	0.0305	A	0.1236	B	
2,5-Dimethyl-benz-aldehyde	***	0.0030	A	0.0029	A	0.0127	B	***
p-Menth-1-en-9-al		0.0410	A	0.0641	B	0.0410	A	*
(*E*)-2-Decenal		0.0080	A	0.0088	A	0.0123	B	
Undecanal	***	0.0059		0.0048		0.0067		
3-Ethylbenzaldehyde	***	0.0011	A	0.0011	A	0.0036	B	***
β-Dodecanal	***	0.0009	A	0.0012	B	0.0011	B	***
				Ketones				
2,3-Octanedione	**	0.0071	A	0.0073	A	0.0059	B	
3-Methyl-cyclopen-ten-1-one	**	0.0007		0.0003		0.0000		*
				Esters				
Hexyl acetate		0.7860	B	0.5974	A	0.4408	A	
3-Hexenyl acetate	***	0.6332	A	0.5362	A	0.3932	B	
2-Hexenyl acetate	*	0.6191	B	0.5167	AB	0.3943	A	
Ethyl octanoate	***	0.0025	A	0.0032	B	0.0021	A	*
5-Ethyldihydro-2(3*H*)--furanone	**	0.0075	A	0.0075	A	0.0059	B	**
5-Ethyl-2(5*H*)-fura-none	***	0.0171		0.0169		0.0132		
2-Methylhexyl pro-panoate	***	0.0010		0.0010		0.0008		
				Esters				
(*Z*)-2-Hexenyl butanoate	***	0.0064		0.0053		0.0045		

Table 3. Continued

Compound	Peach variety	Control		Citric acid		Na benzoate		Interaction
				Esters				
(*E*)-2-Hexenyl hexanoate	***	0.0004		0.0005		0.0009		
Octyl acetate	***	0.0095		0.0095		0.0078		
γ-Decalactone	***	0.0041	A	0.0058	B	0.0046	A	***
				Terpenic compounds				
α-Terpinyl acetate	***	0.0187	A	0.0183	A	0.0133	B	*
α-Cymene	***	0.0160	A	0.0160	A	0.0099	B	**
α-Linalool	***	0.0418		0.0448		0.0407		
2,6-Dimethyl-3,7--octadiene-2,6-diol	***	0.0057	AB	0.0078	B	0.0049	A	
α-Terpineol	**	0.0037	A	0.0042	A	0.0154	B	
α-Cyclocitral	***	0.0038	A	0.0046	A	0.0080	B	
α–Ionene	**	0.0011		0.0014		0.0011		
β-Damascenone	***	0.0053	A	0.0099	B	0.0041	A	***
				Others				
Tetrahydrofuran	*	0.0037	B	0.0031	AB	0.0015	A	*
Hexanoic acid		0.0070	A	0.0070	A	0.0042	B	
2-Ethylfuran	*	0.0148		0.0134		0.0142		
2-Pentylfuran	*	0.1058	B	0.0797	A	0.0686	A	
3,6-Dihydro-4--methyl-2-(2-methyl--1-propenyl)-2*H*-pyran	***	0.0088	A	0.0103	A	0.0063	B	
Benzene	*	0.0028	A	0.0038	A	0.0423	B	*
Benzoic acid		0.0000	A	0.0000	A	0.9853	B	
1,2,3,4-Tetrahydro--1,6,8-trimethyl--naphthalene	***	0.0007		0.0007		0.0004		
1,2-Dihydro-1,1,6-trimethyl-naphthalene	***	0.0059	A	0.0092	B	0.0046	A	
Biphenyl	***	0.0000	A	0.0000	A	0.0056	B	***
2-Methyl-1,1'-biphenyl	***	0.0000	A	0.0000	A	0.0158	B	***

vation. The interaction was expressed in 20 cases, but it arises because the particular volatile was found only in one or two peach varieties, whereas in other it was absent. In other words, the interaction occurs when the effect of preservation (on the quantity, presence or absence of volatiles) is changed according to the peach varieties.

In case of 25 volatiles the treatment with sodium benzoate resulted in a significantly different amount of volatiles compared to control samples and samples treated with citric acid. In fact, 11 were of higher values and 14 were of lower. The preservation with citric acid had significantly different contribution in case of 5 volatiles, compared to the control or samples treated with sodium-benzoate. The increase was noticed in the case of: hexanal, *p*-menth-1-en-9-al, ethyl octanoate, γ-decalactone, and the terpenic compounds 2,6-dimethyl-3,7-octadiene-2,6-diol and β-damascenone. Hexanal, ethyl octanoate and γ-decalactone are compounds typical for peach aroma, already discussed, whereas β-damascenone (cooked-apple-like) and *p*-menth-1-en-9-al were not found in fresh peaches, but they are formed during thermal processing [17,41]. The 2,6-dimethyl-3,7-octadiene-2,6-diol was found in larger amount in Darjeeling tea [42], but it is the first report about its presence in cooked peaches.

Sodium benzoate had the maximal impact on the aldehydes group (on 10 compounds from 20 identified). In fact, its addition decreased the concentration of several aldehydes, like: (*E*)-2-pentenal, heptanal,

(*E,E*)-2,4-hexadienal and (*Z*)-2-heptenal and octanal, while in case of benzaldehyde, decanal, 2,5-dimethylbenzaldehyde, (*E*)-2-decenal and 3-ethylbenzaldehyde it had a positive effect, because the concentration increased. The presence of sodium-benzoate had a negative effect on two esters: (*Z*)-3-hexen-1-ol and 5-ethyldihydro-2(3*H*)-furanone. In the group of terpenic compounds, two of them (α-terpinyl acetate and = *α*-cymene) had lower concentrations than control and samples preserved with citric acid, and two had significantly higher concentrations (*α*-terpineol and *α*-cyclocitral). Further, in Table 3, we can notice the increase in concentration of noxious compounds, like: benzene, benzoic acid (known to provoke urinary, angioedema, asthma and childhood hyperactivity [43]), 2-methyl--1,1'-biphenyl and biphenyl genotoxic to mice [44]. This may cause a less pronounced typical peach odor, and undesirable components.

7 volatile compounds from 57 identified were significantly higher in control samples. In this group can be classified two alcohols: 3-hexen-1-ol (grassy green), (*E*)-2-hexen-1-ol (green banana), two aldehydes: heptanal (fresh, green and citrus) and nonanal (fruity and floral), two esters: hexyl acetate (fruity and floral), 2-hexenyl acetate, as well as 2-pentylfuran (green and fresh). All compounds were already identified in fresh peaches, each having an individual aromatic impact, mostly characterized by fresh notes.

CONCLUSIONS

Differences in peach volatiles regarding seasons and variety were observed in all 4 cultivars. Groups of volatiles were specifically susceptible to monthly rainfall; however a general increase was noticed in the case of some aldehydes, esters, all identified lactones and terpenes in season with less rainfall. Beside seasonal also cultivars differences were observed and statistically evaluated. By applying the multiple group discriminant analysis, it was possible to discriminate all 4 cultivars by two functions. Function 1, which accounted for 56.9% of the variance explained by the model, was influenced more heavily by citric acid, linalool, (*E*)-2--hexenal and benzaldehyde and it was able to separate “Royal Glory“ from “Redhaven“. The second function, which accounted for another 31.7% of the explained variance, seems to be mostly associated with glucose content and to a less extent by sucrose, citric acid, linalool, 1-hexanol, (*E*)-2-hexenal and (*Z*)-3-hexenyl acetate was able to separate similar cultivars “Norman“ and “Maria Marta“.

Cooking by itself, in the other hand has an important impact on the aromatic profile of peaches. However, our interest was oriented in those, which were promoted or/and masked by the added preservatives. The statistical analysis indicated that from 57 identified volatiles, 40 volatiles showed statistically significant difference regarding the way of preservation. In case of 25 volatiles the treatment with sodium benzoate resulted in a significantly different amount of volatiles compared to control samples and samples treated with citric acid. Sodium benzoate had the maximal impact on the aldehyde group (on 10 compounds from 20 identified), a negative effect on two esters: (*Z*)-3-hexen-1-ol and 5-ethyldihydro-2(3H)-furanone. Terpenic compounds reacted in the presence of sodium-benzoate differently, two of them (*α*-terpinyl acetate and *α*-cymene) were of lower concentration, and two were of significantly higher concentration (*α*-terpineol and *α*-cyclocitral) than those observed in the case of control samples and samples preserved with citric acid. The most important and relevant observation came from the fact that the addition of sodium-benzoate caused the increase in concentration of noxious compounds, like: benzene, benzoic acid, 2-methyl-1,1'--biphenyl and biphenyl. All compounds are known to cause adverse health effects. The preservation with citric acid had significantly different contribution in case of only 4 volatiles, and 7 volatile compounds were significantly higher in control samples.

Acknowledgment

The authors would like to thank the Slovenian Research agency for financial support of the post-doctoral project Z4-2287, which enabled us to research the peach aromatic profile and spread the knowledge gained during the study of volatiles in peaches to other fruit and food processing analyses.

REFERENCES

[1] C.H. Crisosto, Peach quality and postharvest technology, Acta Hort. **713** (2006) 479–488.

[2] M. Colaric, R. Veberic, F. Stampar, M. Hudina, Evaluation of peach and nectarine fruit quality and correlations between sensory and chemical attributes**,** J. Sci. Food Agric. **85** (2005) 2611–2616.

[3] E. Costell, M.V. Pastor, L. Izquierdo, L. Durán, Relationships between acceptability and sensory attributes of peach nectars using internal preference mapping, Eur. Food Res. Technol. **211** (2000) 199–204.

[4] M. Esti, M.C. Messia, F. Sinesio, A. Nicotra, L. Conte, E. La Notte, G. Palleschi, Quality evaluation of peaches and nectarines by electrochemical and multivariate analyses: relationships between analytical measurements and sensory attributes, Food Chem. **60** (1997) 659–666.

[5] N. Kakiuchi, A. Ohmiya, Changes in the composition and content of volatile constituents in peach fruits in relation to maturity at harvest and artificial ripening, J. Jap. Soc. Hort. Sci. **60** (1991) 209–216.

[6] C. Aubert, C. Milhet, Distribution of the volatile compounds in the different parts of a white-fleshed peach

(*Prunus persica* L. Batsch), Food Chem. **102** (2007) 375––384.

[7] C. Visai, M. Vanoli, Volatile compound production during growth and ripening of peaches and nectarines, Sci. Hortic.-Amsterdam, **70** (1997) 15–24.

[8] A. Raffo, N. Nardo, M.R. Tabilio, F. Paoletti, Effects of cold storage on aroma compounds of white- and yellow-fleshed peaches, Eur. Food Res. Technol. **226** (2007) 1503–1512.

[9] S. Benedetti, S. Buratti, A. Spinardi, S. Mannino, I. Mignani, Electronic nose as a non-destructive tool to characterise peach cultivars and to monitor their ripening stage during shelf-life, Postharvest Biol. Tec. **47** (2008) 181–188.

[10] J. Brezmes, E. Llobet, X.Vilanova, G. Saiz, X. Correig, Fruit ripeness monitoring using an Electronic Nose, Sensor. Actuat., B **69** (2000) 223–229.

[11] C. Di Natale, A. Macagnano, E. Martinelli, E. Proietti, R. Paolesse, L. Castellari, S. Campani, A. D'Amico, Electronic nose based investigation of the sensorial properties of peaches and nectarines, Sensor. Actuat., B **77** (2001) 561–566.

[12] M.D. Spencer, R.M. Pangborn, W.G. Jennings, Gas chromatographic and sensory analysis of volatiles from cling peaches, J. Agr. Food Chem. **26** (1978) 725–732.

[13] A.A. Kader, C.M. Heintz, A. Chordas, Postharvest quality of fresh and canned clingstone peaches as influenced by genotypes and maturity at harvest, J. Am. Soc. Hort. Sci. **107** (1982) 947–951.

[14] F. Chinnici, U. Spinabelli, C. Riponi, A. Amati, Optimization of the determination of organic acids and sugars in fruit juices by ion-exclusion liquid chromatography, J. Food Compos. Anal. **18** (2005) 121–130.

[15] R. Scherer, A.C.P. Rybka, C.A. Ballus, A.D. Meinhart, J.T. Filho, H.T. Godoy, Validation of a HPLC method for simultaneous determination of main organic acids in fruits and juices, Food Chem. **135** (2012) 150–154.

[16] M. Genard, M. Souty, Modeling the peach sugar contents in relation to fruit growth, J. Am. Soc. Hort. Sci. **121** (1996) 1122–1131.

[17] C. Derail, T. Hofmann, P. Schieberle, Differences in Key Odorants of Handmade Juice of Yellow-Flesh Peaches (*Prunus persica* L.) Induced by the Workup Procedure, J. Agric. Food Chem. **47** (1999) 4742–4745.

[18] S.C. Andrés, L. Giannuzzi, N.E. Zaritzky, Mathematical modeling of microbial growth in packaged refrigerated orange juice treated with chemical preservatives, J. Food Sci. **66** (2001) 724–728.

[19] J.N. Bizri, I.A. Wahem, Citric acid and antimicrobials affect microbiological stability and quality of tomato juice, J. Food Sci. **59** (1994) 130–135.

[20] F. Ceylan, D.Y.C. Fung, J.R. Sabah, Antimicrobial activity and synergistic effect of cinnamon with sodium benzoate or potassium sorbate in controlling *Escherichia coli* O157: H7 in apple juice, J. Food Sci. **69** (2004) FMS102––FMS106.

[21] S. Pao, P.D. Petracek, Shelf life extension of peeled oranges by citric acid treatment, Food Microbiol. **14** (1997) 485–491.

[22] Senesi, R. Pastine, Pre-treatments of ready-to-use fresh cut fruits, Ind. Aliment.-Italy, **35** (1996) 1161–1166.

[23] D. McCann, A. Barrett, A. Cooper, D. Crumpler, L. Dalen, K. Grimshaw, E. Kitchin, K. Lok, L. Porteous, E. Prince, E. Sonuga-Barke, J.O. Warner, J. Stevenson, Food additives and hyperactive behaviour in 3-year-old and 8/9-year-old children in the community: a randomised, double-blinded, placebo-controlled trial. Lancet **370** (2007) 1560–1567.

[24] B.J. Freedman, Asthma induced by sulphur dioxide, benzoate and tartrazine contained in orange drinks, Clin. Exp. Allergy **7** (1977) 407–415.

[25] B. Nair, Effects of sodium benzoate in chronic exposure animal studies were limited to reduced feed intake and reduced growth, Int. J. Toxicol. **20** (2001) 23–50.

[26] S.A.V. Tfouni, M.C.F. Toledo, Determination of benzoic and sorbic acids in Brazilian food, Food Control. **13** (2002) 117–123.

[27] H. Zhang, M. Chang, J. Wang, S. Ye, Sensor Evaluation of peach quality indices using an electronic nose by MLR, QPST and BP network, Actuat., B **134** (2008) 332–338.

[28] C.H. Crisosto, G.M. Crisosto, G. Echeverria, J. Puy, Segregation of peach and nectarine (*Prunus persica* (L.) Batsch) cultivars according to their organoleptic characteristics, Postharvest Biol. Tec. **39** (2006) 10–18.

[29] S. Sansavini, The role of research and technology in shaping a sustainable fruit industry: European advances and prospects, Rev. Bras. Fruitic. **28** (2006) 550–558.

[30] T. Lavilla, I. Recasens, M.L. Lopez, J. Puy, Multivariate analysis of maturity stages, including quality and aroma, in 'Royal Glory'peaches and 'Big Top'nectarines, J. Sci. Food Agric. **82** (2002) 1842–1849.

[31] A. Versari, M. Castellari, G.P. Parpinello, C. Riponi, S. Galassi, Characterisation of peach juices obtained from cultivars Redhaven, Suncrest and Maria Marta grown in Italy. Food Chem. **76** (2002) 181–185.

[32] Y. Wang, C. Yang, S. Li, L. Yang, Y. Wang, J. Zhao, Q. Jiang, Volatile characteristics of 50 peaches and nectarines evaluated by HP–SPME with GC–MS, Food Chem. **116** (2009) 356–364.

[33] M. Riu-Aumatell, M. Castellari, E. López-Tamames, S. Galassi, S. Buxaderas, Characterisation of volatile compounds of fruit juices and nectars by HS/SPME and GC/MS, Food Chem. **87** (2004) 627–637.

[34] R.J. Horvat, G.W. Chapman, J.A. Robertson, F.I. Meredith, R. Scorza, A.M. Callahan, P. Morgens, Comparison of the volatile compounds from several commercial peach cultivars, J. Agr. Food Chem. **8** (1990) 234–237.

[35] R.J. Horvat, G.W. Chapman, Comparison of volatile compounds from peach fruit and leaves (cv. Monroe) during maturation, **J.** Agic. Food Chem. **38** (1990) 1442–1444.

[36] T. Lavilla, I. Recasens, M.L. Lopez, Production of volatile aromatic compounds in big top nectarines and royal glory peaches during maturity, Acta Hort. **553** (2001) 233–234.

[37] J.Y. Do, D.K. Salunkhe, L.E. Olson, Isolation, Identification and Comparison of the Volatiles of Peach Fruit as Related to Harvest Maturity and Artificial Ripening, J. Food Sci. **34** (1969) 618–621.

[38] J.A. Maga, I. Katz, Lactones in foods, Crit. Rev. Food Sci. Nutr. **8** (1976) 1–56.

[39] E.L. Singsaas, Terpenes and the thermotolerance of photosynthesis, New Phytol. **146** (2000) 1–2.

[40] S. Turtola, A.M. Manninen, R. Rikala, P. Kainulainen, Drought stress alters the concentration of wood terpenoids in Scots pine and Norway spruce seedlings, J. Chemic. Ecol. **29** (2003) 1981–1995.

[41] S. Nitz, H. Kollmannsberger, Changes in flavor composition during thermal concentration of apricot purée, Z. Lebensm. Unters. F., A **197** (1993) 541–545.

[42] M. Kawakami, S.N. Ganguly, J. Banerjee, A. Kobayashi, Aroma composition of oolong tea and black tea by brewed extraction method and characterizing compounds of Darjeeling tea aroma**,** J. Agric. Food Chem. **43** (1995) 200–207.

[43] T.E. Tuormaa, The adverse effects of food additives on health: a review of the literature with a special emphasis on childhood hyperactivity, J. Orthomol. Med. **9** (1994) 225–243.

[44] Y.F. Sasaki, S. Kawaguchi, A. Kamaya, M. Ohshita, K. Kabasawa, K. Iwama, K. Taniguchi, S. Tsuda, The comet assay with 8 mouse organs: results with 39 currently used food additives, Mutat. Res.-Gen. Tox. En. **519** (2002) 103–119.

IZVOD

AROMATIČNE MATERIJE RAZLIČITIH SORTI BRESAKA I UTICAJ KONZERVANASA NA FINALNU AROMU KUVANOG VOĆA

Mojca Bavcon Kralj[1], Tjaša Jug[1], Erika Komel[1], Nikita Fajt[1], Kristjan Jarni[2], Jelena Živković[3*], Ibrahim Mujić[4]

[1]*Chamber for Agriculture and Forestry of Slovenia, Agricultural and Forestry Institute Nova Gorica, Nova Gorica, Slovenia*

[2]*Department of Forestry and Renewable Forest Resources, Biotechnical Faculty, University of Ljubljana, Ljubljana, Slovenia*

[3]*Univerzitet u Nišu, Medicinski fakultet, Katedra za hemiju, Niš, Srbija*

[4]*Collegium Fluminense Polytechnic of Rijeka, Rijeka, Croatia*

(Naučni rad)

Breskva je sočan plod drveta *Prunus persica.* Aromu bresaka čine više stotina hemijskih jedinjenja koja pripadaju različitim klasama (alkoholi, estri, aledehidi, ketoni, laktoni, terpenska jedinjenja, itd.). Među materijama koje definišu aromu, kao predstavnici "zelene, nesazrele arome" se ističu (*E*)-2-heksenol i (*E*)-2-heksenal, dok su glavna jedinjenja koja definišu voćnu, zrelu aromu γ-dekalakton i γ-dodekalakton. Tokom sazrevanja sadržaj C6 jedinjenja (heksanala, (*E*)-2-heksenala) opada, dok koncentracija laktona raste. Sazrevanje bresaka i razvoj tipične arome bresaka jako zavisi od sadržaja laktona, (*δ*- i *γ*-dekalaktona). U ovom radu, tokom dvogodišnjeg perioda ispitane su aromatične materije sorti bresaka mesa žute boje, Royal Glory, Redhaven, Maria Marta i Norman. Metoda mikroekstrakcije u čvrstoj fazi – uzorkovanje iz gasovite faze (HS-SPME) je uspešno primenjena za određivanje isparljivih jedinjenja. Cilj našeg rada je bio da se na osnovu rezultata analiza tokom dvogodišnjeg perioda definišu jasne razlike između ispitivanih sorti u pogledu identifikovanih jedinjenja. Takođe, ispitivan je uticaj konzervanasa, natrijum-benzoata i olimunske kiseline, na aromu kuvanih bresaka. Sadržaj isparljivih komponenata je zavisio od mesečnih padavina, odnosno došlo je do povećanje sadržaja nekih aldehida, estara, kao i laktona i terpena u sezoni sa manje padavina. Međutim, pored razlike u sezonama, utvrđene su i razlike između ispitivanih sorti. U cilju razdvajanja – diskriminacije ispitivanih sorti na osnovu aromatičnog profila, korišćena je statistička diskriminantna analiza višestrukih grupa. Iako su jako slične, sorte su razdvojene na osnovu 2 funkcije, fukcije 1 (koja čini 56,9% po primenjenom modelu) i funkcije 2 (31,7%). Sa druge strane, upotreba konzervanasa ispoljava statististički značajan uticaj na aromatski profil kuvanih bresaka. Naime, od 57 identifikovanih isparljivih jedinjenja, kod 40 je utvrđena statistički značajna razliku u pogledu načina konzerviranja. Utvđeno je da je glavni negativan uticaj kao konzervans ispoljio natrijum-benzoat, u poređenju sa kontrolnim uzorkom i uzorcima kod kojih je dodata limunska kiselina.

Ključne reči: Aroma bresaka • Isparljive komponente bresaka • Diskriminantna analiza • Prehrambeni konzervansi • Mikroekstrakcija u čvrstoj fazi

Hemometrijski pristup razvoju kolorimetrijske metode za procenu količine prehrambenih boja u proizvodima od mesa

Radivoj B. Petronijević[1], Vesna F. Matekalo-Sverak[1], Aurelija T. Spirić[1], Ilija K. Vuković[2], Jelena A. Babić[1], Milan P. Milijašević[1], Dejana K. Trbović[1]

[1]*Institut za higijenu i tehnologiju mesa, Beograd, Srbija*
[2]*Univerzitet u Beogradu, Fakultet veterinarske medicine, Beograd, Srbija*

Izvod

Cilj ovog rada je bio da se, merenjem vrednosti parametara boje preseka proizvoda od mesa u CIE (*Commission Internationale de l'Eclairage*, Međunarodna komisija za osvetljenje) *L*a*b** prostoru (*L** – svetloća, *a** – udeo crvene boje i *b** – udeo žute boje) ispita mogućnost procene sadržaja dodate prehrambene boje u proizvodima od mesa. Količina prehrambene boje u uzorcima od mesa određena je metodom visokoefikasne tečne hromatografije sa detekcijom na fotodiodnom sloju (HPLC-PDA), a međusobna zavisnost dobijenih vrednosti i kolorimetrijskih parametara ispitana je višestrukom linearnom regresijom (MLR). Kalibracioni set od 10 proizvodnih partija fino usitnjene barene kobasice, sa tri dodate boje, izrađen je u industrijskim uslovima, i to: kontrolni proizvod bez boje i 9 proizvoda sa različitim količinama dodatih boja E 120 (3,4; 7,5 i 12,5 mg/kg), E 124 (5, 15 i 25 mg/kg) i E 129 (5, 15 i 25 mg/kg). Postavljene su jednačine funkcije zavisnosti količine boje od *L**, *a** i *b** vrednosti. Dobijeni matematički modeli su provereni i primenjeni za procenjivanje sadržaja boje u 21 uzorku fino usitnjenih barenih kobasica sa tržišta. Utvrđeno je da se kolorimetrijskom CIE *L*a*b** metodom mogu, u toku senzorskog ocenjivanja boje proizvoda, proceniti količine dodatih boja u proizvodima od mesa i da se ova metoda može primeniti kao komplementarna HPLC-PDA.

Ključne reči: *prehrambene boje, CIE L*a*b* kolorimetrijska metoda, HPLC-PDA, višestruka linearna regresija (MLR)*.

Dostupno na Internetu sa adrese časopisa: http://www.ache.org.rs/HI/

NAUČNI RAD

UDK 637.5.058:543.544.5:66

Hem. Ind. **68** (6) 781–791 (2014)

doi: 10.2298/HEMIND131204004P

Izgled proizvoda od mesa je jedna od važnijih karakteristika za njegovu prihvatljivost od strane potrošača [1], a zavisi od upotrebljenih sirovina i tehnološkog postupka koji je primenjen u toku proizvodnje. Izgled proizvoda od mesa i njegova prihvatljivost se može poboljšati dodavanjem prehrambenih boja. Najčešće se koriste veštačke i prirodne, crvene, boje. Po propisima EU, ali i u skladu sa nacionalnom regulativom, u fino usitnjenim barenim kobasicama dozvoljena je upotreba boje E 120 (Košenila, karminska kiselina) [2], do količine od 100 mg/kg proizvoda. Veštačke boje čija upotreba je dozvoljena samo u nekim proizvodima od mesa [3] su azo-boje [4] Ponso 4R (E 124) i Alura crvena AC (E 129). Istraživanja koja su poslednjih decenija sprovedena [5,6] pokazuju da sintetičke boje mogu da imaju negativne zdravstvene posledice kod osetljivih osoba i dece. Postoji sumnja da E 120 i neke dozvoljene veštačke, crvene, boje (E 124 i E 129) mogu da izazovu pojavu hiperaktivnosti kod dece, kožna oboljenja kod osetljivih i respiratorne probleme kod astmatičnih osoba [7,8]. Ne postoje pouzdani dokazi da su ove boje, pojedinačno, izazivači navedenih zdravstvenih problema [9], ali postoji opravdana indicija da mogu nepovoljno da utiču kada su u smeši, ili kada su pomešane sa drugim prehrambenim bojama i aditivima [7,10].

Za određivanje količina prirodnih i veštačkih boja u hrani razvijen je veliki broj različitih analitičkih metoda, kao što su spektrofotometrijske [11,12], elektrohemijske [13,14] i razne hromatografske metode (tankoslojna hromatografija, TLC, visokoefikasna tečna hromatografija, HPLC i jonska hromatografija, IC) [15–18] i kapilarna elektroforeza (CE) [19]. Autori saopštavaju da je navedenim metodama moguće određivanje dozvoljenih, prirodnih i sintetičkih, crvenih boja u prehrambenim proizvodima, pojedinačno ili u smeši. Međutim, u najvećem broju slučajeva, navedene metode se odnose samo na određivanje sintetičkih boja u hrani.

CIE (*Commission Internationale de l'Eclairage*, Međunarodna komisija za osvetljenje) [20] *L*a*b** kolorimetrijska metoda se, veoma često, uz senzorsko ocenjivanje, koristi za instrumentalno opisivanje boje proizvoda od mesa [21,22]. Metoda se zasniva na kolorimetrijskom kvantifikovanju vrednosti svetloće (*L**), udela crvene (*a**) i udela žute boje (*b**) površine predmeta na način koji je najsličniji percepciji boje predmeta ljudskog oka. Pošto se za merenje koriste kolorimetri (hromametri), CIE *L*a*b** merenja, za razliku od senzorskih ispitivanja, ne zavise od subjektivnosti ispi-

Prepiska: R.B. Petronijević, Institut za higijenu i tehnologiju mesa, Kaćanskog 13, 11000 Beograd, Srbija.
E-pošta: rpetronijevic@inmesbgd.com
Rad primljen: 4. decembar, 2013
Rad prihvaćen: 22. januar, 2014

tivača. Metoda je brza, ne zahteva komplikovanu pripremu uzoraka i merenja se mogu izvesti i van laboratorije. CIE *L*a*b** kolorimetrijska metoda se, sama ili zajedno sa multivarijantnim statističkim metodama, koristi za kvantitativno određivanje i predikciju promena boje kod proizvoda od mesa nastalih usled promene njegove recepture, atmosfere u koju se proizvod pakuje, načina pakovanja, itd. [23–25], ali se retko koristi u analitičke svrhe, za predikciju količine određene supstance u proizvodu [26]. Iz tih razloga nije postojala mogućnost poređenja dobijenih rezultata sa literaturnim. Merenje boje po CIE *L*a*b** sistemu ne može direktno da se koristi za određivanje količine dodate boje, jer druge obojene materije koje su prisutne u proizvodu, kao što je začinska paprika, ali i kategorija i boja upotrebljenog mesa utiču na boju preseka proizvoda [27,28]. Pouzdanost merenja zavisi od homogenosti boje preseka proizvoda, tako da će merenje *L**, *a** i *b** parametara boje proizvoda koji su fino usitnjeni (fino usitnjene barene kobasice) biti pouzdanije i tačnije nego u proizvodima sa nehomogenom bojom preseka.

Hemometrijska kalibracija analitičkih metoda podrazumeva korišćenje različitih regresionih modela (višestruka linearna regresija, MLR, regresija analizom glavnih komponenti, PCA-R, regresija metodom parcijalnih najmanjih kvadrata, PLS-R i dr) za utvrđivanje zavisnosti između analitičkih rezultata. Izbor modela zavisi od broja ulaznih nezavisnih promenljivih veličina (prediktora) kao i od broja uzoraka u kalibracionom setu. MLR model je najpogodniji za primenu kada je broj ulaznih nezavisnih promenljivih manji od broja uzoraka u kalibracionom setu [29].

Osnovni cilj ovog ispitivanja je bio da se razvije CIE *L*a*b** kolorimetrijska metoda za brzu procenu količina prehrambenih boja u proizvodima od mesa, na osnovu matematičkih modela izvedenih primenom višestruke linearne regresije rezultata dobijenih CIE *L*a*b** kolorimetrijskim i HPLC određivanjima. Drugi cilj je bio da se razvijena CIE *L*a*b** metoda, posle kalibracije i provere na eksperimentalnim proizvodima, primeni za procenu količina boja u fino usitnjenim barenim kobasicama sa tržišta.

EKSPERIMENTALNI DEO

Reagensi

Standardne supstance (Karminska kiselina, E 120, Ponso 4R, E 124, i Alura crvena AC, E 129) nabavljene su od SIGMA-ALDRICH (Nemačka). Organski rastvarači, metanol i acetonitril, su bili HPLC čistoće, CHROMASOLV, Sigma (Nemačka). Voda koja je korišćena za izradu standardnih rastvora boja i puferskog rastvora bila je HPLC čistoće, JT Baker (SAD).

Amonijum-acetat i sirćetna kiselina, koji su korišćeni za pripremu rastvora pufera, bili su p.a. čistoće, MERCK (Nemačka). Puferski rastvor pH vrednosti 7,1 je pripremljen rastvaranjem 3,8541 g amonijum-acetata u 1000 ml vode HPLC čistoće.

Proizvodi od mesa

Za potrebe razvoja CIE *L*a*b** metode multivarijantnom kalibracijom, kao i za proveru MLR modela, izrađeno je 10 proizvodnih partija fino usitnjenih barenih kobasica, prema recepturi za „parisku kobasicu“ (kalibracioni set). Za izradu kobasica korišćeno je svinjsko meso, juneće meso, emulzija kožica, sojino brašno, hidrirane sojine ljuspice, led, začini i aditivi. Sve proizvodne partije „pariske kobasice“ izrađene su u industrijskom pogonu, a svaka partija je, zbog različitih vrsta i količina boja, posebno pripremljena. Eksperimentalnom proizvodu su dodavane sledeće boje: E 120, E 124 i E 129. Vrste i količine boja koje su dodate eksperimentalnim kobasicama prikazane su u tabeli 1. Sintetičke boje (E 124 i E 129) su dodate u većim količinama (od 5 do 25 mg/kg) da bi se postigao sličan intenzitet boje kao sa dodatom prirodnom bojom E 120, koja je dodata u količinama navedenim u tabeli 1.

Tabela 1. Dodate boje eksperimentalnoj „pariskoj kobasici“
Table 1. Food colorants added to the experimental “Parisian sausage”

Proizvodna partija	Boja	Količina, mg/kg
1	–	0,00
2	E 120, Košenila	3,40
3	E 120, Košenila	7,50
4	E 120, Košenila	12,50
5	E 124, Ponso 4R	5,00
6	E 124, Ponso 4R	15,00
7	E 124, Ponso 4R	25,00
8	E 129, Alura crveno AC	5,00
9	E 129, Alura crveno AC	15,00
10	E 129, Alura crveno AC	25,00

CIE *L*a*b** kolorimetrijska metoda, koja je razvijena na osnovu eksperimentalnih model proizvoda, je primenjena za procenu količina boja u 21 proizvodu koji su nabavljeni iz više prodajnih objekata, poreklom od nekoliko domaćih proizvođača i iz uvoza.

Senzorsko ocenjivanje proizvoda

Boja preseka eksperimentalnih proizvoda i proizvoda sa tržišta ocenjivana je kvantitativno-deskriptivnom analizom po Uputstvu metodologije za senzorske analize, SRPS ISO 6658/2001 [30]. Na skali intenziteta od 1 do 5 ocenjivana je boja preseka proizvoda od mesa. Ispitivanja je izvršilo šest obučenih ocenjivača. Za ocenu boje eksperimentalnih proizvoda je korišćena kvantitativno-deskriptivna skala sa sledećim ocenama:

1 – neprihvatljiva boja, 2 – boja na granici prihvatljivosti, 3 – prihvatljiva boja, 4 – veoma prihvatljiva boja i 5 – izuzetno prihvatljiva boja.

Priprema uzoraka za hromatografska ispitivanja

Za izolovanje boja iz proizvoda od mesa korišćena je ubrzana ekstrakcija rastvaračima, pri visokom pritisku i temperaturi (*Accelerated Solvent Extraction*, ASE), [18], na aparatu ASE 100 (Dionex, SAD). Masa uzorka za ispitivanje iznosila je 1 g. Boje iz proizvoda od mesa su ekstrahovane pomoću metanola na temperaturi od 70 °C, u 4 ekstrakciona ciklusa od po 12 min. Ekstrakti su spojeni i potom, na rotacionom vakuum uparivaču, upareni do suva. Suvi ostatak je rastvoren u 2 ml 1:1 zapreminske smeše acetonitrila i amonijum-acetata, 50 mmol/dm^3. Ukupno vreme potrebno za ekstrakciju uzorka je oko 1 h.

HPLC-PDA hromatografija

Količina boje u ispitanim proizvodima od mesa je određena visokoefikasnom tečnom hromatografijom. Sistem za hromatografiju se sastojao od tečnog hromatografa sa autosemplerom Alliance 2695 Separations Module (Waters, SAD), sa detektorom sa fotodiodnim slojem 2996 Photodiode Array Detector (Waters, SAD). Hromatografsko razdvajanje boja je postignuto na Phenomenex Kinetex reverzno-faznoj C18 koloni, dimenzija 150×4,60 mm i veličina čestica 2,6 μm. Mobilna faza se sastojala od rastvora 50 mmol/dm^3 amonijum-acetata pH vrednosti 7,1 (A) i acetonitrila (B). Pri hromatografskom određivanju udeo A u mobilnoj fazi je postepeno opadao od 100 do 40% u toku 12 min od injektovanja dok je istovremeno udeo B rastao od 0 do 60%, a potom je sastav mobilne faze naglo vraćen na početne vrednosti (gradijent mobilne faze). Boje su identifikovane na osnovu njihovih retencionih vremena iz hromatograma izvedenih iz trodimenzionalnih podataka koji su dobijeni detekcijom na fotodiodnom sloju. Potvrda prisustva boja je izvršena na osnovu UV spektara izvedenih iz istih podataka. Radni opseg metode je od 1–100 mg/kg boje u uzorku. Vreme potrebno za akviziciju hromatograma uzorka iznosilo je 15 min. Određivanje vrste i sadržaja boja u eksperimentalnim proizvodima, visokoefikasnom tečnom hromatografijom, je rađeno u 6 ponavljanja. Izračunate su standardne devijacije određivanja, koeficijenti varijacije i povratni prinos (recovery).

Određivanje boje (CIE *L*a*b) kolorimetrijskom metodom**

Merenja *L**, *a** i *b** vrednosti boje preseka eksperimentalnih proizvoda po CIE *L*a*b** sistemu izvršeno je aparatom Chromameter CR-400, Konica Minolta Co. Ltd. (Japan). Proizvodi su snimani, posle kalibracije uređaja, pri sledećim uslovima: prečnik otvora objektiva 8 mm, standardno CIE D65 difuzno osvetljenje, izvor svetlosti – pulsna ksenonska lampa, ugao vidljivosti 0 stepeni. Vrednosti su merene na poprečnim presecima, odmah posle narezivanja. Proizvodi su narezivani poprečno u odnosu na uzdužnu osu, na rastojanju od 1–2 cm, tako da se dobije šest paralelnih preseka proizvoda.

Statistička obrada podataka

Deskriptivna statistika je primenjena za obradu dobijenih rezultata, koji su prikazani u tabelama u obliku "srednja vrednost±standardna devijacija" (*SD*). Statističke značajnosti rezultata su utvrđene *t*-testovima i analizom varijanse (ANOVA). Matematički modeli su dobijeni višestrukom linearnom regresijom (MLR) rezultata CIE *L*a*b** kolorimetrijskih ispitivanja i HPLC određivanja količina boja dodatih eksperimentalnim proizvodima.

Višestruka linearna regresija (*Multiple Linear Regression*, MLR) je data opštom jednačinom oblika:

$$Y_i = \alpha + \beta_1 X_{i,1} + \ldots + \beta_n X_{i,n} + \varepsilon_i \quad (1)$$

gde su Y_i – zavisno promenljiva veličina, $X_{i,j}$ – nezavisno promenljiva veličina, j – broj nezavisno promenljivih, a i – broj merenja, α – odsečak prave, β – koeficijenti, a ε_i – greška merenja. Kraće se jednačina (1) može napisati:

$$Y_i = E(Y|X_i) + \varepsilon_i \quad (2)$$

gde je $E(Y|X_i)$ funkcija eksperimentalno određene zavisno promenljive Y za i merenja nezavisno promenljive X.

Za statističku obradu rezultata i izračunavanja su korišćeni softverski paketi MS Office Excel i JMP 10 Statistical Discovery (SAS Institute, SAD).

REZULTATI

Senzorsko ocenjivanje eksperimentalnih proizvoda od mesa

Senzorske ocene boje eksperimentalne „pariske kobasice" su prikazane u tabeli 2. Na osnovu prikazanih rezultata može da se konstatuje da je boja preseka kontrolnog proizvoda, eksperimentalne barene kobasice bez dodate boje, ocenjena kao prihvatljiva (3,00). Najviše ocene su dobile proizvodne partije 2, 6 i 9 (4,50; 4,42 i 4,40, redom).

Srednje vrednosti senzorskih ocena boje eksperimentalne „pariske kobasice" statistički su upoređene analizom varijanse i Taki–Kramer testom [31] poređenja srednjih vrednosti. Proizvodne partije „pariske kobasice" 2, 6 i 9 su najprihvatljivije u pogledu boje preseka. Njihove ocene su bile između 4,00 i 4,50. Najprihvatljiviju boju preseka je imala „pariska kobasica" sa najmanjim sadržajem E 120 (3,4 mg/kg, proizvodna partija 2), a zatim „pariska kobasica" sa sadržajem E 124 (proizvodna partija 6) i E 129 (proizvodna partija 9), u količini od 15 mg/kg. Za prihvatljivost boje preseka, senzorne ocene „pariske kobasice" proizvod-

Tabela 2. Senzorske ocene boje eksperimentalne „pariske kobasice“
Table 2. Sensory evaluation of the color of experimental “Parisian sausage”

Proizvodna partija	Boja	Prihvatljivost boje preseka
1	–	3,00±0,32
2	E120	4,50±0,45[a]
3	E120	3,83±0,26[b]
4	E120	2,77±0,41[c]
5	E124	3,67±0,41[b]
6	E124	4,42±0,20[a]
7	E124	3,80±0,45[b]
8	E129	3,50±0,45[b]
9	E129	4,40±0,32[a]
10	E129	3,50±0,32[b]

nih partija 3, 5, 7, 8 i 10 su bile između 3,50 i 4,00, a za postojanost boje, u proseku, oko 3,50. Proizvodne partije eksperimentalne „pariske kobasice“ 1 i 4 su, u ovim kategorijama, dobile najmanje ocene. Boja preseka proizvodne partije 1 je bila previše svetla, a partije 4 previše intenzivna.

CIE *L*a*b** kolorimetrijska ispitivanja

Rezultati merenja boje eksperimentalne „pariske kobasice“ prikazani su u tabeli 3. Srednje *L**, *a** i *b** vrednosti eksperimentalnog proizvoda bez dodate boje su bile 73,07, 11,04 i 13,89, redom.

Za proizvode kojima su dodate boje vrednosti *L** su bile manje nego kod kontrolnog proizvoda (od 69,52 do 70,81 za proizvod sa bojom E 120, od 70,14 do 71,33 za proizvod sa bojom E 124 i od 69,78 do 72,14 za proizvod sa bojom E 129). Vrednosti *a** eksperimentalne „pariske kobasice“ sa dodatom bojom su bile veće u odnosu na vrednosti istog parametra kontrolnog proizvoda (od 13,60 do 17,53 za proizvodne partije sa bojom E 120, od 13,19 do 16,27 za proizvode sa bojom E 124 i od 12,43 do 17,50 za proizvod sa dodatom bojom E 129). Vrednosti *b** eksperimentalnih proizvodnih partija sa bojom E 120 su bile manje nego kod kontrolnog proizvoda (od 11,66 do 13,49), dok su vrednosti *b** proizvodnih partija sa bojama E 124 i E 129 bile veće (od 14,26 do 14,55 i od 14,15 do 14,56 redom).

*Tabela 3. L*a*b* vrednosti boje preseka eksperimentalne „pariske kobasice“*
*Table 3. L*a*b* values of the cross-section color of experimental “Parisian sausage”*

Proizvodna partija	*L**	*a**	*b**
1	73,07±0,34	11,04±0,23	13,89±0,18
2	70,81±0,48[a]	13,60±0,27[c]	13,49±0,23[a]
3	70,80±0,39[a]	15,50±0,27[b]	12,96±0,25[b]
4	69,52±0,32[b]	17,53±0,26[a]	11,66±0,17[c]
5	71,33±0,41[a]	13,19±0,99[c]	14,26±0,24[a]
6	70,82±0,43[a]	14,78±0,92[b]	14,29±0,43[a]
7	70,14±0,09[b]	16,27±0,15[a]	14,55±0,11[a]
8	72,14±0,26[a]	12,43±0,17[c]	14,15±0,40[a]
9	70,90±0,21[b]	14,90±0,22[b]	14,36±0,45[a]
10	69,78±0,20[c]	17,50±0,20[a]	14,56±0,51[a]

Zavisnost vrednosti *a**, koja predstavlja udeo crvene boje u CIE *L*a*b** sistemu, od količine dodate boje u eksperimentalnim barenim kobasicama je prikazana na slici 1.

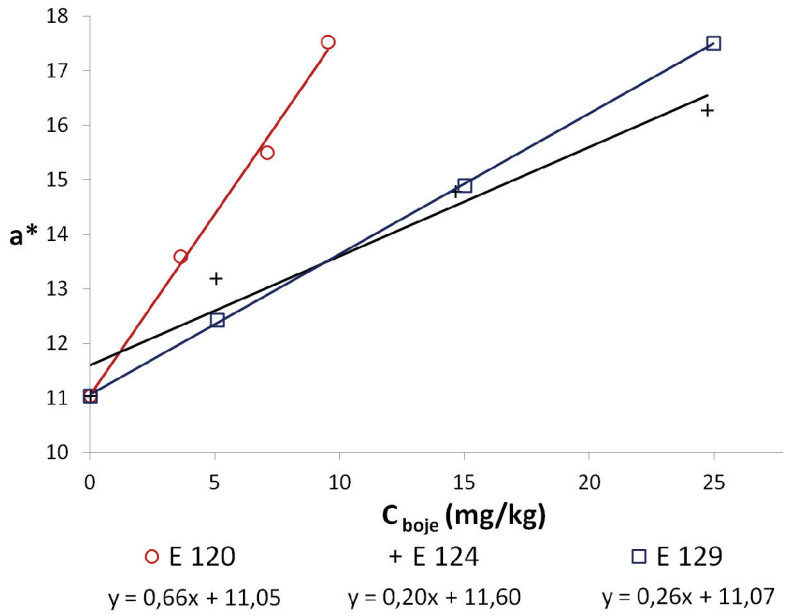

Slika 1 .Zavisnost a vrednosti od količine dodate boje u eksperimentalnim barenim kobasicama.*
Figure 1. Correlation of a value and added food colorant in experimental cooked sausages.*

HPLC ispitivanja

Rezultati određivanja boje tečnom hromatografijom u eksperimentalnim proizvodima su prikazani u tabeli 4.

Vrednosti za povratne prinose kod određivanja boje E 120 u „pariskoj kobasici“ su bile u opsegu od 76,15 do 107,04%, kod određivanja boje E 124 bile su u opsegu od 97,61 do 101,03%, a kod određivanja boje E 129 bile su u opsegu od 99,91 do 101,67%. Standardne devijacije određivanja količina boja u „pariskoj kobasici“ bile su u intervalu od 0,04 do 0,23 mg/kg, za E 120, od 0,31 do 0,54 mg/kg, za E 124 i od 0,18 do 0,26 mg/kg, za E 129.

Višestruka linearna regresija

Za kalibraciju rezultata merenja boje preseka eksperimentalnih proizvoda po CIE $L^*a^*b^*$ sistemu i tečno-hromatografskog određivanja sadržaja boje korišćena je višestruka linearna regresija [29]. Za obradu su upotrebljene vrednosti L^*, a^* i b^* eksperimentalnih proizvoda (nezavisne promenljive, X) i hromatografskog određivanja (zavisna promenljiva, Y). Svaki kalibracioni set za E120, E124 i E129 činile su po tri proizvodne partije sa različitim količinama boje i jedna proizvodna partija bez boje (kontrola). Ispitivanja su urađena u šest ponavljanja, što ukupno predstavlja 24 određivanja po jednom kalibracionom setu. Rezultati višestruke linerne regresije su prikazani u tabeli 5. Na osnovu prikazanih rezultata može se konstatovati da su vrednosti koeficijenata determinacije (R^2) linearnih modela kod „pariske kobasice“0,954, za E 124, 0987, za E 120 i 0,993, za E129, a vrednosti korena srednjeg kvadrata greške modela (*Root Mean Square Error*, *RMSE*) 0,445, 2,228 i 0,881, redom.

Korišćenjem jednačine (1) dobijeni su matematički modeli – regresione jednačine procene sadržaja boja u fino usitnjenim barenim kobasicama:

$$Y_{E120} = 0{,}39L^* + 1{,}77a^* + 0{,}28b^* - 51{,}78 \quad (3)$$

$$Y_{E124} = 0{,}0095L^* + 4{,}90a^* - 1{,}99b^* - 28{,}25 \quad (4)$$

$$Y_{E129} = -1{,}19L^* + 3{,}23a^* + 0{,}51b^* + 43{,}92 \quad (5)$$

gde su Y koncentracije ispitanih boja u proizvodu, izražene u mg/kg.

Tabela 5. Koeficijenti determinacije i statistička značajnost parametara dobijenih pomoću MLR; R^2 – koeficijent determinacije, RMSE – koren srednjeg kvadrata greške modela, Prob>|t| – vrednost verovatnoće kao mera statističke značajnosti
Table 5. Coefficients of determination and statistical significance of parameters obtained by MLR

Parametar	E 120	E 124	E 129
R^2	0,987	0,954	0,993
RMSE	0,445	2,228	0,881
Broj određivanja	24	24	24
Odsečak	51,78	28,25	43,92
	Koeficijenti		
L^*	0,39	0,0095	-1,19
a^*	1,77	4,90	3,23
b^*	0,28	-1,99	0,51
	Prob>|t|		
L^*	0,0491*	0,9930*	0,0702*
a^*	<0,0001*	<0,0001*	<0,0001*
b^*	0,3148*	0,2980*	0,4894*

Rezultati za količine boja u eksperimentalnoj „pariskoj kobasici“ koji su dobijeni hromatografskim određivanjem i odgovarajuće vrednosti koje su izračunate na osnovu jednačina (3)–(5) prikazani su u tabeli 6.

Zamenom L^*, a^* i b^* vrednosti, koje su izmerene za svaki proizvod, u odgovarajućim jednačinama, izračunate su količine boja u tim proizvodima i poređene su sa rezultatima HPLC ispitivanja. Za poređenje je korišćen dvosmerni t-test. Za E 120 i E 129 nije bilo značajnih odstupanja između hromatografski određene količine boje u eksperimentalnim proizvodima i količine boje koja je izračunata matematičkim modelom. U slučaju E 124, postojala je statistički značajna razlika

Tabela 4. Rezultati HPLC-PDA određivanja dodatih boja u eksperimentalnoj „pariskoj kobasici“
Table 4. HPLC-PDA data for the added food colorants to experimental “Parisian sausage”

Proizvodna partija	Boja	Količina dodate boje mg/kg	Određena količina mg/kg	Standardna devijacija mg/kg	Koeficijent varijacije %	Povratni prinos, %
1	–	–	–	–	–	–
2	E120	3,4	3,63	0,22	6,15	107,04
3	E120	7,5	7,10	0,04	0,51	94,62
4	E120	12,5	9,52	0,23	2,37	76,15
5	E124	5	5,05	0,54	10,75	101,03
6	E124	15	14,64	0,31	2,13	97,61
7	E124	25	24,74	0,41	1,68	98,95
8	E129	5	5,08	0,21	4,11	101,67
9	E129	15	15,01	0,18	1,17	100,04
10	E129	25	24,98	0,26	1,03	99,91

*Tabela 6. Količine boja određene HPLC i CIE L*a*b* metodama u eksperimentalnim barenim kobasicama*
*Table 6. Quantities of food colorants determined by HPLC and CIE L*a*b* methods in experimental cooked sausages*

Proizvodna partija	Boja	HPLC određivanje, mg/kg	Izračunato po modelu, mg/kg	Prob>|t|
1	–	–	0,11±0,51	0,634
2	E120	3,63±0,22	3,65±0,42	0,897
3	E 120	7,10±0,04	6,88±0,38	0,204
4	E 120	9,52±0,23	9,61±0,34	0,572
5	E 124	5,05±0,54	6,89±1,85	0,059
6	E 124	14,64±0,31	15,41±2,52	0,493
7	E 124	24,74±0,41	23,24±0,67	**0,002***
8	E 129	5,08±0,21	5,66±0,77	0,131
9	E 129	15,01±0,18	14,62±1,24	0,487
10	E 129	24,98±0,26	24,99±0,33	0,955

između vrednosti eksperimentalno određenih količina i količina izračunatih po matematičkom modelu za količinu boje od 25 mg/kg. Grafički prikaz međusobnih odnosa rezultata dobijenih na osnovu HPLC ispitivanja i modela zasnovanog na CIE *L*a*b** kolorimetrijskoj metodi dat je na slici 2.

Proizvodi sa tržišta

Metoda tečne hromatografije za određivanje boja i CIE *L*a*b** kolorimetrijska metoda su primenjene za ispitivanje fino usitnjenih barenih kobasica sa domaćeg tržišta. Ispitan je ukupno 21 proizvod fino usitnjenih barenih kobasica. Od toga, 18 uzoraka (85,71%) su proizvodi domaćih proizvođača, a tri (14,29%) su proizvodi iz uvoza. Senzorskim ispitivanjem je ocenjena boja preseka proizvoda, CIE *L*a*b** kolorimetrijskom metodom su određeni parametri boje, a tečnom hromatografijom je određena vrsta i količina dodate boje u proizvode. Rezultati ispitivanja su prikazani u tabeli 7. Za 12 (57,14%), od ukupnog broja ispitanih proizvoda, prihvatljivost boje preseka je ocenjena ocenom manjom od 3,50. Od tih proizvoda, četiri (33,33%) je imalo slabo izraženu boju preseka, a 8 (66,67%) suviše intenzivnu boju. Od ukupno 21 ispitanog proizvoda, u 20 (95,24%), utvrđeno je prisustvo boje, a samo u jednom proizvodu (4,76%) nije ustanovljeno prisustvo boje. Od proizvoda u kojima je dokazana boja, u 16 proizvoda (80,00%) je ustanovljena boja E 120, a u četiri (20,00%) boja E 129. Prisustvo boje E 124 nije ustanovljeno ni u jednom od ispitanih proizvoda.

Na rezultate merenja prisustva dodatih boja u proizvodima sa tržišta primenjeni su matematički modeli dobijenim višestrukom linearnom regresijom (jednačine (3) i (5)). Izračunate vrednosti za količine boja u pro-

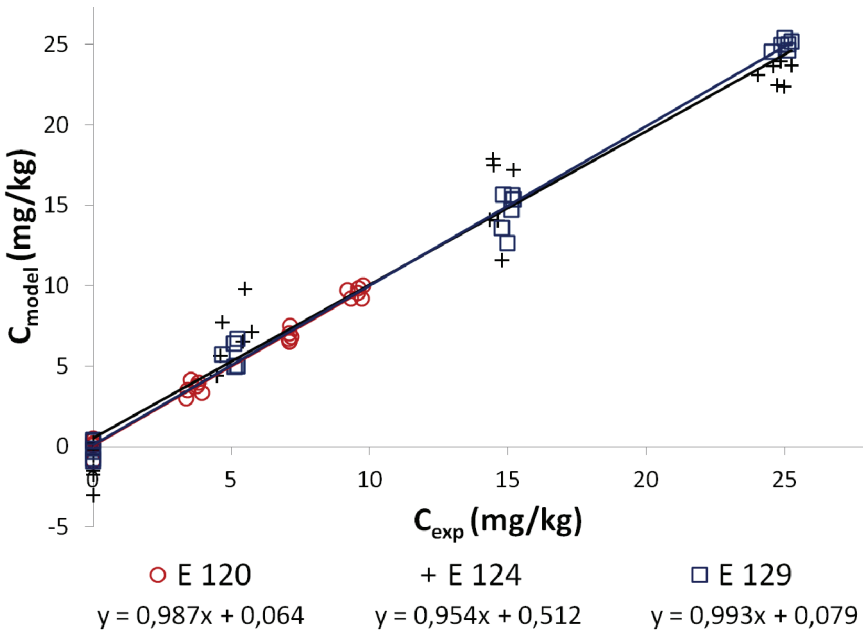

*Slika 2. Provera L*a*b* modela kod određivanja sadržaja boja u eksperimentalnim barenim kobasicama.*
*Figure 2. Evaluation of L*a*b* model in determination of food colorants in experimental sausages.*

*Tabela 7. Senzorske ocene, rezultati CIE L*a*b* i HPLC ispitivanja uzoraka sa tržišta*
*Table 7. Sensory evaluation, CIE L*a*b* and HPLC data for the samples from retail*

R. br.	Senzorska prihvatljivost boje preseka	CIE *L*a*b** merenja boje preseka			Količina boje, mg/kg		Indentifikovana boja[d)]
		*L**	*a**	*b**	HPLC određivanje	Izračunato po modelu	
1	3,08±0,20[b)]	67,60±0,33	15,63±0,23	16,12±,019	3,35±0,16	6,76±0,34	E120
2	4,92±0,20	74,71±0,26	14,30±0,07	13,78±0,14	2,82±0,14	6,50±0,08	E120
3	4,67±0,26	75,79±2,69	13,08±1,85	11,73±0,38	3,27±0,15	4,17±2,31	E120
4	2,83±0,26[a)]	66,25±0,55	16,21±0,18	20,73±0,18	74,95±0,63	73,32±3,81	E129
5	3,00±0,00[a)]	68,11±0,38	15,14±0,26	17,63±0,24	42,45±0,14	41,83±3,08	E129
6	3,25±0,27[b)]	72,78±0,64	8,83±0,20	13,67±0,11	ND[c)]	–3,99±0,20	–
7	3,25±0,27[b)]	63,97±0,46	19,29±0,13	14,92±0,09	3,72±0,11	11,49±0,17	E120
8	4,83±0,26	69,01±0,35	15,61±0,17	12,88±0,09	3,39±0,14	6,35±0,22	E120
9	4,92±0,20	72,24±0,30	14,77±0,14	11,96±0,06	3,07±0,14	5,86±0,16	E120
10	3,58±0,49	68,63±0,53	16,57±0,05	11,98±0,18	3,98±0,15	7,65±0,21	E120
11	3,00±0,32[a)]	66,96±0,44	15,71±0,18	13,65±0,36	3,34±0,14	5,95±0,35	E120
12	2,50±0,32[a)]	68,41±0,26	14,31±0,18	13,90±0,21	2,44±0,16	4,10±0,29	E120
13	3,25±0,65[a)]	69,48±0,44	15,26±0,23	14,97±0,12	19,94±0,23	18,76±2,13	E129
14	2,25±0,50[b)]	68,02±0,62	15,14±0,21	15,57±0,13	2,87±0,13	5,89±0,76	E120
15	4,63±0,25	66,83±0,19	17,01±0,08	12,56±0,15	3,55±0,09	7,90±0,18	E120
16	4,75±0,29	71,35±0,19	14,87±0,09	13,04±0,07	2,92±0,22	5,99±0,22	E120
17	3,38±0,48[a)]	68,92±1,00	14,78±0,13	17,12±0,47	40,38±0,52	37,33±8,17	E129
18	3,38±0,25[a)]	62,53±0,35	19,83±0,24	14,50±0,10	4,69±0,21	11,78±0,42	E120
19	3,00±0,41[a)]	63,60±0,46	19,16±0,19	15,68±0,21	4,32±0,15	11,33±0,21	E120
20	4,00±0,00	67,84±0,19	15,86±0,15	14,32±0,09	3,39±0,21	6,75±0,26	E120
21	4,13±0,25	68,82±0,21	15,45±0,07	14,74±0,07	3,58±0,27	6,52±0,09	E120

[a)]Boja preseka intenzivna; [b)]boja preseka slabo izražena; [c)]ND – nije detektovano prisustvo boje; [d)]identifikacija boje na osnovu UV spektra dobijenog iz PDA podataka

izvodima od mesa, zajedno sa eksperimentalno određenim vrednostima tečno-hromatografskom metodom, su, takođe, prikazane u tabeli 7.

DISKUSIJA

Senzorskim ocenjivanjem boje preseka eksperimentalnih proizvoda utvrđeno je da su proizvodi kojima je dodata boja imali bolju prihvatljivost od kontrolnog proizvoda. Samo proizvod sa najvećom količinom (12,5 mg/kg) dodate boje E 120 je ocenjen lošije od kontrolnog proizvoda, jer je njegova boja bila previše intenzivna. Kolorimetrijskim merenjem boje preseka eksperimentalne „pariske kobasice“ dobijeni su podaci za svetloću boje preseka, *L**, za udeo crvene boje, *a**, i za udeo žute boje, *b**. Eksperimentalna „pariska kobasica“ sa dodatkom boja imala je manje vrednosti za svetloću, u odnosu na proizvod bez dodate boje. Takođe, može da se konstatuje da je sa porastom količine dodate boje opadala vrednost *L**, kod sve tri serije eksperimentalne „pariske kobasice“. Kod proizvoda kojima su dodate boje E 124 i E 129 vrednosti *L** su se linearno smanjivale sa povećanjem količine boje, dok kod „pariske kobasice“ sa dodatom bojom E 120, vrednosti *L** su, sa povećanjem količine boje u proizvodima, nelinearno opadale .

Rezultati kolorimetrijskog određivanja boja E 120, E 124 i E 129 u eksperimentalnoj „pariskoj kobasici“ pokazuju da je između vrednosti *a** i količina sve tri boje u proizvodima postojala linearna zavisnost. Najveći porast vrednosti a* sa povećanjem količine dodate boje je ustanovljen kod „pariske kobasice“ sa dodatom bojom E 120 (nagib prave 0,66), zatim kod proizvoda sa dodatom bojom E 129 (nagib prave 0,26), a najmanji porast je ustanovljen kod proizvoda sa dodatom bojom E 124 (nagib prave 0,20), slika 1. Uzimajući u obzir činjenicu da su količine boje E 120, koje su korišćene pri izradi „pariske kobasice“, bile manje od količina druge dve boje (tabela 2), može se zaključiti da ova boja intenzivno boji proizvode od mesa.

Kolorimetrijska merenja udela žute boje (tabela 3) su pokazala da je eksperimentalna „pariska kobasica“ sa dodatim veštačkim bojama E 124 i E 129 imala veće vrednosti za *b** u odnosu na kontrolni proizvod. Eksperimentalna „pariska kobasica“ kojoj je dodata boja E 120 imala je manju vrednost za *b** u odnosu na proizvode sa sintetičkim bojama E 124 i E 129 i kontrolni proizvod. Na osnovu prikazanih rezultata može da se

konstatuje i da vrednost *b** opada sa povećanjem količine dodate boje, kod proizvodnih partija „pariske kobasice“ kojima je dodata boja E 120. Kod eksperimentalne „pariske kobasice“ sa dodatim sintetičkim bojama, sa porastom količine dodate boje vrednost *b** blago raste.

Rezultati hromatografskih ispitivanja sadržaja boja u eksperimentalnoj „pariskoj kobasici“, koji su prikazani u tabeli 4, pokazuju da su povratni prinosi boja u okviru analitičkih očekivanja, osim u slučaju eksperimentalne „pariske kobasice“ iz proizvodne partije 4, kod koje je vrednost povratnog prinosa bila ispod 80 %. Imajući u vidu da je eksperimentalna „pariska kobasica“ proizvedena u industrijskom pogonu, gde uslovi eksperimentalne proizvodnje nisu optimalni, ovakav rezultat povratnog prinosa može da bude prihvatljiv. U literaturi postoje podaci o primeni HPLC metode sa ASE ekstrakcijom, ali se ona odnosi samo na određivanje veštačkih boja. [18]. Rezultati povratnog prinosa za E 124 i E 129 (97,61–101,30% i 99,91–101,67%, redom), koji su dobijeni u okviru naših istraživanja, su veći u poređenju sa navedenim literaturnim podacima za povratni prinos boje E 124 (76,9–83,6%) i boje E 129 (80,9–84,6%).

Wu i Sun [32] su prikazali obiman pregled metoda merenja boje u širokom spektralnom opsegu, koje su korišćene za kvalitativnu i kvantitativnu kontrolu kvaliteta hrane. Autori navode da je CIE *L*a*b** kolorimetrijska metoda jedna od najčešće korišćenih, zahvaljujući uniformnoj distribuciji boja i zbog činjenice da je najpribližnija percepciji boje ljudskog oka. Međutim, sve navedene metode se koriste za predikciju osobina boje i za senzorsko ocenjivanje pri kontroli kvaliteta hrane. Većina metoda koristi kompleksne algoritme i multivarijantne metode za kalibraciju, kao što je regresija metodom analize glavnih komponenti (PCA-R), ili regresija metodom delimičnih najmanjih kvadrata (PLS-R). Metoda kompjuterske obrade digitalnih snimaka proizvoda [26] je primenjena za određivanje sadržaja šećera u belom grožđu, uz PLS-R kalibraciju. Ove metode se koriste pri obradi skupa podataka, gde je broj prediktora veći od broja uzoraka u kalibracionom setu, kao što je slučaj kod digitalnih fotografija. Sa druge strane, MLR je primenljiva u slučaju kada je broj kalibracionih uzoraka veći od broja prediktora [29]. Stoga je, u ovom istraživanju, MLR korišćena za kalibraciju CIE *L*a*b** metode za određivanje boja u proizvodima od mesa, jer se primenjeni kalibracioni set sastojao od 10 eksperimentalnih proizvoda na čijim presecima su merene vrednosti tri prediktorske promenljive, *L**, *a** i *b**.

Pouzdanost MLR modela za predikciju rezultata može se proceniti na osnovu vrednosti R^2 i *RMSE*. Vrednosti R^2 za sva tri MLR modela (tabela 5) su bliske vrednosti 1, pri čemu je najveća vrednost dobijena kod modela za boju E 129, a najmanja za E 124. *RMSE* vrednost je najmanja kod modela za boju E 120, a najveća kod modela za boju E 124. Prikazane R^2 i *RMSE* vrednosti pokazuju da su modeli za boje E 120 i E 129 pouzdaniji, odnosno da se mogu uspešnije primeniti kod procene količine tih boja u barenim kobasicama od MRL modela za boju E 124. Na osnovu vrednosti verovatnoća (Prob>|t|) dobijenih analizom rezultata MLR, koje su prikazane u tabeli 5, može da se konstatuje da je udeo crvene boje, odnosno vrednost *a**, najuticajniji faktor kod određivanja sadržaja boje CIE *L*a*b** kolorimetrijskom metodom kod svih eksperimentalnih proizvoda. Ovakav zaključak je logičan, s obzirom da dodavanje crvene prehrambene boje u proizvode od mesa najviše utiče na promenu vrednosti *a**. Poređenjem količina boja u eksperimentalnim proizvodima koje su određene tečnom hromatografijom sa količinama boja izračunatim po CIE *L*a*b** modelu, dvosmernim *t*-testom, za boje E 120 i E 129 je potvrđeno dobro slaganje rezultata u celom opsegu ispitivanja, dok je za boju E 124 model pokazao odstupanje pri koncentraciji od 25 mg/kg. Odstupanje može da bude posledica nelinearne zavisnosti koncentracije boje od kolorimetrijskih vrednosti u mernom opsegu, što je, ujedno, uzrok veće vrednosti koja je dobijena za *RMSE* kod ovog modela.

Rezultati primene razvijenih *L*a*b** modela na proizvodima od mesa sa tržišta (tabela 7) pokazuju da se pomoću CIE *L*a*b** modela dobijaju veće vrednosti za sadržaj E 120 nego primenom metode tečne hromatografije. Količine boje E 120 u barenim kobasicama dobijene hromatografskim ispitivanjem bile su u intervalu od 2,44 do 4,69 mg/kg, a CIE *L*a*b** modelom u intervalu od 4,10 do 11,78 mg/kg. Razlike između rezultata dobijenih po CIE *L*a*b** modelu i na osnovu HPLC određivanja mogu poticati od, na primer, količine crvene paprike u ekstraktu paprike dodatom u toku izrade fino usitnjenih barenih kobasica [27,28]. CIE *L*a*b** kolorimetrijskom metodom se meri zbir svih obojenih konstituenata na površini preseka proizvoda, a dodata boja je samo jedna komponenta tog zbira. Pošto je kolorimetrijska CIE *L*a*b** metoda razvijena za procenu količine boje, a ne za precizna određivanja, može se smatrati da su dobijeni rezultati prihvatljivi.

CIE *L*a*b** model za procenu količine boje E 129 u fino usitnjenim barenim kobasicama pokazuje mnogo bolje slaganje rezultata sa rezultatima koji su dobijeni HPLC metodom. Pošto je ispitan mali broj uzoraka, samo četiri, nije moguće izvesti pouzdan zaključak o primeni postavljenog modela kod proizvoda sa tržišta. S obzirom da ni u jednom uzorku iz prometa nije dokazano prisustvo boje E 124, model nije bilo moguće proveriti kod tih proizvoda.

ZAKLJUČAK

Eksperimentalni proizvodi od mesa, fino usitnjene barene kobasice u tipu „pariska kobasica“, kojima su u

toku izrade dodavane različite količine boja E 120, E 124 i E 129, na osnovu senzornog ocenjivanja boje preseka, osim proizvodne partije 4, su imali prihvatljiviju boju preseka od kontrolnog proizvoda i bili su pogodan supstrat za kalibraciju CIE *L*a*b** metode za procenu količina boja kod proizvoda od mesa. Merenjem boje preseka eksperimentalnih proizvoda od mesa izrađenih sa različitim količinama dodatih boja, metodom CIE *L*a*b** kolorimetrije, konstatovano je da se *L** vrednost (intezitet svetlosti) smanjuje, da se *a** vrednost (udeo crvene boje) povećava i da se *b** vrednost (udeo žute boje), kod proizvoda sa dodatom E 120 bojom, smanjuje, a da se povećava kod proizvoda sa veštačkim azo bojama (E 124 i E 129).

Kalibracijom rezultata CIE *L*a*b** merenja prema rezultatima HPLC određivanja primenom MLR modela, razvijena je brza kolorimetrijska metoda za procenu količina boja kod fino usitnjenih proizvoda od mesa. Pouzdanost MLR modela je procenjena na osnovu vrednosti R^2 i *RMSE*. Utvrđeno je da kod rezultata dobijenih MLR modelima za procenjivanje količina boja E 120 i E 129, na osnovu CIE *L*a*b** merenja boje preseka kod eksperimentalnih proizvoda ne postoji značajnost razlike izračunatih vrednosti sa rezultatima dobijenim HPLC određivanjem. Proverom modela za procenu količine boje E 124 je utvrđeno statistički značajno odstupanje kod proizvoda sa količinom od 25 mg/kg boje.

Primenom CIE *L*a*b** i HPLC metoda, boje su utvrđene kod 95,24% ispitanih fino usitnjenih barenih kobasica sa tržišta, kod kojih je upotreba prirodnih boja dozvoljena. Od toga, 80% uzoraka barenih kobasica sadržalo je prirodnu boju E 120 (2,44–4,69 mg/kg), a 20% uzoraka veštačku boju E 129 (19,94–74,95 mg/kg), čija je upotreba zabranjena.

Može da se konstatuje da je CIE *L*a*b** kolorimetrijska metoda, koja je razvijena u okviru ovih ispitivanja, nedestruktivna, pogodna za rutinski rad i obradu velikog broja uzoraka i da se može primeniti za brzo procenjivanje sadržaja prehrambenih boja u proizvodima od mesa.

Zahvalnica

Autori se zahvaljuju Ministarstvu prosvete, nauke i tehnološkog razvoja Republike Srbije na pružanju finansijske pomoći za realizaciju ovoga rada (Projekat III 46009).

LITERATURA

[1] D.J. Troy, J.P. Kerry, Consumer perception and the role of science in the meat industry, Meat Sci. **86** (2010) 214–226.

[2] M. Šmelcerović, D. Đorđević, M. Novaković, Textile dyeing by dyestuffs of natural origin, Hem. ind. **60** (2006) 120–128.

[3] Pravilnik o prehrambenim aditivima, Sl. glasnik RS br. 63/2013.

[4] D.Ž. Mijin, Photodegradation of synthetic dyes under visible and solar light, Hem. ind. **59** (2005) 332–338.

[5] EFSA Panel on Food Additives and Nutrient Sources added to Food (ANS), 2009a. Scientific Opinion on the re-evaluation of Allura Red AC (E 129) as a food additive, EFSA J. 2009; 7(11):1327, 39.

[6] EFSA Panel on Food Additives and Nutrient Sources added to Food (ANS), 2009b. Scientific Opinion on the re-evaluation of Ponceau 4R (E 124) as a food additive, EFSA J. 2009; 7(11):1328, 39.

[7] D. McCann, A. Barrett, C. Cooper, D. Crumpler, L. Dalen, K. Grimshaw, E. Kitchin, K. Lok, L. Porteous, E. Prince, E. Sonuga-Barke, J. O'Warner, J. Stevenson, Food additives and hyperactive behaviour in 3-year-old and 8/9-year-old children in the community: a randomized, double-blinded, placebo-controlled trial, Lancet **370** (2007) 1560–1567.

[8] C. Souvage, Controverse l'hypersensibilité aux additifs alimentaires est une réalité clinique : pour (Controversy hypersensitivity to food additives is a clinical reality: For), Rev. Fr. Allergol. **50** (2010) 288–291.

[9] M.O. Elhkim, F. Fanny Héraud, N. Bemrah, F. Gauchard, T. Lorino, C. Lambré, J.M. Frémy, J.M. Jean-Poul, New considerations regarding the risk assessment on Tartrazine. An update toxicological assessment, intolerance reactions and maximum theoretical daily intake in France, Regul. Toxicol. Pharm. **47** (2007) 308–316.

[10] H.W. Park, C.H. Park, S.H. Park, J.Y. Park, H.S. Park, J. Yang, K.M. Ahn, K.H. Kim, J.W. Oh, K.E. Kim, B.Y. Pyun, H.B. Lee, K.U. Min, Dermatologic adverse reactions to 7 common food additives in patients with allergic diseases: A double-blind, placebo-controlled study, J. Allergy Clin. Immun. **121** (2008) 1059–1061.

[11] S. Altinöz, S. Toptan, Simultaneous determination of Indigotin and Ponceau-4R in food samples by using Vierordt's method, ratio spectra first order derivative and derivative UV spectrophotometry, J. Food Compos. Anal. **16** (2003) 517–530.

[12] E. Dinc, E. Baydan, M. Kanbur, F. Onur, Spectrophotometric multicomponent determination of sunset yellow, tartrazine and allura red in soft drink powder by double divisor-ratio spectra derivative, inverse least-squares and principal component regression methods. Talanta **58** (2002) 579–594.

[13] A.H. Alghamdi, H.M. Alshammery M.A. Abdalla and A.F. Alghamdi, Determination of Carmine Food Dye (E120) in Foodstuffs by Stripping Voltammetry, J. AOAC Int. **92** (2009) 1454–1459.

[14] S. Combeau, M. Chatelut, O. Vittori, Identification and simultaneous determination of Azorubin, Allura red and Ponceau 4R by differential pulse polarography: application to soft drinks, Talanta **56** (2002) 115–122.

[15] E. Andrzejewska, Detection of natural organic dye – Cochineal – in meat products, Rocz. Panstw. Zakl. Hig. **32** (1981) 315–318.

[16] ISO 13496:2000(E), Meat and meat products – Detection of colouring agents -- Method using thin-layer chromatography, 2000.

[17] N. Yoshioka, K. Ichihashi, Determination of 40 synthetic colors in drinks and candies by high-performance liquid chromatography using a short column with photodiode array detection, Talanta **74** (2008) 1408–1413.

[18] Q.G. Liao, W.H. Li, L.G. Luo, Applicability of accelerated solvent extraction for synthetic colorants analysis in meat products with ultrahigh performance liquid chromatography–photodiode array detection, Anal. Chim. Acta **716** (2012) 128–132.

[19] M. Ryvolova, P. Taborsky, P. Vrabel, P. Krasensky, J. Preisler, Sensitive determination of erythrosine and other red food colorants using capillary electrophoresis with laser-induced fluorescence detection, J. Chromatogr., A **1141** (2007) 206–211.

[20] CIE Commission Internationale de l'Eclairage, International Commission on Illumination, http:// //www.cie.co.at/

[21] Z. Pejkovski, A. Silovska-Nikolova, K. Belichovska, L. Gasperlin, T. Polak, B. Žlender, S. Lilić, H. Ockerman, Impact of different vegetable fats and oils on instrumentally measured color and texture of processed chicken sausages, Tehnologija mesa **50** (2009) 238–242.

[22] D. Vasilev, I. Vuković, V. Tomović, M. Jokanović, N. Vasiljević, M. Milanović-Stevanović, M. Tubić, Some important physical, physico-chemical and sensory quality properties of functional fermented sausages, Tehnologija mesa **50** (2009) 342–350.

[23] C. Sheridan, M. O'Farrell, E. Lewis, C. Flanagan, J. Kerry and N. Jackman, A comparison of CIE *L*a*b** and spectral methods for the analysis of fading in sliced cured ham, J. Opt. A-Pure Appl. Op. **9** (2007) S32–S39.

[24] D. Ansorena, M.P. De Peña, I. Astiasarán, J. Bello, Colour evaluation of chorizo de Pamplona, a Spanish dry fermented sausage: Comparison between the CIE *L*a*b** and the Hunter lab systems with illuminants D65 and C, Meat Sci. **46** (1997) 313–318.

[25] R. Korifi, Y. Le Dréau, J.F. Antinelli, R. Valls, N. Dupuya, CIE *L*a*b** color space predictive models for colorimetry devices – Analysis of perfume quality, Talanta **104** (2013) 58–66.

[26] F.J. Rodríguez-Pulido, B. Gordillo, M.L. González-Miret, F.J. Heredia, Analysis of food appearance properties by computer vision applying ellipsoids to colour data, Comput. Electron. Agr. **99** (2013) 108–115.

[27] J. Fernández-López, J.A. Pérez-Alvarez, E. Sayas-Barberá, F. López-Santoveña, Effect of Paprika (*Capsicum annum*) on Color of Spanish-type Sausages During the Resting Stage, J. Food Sci. **67** (2002) 2410–2414.

[28] M. Alvarez-Ortí, R. Gómez, J. E. Pardo, Manufacture of red line meat products with higher colour stability and improved visual attractiveness, J. Food Agric. Environ. **7** (2009) 16–18.

[29] J. N. Miller, J.C. Miller, Statistics and chemometrics for analytical chemistry, 5th ed., Pearson Education Limited, Harlow, 2005.

[30] SRPS ISO 6558 2001. Senzorske analize, Metodologija, Opšte uputstvo, 2001.

[31] C.W. Dunnett, Pairwise multiple comparisons in the homogeneous variance, unequal sample size case, J. Am. Stat. Assoc. **75** (1980) 789–795.

[32] D. Wu, D.-W. Sun, Colour measurements by computer vision for food quality control – A review, Trends Food Sci. Tech. **29** (2013) 5–20.

SUMMARY

THE CHEMOMETRIC APPROACH IN DEVELOPMENT OF THE COLORIMETRIC METHOD FOR THE ESTIMATION OF FOOD COLORANTS IN MEAT PRODUCTS

Radivoj B. Petronijević[1], Vesna F. Matekalo-Sverak[1], Aurelija T. Spirić[1], Ilija K. Vuković[2], Jelena A. Babić[1], Milan P. Milijašević[1], Dejana K. Trbović[1]

[1]*Institute of Meat Hygiene and Technology, Belgrade, Serbia*
[2]*University of Belgrade, Faculty of Veterinary Medicine, Belgrade, Serbia*

(Scientific paper)

The aim of this research was to develop a novel colorimetric method based on mathematical models, by multiple linear regression (MLR), from the CIE *L*a*b** measurements and data of the HPLC determination of food colorants. Calibration set of 10 production batches of finely grinded cooked sausage with added food colorants was manufactured in industrial conditions as follows: one control batch and 9 products with various quantities of added food colorants: E120 (3.4, 7.5 and 12.5 mg/kg), E 124 (5.0, 15.0 and 25.0 mg/kg) and E 129 (5.0, 15.0 and 25.0 mg/kg). The estimation of the added food colorants was assessed by measuring *L**, *a** and *b** parameters of cross-section. The quantification of food colorants was achieved by HPLC-PDA. Food colorants were extracted from meat products using accelerated solvent extraction (ASE). Quantification of food colorants was achieved in the range from 1 to 100 mg/kg, and recovery values were from 76.1 to 107.04%, for E 120, from 97.61 to 101.03%, for E 124 and from 99.91 to 101.67% for E 129. Correlation of the results obtained using HPLC and colorimetric measuring data was assessed by multiple linear regression (MLR). The results from colorimetric and chromatographic determinations in four experimental batches (three batches with different quantities of food colorants and one control batch) were used for calibration. The coefficients of determination (R^2) for linear models in experimental batches were 0.954, for E 124, 0.987, for E 120 and 0.993, for E 129. The correlation functions of food colorant quantities and corresponding *L*a*b** values were established. The obtained mathematical models were tested for the estimation of the content of dyes in 21 samples of finely grinded cooked sausages purchased in retail stores. Food colorants were confirmed in 20 samples (95.24%), and one sample (4.76%) did not contain any of these compounds. Out of the positive samples, sixteen samples (80.00%) contained E 120, while four samples (20.00%) contained E 129. Food colorant E124 was not established in any of the analysed samples. The colorimetric CIE *L*a*b**method might be used during sensory evaluation of meat products for the assessment of the added food colorants.

Keywords: Food colorants • CIE *L*a*b** Colorimetric method • HPLC-PDA • MLR

Kinetic model for the sorption of copper ions onto sugar beet shreds

Mirjana M. Brdar, Marina B. Šćiban, Dragana V. Kukić, Tatjana M. Došenović

University of Novi Sad, Faculty of Technology, Serbia

Abstract

Adsorption kinetics is of great significance to evaluate the performance of adsorption process. The kinetics of copper ions adsorption onto different sized sugar beet shreds has been considered. Sugar beet shreds are very promising adsorbents due to their convenient chemical composition and availability in relatively large quantities in many countries. Experimental data were fitted with pseudo-first and pseudo-second-order kinetic models. Also, we used the intraparticle diffusion model for further analysis of kinetics. The coefficient of determination indicates that the pseudo-second-order equation, obtained by using nonlinear least square method, was the most appropriate model for the description of copper ions adsorption onto sugar beet shreds. The adsorption capacities at equilibrium, for a particle size of 224–400 μm, 400–750 μm and 750–1000 μm, are 10, 9 and 8.6 mg/g, respectively. By using intraparticle diffusion model proposed by Weber and Morris, it was obtained that there exist two different stages in adsorption: fast initial adsorption which is further limited by intraparticle diffusion.

Keywords: adsorption, sugar beet shreds, kinetic models, pseudo-first order, pseudo-second order, intraparticle diffusion model.

Available online at the Journal website: http://www.ache.org.rs/HI/

SCIENTIFIC PAPER

UDC 544.723.2:633.41

Hem. Ind. **68** (6) 793–799 (2014)

doi: 10.2298/HEMIND130830005B

Wastewaters of many industries, such as metal plating facilities, mining operations, fertilizer industries, tanneries, paper industries, production of batteries, pesticides, etc., contain heavy metals which are of major concern due to their toxicity, bioaccumulation tendency and non-biodegradability. Consequently, it is necessary to remove metal ions from effluents [1]. Conventional precipitation method of heavy metals removal from wastewaters has serious limitations regarding efficiency, operating conditions and sludge production. The use of different biomass, such as wood and agro-industry waste, as adsorbent is an alternative technology for removing metal ions from wastewaters that is called biosorption [2]. Advantages of biosorption over conventional methods are low cost, high efficiency for dilute solutions, minimal amount of sludge, no additional nutrient requirement and possibility of biosorbent regeneration and metal recovery [3]. Agro-industry waste and by-products of cellulosic origin are convenient low-cost adsorbents because they are inexhaustible and non-hazardous materials. In this study, the dried sugar beet shreds, a by-product of sugar industry, are investigated as adsorbents. Sugar beet shreds which are usually used as animal feed, a source of pectin or as a substrate for bioethanol production, also have certain adsorption properties. If production of bioethanol from sugar beet, as a fuel, increases in the future, the sugar beet shreds will be obtained in large quantities as by-products. On the other hand, more than 40% of shreds dry matter is pectic substance. Pectin is known to strongly bind metal cations in aqueous solutions due to a number of carboxyl functional groups. Therefore, sugar beet shreds are very promising adsorbents [4]. The aim of this paper is to research influence of adsorbent particle size on adsorption kinetics.

In order to use agro-industrial waste material as adsorbent, in actual treatment plants for removing of heavy metals from wastewaters, it is necessary to conduct adsorption kinetic experiments [5,6]. Kinetic studies provide information about possible mechanism of adsorption and reactions that occur on the adsorbent surface. They can also help in understanding the rate controlling step of the mass transfer process which affects the overall rate of adsorption. In recent years, several mathematical models have been proposed to describe adequately the kinetic process of adsorption [7–9]. According to [7] the most crucial factor for effective system design is predicting the rate of adsorbate removal. Adsorption kinetics of copper ions onto other different adsorbent has been investigated in many papers [10–13].

In this study, the kinetic studies have been carried out by batch reactions with various particle sizes of sugar beet shreds as adsorbents. The pseudo-first and pseudo-second-order equation were analyzed, as well as the intraparticle diffusion model. The method of least square was used to predict which model better match the experimental data. Mathematica 6, Wolfram Research software tool was used for calculation.

Correspondence: M.M. Brdar, University of Novi Sad, Faculty of Technology, Bul. cara Lazara 1, 21000 Novi Sad, Serbia.
E-mail: mbrdar@tf.uns.ac.rs
Paper received: 30 August, 2013
Paper accepted: 28 January, 2014

EXPERIMENTS

Materials

Water solution of $CuSO_4$ concentration of about 50 mg/L was prepared by diluting 0.25 mol/L stock salt solution with demineralised water, just before experiments. pH adjustment was made using HNO_3 solution. All chemicals used were of analytical reagent grade.

Dry sugar beet shreds were obtained from nearby sugar refinery. They were milled on a laboratory mill (MiagBraunschweig DOXY 71b/4) and sieved through a set of sieves (Bűhler MLU-300) in order to obtain different particle size. Three different ranges of particle size were used in experiments: 224–400 μm, 400–750 μm and 750–1000 μm.

Batch adsorption studies

The batch experiments were carried out by shaking 5 g of sugar beet shreds of different particle size in 1 L of aqueous solution of Cu(II) at pH 4. Experimental pH value is chosen to be under the pH value that induces copper hydroxide precipitation [14]. Suspensions were shaken at different time intervals (2 to 180 min). After reaction time, suspensions were filtered through a filter paper (Macherey-Nagel 651/120). Concentrations of copper ions in aqueous solutions were determined before (c_0) and after (c) adsorption process by complexometric titration [15]. Experiments were duplicated and results were averaged.

The amount of heavy metal ions adsorbed per specified amount of adsorbent (q) was calculated as follows:

$$q = \frac{c_0 - c}{m} \tag{1}$$

where m is a mass of adsorbent per liter of solution.

Kinetic models

Adsorption kinetics depends on the sorbate–sorbent interactions and experimental conditions. Various models can be used to analyze the kinetics of sorption process. Two of them, pseudo-first-order and pseudo-second-order model, have been widely used to describe sorption without any assumption of process conditions [16].

Pseudo-first-order model was introduced by Lagergren in 1898 [17]. It was the first model which describes kinetic of adsorption and it can be presented as follows:

$$\frac{\mathrm{d}q}{\mathrm{d}t} = k_1(q_\mathrm{e} - q) \tag{2}$$

where q_e and q are the adsorption capacities at equilibrium and time t, respectively, and k_1 is the pseudo-first-order constant for the kinetics model.

In many manuscripts the Lagergren equation was applicable only to first 20 or 30 min of adsorption [18]. This kinetic model has been mostly used to describe the adsorption of pollutants from wastewater in different fields.

Literature survey has shown that the number of publications referring to other kinetic models such as the pseudo-first-order model, intraparticle diffusion model and Elovich equation are about one-third of that to the pseudo-second-order model [19]. Pseudo-second-order model is expressed with the following equation:

$$\frac{\mathrm{d}q}{\mathrm{d}t} = k_2(q_\mathrm{e} - q)^2 \tag{3}$$

where q_e and q are the adsorption capacities at equilibrium and time t, respectively, and k_2 is the pseudo-second-order constant for that model. It was suggested by Ho and McKay [20]. All of the constants, both in pseudo-first and pseudo-second order model, have been calculated from the experimental results.

Nonlinear regression methods for determining the parameters of these two kinetic models for the experimental data were used [21]. Which model better describes the fit of the experimental data is determined by some error function. Since non-linear regression implicitly minimizes the sum of squares of the errors to determine the equation parameters, the coefficient of determination R^2 was chosen as the error function for the kinetic model analysis. Mathematica 6, Wolfram Research software tool was used for calculation.

Since the above two equations could not definitely reveal the adsorption mechanism, another kinetic model named intraparticle diffusion model was used in the present study. This model was discovered by Weber and Morris [22]. They found that in many adsorption cases solute uptake varies almost proportionally with $t^{1/2}$ rather than with the contact time t, so this model has the following interpretation

$$q = k_\mathrm{int}\, t^{1/2} + a \tag{4}$$

where k_int is the intraparticle diffusion rate constant and a is a constant for any experiment. Equation (4) can be written as:

$$q_\mathrm{ref} = k_\mathrm{int} {t_\mathrm{ref}}^{1/2} + a \tag{5}$$

After some simple calculation we obtain:

$$\frac{q}{q_\mathrm{ref}} = 1 - R_\mathrm{i}\left[1 - \left(\frac{t}{t_\mathrm{ref}}\right)^{1/2}\right] \tag{6}$$

where $R_\mathrm{i} = k_\mathrm{int} {t_\mathrm{ref}}^{1/2} / q_\mathrm{ref}$, which is defined as the initial adsorption factor of the intraparticle diffusion model. Also, R_i can be expressed as:

$$R_i = 1 - \frac{a}{q_{ref}} \quad (7)$$

When a = 0, *i.e.*, R_i = 1, there is no initial adsorption behavior in an absorption system. When R_i = 0.1, the initial point is at q/q_{ref} = 0.9, which means that the initial adsorption has already reached 90%; later on, the adsorption proceeds following intraparticle diffusion mechanism. The R_i value is divided into four zones: 0.9 < R_i < 1 is called weakly initial adsorption (zone 1); 0.5 < R_i < 0.9 intermediately initial adsorption (zone 2); 0.1 < R_i < 0.5 strongly initial adsorption (zone 3) and R_i < 0.1 approaching completely initial adsorption (zone 4).

If the adsorption process follows the intraparticle diffusion model, a plot of q against $t^{1/2}$ should be a straight line. The intraparticle diffusion rate constant, k_{int}, can be calculated from the slope of the straight line. Nevertheless, it is common to observe multilinearity on the above mentioned plot, which reveals the different stages in adsorption involving external mass transfer and intraparticle diffusion [23].

RESULTS AND DISCUSSION

The kinetic studies have been carried out by batch reactions with various particle sizes of sugar beet shreds as adsorbents (Figure 1). The removal of copper ions by shreds with different particle sizes showed that the adsorption capacity and removal rate were increased with a decrease in particle diameter. The explanation is in the following, the higher adsorption with smaller adsorbent particle is attributed to the fact that smaller particles yield larger specific surface area. Also, the surface area of small particles is more accessible which facilitates adsorbate diffusion to the active sites. Therefore, using adsorbents with smaller particles can be achieved faster as well as more efficient adsorption.

In this paper, the pseudo-first and pseudo-second order kinetic models were used to determine the rate of adsorption. In Table 1 the kinetic parameters for experimental data were presented obtained by using pseudo-first and pseudo-second-order model. Both equations give high coefficient of determination for all experimental data. The higher coefficient of determination for pseudo-second-order equation suggested that it was better model to explain kinetics of adsorption for experimental data. Figures 2–4 show the pseudo-first and pseudo-second-order equations obtained by using the non-linear methods for different particle sizes, 224–400 μm, 400–750 μm and 750–1000 μm, respectively.

Table 1. Kinetic parameters obtained from experimental data for different particle size

Particle size	Parameter	Pseudo-first	Pseudo-second
224–400 μm	q_e	9.2868	10.0000
	k	0.3807	0.0558
	R^2	0.9585	0.9883
400–750 μm	q_e	8.3400	9.0000
	k	0.3343	0.0521
	R^2	0.9336	0.9824
750–1000 μm	q_e	7.8902	8.6000
	k	0.2727	0.0436
	R^2	0.9437	0.9863

The coefficient of determination in Table 1 showed that the best model to describe the kinetics of adsorption is pseudo-second-order equation. The experimental adsorption capacities at equilibrium (q_e, Figure 1) best matches with values obtained by pseudo-sec-

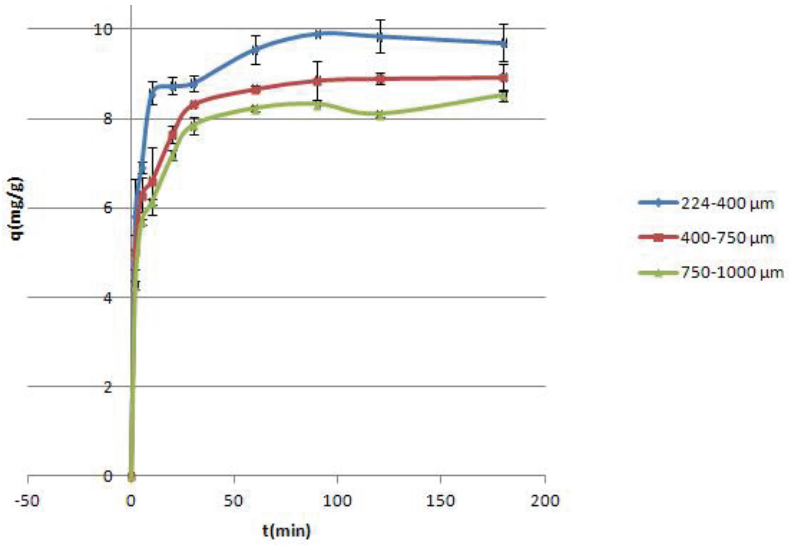

Figure 1. Effect of contact time and particle size of sugar beet shreds on the adsorption of copper ions.

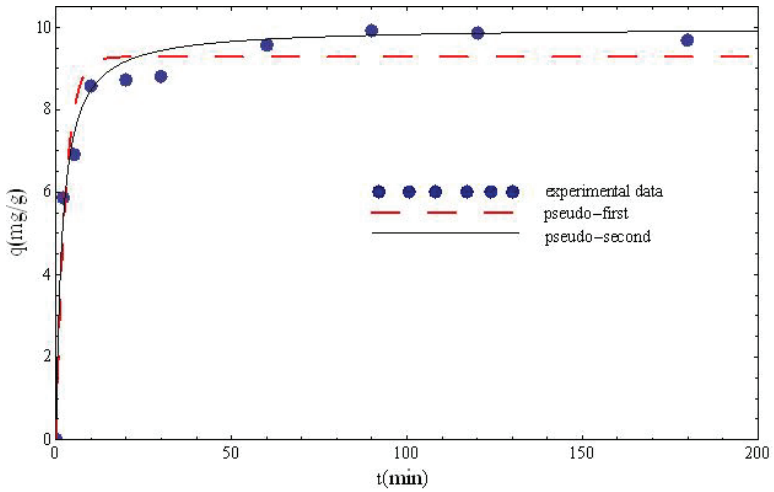

Figure 2. Pseudo-first and pseudo-second-order kinetic equations obtained by using the non-linear methods at particle sizes 224–400 μm.

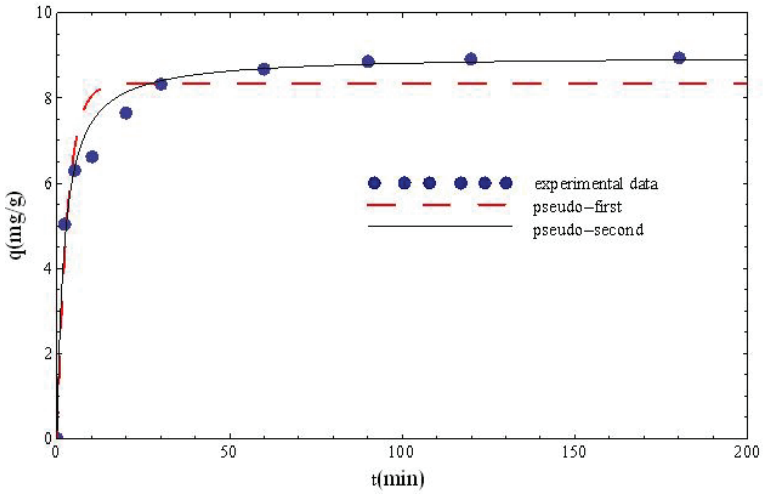

Figure 3. Pseudo-first and pseudo-second-order kinetic equations obtained by using the non-linear methods at particle sizes 400–750 μm.

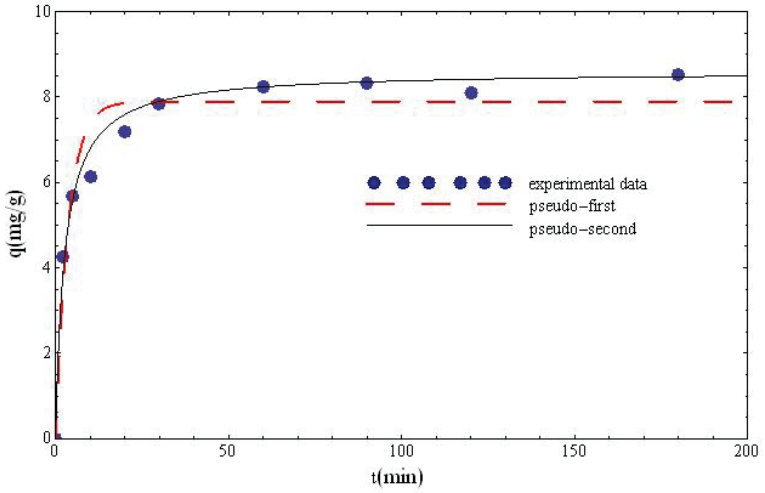

Figure 4. Pseudo-first and pseudo-second-order kinetic equations obtained by using the non-linear methods at particle sizes 750–1000 μm.

ond-order kinetics model (Table 1). This is another confirmation of the success of this model.

In Figure 5 it is observed that there are two linear portions which elucidate the two adsorption stages. The first adsorption stage is external mass transfer at initial period and the second is intraparticle diffusion. The slope of the linear portion suggests that the rate of intraparticle diffusion k_{int}, listed in Tables 2 and 3, increases with decreasing of particle size. The first adsorption state is represented by rapid adsorption (zone 1) while the second state is represented by deceleration (zone 3). Further, the first straight portion is attributed to a macropore diffusion process and the second linear portion can be ascribed to a micropore diffusion process. It is clear from Figure 5 that the first stage is faster than the second one. The slope decreases with increasing of particle size, which can be explained by poor accessibility of larger particles pores surface for the adsorbates.

CONCLUSIONS

The kinetics of adsorption of copper ions from water solution by sugar beet shreds was explained using the pseudo-first and pseudo-second-order kinetic and intraparticle diffusion models. The adsorption equilibrium for copper ions adsorption onto different sized sugar beet shreds was reached in 30 min. The adsorption capacity and removal rate were increased with a decrease in sugar beet shreds particle diameter. The coefficient of determination showed that the best model to describe the kinetics of adsorption is pseudo-second-order equation. The adsorption capacities at equilibrium, for a particle size of 224–400 μm, 400–750 μm and 750–1000 μm, are 10, 9 and 8.6 mg/g, respectively. By using intraparticle diffusion model proposed by Weber and Morris, it was obtained that there exist two different stages in adsorption: fast initial adsorption which is further limited by intraparticle diffusion.

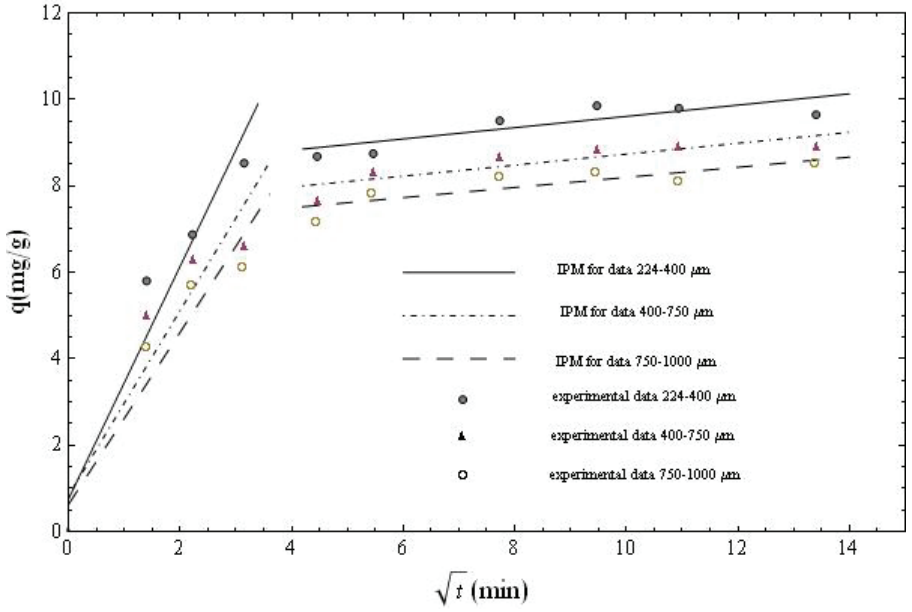

Figure 5. Intraparticle diffusion plot for the sorption of copper ions onto sugar beet shreds.

Table 2. First adsorption stage – intraparticle diffusion model for zone 1

Particle size	k_{int}	a	R_i	R^2
224–400 μm	2.6899	0.7586	0.9241	0.9667
400–750 μm	2.1396	0.8364	0.9071	0.9363
750–1000 μm	1.9905	0.6324	0.9265	0.9546

Table 3. Second adsorption stage – intraparticle diffusion model for zone 3

Particle size	k_{int}	a	R_i	R^2
224–400 μm	0.1304	8.3052	0.1695	0.9576
400–750 μm	0.1265	7.4694	0.1701	0.9688
750–1000 μm	0.1171	7.0269	0.1829	0.9325

Acknowledgement

The work presented here was supported by the Project number 3471 of the Provincial Secretariat of Science and Technological Development of AP Vojvodina and MNTRRS (project 174009).

REFERENCES

[1] F. Fu, Q. Wang, Removal of heavy metal ions from wastewaters: A review, J. Environ. Manage. **92** (2011) 407–418.

[2] D. Sud, G. Mahajan, M.P. Kaur, Agricultural waste material as potential adsorbent for sequestering heavy

metal ions from aqueous solutions – A review, Bioresource Technol. **99** (2008) 6017–6027.

[3] S.O. Lesmana, N. Febriana, F.E. Soetaredjo, J. Sunarso, S. Ismadji, Studies on potential applications of biomass for the separation of heavy metals from water and wastewater, Biochem. Eng. J. **44** (2009) 19–41.

[4] V.M. Dronnet, C.M.G.C. Renard, M.A.V. Axelos, J.-F. Thibault, Binding of divalent metal cations by sugar-beet pulp, Carbohyd. Polym. **34** (1997) 73–82.

[5] Y.S. Ho, J.C.Y. Ng, G. McKay, Kinetics of pollutant sorption by biosorbents, Rev. Separ. Purif. methods **29** (2000) 189–232.

[6] R.B. Garcia-Reyes, J.R. Rangel-Mendez, Adsorption kinetics of chromium(III) ions on agro-waste materials, Bioresource Technol. **101** (2010) 8099–8108.

[7] W. Plazinski, W. Rudzinski, A. Plazinska, Theoretical models of sorption kinetics including a surface reaction mechanism: A review, Adv. Colloid Interf. Sci. **152** (2009) 2–13.

[8] H. Qiu, L. Lv, B. Pan, Q. Zhang, W. Zhang, Q. Zhang, Critical review in adsorption kinetic models, J. Zhejiang Univ. Sci., A **10** (2009) 716–724.

[9] S.S. Gupta, K.G. Bhattacharyya, Kinetics of adsorption of metal ions on inorganic materials: A review, Adv. Colloid Interf. Sci. **162** (2011) 39–58.

[10] A.E. Ofomaja, E.B. Naidoo, Biosorption of copper from aqueous solution by chemically activated pine cone: A kinetic study, Chem. Eng. J. **175** (2011) 260–270.

[11] K.S. Tong, M. Jain Kassim, A. Azraa, Adsorption of copper ion from its aqueous solution by a novel biosorbent Uncaria gambir: Equilibrium, kinetics, and thermodynamic studies, Chem. Eng. J. **170** (2011) 145–153.

[12] B. Al-Rashdi, C. Tizaoui, N. Hilal, Copper removal from aqueous solutions using nano-scale diboron trioxide/ /titanium dioxide (B_2O_3/TiO_2) adsorbent, Chem. Eng. J. **183** (2012) 294–302.

[13] E. Demirbas, N. Dizge, M.T. Sulak, M. Kobya, Adsorption kinetics and equilibrium of copper from aqueous solutions using hazelnut shell activated carbon, Chem. Eng. J. **148** (2009) 480–487.

[14] M. Šćiban, M. Klašnja, Wood sawdust and wood originate materials as adsorbents for heavy metal ions, Holz Roh Werkstoff **62** (2004) 69–73.

[15] I. Sajo, Complexometry, 1st ed., Muszakikonykiado, Budapest, 1973 (in Hungarian)

[16] W. Rudzinski, W. Plazinski, Kinetics of solute adsorption at solid/solution interfaces: a theoretical development of the empirical pseudo-first and pseudo-second order kinetic rate equations, based on applying the statistical rate theory of interfacial transport, J. Phys. Chem., B **110** (2006) 16514–16525.

[17] S. Lagergren, Zurtheorie der sogenannten adsorption gelöesterstoffe, Kungliga Svenska Vetenskapsakademiens. Handlingar **24** (1898) 1–39.

[18] Y.S. Ho, G. McKay, A comparison of chemisorption kinetic models applied to pollutant removal on various sorbent, Trans. IchemE 76, B (1998) 332–340.

[19] F.-C. Wu, R.-L. Tseng, S.-C. Huang, R.-S. Juang, Characteristics of pseudo-second-order kinetic model for liquid-phase adsorption: A mini-review, Chem. Eng. J. **151** (2009) 1–9.

[20] Y.S. Ho, G. McKay, Pseudo-second order model for sorption processes, Process Biochem. **34** (1999) 451–465.

[21] Y.S. Ho, Second-order kinetic model for the sorption of cadmium onto tree fern: A comparison of linear and non-linear methods, Water Res. **40** (2006) 119–125.

[22] W.J. Weber,Jr., J.C. Morris, Kinetics of adsorption on carbon from solution, J. Sanit. Eng. Div. Am. Soc. Civ. Eng. **89** (SA2) 31–39.

[23] X.Y. Yang, B. Al-Duri, Kinetic modeling of liquid phase adsorption of reactive dyes on activated carbon, J. Coll. Interf. Sci. **287** (2005) 25–34.

IZVOD

Kinetika adsorpcije jona bakra na izluženim repinim rezancima šećerne repe

Mirjana M. Brdar, Marina B.Šćiban, Dragana V. Kukić, Tatjana M. Došenović

Univerzitet u Novom Sadu, Tehnološki fakultet, Srbija

(Naučni rad)

Otpadne vode mnogih industrija, kao što su industrija prerade metala, eksploatacija ruda, proizvodnja đubriva, papira, baterija, prerada kože, itd, sadrže teške metale koji predstavljaju problem sa stanovišta zaštite životne sredine jer su toksični, imaju tendenciju biakumulacije i nisu biorazgradljivi, pa ih je neophodno ukloniti iz efluenata. Među mnogobrojim dostupnim tehnikama najbolje rezultate je pokazala adsorpcija aktivnim ugljem, međutim, njenu primenu uveliko ograničava visoka cena. Potraga za novim, jeftinijim adsorbentima poput biomase dovela je do razvoja nove tehnologije poznate pod nazivom biosorpcija. Prednosti ove metode su, osim niže cene, visoka efikasnost i mogućnost regeneracije adsorbenta. Poljoprivredni otpad, koji u svojoj strukturi sadrži celulozu, je vrlo pogodan za ove svrhe jer je jeftin i dostupan u velikim količinama. Izluženi rezanci šećerne repe se obično koriste kao stočna hrana, izvor pektina ili supstrat za proizvodnju bioetanola, ali imaju i sposobnost adsorpcije jona teških metala. Oko 40% suve materije repinih rezanaca čini pektin koji veže katjone metala iz vodenih rastvora zbog brojnih funkcionalnih grupa koje sadrži. Za ocenu efikasnosti procesa adsorpcije značajno je određivanje kapaciteta adsorbenta, kinetike adsorpcije i ostalih uslova rada koji će dati najbolje rezultate pri primeni nekog adsorbenta. U ovom radu ispitana je kinetika adsorpcije jona bakra na izluženim repinim rezancima šećerne repe. Eksperimenti su izvedeni šaržno primenom rezanaca šećerne repe različitih veličina čestica: 224–400 μm, 400–750 μm i 750–1000 μm. Ravnoteža u procesu adsorpcije je postignuta nakon 30 min, a kapacitet i brzina adsorpcije su rasli sa smanjenjem veličina čestica adsorbenta. Za opisivanje kinetike adsorpcije su primenjene nelinearne jednačine pseudo-prvog i pseudo-drugog reda, kao i model difuzije unutar čestica. Za proračun je korišćen softver Mathematica 6. Rezultati su pokazali da je jednačina pseudo-drugog reda dobijena nelinearnom metodom najmanjih kvadrata najbolji model za opisivanje adsorpcije jona bakra na izluženim rezancima šećerne repe. Modelom difuzije unutar čestica je pokazano da postoje dva stanja prilikom adsorpcije. Prvo stanje karakteriše brza adsorpcija (zona 1), dok u drugom dolazi do zasićenja, te brzina adsorpcije opada (zona 3).

Ključne reči: Adsorpcija • Rezanci šećerne repe • Kinetički modeli • Pseudo-prvi red • Pseudo-drugi red • Model difuzije unutar čestice

Effect of goat breed on the meat quality

Snezana D. Ivanovic[1], Zoran M. Stojanovic[2], Ksenija D. Nesic[1], Boris P. Pisinov[1], Milan Ž. Baltic[3], Jovanka V. Popov-Raljic[4], Jelena M. Đurić[3]

[1]*Institute of Veterinary Medicine of Serbia, Belgrade, Serbia*
[2]*Serbian Environmental Protection Agency SEPA, Belgrade, Serbia*
[3]*Faculty of Veterinary Medicine Belgrade University, Belgrade, Serbia*
[4]*Faculty of Agriculture, Zemun, Serbia*

Abstract

The quality of goat meat has recently become an important aspect in the marketing of goats in Serbia. The aim of this study was to compare some goat meat quality parameters of various races and to determine the differences between them. Goat breeds were Balkan goat and Serbian white goat, both female in the age of four years. Analysis of quality parameters: chemical composition (moisture, protein, total fat, ash,), pH value, fatty acids, amino acids, microelements content, tenderness, cooking loss and colour measurements were done. Statistically significant difference was found between the samples of two groups of goat meat ($P < 0.05$) in relation to: live weight (kg), water (%), fat (%), protein (%) and ash (%), among 11 of 15 tested fatty acids, amino acid leucin, sensory examination of fresh meat for the palpatory evaluated firmness and in the content of copper and zinc. Statistically significant differences between the groups did not existed regarding the pH value, fatty acids eicosenoic, cis-heptadecenoic, t-elaidic, t-linolelaidic and amino acids alanine, arginine, aspartic acid, cysteine, glutamic acid, glycine, histidine, isoleucine, lysine, methionine, phenylalanine, proline, serine, threonine, tryptophan, tyrosine and valine. Also there was no statistically significant difference in instrumental testing of the meat color, sensory evaluation of surface color, visual evaluated structure, olfactory evaluated odor and iron and manganese. These results suggest that the race of animal has an impact on meat quality.

Keywords: chemical composition, goat, meat, quality, race.

Available online at the Journal website: http://www.ache.org.rs/HI/

PROFESSIONAL PAPER

UDC 636.39:637.5'63.9:54

Hem. Ind. **68** (6) 801–807 (2014)

doi: 10.2298/HEMIND131201006I

Goat meat has about the same nutritional value as meat of sheep (more precisely, more protein and less fat compared to sheep meat). Anaeto *et al*. [1] consider that, due to its molecular structure, goat meat is easier to digest. The goat meat in the human diet, according to Anaeto *et al*. [1] is a healthier alternative compared to other types of red meat as it contains low levels of saturated fatty acids and cholesterol. According to Devendra [2], the polyunsaturated fatty acids are prevalent in meat of goats, and a diet rich in unsaturated fatty acids is correlated with a reduced risk of stroke and coronary diseases. In addition, the essential amino acids such as lysine, threonine and tryptophan are present in the meat of goats. Regardless of the nutritional value, it is still less appreciated due to the specific scents and flavors, even more so if the animal is older [3].

Growing and goat meat consumption, despite this qualitative composition, is conditioned by religion, traditions and customs, as well as by market and consumer habits [4]. According to official data of the Serbian Chamber of Commerce in 2011, the number of goats in Serbia is 130.000. They are grown in the mountainous, less economically developed areas, with 1–2 animals per household, or in mini farms (20, 30, 50 and more goats). Regarding composition of the present breeds of goats, Alpino (2–3%), Serbian white breed (15%), various hybrids (35%) and Balkan (47%) goats are present. The production of goats in Serbia is focused on milk and meat production, where the milk is a priority [5]. In the world, especially in Asia and Africa, the goat and kid meat is of great importance in human nutrition. The goat meat is increasingly required in developed countries due to its high nutritional value [6–8].

Since the testing of fattening and slaughter characteristics of Balkan goats, purebred grown in Serbia (Alpine, Sanen, Bunte Deutsche Edelziege and others), are not so common, there is really little literature data regarding these properties of goats and kids [9]. This paper presents the characteristics of production, as well as some carcass characteristics of domestic Balkan goat and Bunte Deutsche Edelziege race. Balkan goat still in a large percentage (about 47%) participates in the racial composition of the population of goats being raised in Serbia [10]. In Serbia, little is known about the quality of goat meat compared with other species, par-

Correspondence: S. Ivanovic, Institute of Veterinary Medicine of Serbia, Autoput 3, 11070 Belgrade, Serbia.
E-mail: snezaivanovic@gmail.com
Paper received: 1 December, 2013
Paper accepted: 31 January, 2014

ticularly the lack of knowledge of the meat quality of autochthonous goat breeds and there is practically no information on the characteristics of meat of goats and kids of Serbian White and Balkan goat. In addition, the quality of goat meat has recently become an important aspect in the marketing of goats in Serbia.

The aim of this study was to collect and compare data on the quality of meat of domestic Serbian white and Balkan goat of the same age.

MATERIALS AND METHODS

Source of goat meat

Material was used from two races of goat meat (20 goats from each), Balkan goat and Serbian white goat, both female in the age of four years. The goats were got from private farms in the rural area of Stara Planina. The goats were raised at the same time. Objects for the goats were with conditions that were satisfactory for goat breeding. Watering was *ad libitum*.

Plane of nutrition

Diet of goats during the winter consisted of hay which was collected from natural pastures (3.5 kg per day) and concentrate (0.25 kg per day). In the summer months, the goats were pastured and fed with concentrate in the amount of 0.25 kg per day. The concentrate was made of maize meal, wheat bran with added sodium chloride and premix. Goats were slaughtered in an experimental slaughter house in the Institute for animal husbandry.

Analysis of quality parameters

Material used for the determination of chemical composition, fatty and amino acids, microelements content was *m. longissimus dorsi* from left side of halves. For tenderness, cooking loss, colour measurement and sensory analysis the same muscle from the right side of halves was used.

Moisture content [11], fat content [12], ash content [13], protein content [14] and pH value [15] were all determined according to ISO. Chemical parameters and pH were measured in meat 24 h after slaughter.

Modified Folch–Lees method [16] was applied for lipid extraction from 1 g homogenized tissue with chloroform–methanol mixture (2:1, *V*/*V*). The combined extracts were washed, filtered and evaporated to obtain purified lipid fraction. After the lipid hydrolysis with KOH in methanol, esterification of the fatty acids to methyl esters was performed, evaporated to dryness in a stream of nitrogen. Analysis of FAMEs was performed by gas chromatography technique (GC6890N, Agilent Tech., USA) comparing with FAMEs standard (Supelco, USA) [17].

The amino acids composition was determined by AOAC method 982.30 [18], for most amino acids by acid hydrolysis with 6 M HCl for 24 h at 110 °C, total sulfur amino acid after performic acid oxidation followed by acid hydrolysis and tryptophan after alkaline hydrolysis. Dabsyl amino acids were prepared from hydrolyzate [19] after reagent was added, dried under vacuum, redissolved and separated using a Waters Breeze HPLC System (Waters Corporation, Milford, MA) consisted of a binary pump (Waters 1525), UV/Vis detector (Waters 2487), reversed-phase column SUPELCOSIL LC-DABS (15 cm×4.6 mm ID, particle size 3 μm) equipped with a guard column Supelguard™ LC-18-T and a two-eluent mobile phase potassium dihydrogen phosphate as solvent A, and acetonitrile:2-propanol (75:25) as solvent B at a flow rate 2 mL/min at room temperature. The eluted DABS-AA and DABS-norleucine, as internal standards, were detected by UV/Vis detector at 436 nm wavelengths, respectively. A commercial amino acid mixture (Sigma, St. Louis, MO) was used as standard.

The microelements analysis was conducted by FAAS technique according to AOAC method 999.10 [20], using advanced microwave digestion system Ethos 1 (Milestone, Italy) and atomic absorption spectrophotometry AAnalyst 300 with HCL-lamps (Perkin-Elmer, USA). Dried samples (0.2–0.5 g) are digested with nitric acid and hydrogen peroxide in microwave oven. The microelements were determined at characteristic wavelengths separately for each element and calculated. Commercial individual standards (Merck, Germany) were used to prepare the standard calibration mixtures.

Principle of the method is to determine the mass loss due to heat treatment by measuring the weight before and after completing the heating and subsequent cooling of the sample. Goat meat is heat treated by boiling in a water bath at 90 °C for 60 min.

Tenderness was determined by Warner–Bratzler instrument. It was done by measurement of force, expressed in lb and converted into N, which was required to cut a cylindrical sample obtained by drill 0.5 inches in diameter in the direction of muscle fibers from heat-treated and cooled sample. The result was expressed as the mean value of 8 to 10 measurements [21].

The color was measured on the fresh meat cuts (*musculus longissimus dorsi)*, from the right side of each carcass (n = 20, for each sample). CIE, CIEL*a*b* [22] were determined using Minolta chromameter CR 400 (Minolta Co. Ltd., Osaka, Japan) in D-65 lighting, with standard angle of 2 degrees of shelter and 8 mm aperture of the measuring head. These results were expressed in CIE system as the average: y (reflectance or brilliance, %), λ (dominant wavelength, nm) and P (color purity, %) [23] and in CIEL*a*b* as: L* (psy-

chometer light), *a** (psychometer tone) and *b** (psychometer chroma).

The sensory evaluation included appearance (color and surface), texture (structure and firmness) and aroma (odour) in each part of the meat (*musculus longissimus dorsi*). The same sensory evaluation was made on meat backed in Al folia at the temperature of 225 °C up to achieving of 75 °C in the inner part of meat, as well the textural characteristics – softness, chewiness and tenderness, and flavor (smell and taste). The sensory evaluation was made by ten trained assessors, according to relevant ISO [24]. Sensory analysis was made by according to the methodology described by the Ivanovic *et al*. [3].

Data obtained in this study were analyzed by descriptive and analytical statistical parameters: mean value (*M*), standard deviation (*SD*) by using MS Excel 2003 and analysis of variance ANOVA. The differences between the averages were compared by t-test at the level of significance of 95% [25].

RESULTS AND DISCUSSION

Live weight, chemical composition, pH value, tenderness, cooking loss and microelements

The populations of Serbian white goats had bigger live weight ($P < 0.05$) than Balkan goats. The average water means, total fats, proteins and ash expressed as percentage, showed that there were differences between compared groups ($P < 0.05$). The pH value of populations of Serbian White goats meat did not differ ($P>0.05$) from Balkan goat. Regarding tenderness and cooking loss, there were significant differences ($P < < 0.05$) between compared groups. There was a statistically significant difference ($P < 0.05$) in the content of copper and zinc between the samples, while in the content of iron and manganese was no statistically significant difference ($P > 0.05$) in these same samples of meat.

Results for moisture percentage and fat percentage which are shown in Table 1 and refer to the Balkan goat meat, are not in accordance with the results that we got from an earlier study for chemical and sensory characteristics of Bunte Deutsche Edelziege and Balkan goat meat [3]. Results for protein, ash and pH, which refer to the Balkan goat meat (Table 1), are consistent with those in previous study [3].

Wattanachant *et al.* [26] examined the quality characteristics of raw goat meat obtained from different ages and breeds of goats: Anglonubia×Tai native aged one and three and race Saanan×Tai native in age of seven years, 24 h after slaughter. Comparing the results of these authors for the breed Anglonubia×Tai native, aged three years, for moisture %, fat %, protein %, ash %, pH value, cooking loss % and tenderness, g/cm^2, it could be noted that they are not in line with the results shown in the Table 1. Sen *et al*. [27] examined the quality of the meat of one year old goats. Their results for moisture % and protein % are in agreement with our results concerning the Balkan goat meat, while fat %, pH and cooking loss % are not in line with our results, but tenderness comply. Our results, except pH, which are related to the Serbian white goat, are in agreement with the results of Paleari *et al.* [28], but the results obtained for the Balkan goat are inconsistent.

Results shown in Table 1 are not in agreement with the results of Webb *et al.* [29] who presented in their review paper the mineral concentrations in muscle for Cu, Mn, Fe and Zn.

Fatty acid analysis

The results of fatty acid composition in *m. longissimus dorsi* of Serbian White goat and Balkan goat, slaughtered at the age of four years, are presented in Table 2. Comparison between them showed that the lauric, myristic, pentadecanoic, pentadecenoic, palmitic, palmitoleic, margaric, stearic, oleic, linoleic, alfa linolenic and eicosenoic fatty acids statistically significantly differ ($P < 0.05$). There was no statistically significant difference ($P > 0.05$) between compared groups in content of cis – heptadecenoic, t – elaidic, t – linolelaidic and eicosenoic fatty acids. The ratio of unsaturated/saturated fatty acids in meat of Serbian white goats was 0.96 and in Balkan goats was 0.92.

The results obtained in this study are not entirely consistent with the results we obtained in the previous

Table 1. Live weight, chemical composition, pH value, tenderness, cooking loss and microelements (mg/kg) of goat meat of Serbian white goat and Balkan goat; a,b – means within the same column with different superscripts differ significantly (P < 0.05)

Parameter, *n* = 20	*M±SD*		Parameter, *n* = 20	*M±SD*	
	Serbian white goat	Balkan goat		Serbian white goat	Balkan goat
Live weight, kg	50.90±3.29^b	44.70±1.13^a	Ash, %	1.06±0.01^b	1.04±0.01^a
Water, %	75.42±0.30^b	74.51±0.13^a	pH value	5.67±0.03	5.67±0.03
Fat, %	3.55±0.40^a	3.92±0.14^b	Tenderness, kg/cm^2	7.25±0.81^a	7.75±0.73^b
Proteins, %	19.95±0.48^a	20.55±0.05^b	Cooking loss, %	39.41±1.99^a	40.60±1.68^b
Copper	0.73±0.17^b	0.58±0.15^a	Manganese	0.06±0.02	0.07±0.02
Iron	7.25±1.22	6.51±1.18	Zinc	4.08±0.40^a	4.56±0.48^b

Table 2. Fatty acid composition of Serbian white and Balkan goat, mg/g of meat; a,b – means within the same column with different superscripts differ significantly (P < 0.05)

Parameter, *n* = 20	*M±SD*		Parameter, *n* = 20	*M±SD*	
	Serbian white goat	Balkan goat		Serbian white goat	Balkan goat
Lauric acid (C12:0)	0.34±0.03[b]	0.29±0.01[a]	t-Elaidic acid (C18:1)	0.13±0.05	0.11±0.03
Myristic acid (C14:0)	2.46±0.05[b]	1.32±0.03[a]	Oleic acid (C18:1)	13.96±0.23[a]	15.23±0.19[b]
Pentadecanoic acid (C15:0)	0.37±0.03[b]	0.26±0.02[a]	t-Linolelaidic acid (C18:2)	0.12±0.04	0.10±0.04
Pentadecenoic acid (C15:1)	0.15±0.01[b]	0.06±0.01[a]	Linoleic acid (C18:2)	0.86±0.04[a]	1.32±0.02[b]
Palmitic acid (C16:0)	9.12±0.16[a]	11.91±0.31[b]	AlfaLinolenic acid (C18:3)	0.20±0.01[a]	0.47±0.01[b]
Palmitoleic acid (C16:1)	1.77±0.08[b]	1.23±0.03[a]	Eicosenoicacid (C20:1)	0.07±0.01	0.08±0.01
Margaric acid (C17:0)	0.50±0.03[b]	0.08±0.01[a]	SFA	17.80	20.02
cis-Heptadecenoic acid (C17:1)	0.05±0.02	0.07±0.02	USFA	17.31	18.67
Stearic acid (C18:0)	5.00±0.10[a]	6.16±0.19[b]	USFA/SFA	0.96	0.92

study. During the year 2012 we investigated a fatty acid composition in Bunte Deutsche Edelziege race, of different age, six and three years old [30]. Paleari *et al*. [28] examined the fatty acids in fresh thigh 2–3-year-old goats, race Frisa×Frontalasca crosses. The findings of fatty acids: lauric acid, myristic acid, pentadecanoic acid, palmitic acid, margaric acid, stearic acid and linoleic acid, are not in agreement with our results shown in Table 2.

Webb *et al.* [29] in their paper show the values of fatty acids for Boer goats meat: tridecanoic acid, myristic acid, pentadecanoic acid, palmitic acid, palmitoleic acid, margaric acid, stearic acid, oleic acid, eicosenoic acid, saturated fatty acids and unsaturated fatty acids. These values do not comply with our results shown in Table 2.

Zervas and Tsiplakou [31] in their review paper showed the percentage of individual fatty acids in muscle tissue. The results that we obtained (Table 2) are consistent with the values presented by Zervas and Tsiplakou [31] for palmitic acid, palmitoleic acid, stearic acid and oleic acid, but did not agree with the values for myristic acid, linoleic acid and alpha linolenic acid.

Amino acid analysis

Table 3 shows the results of the amino acid composition (g/100 g) of protein in the *musculus longissimus dorsi* of Serbian white and Balkan goats. It could be noted that between the amino acid alanine, arginine, aspartic acid, cysteine, glutamic acid, glycine, histidine, isoleucine, lysine, methionine, phenylalanine, proline, serine, threonine, tryptophan, tyrosine and valine difference was not statistically significant ($P > 0.05$), while between the amino acid leucine there was a statistically significant difference ($P < 0.05$) between the analyzed samples.

Webb *et al*. [29] in their paper showed the presence of the amino acids in meat of one year old goats. The results of these authors agree with the results given in Table 3.

Ferreira [32] in his study gave the amino acids content present in carcass of Boer goats. These results are somewhat lower than the values presented in Table 3.

Brzostowski et al. [33] examined amino acid profile of protein in meat from male kids race French Alpine. The results listed there are in agreement with the results shown in Table 3.

Table 3. Amino acid composition (g/100 g) of Serbian white goat and Balkan goat protein; a,b – means within the same column with different superscripts differ significantly (P < 0.05)

Parameter, *n* = 20	*M±SD*		Parameter, *n* = 20	*M±SD*	
	Serbian white goat	Balkan goat		Serbian white goat	Balkan goat
Alanine	4.93±0.87	4.98±0.95	Lysine	8.36±1.55	8.11±1.60
Arginine	5.44±0.86	5.54±0.89	Methionine	3.20±0.57	3.51±0.60
Aspartic acid	8.66±0.95	8.74±0.90	Phenylalanine	4.22± 0.76	4.55±0.75
Cysteine	1.02±0.21	1.04±0.22	Proline	3.45±0.80	3.37±0.84
Glutamic acid	14.41±1.70	13.95±1.59	Serine	3.92±0.82	3.89±0.87
Glycine	3.97±0.80	3.91±0.78	Threonine	4.84±0.94	4.97±0.90
Histidine	3.62±0.72	3.84±0.73	Tryptophan	1.19±0.27	1.27±0.33
Isoleucine	4.63±0.91	4.71±0.96	Tyrosine	4.17±0.78	4.44±0.75
Leucine	8.13±0.22[a]	8.38±0.33[b]	Valine	4.97±0.92	5.05±0.96

Instrumental determination of color

Table 4 shows the results of instrumental analyses of the *musculus longissimus dorsi* of the mentioned goat breeds in CIE and CIEL**a***b** system. According to the values of the parameters of this system it could be seen that there were no statistically significant differences ($P > 0.05$), *i.e*., there was no difference in color between the samples.

Results obtained by instrumental determination of color in this study (Table 4) are in correlation with the results from our previous investigation regarding Balkan goat and Bunte Deutsche Edelziege goat [3].

Our results are not in agreement with the results of Wattanachant *et al*. [26] who investigated the quality characteristics of raw goat meat obtained from different ages and breeds. The values presented in Table 4 comply with the results by mentioned authors for the breed Anglonubian×Thai native goats aged 3 years. Results shown in Table 4 are compatible to the results of Teixeira *et al*. [34] who investigated ageing effect on fresh meat color.

Sensory analysis

Sensory evaluation of fresh meat (Serbian white goat (n = 10) and Balkan goat (n = 10) is presented in the Table 5.

differences were not found ($P > 0.05$). The color of meat of Balkan goat obtained in the evaluation was 19.80 and of Serbian white goat meat was 19.50. Visual structure and firmness of fresh meat were also similar ($P > 0.05$). Structure was evaluated for meat of Balkan goat as 12.80 and for Serbian white goat meat 12.50.

During sensory evaluation of fresh goat meat samples, significant differences were found ($P < 0.05$) for the examined characteristic, palpatory evaluated firmness, between groups with 13.00 for meat of Balkan goat and 12.00 for Serbian white goat. Olfactory odor was evaluated for Balkan goat meat with 48.00 and for Serbian white goat meat with 48.00, which means that there was no statistically significant difference ($P > 0.05$). Sensory evaluation is very difficult to compare with the findings of other authors.

CONCLUSION

Comparing the results of analysed meat quality parameters of two goat races, Balkan goat and Serbian White goat, significant differences were noted in water means, total fats, proteins, ash, cooking loss, as well as for amino acid leucine content and in sensory evaluation of fresh meat for the palpatory evaluated firmness. Statistically significant difference ($P < 0.05$) for

*Table 4. Colour parameters of the m. longissimus dorsi of Serbian white and Balkan goats expressed in CIE and CIEL*a*b* system; reflectance – y, dominant wavelength – λ, P (color purity, %), lightness – L*, redness – a*, yellowness – b**

Parameter, n = 20	M±SD		Parameter, n = 20	M±SD	
	Serbian white goat	Balkan goat		Serbian white goat	Balkan goat
y / %	78.29±1.16	77.69±0.96	L^*	33.83±1.84	32.77±2.01
λ / nm	656.07±7.70	659.12±7.73	a^*	20.46±1.20	19.78±1.25
P / %	21.24±1.50	20.24±1.89	b^*	4.94±0.50	4.63±0.50

Table 5. Sensory evaluation of fresh meat of Serbian white and Balkan goats (M±SD); a,b – means within the same column with different superscripts differ significantly (P < 0.05)

Attributes, n = 10	Appearance	Texture		Flavour	Percentage of maximal possible quality 100	Weighted average 100/20
	Colour surface	Visual evaluated structure	Palpatory evaluated firmness	Olfactory evaluated odour		
	Coefficient of importance					
	4	3	3	10		
Serbian white goat	19.50±0.43	12.50±0.38	12.00±0.40[a]	48.00±0.49	92.00	4.60
Balkan goat	19.80±0.42	12.80±0.41	13.00±0.43[b]	48.00±0.49	93.60	4.68

During the sensory evaluation of fresh meat of goats a statistically significant difference ($P<0.05$) for the characteristic palpatory evaluated firmness between the groups was noted, while the surface color, visual evaluated structure, evaluated olfactory odor showed no statistically significant difference ($P > 0.05$).

Results of sensory evaluation are presented in Tables 5. Among the color of fresh meat, statistical

copper and zinc content was also present, while the ration of unsaturated/saturated fatty acids in Serbian white was 0.96 and in Balkan goats 0.92.

Acknowledgements

The research was done within the project TR 31053, Implementation of new biotechnological solutions in breeding of cattle, sheep and goats for the purpose of

obtaining biologically valuable and safe food, funded by the Ministry of Education and Science of the Republic of Serbia.

REFERENCES

[1] M. Anaeto, J.A. Adeyeye, G.O. Chioma, A.O. Olarinmoye, G.O. Tayo, Goat products: Meeting the challenges of human health and nutrition. ABJNA http:// //www.scihub.org/ABJNA, 2010.

[2] C. Devendra, The nutritional value of goat meat, in Proceedings (IDRC- 268e) of goat meat production in Asia, 1988, pp. 76–86.

[3] S. Ivanovic, J. Popov-Raljic, Z.M. Baltic, M. Zujovic, Z. Tomic, S. Lilic, I. Pavlović, Chemical and sensory characteristics of bunte deutsche edelziege and balkan goat meat, Afr. J. Biotechnol. **10** (2011) 18433–18439.

[4] S. Ivanovic, M. Zutic, I. Pavlović, M. Zujovic, Goat meat – important food stuff or vector of zoonotic microorganisms, in Proceedings of IV International symposium of livestock production, Struga, Makedonija, 2009, p. 65.

[5] M. Zujovic, N. Memisi, S. Ivanovic, Present status, possibilities and perspective of development of goat production in republic of Serbia, in Proceedings of 3rd International congress on animal husbandry "New Perspectives and Challenges of Sustainable Livestock Production", Biotech. Anim. Husbandry **27** (2011) 431––443.

[6] J.P. Dubeuf, P. Morand-Fehr, R. Rubino, Situation, changes and future of goat industry around the world, Small Ruminant Res. **51** (2004) 165–173.

[7] M. Todaro, A. Corrao, M.L. Alicata, R. Shinelli, P. Giaccone, A. Priolo, Effects of litter size and sex on meat quality traits of kid meat, Small Ruminant Res. **54** (2004) 191–196.

[8] J.N.B. Shrestha, M.H. Fahmy, Breeding goats for meat production: a review. 1. Genetic resources, management and breed evaluation, Small Ruminant Res. **58** (2005) 93–106.

[9] N. Memisi, Quantitative analisis of body development and production traits of Domestic Balkan goats. Ph.D. Thesis, Faculty of Agriculture, Belgrade, 2000.

[10] M. Zujovic, Z.Tomic, P.M. Petrovic, C. Mekic, S. Ivanovic, Z.Nesic, Development and perspective of goat production in Serbia, Biotech. Anim. Husbandry **22** (2006) 43––56.

[11] ISO 1442, Meat and meat products - Determination of moisture content, International Organization for Standardization, Geneva, 1998.

[12] ISO 1443, Meat and meat products – Determination of total fat content, International Organization for Standardization, Geneva, 1992.

[13] ISO 936, Meat and meat products – Determination of total ash. International Organization for Standardization, Geneva, 1999.

[14] ISO 937, Meat and meat products – Determination of nitrogen content. International Organization for Standardization, Geneva, 1992.

[15] ISO 2917, Meat and meat products – Measurement of pH, Reference method, International Organization for Standardization, Geneva, 2004.

[16] J. Folch, M.Lees, G.H.S. Stanley, Eine einfache MethodezurIsolierung und Reinigung der Lipideaustierisch Gewebe, J. Biol. Chem. **1** (1957) 497–509.

[17] ISO 5508, Animal and vegetable fats and oils – Analysis by gas chromatography of methyl esters of fatty acids, International Organization for Standardization, Geneva, 1990.

[18] AOAC, Protein Efficiency Ratio, in: W. Horwitz (Ed.) Official Methods of Analysis of AOAC International, 17th ed., Gaithersburg, MD, 2000.

[19] V. Stocchi, G. Piccoli, M. Magnani, F. Palma, B. Biagiarelli, L. Cucchiarini, Reversed-phase high-performance liquid chromatography separation of dimethylaminoazobenzene sulfonyl- and dimethylaminoazobenzene thiohydantoin-amino acid derivatives for amino acid analysis and microsequencingstudies at the picomole level, Anal. Biochem. **178** (1989) 107–117.

[20] AOAC, Lead, Cadmium, Zinc, Copper, and Iron in Foods, Atomic Absorption Spectrophotometry after Microwave Digestion. in Official Methods of Analysis of AOAC International, 17th ed., 999.10, W. Horwitz, ed., Gaithersburg, MD, 2000.

[21] S. Ivanovic**,** Investigation of the influence of probiotics on the selected indicators of broiler's meat hygiene and quality. Ph.D. Thesis, Univ. Belgrade, 2003

[22] CIE Colorimetry (2nd ed.), Publication CIE No. 15.2, Central Bureau of the Commission Internationale de L'Ectarge, Vienna, 1986.

[23] CIE Colorimetry Committee, Technical notes: working program on color differences. J. Opt. Soc. Am. **64** (1986) 896–897.

[24] ISO 8586-1, Sensory analysis-General guidance for the selection, training and monitoring of assessors. International Organization for Standardization, Geneva, 1993.

[25] S. Hadzivukovic, Statistical methods, University of Belgrade, Faculty of Agriculture, Belgrade, 1991 (in Serbian)

[26] S. Wattanachant, T.Sornprasitt, Y. Polpara, Quality characteristics of raw and canned goat meat in water, brine, oil and Thai curry during storage, Songklanakarin, J. Sci. Technol. **30** (2008) 41–50.

[27] A.R. Sen, A.Santra, S.A. Karim, Carcass yield, composition and meat quality attributes of sheep and goat under semiarid conditions, Meat Sci. **66** (2004) 757–763.

[28] M. Paleari, V. Moretti, G. Beretta, F. Caprino, Chemical parameters, fatty acids and volatile compounds of salted and ripened goat thigh, Small Ruminant Res. **74** (2008) 140–148.

[29] E.C. Webb, N.H. Casey, L. Simela, Goat meat quality, Small Ruminant Res. **60** (2005) 153–166.

[30] S. Ivanovic, Z. Stojanovic, B. Pisinov, K. Nešić, I. Pihler, N. Maksimović, N. Stanišić, Influence of slaughter age on meat quality of goat, in Proceedings of 15th International Feed Technology Symposium "Feed-to-food"/ /cost feed for health joint Workshop, Novi Sad, 2012, pp. 284–289.

[31] G. Zervas, E. Tsiplakou, The effect of feeding systems on the characteristics of products from small ruminants, Small Ruminant Res. **101** (2011) 140–149.
[32] A.V. Ferreira, Essential amino acid requirements of meat and milk goats, South Afr. J. Anim. Sci. **34** (2004) 46–48.
[33] H. Brzostowski, R. Niżnikowski, Z. Tański, Quality of goat meat from purebred French Alpine kids and Boer cross-breeds, Arch. Tierz. Dummerstorf **51** (2008) 381–388.
[34] A. Teixeira, E. Pereira, E.S. Rodrigues, Goat meat quality. Effects of salting, air-drying and ageing processes, Small Ruminant Res. **98** (2011) 55–58.

IZVOD

UTICAJ RASE KOZA NA KVALITET MESA

Snezana D. Ivanovic[1], Zoran M. Stojanovic[2], Ksenija D. Nesic[1], Boris P. Pisinov[1], Milan Ž. Baltic[3], Jovanka V. Popov-Raljic[4], Jelena M. Đurić [3]

[1]*Naučni institut za veterinarstvo Srbije, Beograd, Srbija*
[2]*Agencija za ispitivanje životne sredine, Beograde, Srbija*
[3]*Fakultet veterinarske medicine, Univerziteta u Beogradu, Beograd, Srbija*
[4]*Poljoprivredni fakultet, Zemun, Srbija*

(Stručni rad)

Kozije meso ima otprilike istu hranljivu vrednost kao i ovčije (bliže rečeno više belančevina, a manje masti). Zbog niske zastupljenosti zasićenih masnih kiselina i holesterola, kozije meso u ishrani ljudi je zdravija alternativa u poređenju sa drugim vrstama crvenog mesa. Bez obzira na nutritivnu vrednost, ono je ipak manje cenjeno zbog specifičnog mirisa i ukusa koji su intenzivniji kod starijih životinja. U Srbiji se malo zna o kvalitetu kozijeg mesa u poređenju sa ostalim vrstama, a posebno je nedovoljno poznavanje kvaliteta mesa autohtonih rasa koza. Cilj ovog istraživanja bio je da se prikupe i uporede podaci hemijskog sastava, pH vrednosti, sastava masnih i amino kiselina, pojedinih mikroelemenata, boje i mekoće (instrumentalno), senzorne analize svežeg mesa i određivanje kala toplotne obrade srpske bele i balkanske koze iste starosti. Iz uzoraka *m. longissimus dorsi,* uzetih nakon klanja navedenih životinja, ispitivan je hemijski sastav i pH vrednost, primenom ISO metoda. Sastav masnih kiselina i određen je primenom gasne hromatografije (GC6890N, Agilent Tech., USA) i poređen je sa standardom masnih kiselina (standard mix of FAMEs 37, Supelco, USA). Aminokiseline u navedenim uzorcima određene su nakon hidrolize tkiva primenom AOAC metode 982.30. Određivanje mikroelemenata u mesu koza vršeno je u metodom AOAC method 999.10. Princip metode za određivanje kala toplotne obrade sastoji se u određivanju gubitka mase usled toplotne obrade uzorka. Određivanje mekoće je obavljeno aparatom Warner–Bratzler. Boja svežeg mesa je takođe određivana u *m. longissimus dorsi* upotrebom Minolta chromameter CR-400. Senzornu analizu su radili obučeni ocenjivači u skladu sa ISO metodom. Dobijeni rezultati su statistički obrađeni primenom programa MS-Excel 2003, ANOVA, i utvrđene razlike srednjih vrednosti poređene *t*-testom na nivou značajnosti 99 i 95%. Na osnovu dobijenih rezultata može se zaključiti da je postojala statistički značajna razlika u kvalitetu mesa između ispitivanih uzoraka.

Ključne reči: Hemijski sastav • Koze • Meso • Kvalitet • Rase

Influence factors of photocatalytic activity of the filter media modified by TiO_2

Rongyan Shen, Guoyong Feng, Yuting Liang, Xingqing Zhao, Wenyi Zhang

School of Environmental and Safety Engineering, ChangZhou University, Changzhou, China

Abstract

The gangue filter media was modified by the titanium dioxide (TiO_2) through the liquid phase deposition method. Some influence factors of photocatalytic activity were investigated, including the mole ratio of initial solution, the water bath temperature, the deposition time, the calcination temperature and the heat preservation time of calcination. The morphology of the film was examined by SEM, EDS and crystallite structure by X-Ray Diffraction (XRD). The SEM, EDS and XRD data showed that new TiO_2 crystal was found in the modified filter media. And the specific surface area of the modified filter media greatly increased. By the orthogonal experiment, the optimum parameters of modification were $(NH_4)_2TiF_6$:H_3BO_3 = 1:2, water bath temperature of 80 °C, deposition time of 5 h, calcination temperature of 500 °C, and 1 h heat preservation time of calcination. Under above conditions, the heavy nitrogen wastewater of 1589.94 mg/L COD and 18750 times chroma was treated by the modified filter media. After 1 h catalytic reaction, the decolorization rate and COD removal rate reached 65.89 and 47.87%, respectively.

Keywords: TiO_2, liquid phase deposition, heavy nitrogen, decolorization rate, COD.

Available online at the Journal website: http://www.ache.org.rs/HI/

SCIENTIFIC PAPER

UDC 544.526.5:546.824–31

Hem. Ind. **68** (6) 809–818 (2014)

doi: 10.2298/HEMIND131017010S

2-Diazo-4,6-dinitrophenol (DDNP) has been widely used in commercial and military detonators as an important and effective primary explosive. It is an energetic compound without lead [1,2], and its good energy capability is comparable with that of high explosives. Among existing primary explosives, DDNP is a very promising initiator [3,4]. But in the process of DDNP producing, large amount of heavy nitrogen wastewater was produced, which had the characteristics of higher chroma, higher COD, higher toxicity, complicated composition, etc. [5]. If the heavy nitrogen wastewater without being treated was discharged into river, it would severely pollute the environment and threaten the health of people living in the downstream [6]. This problem has attracted the researchers' attention and puzzled the local industry and environmental protection institution.

Nowadays, the main treatment methods of heavy nitrogen wastewater are adsorption method, microelectrolysis/H_2O_2 method, and biochemistry method, etc. But the initial cost of these methods was high. Some enterprises could not afford it. And some methods are in the period of exploration, and it is difficult for them to be applied and promoted.

Photocatalytic oxidation is a newly developed technology for wastewater treatment [7,8]. Sunlight was used as a potential radiation source in this method. It could stimulate the generation of hole and electron pair for the catalyst, so strong redox occurred in this method. Many pollutants such as refractory organics could be treated by this method. It was difficult for the heavy nitrogen wastewater of higher chroma to be treated. So, it is particularly important for the heavy nitrogen wastewater to find an economic and efficient treatment technology.

Titanium dioxide (TiO_2) is widely used as a photocatalyst in the photocatalytic oxidation method because it is relatively highly efficient, cheap, non-toxic, chemically and biologically inert and photo stable [9–13]. TiO_2 in the anatase phase has been used as an excellent photocatalyst and it is well applied for purification [9,10]. As a promising material, TiO_2 has been used in the photocatalytic degradation of polluted water and air [9–11]. TiO_2 was also widely applied in pollutants processing, sensors, photovoltaics and dye-sensitized solar cells due to its nontoxicity, highstability and photoelectric properties [14–19].

Photocatalytic oxidation was an effective method for the chroma reduction of wastewater [11–18], and it was easy to be operated. In this study, the feasibility of photocatalytic oxidation for heavy nitrogen wastewater was explored. The core was to investigate the influence factors of modification and the photocatalytic activity of the filter media modified by TiO_2. And the optimum technological conditions of modification were determined by the orthogonal experiment.

Correspondence: R. Shen, School of Environmental and Safety Engineering, ChangZhou University, Changzhou 213164, China.
E-mail: ryshen@cczu.edu.cn
Paper received: 17 October, 2013
Paper accepted: 20 January, 2014

EXPERIMENTAL

Preparation of the filter media

The main materials for the preparation of the filter media were coal gangue, waste glass, little $CaCO_3$ as the additive, and the volatile organic matter as the forming agent. Gangue was selected from the deserted gangue in the coal mine, and the waste glass was the ordinary flat glass. Coal gangue and waste glass were fine ground in the ball mill and uniformly mixed according to certain ratio. Forming agent along with the little blended powder were put into the ball mill as the mother bulb. The blended materials were continuously added onto the scrolling ball particles and sprayed by a small sprayer. Then the mother bulb grew bigger and denser. After certain time, the bigger mother bulb was filtered by the 5 mm sieve and the smaller mother bulb was returned into the rotary. The average remaining time of the ball in ball mill was 1h and the particle sizes were between 3 mm and 6 mm. Then the raw ball was roasted in the muffle furnace under the certain technological conditions.

Preparation of the filter media modified by TiO_2

The filter media modified by TiO_2 was prepared by the liquid phase deposition method using the gangue filter media as the carrier, and $(NH_4)_2TiF_6$ and H_3BO_3 as precursors. Firstly, the solutions of $(NH_4)_2TiF_6$ and H_3BO_3 were prepared with the distilled water. And 250 mL reaction solution in different ratios was acquired in the coating container by taking certain volume of two solutions. Secondly, the coating container was put into the constant temperature water bath, and 100 g filter media was put into the coating container under the condition of stir. The filter media was taken out from the coating container after it had deposited for certain time at constant temperature. Thirdly, the filter media was washed with the distilled water and then was dried in the dryer at 120 °C. Fourthly, the dried filter media was put into the muffle furnace whose temperature rose from the room temperature to the set temperature at the speed of 15 °C/min. After certain time the gangue filter media modified by TiO_2 was obtained. The preparation device is shown in Figure 1.

Photocatalytic reaction device

Photocatalytic reactor was the laminated glass container. The interlayer was photocatalytic reaction unit filled with the filter media modified by TiO_2 (Figure 2). The filling rate of the filter media was 50% and the volume was about 250 ml. 50 cm length quartz glass tube was placed in the internal device of the photocatalytic reactor. 25 W ultraviolet illumination tube was placed in the quartz glass tube. Glass tube mouths of 1 cm inner diameter were set in each side of the reactor, and water inflowed from upper orifice. Oxygen was generated by air pump. The reactor was washed with the original solution, and timing began when appropriate solution was taken into the reactor.

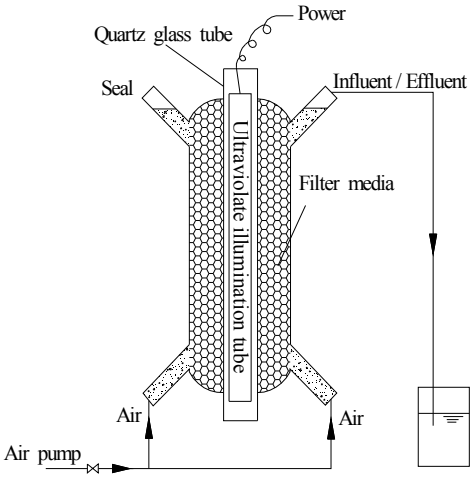

Figure 2. The test device of photocatalytic reaction.

Water samples and analysis method

Heavy nitrogen wastewater was used as the target degradation substrate and COD removal rate and decolorization rate were evaluated. The COD value was

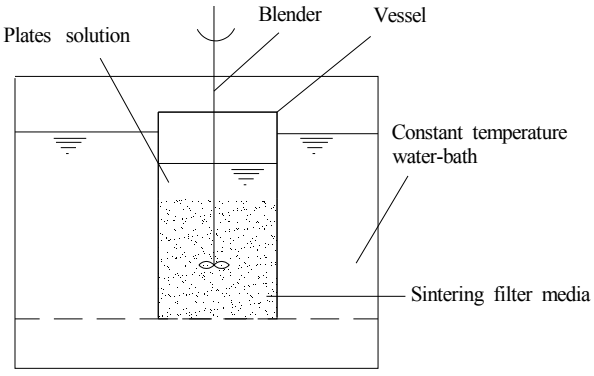

Figure 1. The device for the preparation of the modified filter media.

measured by the potassium dichromate method. The decolorization rate was used to measure the degradation effect of the modified filter media. And the variation of absorbency was characteristic of decolorization efficiency. The computation formula was as follows:

$$\eta = 100\frac{A_0 - A}{A_0} \quad (1)$$

where A_0 and A are the absorbency of wastewater at the initial time and t time, respectively. Absorbency was determined by 722 s visible spectrophotometer. And the wavelength value was 420 nm.

RESULTS AND DISCUSSION

Particle morphology and physicochemical properties of TiO_2 film

SEM. Figure 3 shows that the SEM images of the modified and unmodified filter media under different magnification. Figure 3c and d were the corresponding enlarged images of Figure 3a and b, respectively. Figure 3b shows that the surface of modified filter media had brighter background. As TiO_2 thin film had reflection, and light left the uneven surface after multiple reflections. The absorption and utilization of light would inevitably increase. It was good for the catalytic reaction. Although the surface of unmodified filter media was very rough, and there were large irregular holes in the surface. But the surface of particle was smoother. Figure 3d shows that many evenly distributed 30–50 nm bumps existed in the surface of the modified filter media. They were TiO_2 grain particles and these particles piled up in together in different ways. This made the microstructure of the surface of the modified filter media change. And the specific surface area of the modified filter media was greatly improved. It was good for the particle to be adsorbed on the surface. Then more ultraviolet light was adsorbed. So TiO_2 film had good photocatalytic performance [20].

EDS. Figure 4 shows the EDS electron energy spectrum diagram of the modified and unmodified filter media. From the diagram we can see that the main components of the unmodified filter media were silicon, aluminum, oxygen, carbon, calcium and iron. Titanium element was found in the energy spectrum diagram of the modified filter media and existed in the form of TiO_2. The weight percentage and atomic percentage of the titanium were 0.99 and 0.40%, respectively (Figure 4b).

XRD. In order to further research the crystallography characteristics of modified and unmodified filter media, XRD was conducted. The results were shown in Figure 5. By the qualitative analysis, a great quantity of alpha quartz crystal, calcium scale quartz, and feldspar existed in the mineral phase structure of the filter media. TiO_2 crystal did not be found in the unmodified

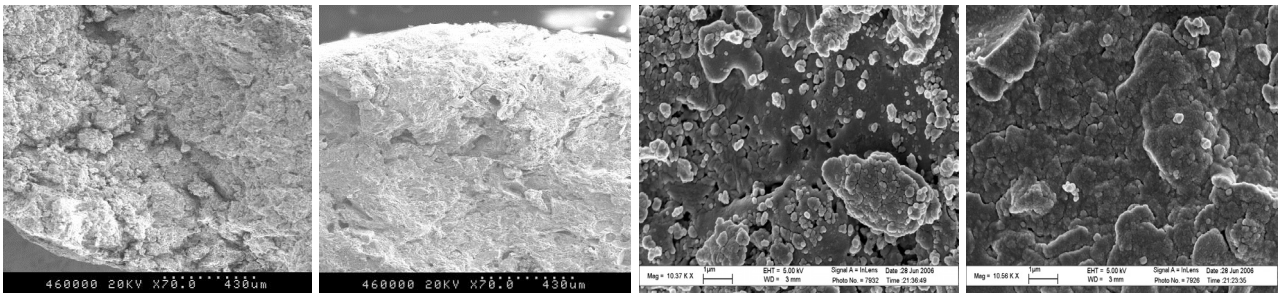

(a) (b) (c) (d)

Figure 3. Image of SEM (unmodified and modified).

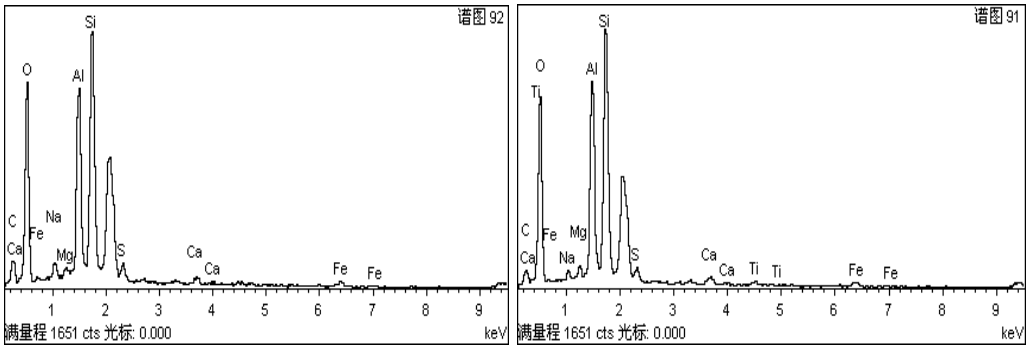

(a) (b)

Figure 4. Image of EDS (unmodified and modified).

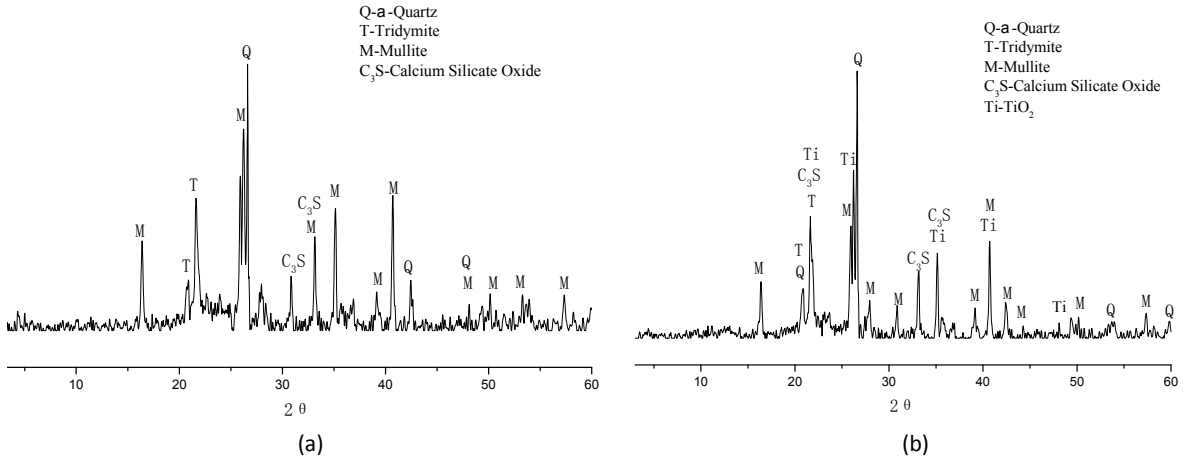

Figure 5. Image of XRD.

filter media. New TiO_2 crystal was found in the modified filter media. The superposition phenomenon was found in the diffraction peak of TiO_2 crystals and calcium feldspar crystal.

Specific surface area and void fraction. The specific surface area and void fraction of modified and unmodified coal gangue filter media were shown in Table 1. The specific surface area of the modified filter media has been increased by 70%. The main reason was that the microstructure was formed because of the high dispersion degree of nano TiO_2 at the surface of the filter media. After the treatment of high temperature, amorphous TiO_2 was transformed into the anatase phase. Specific surface area significantly increased owing to the crystallization of the element and the formation of microporous [21]. According to the physical and chemical theory, the solid with big specific surface area often was in the unstable state and its surface always tended to become smooth [22]. Such surface had good adsorption performance and could provide more catalytic activity center for the reaction, and the catalytic reaction could smoothly happen.

Table 1. Specific surface area and void fraction of modified and unmodified filter media

Filter media	Specific surface area m^2/g	Void fraction %
Unmodified	4.6	48.51
Modified	7.8	49.63

Analysis of influence factors of modification

In this paper, the heavy nitrogen wastewater of 18750 times chroma and 1589.94 mg/L COD was treated by the filter media modified by TiO_2. And the photocatalytic activity of the modified film was investigated. All photocatalytic reaction times were setting for 1h. In the process of TiO_2 film preparation, its photocatalytic performance was influenced by many factors. In this study, the mole ratio of initial solution, deposition temperature, deposition time, heat treatment temperature, and heat preservation time were studied.

Mole ratio of initial solution. H_3BO_3 and $(NH_4)_2TiF_6$ of different mole ratios were mixed and stirred at 80 °C for 5 h, and then were heated at 450 °C for 1 h. Under this condition, the modified film was obtained and its photocatalytic performance was studied.

Figure 6 shows the composition of the plating solution obviously affected the photocatalytic activity. The decolorization rate and COD removal rate increased at first and then declined. When the mole ratio of H_3BO_3 and $(NH_4)_2TiF_6$ was 3:1, the decolorization and COD removal rates reached the maximum which are 46.67 and 28.90%, respectively. The transparency of the deposition film was determined by the composition of reaction solution. When the concentration of $(NH_4)_2TiF_6$ was higher, the speed of the hydrolysis and the film formation grew faster. When large amount grain deposited in very short time, the film was thick and opaque. But when the concentration of $(NH_4)_2TiF_6$ was lower, the film formation was slow. So film was transparent. If the concentration of $(NH_4)_2TiF_6$ was too lower, it was difficult for the film to form because it was difficult for $[TiF_6]^{2-}$ to hydrolyze [11,23]. Meantime, the pH value of the initial solution effected the dehydration, polymerization, and TiO_2 phase [24–27].

The pH value of the precursor solution is a decisive factor in controlling the final particle size [28], shape [29], phase [30] and agglomeration [31] due to its influence on the relative rates of hydrolysis and polycondensation. The coordination Ti^{4+} and OH^- depended of the pH [24]. In the pH 2 solutions ($[Ti(OH)_2(H_2O)_4]^{2+}$), rod-like rutile formed. In the pH 4 solutions ($[Ti(OH)_4(H_2O)_2]^0$), the skewed chains of the anatase structure formed. And small quantities of the rutile structure existed in the precursor species and decreased the critical size of anatase-to-rutile transfor-

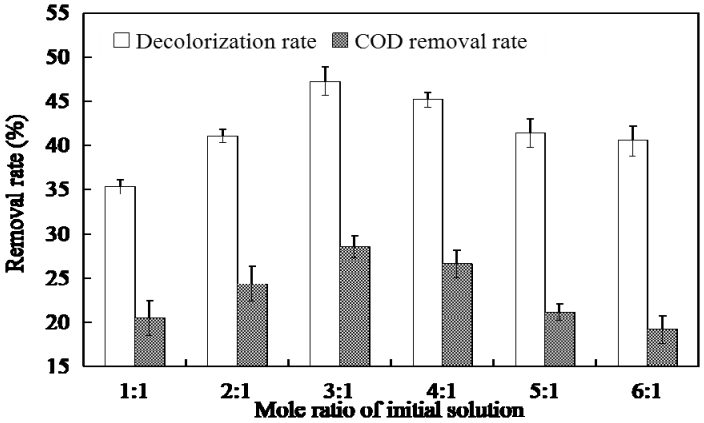

Figure 6. Effect of the mole ratio of initial solution on removal rate.

mation [24]. The probabilities of polycondensation occurred in the pH 7 solutions ($[Ti(OH)_6]^{2-}$). So anatase and rutile cocrystallized from the solutions. In the pH 9 solutions ($[Ti(OH)_7]^{3-}$), much structural and free water in the netlike precursor structure was involved during the process of polymerization. The presence of excessive OH^- would hinder the orientation movement of crystal nucleus. Thus, the disordered precursor structure would easily crystallize into the anatase phase. These provided a deep insight into the formation mechanism of anatase or rutile at different pH values [24].

H_3BO_3 did not affect the film thickness but the speed of film formation. When H_3BO_3 content was too low, the mixed solutions was not stable and tended to hydrolyze. So the speed of $[TiF_6]^{2-}$ hydrolysis was very rapid. While H_3BO_3 content was too high, the hydrolysis of $[TiF_6]^{2-}$ was inhibited. So the film formation was hard. When the concentrations of $(NH_4)_2TiF_6$ and H_3BO_3 were in the range of 0.08–0.20 mol/L and 0.10–0.50 mol/L, respectively, the optimal condition of film formation reached [32]. When the mole ratios of H_3BO_3 and $(NH_4)_2TiF_6$ were from 2 to 4, the transparent film could be obtained. Therefore, 0.10 mol/L $(NH_4)_2TiF_6$ and the mole ratios 2, 3, and 4 of H_3BO_3 and $(NH_4)_2TiF_6$ were chosen in this study.

*Water bath temperatur*e. Due to the endothermic process of the film formation, temperature effected the formation of film. When temperature was higher, the speed of the film formation was quicker. But too high temperature would cause the evaporation of the plating solution. So the spot existed in the surface of the film and it was not suitable for the film formation. When $c_{H_3BO_3}$:$c_{(NH_4)_2TiF_6}$ was 3:1, the mixed solution was deposited for 5 h and then heated at 450 °C for 1 h. Under this condition, the modified film was obtained and its photocatalytic performance was studied.

Figure 7 shows TiO_2 film had certain catalytic activity when water bath temperature is from 50 to 90 °C. Hence, the temperature range of the liquid phase deposition film is wide. With the rising of water bath temperature, the decolorization rate and COD removal rose at first and then declined. When water bath temperature was 70 °C, the removal rates reached the highest values which are 52.00 and 34.45%, respect-

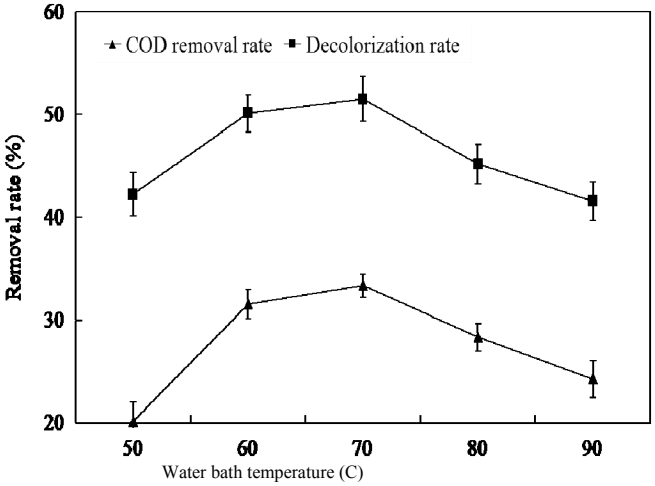

Figure 7. Effect of water bath temperature on removal rate.

ively. With the rising of temperature, the time that the turbid phenomenon emerged in the plating solution obviously reduced. According to the collision theory of chemical reaction, at lower temperature, $[Ti(OH)_6]^{2-}$ and –OH at the surface of the filter media would fully contact and collide. And the dehydration and the polymerization reaction happened [33,34]. TiO_2 film generated at the surface. With the rising of temperature, the thermodynamic movement of molecular sped up and the dehydration and polymerization of $[Ti(OH)_6]^{2-}$ and –OH sped up. Therefore, with the rising of temperature in low temperature range, COD removal rate also increased. But when temperature continued to rise, the speed of the dehydration and polymerization of $[Ti(OH)_6]^{2-}$ was higher than that of $[Ti(OH)_6]^{2-}$ and –OH. Dehydration and polymerization of $[Ti(OH)_6]^{2-}$ might be the main process of film formation. The polymer chains emerged in this process covered the surface of matrix, and the dehydration and polymerization of $[Ti(OH)_6]^{2-}$ and –OH was impeded. This caused the reduction of film adhesion. Hence, when temperature rose to the critical value, the removal rates declined. Based on above analysis, water bath temperature effected the deposition and the adhesion of film. The optimal temperature was 70 °C in this study.

Deposition time. At certain water bath temperature, the thickness of photocatalytic film changed with the variation of deposition time. In this study, the conditions of $c_{H_3BO_3}$:$c_{(NH_4)_2TiF_6}$ of 3:1 and 80 °C water bath were chosen, the solution was deposited for different time and then heated at 450 °C for 1h. The photocatalytic performance of the modified film obtained under above condition was studied.

Figure 8 shows TiO_2 film had photocatalytic activity when the deposition time was from 3 to 6 h. The decolorization rate and COD removal rate rose at first and then decreased with the rising of deposition time. When deposition time was 5 h, the removal rates reached the maximum which were 52.00 and 34.45%, respectively. At certain water bath temperature, when deposition time increased, film became thicker. Its photocatalytic activity has been increased. But when the film thickness was out of certain range, its photocatalytic activity would decline because certain depth existed both in the illumination of ultraviolet and in the photocatalytic reaction of film [11]. Meanwhile, deposition temperature affected the deposition time. Generally, the higher the temperature was, the greater the deposition rate was, the shorter the film formation time of certain thickness was. So there was close relationship between deposition time and film thickness. In this study, the optimal deposition time was 5 h.

*Calcination temperature***.** During the preparation of TiO_2 photocatalyst, heat treatment temperature was an important parameter. Under the conditions of 5 h deposition time, $c_{H_3BO_3}$:$c_{(NH_4)_2TiF_6}$ of 3:1, and water bath temperature of 80 °C, the mixed solution was treated at different calcination temperature for 1 h. The effects of calcination temperature on the photocatalytic activity of TiO_2 film were studied.

Figure 9 shows the decolorization rate and COD removal rate rose at first and then declined with the rising of calcination temperature. When calcination temperature was 500 °C, the decolorization rate and COD removal rate reached the maximum which were 58.40 and 36.97%, respectively. Before sintering, TiO_2 existed in amorphous state. Anatase phase TiO_2 could be obtained by heat treatment. With the rising of sintering temperature, the anatase phase gradually transformed into the rutile phase. Calcination effected not only the physical and chemical properties of nanocrystal of titanium oxide but also the size of grain. When calcination temperature was from 300 to 500 °C, catalyst had the best photocatalytic activity [35–37]. Because calcination could let the gel become dense at above temperature, and the particle size of micropore increased with the enlargement of sintering grain. So the crystallinity of dried anatase phase and mixed

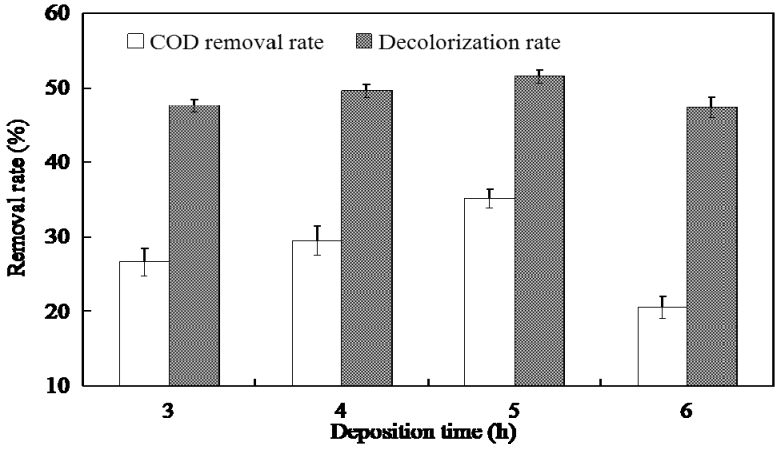

Figure 8. Effect of deposition time on removal rate.

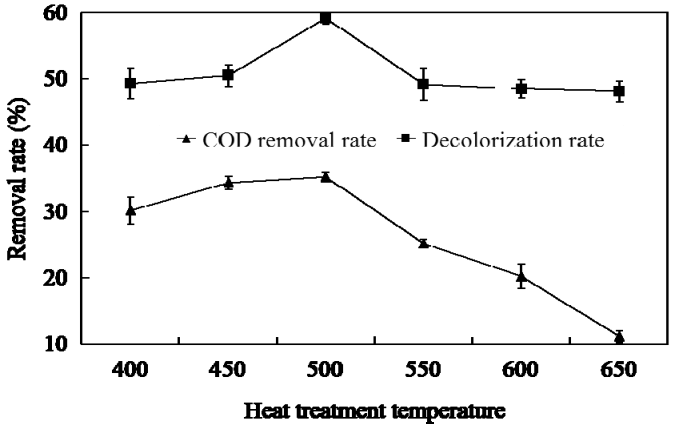

Figure 9. Effect of heat treatment temperature on removal rate.

phases was obviously improved. When calcination temperature was less than 550 °C, anatase phase mainly existed [37]. When calcination temperature was 550 °C, the rutile phase mainly existed and its proportion gradually increased with the rising of temperature. When calcination temperature was more than 700 °C, rutile phase mainly existed. The photocatalytic performance of TiO_2 strongly depended on its crystal phase and surface area [37]. The pure rutile phase TiO_2 hardly had catalytic activity. But the anatase phase of higher surface area had better photocatalytic activity. When small amount anatase phase transformed into the rutile phase, the catalytic activities of mixed phases were higher than those of pure anatase phase TiO_2 [35–37]. In this study, the optimal temperature of heat treatment was 500 °C.

Heat preservation time of calcination. According to the optimal conditions of single factor experiment, when the ratio of $c_{H_3BO_3}$ and $c_{(NH_4)_2TiF_6}$ was 3:1, the deposition time was 5 h, and the water bath temperature was 70 °C, the plating solution was treated at 500 °C for different time. The photocatalytic performance of the modified film obtained under above conditions was studied.

Figure 10 shows the heat preservation time affected the photocatalytic activity of modified filter media. The decolorization rate and COD removal rate increased at first and then declined with the rising of time, and the photocatalytic activity was highest when the heat treatment time was 2 h. The decolorization rate and COD removal rate were 63.73 and 41.84%, respectively. Anatase phase TiO_2 gradually transformed the rutile phase with the increasing calcination time. With the increasing proportion of rutile phase, the photocatalytic performance of TiO_2 film would be significantly affected. So the heat preservation time of calcination should be controlled. The optimal heat treatment time was 2 h in this study.

Orthogonal experiment of optimal process parameters

To determine the optimal parameters of the gangue filter media modified by TiO_2, the decolorization rate was evaluated. $c_{H_3BO_3}$:$c_{(NH_4)_2TiF_6}$ of plating solution, water

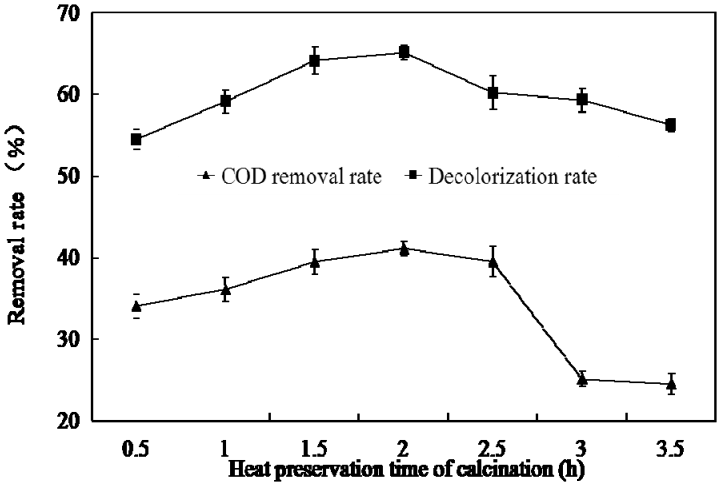

Figure 10. Effect of heat preservation time of calcination on removal rate.

bath temperature, calcination temperature, and heat preservation time of calcination were chosen, each factor taking three levels. The orthogonal experiment of four factors and three levels was arranged (Table 2). The concerned results are shown in Tables 3 and 4.

Table 2. Factors and levels of orthogonal experiment

Level	Factor			
	$c_{H_3BO_3}$:$c_{(NH_4)_2TiF_6}$	Reaction temperature, °C	Calcination temperature, °C	Calcination heat preservation time, h
	A	B	C	D
1	2:1	60	450	1
2	3:1	70	500	2
3	4:1	80	550	3

Table 3. Schemes and results of orthogonal experiment

Number	A	B	C	D	COD removal, %
1	2:1	60	450	1	42.63
2	2:1	70	500	2	45.76
3	2:1	80	550	3	43.52
4	3:1	60	500	3	37.64
5	3:1	70	550	1	35.79
6	3:1	80	450	2	37.85
7	4:1	60	550	2	28.40
8	4:1	70	450	3	33.70
9	4:1	80	500	1	36.74

Table 4 shows the effect order of each factor on the photocatalytic activity of the filter media modified by TiO_2 is A > C > B > D in the heavy nitrogen wastewater. The optimal parameters were $c_{H_3BO_3}$:$c_{(NH_4)_2TiF_6}$ of 2:1 (0.1 mol/L $(NH_4)_2TiF_6$), water bath temperature of 80ºC, calcination temperature of 500 °C, and heat preservation time of 1 h. When the filter media was modified under above conditions, the decolorization rate and COD removal reached 65.89 and 47.87%, respectively. The rates were higher than any group of the orthogonal experiment.

CONCLUSION

The sintering filter media was modified by TiO_2 and its photocatalytic performance was preliminary studied. The results showed that the filter media hardly had photocatalysis before it was modified. But after it was modified by TiO_2, the decolorization rate and COD removal rate increased in different degree. The morphology of the modified filter media was examined by SEM, EDS and crystallite structure by XRD. The SEM, EDS, and XRD data showed that new TiO_2 crystal was found in the modified filter media. And the specific surface area of the modified filter media greatly increased. So it was an important method for the sintering filter media to be modified by TiO_2 to improve its photocatalytic activity. And it also showed that TiO_2 was an excellent photocatalyst.

Many factors affected the modification of the filter media modified by TiO_2. The orthogonal experiment showed that the optimal preparation parameters of the sintering filter media modified by TiO_2 separately were the ratio of H_3BO_3 and $(NH_4)_2TiF_6$ for 2:1, water bath temperature for 80 °C, deposition time for 5 h, calcination temperature for 500 °C, and heat preservation time of calcination for 1 h. The heavy nitrogen wastewater of 1589.94 mg/L COD and 18750 times chroma was treated by the filter media modified by TiO_2 under above technological conditions. And the decolorization rate and COD removal rate were 65.89 and 47.87%, respectively.

Acknowledgements

The authors are grateful to the Jiangsu Province Natural Scientific Foundation (BK2011233 and BK2012159) and the Major Science and Technology Program for Water Pollution Control and Treatment (2012ZX07301001c) for the financial support of this work.

Table 4. Range analysis of orthogonal experiment

Number	$c_{H_3BO_3}$:$c_{(NH_4)_2TiF_6}$	Water bath temperature, °C	Calcination temperature, °C	Calcinations heat preservation time, min
K1	131.91	108.67	114.18	115.16
K2	111.28	115.25	120.14	112.01
K3	98.84	118.11	107.71	114.86
K1/3	43.97	36.22	38.06	38.39
K2/3	37.09	38.42	40.05	37.34
K3/3	32.95	39.37	35.90	38.29
R	11.02	3.15	4.14	1.05

REFERENCES

[1] M.H.V. Huynh, M.A. Hiskey, T.J. Meyer, M. Wetzler, Green primaries: environmentally friendly energetic complexes, PNAS **103** (2006) 5409–5412.

[2] M.B. Talawar, R. Sivabalan, T. Mukundan, H. Muthurajan, A. K. Sikder, B. R. Gandhe, A. Subhananda Rao, Environmentally compatible next generation green energetic materials (GEMs), J. Hazard. Mater. **161** (2009) 589–607.

[3] L.V. De Yong, G. Campanella, A study of blast characteristics of several primary explosives and pyrotechnic compositions, J. Hazard. Mater. **21** (1989) 125–133.

[4] R.G. Jiang, Z. T. Liu, Initiating Explosive, Vol. 1, Ordnance Industry Press of China, Beijing, 2006.

[5] A.P. Zhou, Study on diazodinitrophenol production wastewater, Explosive Materials **4** (1994) 12–13.

[6] X.H. Luo, X.F. Ye, The status and prospects of DDNP wastewater treatment, J. Xinjiang Norm. Univer. (Nat. Sci. Ed.) **4** (2011) 31–33.

[7] A. Troupis, A. Hiskia, E. Papaconstantinou, Photocatalytic reduction recovery of silver using polyoxometalates, Appl. Catal., B **42** (2003) 305–315.

[8] K. Rajeshwar, C.R. Chenthamarakshan, Y. Ming, W. Sun, Cathodic photoprocesses on titania films and in aqueous suspensions, J. Electroanal. Chem. (2002) 538–539.

[9] W.K. Jo, J.T. Kim, Application of visible light photocatalysis with nitrogen-doped or unmodified titanium dioxide for control of indoor-level volatile organic compounds, J. Hazard. Mater. **164** (2009) 360–366.

[10] K. Ubonchonlakate, L. Sikong, F. Saito, Photocatalytic disinfection of *P.aeruginosa* bacterial Ag-doped TiO_2 film, Procedia Eng. **32** (2012) 656–662.

[11] M.R. Hoffmann, S.T. Martin, W. Choi, D.W. Bahnemannt, Environmental applications of semiconductor photocatalysis, Chem. Rev. **95** (1995) 69–96.

[12] R.S. Sonawane, B.B. Kale, M. K. Dongare, Preparation and photocatalytic activity of Fe–TiO_2 thin films prepared by sol–gel dip coating, Mater. Chem. Phys. **85** (2004) 52–57.

[13] X. Wu, Q. Wei, J. Zhaohua, Influence of Fe^{3+} ions on the photocatalytic activity of TiO_2 films prepared by microplasma oxidation method, Thin Solid Films **496** (2006) 288–292.

[14] M. Takeshi, N. Kaori, S. Kazuyuki, K. Kazumi, Preparation of nanoporous TiO_2 film with large surface area using aqueous sol with trehalose, Mater. Lett. **58** (2004) 2751–2753.

[15] C. Wang, Y.H. Ao, P.F. Wang, J. Hou, J. Qian, S.H. Zhang, Preparation, characterization, photocatalytic properties of titania hollow sphere doped with cerium, J. Hazard Mater. **178** (2010) 517–521.

[16] C. Wang, Y.H. Ao, P.F. Wang, J. Hou, J. Qian, Photocatalytic performance of Gd ion modified titania porous hollow spheres under visible light, Mater. Letts. **64** (2010) 1003–1006.

[17] S. Biswas, M.F. Hossain, T. Takahashi, Y. Kubota, A. Fujishima, Photocatalytic activity of high-vacuum annealed CdS–TiO_2 thin film, Thin Solid Film **516** (2008) 7313––7317.

[18] V. Houškova, V. Štengl, S. Bakardjieva, N. Murafa, Photoactive materials prepared by homogeneous hydrolysis with thioacetamide: Part 2 – TiO_2/ZnO nanocomposites, J. Phys. Chem. Solid **69** (2008) 1623–1631.

[19] H.C. Lee, W.S. Hwang, Substrate effects on the oxygen gas sensing properties of SnO_2/TiO_2 thin films, Appl. Surf. Sci. **253** (2006) 1889–1897.

[20] Y.J. Zhang, J.N. Shen. The crystallization heat treatment of the TiO_2 photocatalytic nanofilm, Rare Metal Mater. Eng. **35** (2006) 92–95.

[21] Z.J. Li, B. Hou, Y. Xu, D. Wu, Y.H. Sun, Preparation and characterization of silica-modified titanium dioxide nanoparticles by coprecipitation method, J. Phys. Chem. **21** (2005) 229–233.

[22] X.P. Yi, H.P. Deng, Application of modified filter material in water treatment and its mechanism study, Water Purification Technology **18** (2000) 25–27.

[23] C.K. Xu, P.H. Shin, L.L. Cao, J.M. Wu, D. Gao, Ordered TiO_2 nanotube arrays on transparent conductive oxide for dye-sensitized solar cells, Chem. Mater. **22** (2010) 143–148.

[24] W.W. Zhang, S.G. Chen, S.Q. Yu, Y.S. Yin, Experimental and theoretical investigation of the pH effect on the titania phase transformation during the sol–gel process, J. Cryst. Growth **308** (2007) 122–129.

[25] H. Cheng, J. Ma, Z. Zhao, L. Qi, Hydrothermal preparation of uniform nanosize rutile and anatase particles, Chem. Mater. **7** (1995) 663–671.

[26] A. Pottier, C. Chaneac, E. Tronc, L. Mazerolles, J. Jolivet, Synthesis of brookite TiO_2 nanoparticles by thermolysis of $TiCl_4$ in strongly acidic aqueous media, J. Mater. Chem. **11** (2001) 1116–1121.

[27] H. Yin, Y. Wada, T. Kitamura, S. Kambe, S. Murasawa, H. Mori, T. Sakata, S. Yanagida, Hydrothermal synthesis of nanosized anatase and rutile TiO_2 using amorphous phase TiO_2, J. Mater. Chem. **11** (2001) 1694–1703.

[28] T. Sugimoto, X. Zhou, A. Muramatsu, Synthesis of uniform anatase TiO_2 nanoparticles by gel–sol method: 3. Formation process and size control, J. Colloid Interface Sci. **259** (2003) 43–52.

[29] H. Yin, Y. Wada, T. Kitamura, T. Sumida, Y. Hasegawa, S. Yanagida, Novel approaches to anatase and rutile nanocrystallites direct from $TiCl_4$, J. Mater. Chem. **12** (2002) 378–383.

[30] Y. Li, T.J. White, S.H. Lim, Low-temperature synthesis and microstructural control of titania nano-particles, J. Solid State Chem. **177** (2004) 1372–1381.

[31] M. Sugiyama, H. Okazaki, S. Koda, Size and shape transformation of TiO_2 nanoparticles by irradiation of 308-nm laser beam, Jap. J. Appl. Phys. **41** (2002) 4666–4674.

[32] G.D. Jiang, Z.F. Lin, C. Chen, L.H. Zhu, Q. Chang, N. Wang, W. Wei, H.Q. Tang, TiO_2 nanoparticles assembled on graphene oxide nanosheets with high photocatalytic activity for removal of pollutants, Carbon **49** (2011) 2693–2701.

[33] Y.Q. Wang, Y.J. Hou, J. Zhang, G. Ruan, Kinetics of dehydration polymerization of aspartic acid and syn-

thesis of polyaspartate catalyzed by potassium bisulfate, Polym. Internat. **53** (2004) 156–162.

[34] H. Wu, X.S. Li, M.C. Nie, B. Li, Z.Y. Jiang, Integral PVA-PES composite membranes by surface segregation method for pervaporation dehydration of ethanol, Chin. J. Chem. Eng. **19** (2011) 855–862.

[35] W. Natda, I. Burapat, W. Khatcharin, P. Sukon, Influence of calcination temperature on anatase to rutile phase transformation in TiO_2 nanoparticles synthesized by the modified sol–gel method, Mater. Lett. **82** (2012) 195––198.

[36] K.R. Zhu, M.S. Zhang, J.M. Hong, Z. Yin, Size effect on phase transition sequence of TiO_2 nanocrystal, Mater. Sci. Eng., A **403** (2005) 87–93.

[37] A.O. Araoyinbo, M.N. Ahmad Fauzi, S. Sreekantan, A. Aziz, Preparation and characterization of thin film TiO_2 dip coated on non-conductive substrate prepared from tetraethyl orthotitanate precursor, Asian J. Appl. Sci. **3** (2010) 35–43.

IZVOD

ISPITIVANJE FAKTORA KOJI UTIČU NA FOTOKATALITIČKU AKTIVNOST FILTERA MODIFIKOVANIH TiO_2

Rongyan Shen, Guoyong Feng, Yuting Liang, Xingqing Zhao, Wenyi Zhang

School of Environmental and Safety Engineering, ChangZhou University, Changzhou, China

(Naučni rad)

Gangue filter je modifikovan pomoću titan-dioksida (TiO_2) metodom depozicije u tečnoj fazi. Ispitivani su neki činioci koji utiču na fotokatalitičku aktivnost, kao što je molarni odnos početnog rastvora, temperatura vodenog kupatila, vreme depozicije, temperatura kalcinacije i dužina kalcinacije. Morfologija filma je ispitivana pomoću SEM i EDS, a kristalna struktura pomoću difrakcije X-zraka (XRD). Podaci dobijeni pomoću SEM, EDS i XRD su pokazali da je u modifikovanom filteru pronađena nova TiO_2 kristalna faza. Specifična površina modifikovanog filtera je značajno povećana. Kod vertikalnog eksperimenta optimalni parametri modofikacije su: $(NH_4)_2TiF_6$:H_3BO_3 = 1:2, temperatura vodenog kupatila 80 °C, vreme depozicije 5 h, temperatura kalcinacije od 500 °C i dužina kalcinacije 1 h. Pod pomenutim uslovima, otpadna voda teškog azota od 1589,94 mg/L COD i 18750 puta veće koncentracije hroma tretirana je pomoću modifikovanog filtera. Posle 1 h katalitičke reakcije, brzina obezbojavanja i brzina COD odstranjivanja je dostigla 65,89 i 47,87%, redom.

Ključne reči: TiO_2 • Depozicija u tečnoj fazi • Teški azot • Brzina obezbojavanja • COD

SADRŽAJ VOLUMENA 68.

Sveska 1

Sveska 2

Sveska 3

Sveska 4

Sveska 5

Sveska 6

Polimeri

INDEKS AUTORA 2014